

**ÉCOLE DOCTORALE ED222 - SCIENCES CHIMIQUES**  
**UMR7199 – LCAMB**  
**Laboratoire de Conception et Application des Molécules**  
**Bioactives**

**THÈSE** présentée par :  
**Elisabetta TOBALDI**

soutenue le : **09 Avril 2019**

pour obtenir le grade de : **Docteur de l'université de Strasbourg**

Discipline/ Spécialité : Chimie Organique

**Acid Catalysed Abiotic Reactions in  
Biological System:  
From Design to In Vivo Proof of  
Concept**

**THÈSE dirigée par :**

**M. WAGNER Alain**

Directeur de recherche, UMR 7199, Université de Strasbourg

**M. BECHT Jean-Michel**

Maître de Conférences HDR, IS2M, Université Haute-Alsace

**RAPPORTEURS :**

**M. WARD Thomas**

Professeur, Department of Chemistry, University of Basel

**M. TARAN Frédéric**

Directeur de recherche, SCBM, CEA Saclay



# TABLE OF CONTENT

<b>LIST OF ABBREVIATIONS</b>	<b>4</b>
<b>I – INTRODUCTION</b>	<b>6</b>
1. ABIOTIC REACTIONS IN BIOLOGICAL ENVIRONMENT .....	6
2. DEFINITION OF THE PROJECT: OBJECTIVES AND MAIN CHALLENGES.....	10
<b>I – INTRODUCTION</b>	<b>15</b>
1. RÉACTIONS ABIOTIQUES EN MILIEU BIOLOGIQUE .....	15
2. DEFINITION DU PROJET: OBJECTIFS ET PRINCIPAUX DEFIS.....	20
<b>II – IDENTIFICATION AND MODULATION OF THE ACETAL SUBSTRATE</b>	<b>27</b>
<b>1. OBJECTIVES</b> .....	<b>27</b>
1.1 LIST OF TARGETED ACETAL SUBSTRATES ACCORDING TO THEIR STABILITY	27
1.2 FRET PROBES AS TOOLS TO MONITOR HYDROLYSIS AT “ <i>IN VIVO</i> -LIKE” CONCENTRATION OF SUBSTRATES	27
<b>2. IDENTIFICATION OF HYDROPHOBIC ACETAL CLEAVABLE AT pH &lt; 4</b> .....	<b>31</b>
2.1 IDENTIFICATION OF ACETAL <b>APN6</b> AS CANDIDATE FOR HYDROLYSIS AT pH < 4	31
2.1.1 FRET probe of APN6.....	32
2.2.2 Profile of APN6 stability towards hydrolysis at different pH.....	33
2.2 IDENTIFICATION OF <b>APNM5</b> AS SECOND CANDIDATE FOR HYDROLYSIS AT pH < 4	35
2.2.1 Design of APNM5 to reach hydrolysis at pH < 4 and pH > 2 .....	35
2.2.2 Synthesis of acetal APNM5 .....	35
2.2.3 Synthesis and purification of FRET probe of acetal APNM5.....	44
2.2.4 Profile of F-APNM5 stability towards hydrolysis at different pH .....	46
<b>3. IDENTIFICATION OF HYDROPHILIC ACETAL CLEAVABLE AT pH &lt; 4</b> .....	<b>49</b>
3.1 DESIGN AND SYNTHESIS OF <b>PEGAM5</b> : THE HYDROPHILIC EQUIVALENT OF <b>F-APNM5</b>	49
3.1.1 Design of PEGAM5 .....	49
3.1.2 Evaluation of Huckel charges on the new acetal model .....	49
3.1.3 Synthesis of PEGAM5.....	50
<b>4. IDENTIFICATION OF ACETAL CLEAVABLE AT pH &gt; 4</b> .....	<b>53</b>
4.1 DESIGN AND SYNTHESIS OF ACETAL CLEAVABLE AT pH > 4 AND STABLE AT pH > 6	53
4.1.1 Design of acetal A2M5 and A2M6.....	53
4.1.2 Synthesis of A2M5 and A2M6.....	53
4.1.3 Synthesis of FRET probes F-A2M5 and F-A2M6 .....	55

4.2 PROFILE OF <b>F-A2M5</b> AND <b>F-A2M6</b> STABILITY TOWARDS HYDROLYSIS AT DIFFERENT PH	57
4.3 <i>IN VITRO</i> EVALUATION OF <b>F-A2M5</b> AND <b>F-A2M6</b> CLEAVABILITY IN CELLS	58
<b>5. IDENTIFICATION OF ACETAL STABLE TOWARDS HYDROLYSIS AT VERY LOW PH</b> .....	<b>61</b>
5.1 INTRODUCTION	61
5.1.1 Maleimide group in bioconjugation .....	61
5.1.2 SMCC vs MD amine-to-thiol heterobifunctional linkers .....	62
5.2 STRUCTURAL INVESTIGATION OF MALEIMIDE-ACETAL LINKERS FOR ACID AND SERUM STABILITY	63
5.2.1 Design and synthesis of MD linker analogues .....	63
5.2.2 Synthesis of FRET probes of MIA linkers.....	65
5.3.3 Profile of MIAs stability towards acetal hydrolysis at various pH.....	66
5.3.4 Profile of succinimide ring-opening in PBS .....	68
5.3.5 Profile of succinimide ring-opening in plasma. ....	69
5.3.6 Assessment of thiol exchange with HSA in plasma.....	70
5.3 CONCLUSION: OVERVIEW OF MALEIMIDE-ACETAL LINKERS' STRUCTURE-REACTIVITY RELATIONSHIP	71
<b>6. CONCLUSION</b> .....	<b>73</b>
<b><u>III – IDENTIFICATION OF THE BIOCOMPATIBLE ACID CATALYST</u></b> .....	<b>75</b>
<b>1. INTRODUCTION</b> .....	<b>75</b>
1.1 OBJECTIVES	75
1.2 SETUP OF THE CATALYST'S SCREENING	76
1.2.1 Definition of camphor sulfonic acid as positive control .....	77
1.2.2 Identification of the co-solvent for tests in aqueous media .....	78
1.2.3 Setup of catalyst's screening general conditions.....	79
1.2.4 Heterogeneous catalysts: reaction monitoring .....	80
<b>2. IDENTIFICATION OF A HYDROPHOBIC HETEROGENEOUS ACID CATALYST</b> .....	<b>82</b>
2.1 SCREENING OF HOMOGENEOUS CATALYSTS	82
2.2 SCREENING OF HETEROGENEOUS CATALYSTS	85
2.2.1 Screening of commercial catalysts .....	85
2.2.2 Screening of synthetic catalysts: modified silica.....	87
2.2.3 Screening of synthetic catalysts from IS2M.....	89
2.2.4 Screening of synthetic catalysts: modified Merrifield resin .....	90
2.3 SCREENING'S RESULTS: SYNOPSIS	92
2.4. INVESTIGATION OF THE ADSORBANCE RATE OF NAFION NR50 AND AMBERLYST A-15	93
2.5 APPROACHES TOWARDS THE QUANTIFICATION OF HYDROLYSIS IN SOLID ADSORBENT CATALYSTS	96
2.5.1 First quantitative hydrolysis evaluation method: wash out of reaction prodcts.....	96
2.5.2 Second quantitative hydrolysis evaluation method: imaging with UV transilluminator .....	98
2.5.3 Third quantitative hydrolysis evaluation method: imaging with Confocal Microscope .....	101

2.5.4 Conclusion on quantitative hydrolysis evaluation methods .....	103
2.6 INVESTIGATION OF NAFION NR50 ACIDIFICATION OF BUFFERED MEDIA .....	104
2.7 INVESTIGATION OF OTHER COMMERCIAL FORMS OF NAFION NR-50 .....	113
2.8 INVESTIGATION OF NAFION NR50 ACTIVITY IN COMBINATION WITH HYDROPHILIC ACETAL <b>PEGAM5</b> .....	114
<b>3. IDENTIFICATION OF A HYDROPHILIC HETEROGENEOUS ACID CATALYST .....</b>	<b>116</b>
3.1 ENCAPSULATION OF PAASA INTO ALGINATE BEADS .....	117
3.2 DESIGN AND TEST OF A TAILORED HYDROPHILIC HETEROGENOUS CATALYST .....	117
3.2.1 Formulation of PEG-acid polymer composition .....	118
3.2.2 Tests of PEG-AASA-20% beads with F-APNM5 .....	120
3.2.3 Tests of PEG-AASA-20% co-polymer with F-A2M5 and F-A2M6 .....	121
3.2.4 Tests of PEG-AASA-20% beads with PEGAM5 .....	122
3.3 CONCLUSION ON THE IDENTIFICATION OF THE HYDROPHILIC HETEROGENEOUS ACID CATALYST .....	125
<b>4. INVESTIGATION OF CATALYSTS INNER ACIDITY .....</b>	<b>126</b>
4.1 QUALITATIVE INVESTIGATION OF ACIDITY WITH PH UNIVERSAL INDICATOR .....	126
4.2 QUANTITATIVE DETERMINATION OF ACIDITY WITH CONFOCAL MICROSCOPE .....	127
4.2.1 Identification of ratiometric probe for confocal microscope .....	127
4.2.2 Determination of acidity of Nafion .....	131
4.2.3 Determination of acidity of PEG-AASA beads .....	136
<b>5. CORRELATION BETWEEN OBSERVED HYDROLYTIC ACTIVITY AND CALCULATED ACIDITY OF NAFION NR50 AND PEG-AASA-20% WITH DIFFERENT ACETAL SUBSTRATES.....</b>	<b>139</b>
<b><u>IV – TOWARDS <i>IN VIVO</i> PROOF OF CONCEPT</u></b> .....	<b>143</b>
<b>1. OBJECTIVES .....</b>	<b>143</b>
<b>2. <i>IN VIVO</i> PROOF OF CONCEPT SETUP .....</b>	<b>144</b>
2.1 CHOICE OF CATALYST AND SUBSTRATE .....	144
2.2 <i>In Vivo</i> PROOF OF CONCEPT: CHALLENGES AND PLANNING .....	144
2.2.1 Constraint relative to the use of Nafion beads .....	144
2.2.2 Constraint relative to the use of F-APNM5 .....	145
2.2.3 Test of Nafion-hFGF beads with F-APNM5 from Kolliphor® solution.....	145
2.2.4 In vivo experiments planning .....	146
<b>3. CONCLUSION .....</b>	<b>149</b>
<b><u>V – LATE STAGE FUNCTIONALIZATION OF ANTICANCER AGENTS</u></b> .....	<b>151</b>
<b>1. INTRODUCTION .....</b>	<b>151</b>
<b>2. PROJECT PLANNING .....</b>	<b>152</b>
2.1 SELECTION OF PROCEDURES .....	152
2.2 REACTION CONDITIONS .....	153
2.3 EXPERIMENTAL PLANNING .....	153

2.4 SELECTION OF ANTICANCER AGENTS AS SUBSTRATES	154
<b>3. PRELIMINARY RESULTS</b>	<b>159</b>
3.1 ISOMERIZATION OF PACLITAXEL	159
3.2 STABILITY TESTS FOR SOLVENTS AND TEMPERATURES	160
<b>4. CONCLUSION ON LATE STAGE FUNCTIONALIZATION</b>	<b>163</b>
<b><u>VI. CONCLUSIONS AND PERSPECTIVES</u></b>	<b><u>165</u></b>
<b><u>VI. CONCLUSIONS ET PERSPECTIVES</u></b>	<b><u>168</u></b>
<b><u>VIII. EXPERIMENTAL PROCEDURES</u></b>	<b><u>171</u></b>
DETAILED INDEX	171
1. CHEMICAL SYNTHESSES	173
2. STABILITY OF FRET PROBES IN AQUEOUS MEDIA	216
3. SCREENING OF CATALYSTS AND HYDROLYSIS TESTS	221
4. RATIOMETRIC ANALYSIS	227
5. <i>IN VITRO</i> AND <i>IN VIVO</i> EXPERIMENTS	228
6. LATE STAGE FUNCTIONALIZATION	230
<b><u>TABLE OF ILLUSTRATIONS</u></b>	<b><u>231</u></b>
<b><u>REFERENCES</u></b>	<b><u>239</u></b>
<b><u>APPENDIX</u></b>	<b><u>247</u></b>
A. CATALYSTS' SCREENING	247
B. NAFION NR50'S WASHING PRE-TREATMENT SCREENING	251
C. LATE STAGE FUNCTIONALIZATION: SOLVENT AND TEMPERATURE STABILITY TESTS..	261
<b><u>ACKNOWLEDGMENTS</u></b>	<b><u>283</u></b>

## LIST OF ABBREVIATIONS

ACN	acetonitrile
ADC	antibody-drug conjugates
ADME	absorption, distribution, metabolism and excretion
alloc	allyloxy carbonyl
AMBN	azobisisoamylonitrile
APN	arylpropiolonitrile
BCN	bicyclononine
BEP	2-bromo-1-ethyl-pyridinium tetrafluoroborate
BHQ-2	black hole quencher, type 2
BSA	bovine serum albumine
CAN	cerium ammonium nitrate
CDX	cyclodextrin
CLSM	confocal laser scanning microscope
CSA	camphor sulfonic acid
Ctrl	control
CuAAC	copper-catalysed alkyne-azide cycloaddition
DCM	dichloromethane
DMF	dimethyl formamide
DMSO	dimethyl sulfoxide
DSC	disuccinimidyl carbonate
EDG	electron-donating group
ESI	electron spray ionization
EWG	electron-withdrawing group
FDA	Food and Drug Administration
FRET	Förster resonance energy transfer
hFGF	human fibroblast growth factor
HPLC	high performance liquid chromatography
HR-ESI-MS	high resolution – electron spray ionization – mass spectrometry
HSA	human serum albumin
IEDDA	inverse electron demand Diels-Alder

IPA	isopropyl alcohol
IS2M	Institut de Science des Matériaux
IV	intravenous
LC-MS	liquid chromatography – mass spectrometry
mQ	milliQ
MR	Merrifield resin
NMR	nuclear magnetic resonance
PBS	phosphate buffer saline
PEG	polyethylene glycol
PMA	phosphomolybdic acid
PMI	photomultiplier
py	pyridine
SPAAC	strain-promoted alkyne-azide cycloaddition
TBAF	tetrabutylammonium fluoride
TCO	trans-cyclooctene
TFA	trifluoroacetic acid
THF	tetrahydrofuran
TM	transition metal(s)
TMP	tetramethyl piperidine
TRIS	tris(hydroxymethyl)aminomethane
UV	ultraviolet



# I – INTRODUCTION

## 1. ABIOTIC REACTIONS IN BIOLOGICAL ENVIRONMENT

From a chemical point of view, living organisms are probably the most fascinating systems that have ever existed. A massive amount of chemical and physical phenomena take place at the same time, in perfect coordination and balance, auto-regulated and mostly self-repaired. A system so intricate that apparently even the slightest perturbation could have the potential to trigger a cascade of unpredicted events and yet a system so highly buffered that proved to be able to sustain external stress without deadly consequences. A system whose secrets we have been trying to unravel and to reproduce since ever.

Interacting with such a complex world by physical entities -like X-rays, UV light, magnetic field- and by introduction of chemicals has always been with the aim to either decode, study, reproduce and ameliorate it (biochemistry, chemical biology and all their sub subjects) or to rebalance it in case of malfunctions (medicinal chemistry, diagnosis and treatment of diseases).

In almost all the cases, this is translated into the introduction of a xenobiotic (from the Greek: “xeno” = stranger, foreign) into a living organism. This foreign chemical would react with other more or less complex entities present in such a crowded environment, from the smallest species (protons, inorganic ions, metals, oxygen...) to the most complex and structured biomolecules (proteins, enzymes, cell organelles).

Either way, the aim is to prepare xenobiotics which would possibly undergo or regulate a selected reaction, according to the final goal: for the chemical biologist it would be the labelling of a metabolite, a protein, an enzyme, a part of the cell or even the whole cell in order to gain information from it; for a medicinal chemist it could be the stimulation or the inhibition of a certain metabolic pathway; the activation in situ of an anticancer agent; the transformation of a undesired metabolite to another molecule more easily excreted from the body. Carrying out those reactions in a hyper-regulated and crowded environment is extremely challenging because the xenobiotic introduced must selectively react with its counterpart, without causing undesired side-reactions and adverse effects on the short and long term.

Selectivity can be gained in different ways: **i**) by finding xenobiotic substrates which perfectly fit the biomolecule of interest, it is the case for example of enzymatic substrates, inhibitors,

antibody drug conjugates; **ii**) by exploiting extremely selective chemical reactions which are not performed by living systems. The second concept was introduced in 2003 by C. Bertozzi and grew exponentially since then. Biorthogonal reactions require the use of functionalities with no counterparts *in vivo* and are extremely selective, nontoxic (or presenting minimal toxicity) and highly efficient under physiological conditions.<sup>1,2</sup>

Biorthogonal applications typically proceed in two steps. First, the substrate (a biomolecule of interest, like a metabolite, an enzyme inhibitor, etc.) is modified with a bioorthogonal functional group and introduced into the cell. The modification must not alter the normal bioactivity of the target. Then a probe containing the complementary functional group is introduced to react and label the substrate.<sup>3</sup>

Over the years, the concept of bioorthogonal chemistry has been broadened to a pool of applications, not limited to biomolecular tagging and modification *in cellulo*.

The next frontier in chemical biology is to move toward completely abiotic reaction systems in which both the substrate, the promoter and the reaction itself are designed and prepared via organic synthesis (from the Greek: prefix “a” = “not”, “abiotic” = “not derived from living organisms”). The aim is to reproduce the selectivity and efficiency of biological processes -as in the case of bioorthogonal chemistry- while keeping the controllability in every single part.

The introduction of an abiotic reaction trigger in a living system encounters many challenges about toxicity, loss of activity and substrate competition, especially in the case of metal catalysts. Only few studies aiming at *in vivo* applications of completely abiotic reaction systems have been able to demonstrate the concept in complex living organism (mice, zebrafish, etc.). One example of biorthogonal chemistry applied to abiotic system was published by Oneto *et al.* in 2016.<sup>4</sup> The reaction is the well-known inverse-electron demand Diels-Alder (IEDDA) reaction between tetrazine and trans-cyclooctene (TCO). The xenobiotic substrate is a TCO modified anticancer drug (pro-drug) and the abiotic promoter (in this case the bioorthogonal counterpart of TCO) is a heterogeneous biocompatible hydrogel (alginate polymer) modified with tetrazine. The hydrogel is pre-implanted in a desired location (e.g. next to a tumoral tissue), assuring the concentration and activation of the pro-drug in the location of choice. The system was successfully tested in mice using the doxorubicin pro-drug, comparing their local drug activation system to classical chemotherapy.

Another recent work, performed in our group, exploits the selectivity of strain-promoted alkyne-azide cycloaddition (SPAAC) for the inactivation and fast clearance of an anticoagulant

drug in mice.<sup>5</sup> In this case the xenobiotic substrate is the anticoagulant agent Warfarin modified with an azide and the abiotic reagent is a clearing agent bearing a bicyclononyne motif (BCN-peg6-OH). The *in vivo* bioorthogonal reaction between the circulating drug and the BCN leads to the formation of an inactivated product which is cleared from the bloodstream. Bioorthogonal strategies rely also on the use of metals as abiotic catalysts for reactions in living systems, a fact which is not surprising given their great performances in classical organic chemistry.<sup>6</sup> The efficiency and selectivity of Transition Metals (TM) as catalysts for new-to-nature reactions is however counterbalanced by their cytotoxicity and deactivation in biological media.<sup>7</sup> To overcome these issues, TM are used as homogeneous complexes, incorporated into nanoparticles or enclosed in resins and microspheres. To date only a few metal-catalysed abiotic reactions have been proven in complex living organism. The pioneer in such direction is probably the work presented by Bradley's group in 2011 in which palladium nanoparticles trapped within polystyrene microspheres were proved to catalyse allylcarbamate cleavage and Suzuki-Miyaura cross-coupling in cells for the first time.<sup>8</sup> As the author claim in the conclusion of their article "this investigation provides the basis for the customization of heterogeneous unnatural catalysis as tools for creative applications in chemical biology, pharmacology and, potentially, in medicine". A prediction which proved to be correct given that since then many other examples of metal-catalysed reactions *in cellulo* were reported.<sup>9-11</sup> However, only a few and very recent works were able to go over cell-based systems and reach the stage of *in vivo* proof of concept and application in mice or zebrafish. In 2014, Weiss *et al.* reported an abiotic palladium-catalysed system composed by a modified 5-fluorouracil prodrug as xenobiotic substrate and palladium-functionalized polyethylene glycol-polystyrene resins as abiotic catalyst.<sup>12</sup> The reaction is the activation of the 5-fluorouracil drug in the extracellular tumoral environment since the Pd-resin are bigger than cells (diameter = 150  $\mu\text{m}$ ) and are supposed to be implanted intratumorally. The authors were able to demonstrate the biocompatibility of such resins, as well as their activity toward carbamate cleavage, in zebrafish embryos. Very recently, Miller and co-workers investigated the biocompatibility, localization in mice and use for doxorubicin drug release of a nano-encapsulated palladium catalyst.<sup>13</sup> Their system is composed by pro-doxorubicin (doxorubicin protected with allyloxycarbonyl "alloc" group as xenobiotic substrate and Pd-nanoparticles as abiotic promoter injected intravenously and uptaken by tumoral cells.

In the same year (2017), Tsubokura et al. presented a propargyl ester amidation reaction catalysed by gold within live mice.<sup>14</sup> In this case the metal was linked to a glycoalbumin in order to achieve specific localization of the reaction.

Those listed are examples of recent outstanding results obtained in the application of abiotic controllable bioorthogonal reactions in living systems. Some excellent reviews published very recently (2018) collect the most recent advances in the field.<sup>15-17</sup>

The challenges encountered when researcher try to translate an abiotic reaction from in vitro to in vivo -which include toxicity of the catalyst (the metal itself, nanoparticles), uncontrolled localization, deactivation of the catalyst- pushed us to consider as abiotic promoter other than transition metals.

Our objective is to define a system whose components are tailor-made (in order to get total controllability and possibility to modify according to needs) and whose performances are close to those of natural bioprocesses (high selectivity, efficiency and localization/compartmentalization). Thus, we took inspiration directly from those bioprocesses whose performances we aim to reach, by identifying in Brønsted acid catalysis the model reaction for this project. As a matter of fact, almost every biological process is pH-dependent, from those in which  $H^+$  is a direct participant (e.g. reactions catalysed by acid hydrolase class of enzymes) to those in which there is no apparent role for  $H^+$  ion.<sup>18</sup>

In the next section we define our project, objectives and main challenges regarding the design of a biological-inspired and totally abiotic reaction system which is conceived with the purpose of being applied in vivo.

## 2. DEFINITION OF THE PROJECT: OBJECTIVES AND MAIN CHALLENGES

Herein we present the description of a completely abiotic system composed by **i)** a substrate and **ii)** a reaction promoter (*i.e.* a catalyst) which are dependent on each other. The whole system “substrate + promoter” is conceived to work in the biological environment without interfering with it, thus giving a high reaction selectivity and a precise localization.

In the attempt to mimic the efficiency and selectivity of nature, we have investigated a way to trigger abiotic reactions which takes inspiration from biological processes: Brønsted acid catalysis.

The concentration of protons in the biological system is finely regulated and changes in pH are the triggers of many natural processes. Proton concentration is not the same neither in every part of the body, nor in every compartment of the cell.<sup>19</sup> The natural pH range is between 4.5 and 7.4, with some exceptions like gastric fluids (pH=2). The normal cell and extracellular environment have a pH value of 7.4; late endosomes have pH values between 5.5 and 6.5; lysosomes present even lower values, from pH = 4.5 to pH = 5.5. Extracellular tumour environment has a pH slightly more acidic than normal (pH = 6.5) thanks to the hypoxia conditions. Given that, our approach is to conceive an acid catalysed reaction which is triggered outside this range, *i.e.* at pH less than 4, in order to avoid undesired triggering in the slightly acidic compartments of the cell. To make this approach possible we thus need to design an acidic micro-environment that will retain its acidity within the highly buffered biological surrounding. The main challenge consists in identifying a heterogeneous material that fulfils this requirement. To achieve this ambitious aim, we will delve into catalysts of different nature (hydrophobic, hydrophilic) and, if necessary, design and synthesize solid acidic catalysts with tailored features.

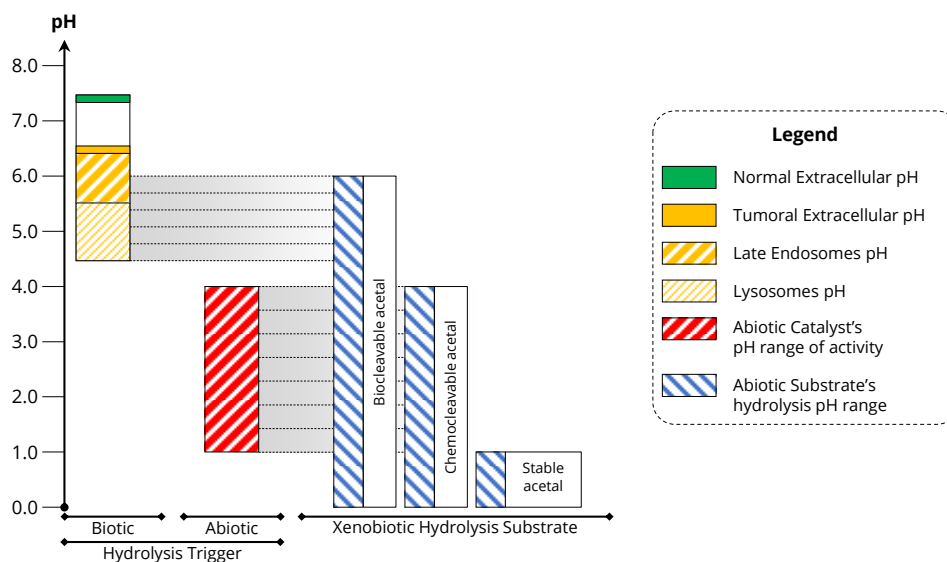
Regarding the reaction to be performed, we opted for the hydrolysis of cyclic acetals. This reaction is acid catalysed, requires the presence of water and is a bond-breaking reaction which can find applications in strategies based on the release of a payload.

Acetals' properties include cleavability in mild conditions, solubility in aqueous solvents and low hydrophobicity. Acetal linkers have been used as cleavable linkers for applications in fields like drug development, proteomics, imaging and DNA sequencing.<sup>20-22</sup> Thus, acetals have always been designed in order to have a precise hydrolysis rate, either to hydrolyse selectively in specific cell organelles (lysosomes and late endosomes) at pH around 5 either to be stable and serve as non-cleavable linkers.

In this work the structure-reactivity relationship of cyclic acetal linkers will be investigated in order to identify suitable substrates cleavable in different ranges of pH. We aim to design and synthesize acetals which falls into the following three categories:

- Acetals cleavable at pH < 4. This class of acetals can be cleaved in a range of pH which matches that of the suited acidic catalyst. Such combination of acetal and catalyst would compose a good candidate for a xenobiotic reaction system which would not interfere with the natural biological processes.
- Acetals cleavable between pH = 4 and pH = 5. This kind of acetals can be cleaved in the range of pH of lysosomes and late endosomes; thus, they would be excellent candidates for releasing strategies inside cells.
- Non-cleavable acetals. Acetals which could be used as stable water-soluble component in non-cleavable linkers.

The following figure resumes our objectives with the aid of a pH scale. The bands depicted corresponds to **i)** the natural pH ranges in cell and extracellular environment (first band), **ii)** the target pH activity for the heterogeneous acid catalyst suitable for *in vivo* catalysis (red band) and **iii)** the various pH ranges at which the abiotic acetals' hydrolysis is triggered according to the desired applications (blue bands).



**Figure 1.** Representation of the objectives pursued. The first band on the left represents the range of pH covered by cells and extracellular environment. The second red band represents the range of pH covered by the abiotic acid catalyst. The three blue bands on the right represent the pH ranges in which the hydrolysis of different abiotic acetal substrates is supposed to be triggered. Grey faded horizontal bands are used to show the matching between the abiotic substrates and the corresponding hydrolysis promoters.

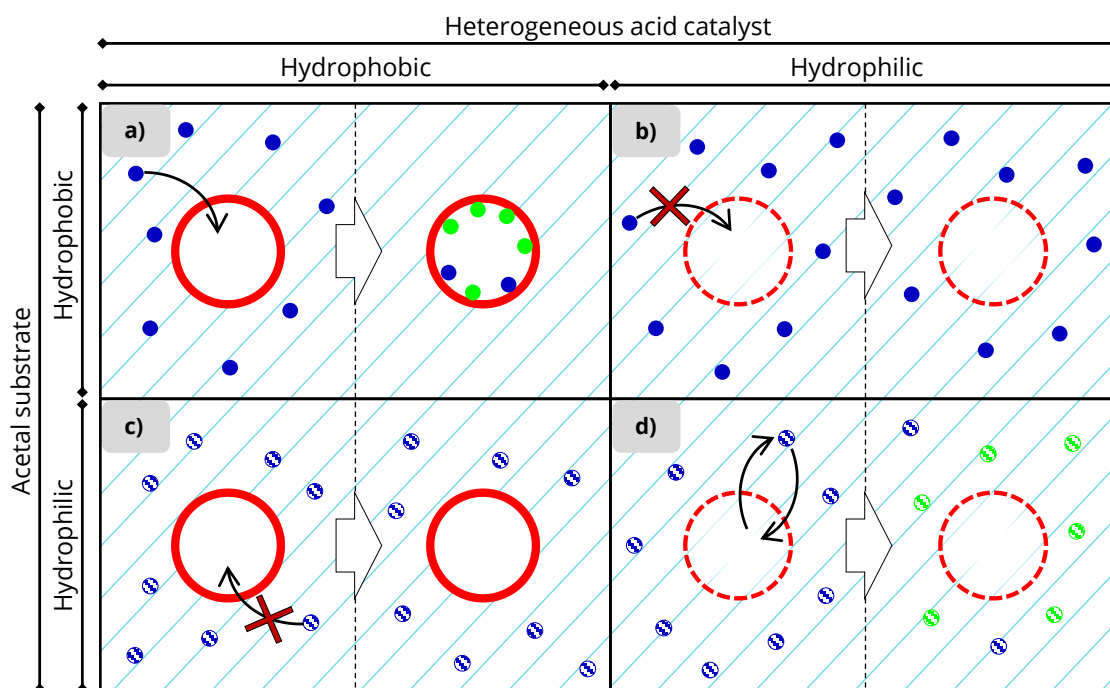
The figure shows the ideal pH range at which a catalyst suitable for *in vivo* applications would be active. Such value matches with the pH range in which the corresponding xenobiotic acetal substrate is hydrolysed. Both do not overlap with that of cell's acidic compartments. On the other hand, the abiotic acetal designed to be hydrolysed in mild acidic conditions ( $\text{pH} > 4$ ) matches the pH ranges of lysosomes and late endosomes, while the third kind of acetal substrate is extremely stable at low pH and does not have a corresponding trigger for its hydrolysis.

The chemical nature of the acetals cleavable at  $\text{pH} < 4$  has to be investigated in combination to that of its corresponding abiotic heterogeneous acid catalyst. The interaction between the acetal substrate, the catalyst and the aqueous media can be related to the hydrophobic or hydrophilic nature of both the catalyst and the acetal, without taking into account the binding to plasmatic proteins.

Four possible combinations are examined:

- A.** Hydrophobic acetal + hydrophobic catalyst: the catalyst has minimum exchange with the aqueous media. The acetal has much more affinity to the catalyst than to the solvent, so it is expected to adsorb into the solid catalyst, where the hydrolysis can occur thanks to its acidity.
- B.** Hydrophilic acetal + hydrophobic catalyst: the acetal has affinity for the aqueous environment and therefore presents much less interaction with the catalyst. Thus, the hydrolysis is not expected to take place.
- C.** Hydrophobic acetal + hydrophilic catalyst: in this case too, the lack of affinity between the substrate and the catalyst will likely result in the absence of acetal cleavage.
- D.** Hydrophilic acetal + hydrophilic catalyst: the acetal, the catalyst and the aqueous media can exchange with each other. In this case the substrate can be adsorbed by the catalyst, hydrolysed because of its inner acidity and then the product can be released, thanks to the affinity with the aqueous solvent.

**Figure 2** shows the four described combinations of acetal substrate and acidic catalyst. The solid catalyst is represented as a spherical bead. The contour of the sphere is plain for the hydrophobic catalyst (to represent the lack of interactions with the solvent) and is dotted for the hydrophilic one (to represent the exchange with water). The substrate is symbolized by blue dots, while the product of the hydrolysis is represented by green dots. Dots are plain in case of hydrophobic chemicals and striped if hydrophilic.



**Figure 2.** Representation of the four possible scenarios given by the combination of the substrate and the solid catalyst. Hydrophobic catalyst is symbolized by a sphere with a plain contour, while the hydrophilic catalyst's symbol has a dotted contour. The substrate and the product are represented as, respectively, blue and green dots. Dots are plain for the hydrophobic substrate and striped for the hydrophilic one. **a)** Hydrophobic substrate + hydrophobic catalysts; **b)** hydrophobic substrate + hydrophilic catalysts; **c)** hydrophilic substrate + hydrophobic catalyst and **d)** hydrophilic substrate + hydrophilic catalyst.

Scenarios **A** and **D** in which the substrate and catalyst have matching features are more likely to carry out acetal hydrolysis. The two situations diverge in the interaction between the substrate and the catalyst. We hypothesized that in the first case the hydrophobic interaction leads to the irreversible adsorbance of the acetal into the solid catalyst. The lack of release of neither the substrate nor the products may seem a significant drawback. Actually, in the optic of setting up a first *in vivo* proof of concept, this is exactly what is needed. In order to prove that hydrolysis has been achieved in the living system, an adsorbent solid catalyst allows to: **(i)** concentrate the probe in one spot, making easier to detect the fluorescence of the product; **(ii)** affirm that the hydrolysis was achieved only thanks to the catalyst.

In the second case the hydrophilic nature of both the substrate and the catalyst allows the product (= released payload) to stay in solution and interact with the biological environment, implementing its function(s). Given the higher degree of exchange between the catalyst and the aqueous solvent, finding a catalyst which can maintain its acidity in the buffered media



appears even more challenging than in previous case. In this matter, the expertise of Dr. Jean-Michel Becht and Dr. Lavinia Balan, researchers at the Institute of Materials in Mulhouse (IS2M, “Institut de Science des Matériaux”, Université Haute Alsace), our partner for this doctoral project, is essential for the formulation and the production of solid polymer specifically tailored to meet all our requirements (biocompatibility, hydrophilicity and acidity).

The first issue addressed in chapter **II** is the identification of the acetal and the modification of its chemical structure in order to tune its stability towards hydrolysis. Once hydrophobic and hydrophilic acetals cleavable in the desired range of pH far from the biological one (*i.e.* pH < 4) have been recognized, in chapter **III** the attention will be focused on identifying the corresponding hydrophobic and hydrophilic acid catalysts active in that range of pH. Then, experiments *in vivo* will be defined in detail in chapter **IV** and are expected to proof our hypothesis.

Finally, the possible applications of this abiotic system based on acetal hydrolysis are addressed. As mentioned above, this bond-breaking reaction could be exploited by payload-releasing techniques, if the payload presents a diol motif in its chemical structure. Since most of the currently used xenobiotics do not present a diol in their structure, we postulated that it is possible to modify the complex chemical structure of active molecules to insert a diol function without endangering their activity. In chapter **V** we broaden the scope from diol insertion to a pool of late-stage functionalization reactions of anticancer agents with the aim to find mild procedures which can be applied to a wide group of complex compounds to enhance their activity and performance.

# I – INTRODUCTION

## 1. RÉACTIONS ABIOTIQUES EN MILIEU BIOLOGIQUE

D'un point de vue chimique, les organismes vivants sont probablement les systèmes les plus fascinants qui aient jamais existé. Une multitude de phénomènes chimiques et physiques se produisent simultanément, parfaitement coordonnés et équilibrés, auto-régulés et principalement réparés. Un système si complexe qu'apparemment même la plus petite perturbation pourrait potentiellement déclencher une cascade d'imprévus et pourtant un système si fortement amorti qu'il a été capable de supporter le stress extérieur sans conséquences mortelles. Un système dont nous essayons de dévoiler les secrets et de les reproduire depuis toujours.

Interagir avec un monde aussi complexe par des entités physiques - rayons X, rayons UV, champs magnétiques - et par l'introduction de produits chimiques a toujours eu pour objectif de le décoder, de l'étudier, de le reproduire et de l'améliorer (biochimie, biologie chimique et tous leurs sous-sujets) ou de le rééquilibrer en cas de dysfonctionnements (chimie médicale, diagnostic et traitement des maladies).

Dans presque tous les cas, cela se traduit par l'introduction d'un xénobiotique (du grec : "xeno" = étranger, étranger) dans un organisme vivant. Ce produit chimique étranger réagirait avec d'autres entités plus ou moins complexes présentes dans un environnement aussi encombré, des plus petites espèces (protons, ions inorganiques, métaux, oxygène...) aux biomolécules les plus complexes et structurées (protéines, enzymes, organites cellulaires).

Quoi qu'il en soit, l'objectif est de préparer des xénobiotiques susceptibles de subir ou de réguler une réaction choisie, en fonction du but final: pour le biologiste chimiste, il s'agirait de marquer un métabolite, une protéine, une enzyme, une partie de la cellule ou même toute la cellule pour en tirer des informations; pour un chimiste spécialisé en médecine, il pourrait s'agir de la stimulation ou de l'inhibition d'une certaine voie métabolique; l'activation in situ d'un agent anticancéreux; la transformation d'un métabolite indésirable en une autre molécule plus facilement excrétée par l'organisme. Réaliser ces réactions dans un environnement hyper-régulé et surpeuplé est extrêmement difficile, car le xénobiotique introduit doit réagir de manière sélective avec son homologue, sans provoquer de réactions indésirables ni d'effets indésirables à court et à long terme.

La sélectivité peut être obtenue de différentes manières : **i)** en recherchant des substrats xénobiotiques parfaitement adaptés à la biomolécule d'intérêt, c'est le cas par exemple des substrats enzymatiques, des inhibiteurs, des anticorps conjugués ; **ii)** en exploitant des réactions chimiques extrêmement sélectives qui ne sont pas effectuées par des systèmes vivants. Le deuxième concept a été introduit en 2003 par C. Bertozzi et a connu une croissance exponentielle depuis. Les réactions biorthogonales nécessitent l'utilisation de fonctionnalités sans contrepartie *in vivo* et sont extrêmement sélectives, non toxiques (ou présentant une toxicité minimale) et hautement efficaces en conditions physiologiques.<sup>1,2</sup>

Les applications bioorthogonales se déroulent généralement en deux étapes. Tout d'abord, le substrat (une biomolécule d'intérêt, comme un métabolite, un inhibiteur d'enzyme, etc.) est modifié avec un groupe fonctionnel bioorthogonal et introduit dans la cellule. La modification ne doit pas altérer la bioactivité normale de la cible. Ensuite, une sonde contenant le groupe fonctionnel complémentaire est introduite pour réagir et marquer le substrat.<sup>3</sup>

Au fil des ans, le concept de chimie bioorthogonale a été élargi à un ensemble d'applications, qui ne se limite pas au marquage biomoléculaire et à la modification de la cellule.

La prochaine frontière en biologie chimique consiste à adopter des systèmes de réaction complètement abiotiques dans lesquels le substrat, le promoteur et la réaction elle-même sont conçus et préparés via une synthèse organique (du grec : préfixe «a» = «non», «abiotique»). = "Non dérivé d'organismes vivants"). L'objectif est de reproduire la sélectivité et l'efficacité des processus biologiques - comme dans le cas de la chimie bioorthogonale - tout en préservant la contrôlabilité dans chaque partie.

L'introduction d'un déclencheur de réaction abiotique dans un système vivant pose de nombreux problèmes de toxicité, de perte d'activité et de compétition du substrat, en particulier dans le cas des catalyseurs métalliques. Seules quelques études portant sur des applications *in vivo* de systèmes de réaction complètement abiotiques ont été en mesure de démontrer le concept dans un organisme vivant complexe (souris, poisson zèbre, etc.).

Un exemple de chimie biorthogonale appliquée au système abiotique a été publié par Oneto et al. en 2016.<sup>4</sup> La réaction est la réaction de Diels-Alder (IEDDA) à demande d'électrons inversée bien connue entre la tétrazine et le trans-cyclooctène (TCO). Le substrat xénobiotique est un médicament anticancéreux modifié par le TCO (précurseur du médicament) et le promoteur abiotique (dans ce cas le pendant bioorthogonal du TCO) est un hydrogel hétérogène biocompatible (polymère d'alginate) modifié avec de la tétrazine. L'hydrogel est

préimplanté à un emplacement souhaité (par exemple à proximité d'un tissu tumoral), en assurant la concentration et l'activation du pro-médicament à l'emplacement de choix. Le système a été testé avec succès chez des souris avec le pro-médicament de doxorubicine, en comparant leur système d'activation de médicament local à la chimiothérapie classique.

Un autre travail récent, réalisé dans notre groupe, exploite la sélectivité de la cycloaddition d'alkyne-azide (SPAAC) promue par souche pour l'inactivation et la clairance rapide d'un anticoagulant chez la souris<sup>5</sup>. Dans ce cas, le substrat xénobiotique est l'agent anticoagulant modifié par la warfarine un azoture et le réactif abiotique est un agent de clarification portant un motif bicyclononyne (BCN-peg6-OH). La réaction bioorthogonale *in vivo* entre le médicament en circulation et le BCN conduit à la formation d'un produit inactivé qui est éliminé de la circulation sanguine.

Les stratégies bioorthogonales reposent également sur l'utilisation de métaux comme catalyseurs abiotiques pour les réactions dans les systèmes vivants, ce qui n'est pas surprenant compte tenu de leurs excellentes performances en chimie organique classique.<sup>6</sup> L'efficacité et la sélectivité de Métaux des Transition (MT) en tant que catalyseurs de Les réactions de nature sont toutefois contrebalancées par leur cytotoxicité et leur désactivation dans les milieux biologiques.<sup>7</sup> Pour surmonter ces problèmes, les MT sont utilisées sous forme de complexes homogènes, incorporés dans des nanoparticules ou enfermés dans des résines et des microsphères. À ce jour, seules quelques réactions abiotiques catalysées par des métaux ont été prouvées dans des organismes vivants complexes. Le pionnier dans cette direction est probablement le travail présenté par le groupe Bradley en 2011 dans lequel il a été prouvé que des nanoparticules de palladium piégées dans des microsphères de polystyrène catalysaient le clivage d'allylcarbamate et le couplage croisé de cellules de Suzuki-Miyaura<sup>8</sup>. Comme le prétendent les auteurs dans la conclusion de leur article "cette enquête fournit la base pour la personnalisation de la catalyse non naturelle hétérogène en tant qu'outils pour des applications créatives en biologie chimique, en pharmacologie et, éventuellement, en médecine". Une prédiction qui s'est avérée correcte étant donné que depuis lors, de nombreux autres exemples de réactions catalysées par un métal chez les cellules ont été rapportés<sup>9-11</sup>. Cependant, seuls quelques travaux très récents ont pu passer en revue les systèmes à base de cellules et atteindre le stade de preuve de concept et application *in vivo* chez la souris ou le poisson zèbre.

En 2014, Weiss et al. ont rapporté un système abiotique catalysé par le palladium composé d'un promédicament modifié au 5-fluorouracile en tant que substrat xénobiotique et de résines de polyéthylène glycol-polystyrène fonctionnalisées au palladium en tant que catalyseur abiotique<sup>12</sup>. La réaction consiste en l'activation du médicament 5-fluorouracile dans l'environnement tumoral extracellulaire, car La résine de palladium est plus grosse que les cellules (diamètre = 150  $\mu\text{m}$ ) et est supposée être implantée par voie intratumorale. Les auteurs ont pu démontrer la biocompatibilité de telles résines ainsi que leur activité vis-à-vis du clivage des carbamates dans les embryons de poisson zèbre.

Très récemment, Miller et ses collaborateurs ont étudié la biocompatibilité, la localisation chez la souris et l'utilisation de la doxorubicine dans la libération d'un catalyseur au palladium nano-encapsulé.<sup>13</sup> Leur système est composé de pro-doxorubicine (doxorubicine protégée par un groupe «ally» carbonylé «allô»), comme le xénobiotique et des nanoparticules de Pd en tant que promoteur abiotique injectés par voie intraveineuse et absorbés par les cellules tumorales.

La même année (2017), Tsubokura et al. a présenté une réaction d'amidation d'ester de propargyle catalysée par de l'or chez des souris vivantes.<sup>14</sup> Dans ce cas, le métal était lié à une glycoalbumine afin d'atteindre une localisation spécifique de la réaction.

Celles-ci sont des exemples de résultats remarquables récents obtenus dans l'application de réactions bioorthogonales contrôlables abiotiques dans des systèmes vivants. Quelques excellentes critiques publiées très récemment (2018) rassemblent les dernières avancées dans le domaine<sup>15-17</sup>.

Les difficultés rencontrées lorsque les chercheurs ont tenté de traduire une réaction abiotique d'in vitro à in vivo, notamment la toxicité du catalyseur (le métal lui-même, les nanoparticules), la localisation incontrôlée, la désactivation du catalyseur, nous ont incités à considérer le promoteur abiotique comme autre que les métaux de transition.

Notre objectif est de définir un système dont les composants sont taillés sur mesure (afin d'obtenir une contrôlabilité totale et une possibilité de modification en fonction des besoins) et dont les performances sont proches de celles des bioprocédés naturels (sélectivité élevée, efficacité et localisation / compartimentation). Ainsi, nous nous sommes inspirés directement des bioprocédés dont nous souhaitons atteindre les performances, en identifiant dans la catalyse acide de Brønsted le modèle de réaction pour ce projet. En fait, presque tous les processus biologiques dépendent du pH, de ceux dans lesquels H<sup>+</sup> est un participant direct

(par exemple, des réactions catalysées par des enzymes de la classe des hydrolases acides) à ceux dans lesquels il n'y a aucun rôle apparent pour l'ion  $H^+$ .<sup>18</sup>

Dans la section suivante, nous définissons notre projet, nos objectifs et les principaux défis en ce qui concerne la conception d'un système de réaction totalement abiotique d'inspiration biologique conçu pour être appliqué in vivo.

## 2. DEFINITION DU PROJET: OBJECTIFS ET PRINCIPAUX DEFIS

Nous présentons ici la description d'un système complètement abiotique composé de i) un substrat et ii) d'un promoteur de réaction (c'est-à-dire un catalyseur) qui dépendent l'un de l'autre. L'ensemble du système «substrat + promoteur» est conçu pour fonctionner dans l'environnement biologique sans interférer avec celui-ci, donnant ainsi une sélectivité élevée à la réaction et une localisation précise.

Dans le but d'imiter l'efficacité et la sélectivité de la nature, nous avons étudié un moyen de déclencher des réactions abiotiques inspirées des processus biologiques: la catalyse acide de Brønsted.

La concentration de protons dans le système biologique est régulée avec précision et les changements de pH déclenchent de nombreux processus naturels. La concentration en protons n'est pas la même, ni dans toutes les parties du corps, ni dans tous les compartiments de la cellule.<sup>19</sup> La plage de pH naturel est comprise entre 4,5 et 7,4, à quelques exceptions près comme les fluides gastriques (pH = 2). La cellule normale et l'environnement extracellulaire ont une valeur de pH de 7,4; les endosomes tardifs ont un pH compris entre 5,5 et 6,5; Les lysosomes présentent des valeurs encore plus faibles, de pH = 4,5 à pH = 5,5. L'environnement tumoral extracellulaire a un pH légèrement plus acide que la normale (pH = 6,5) en raison des conditions d'hypoxie. Compte tenu de cela, notre approche consiste à concevoir une réaction catalysée par un acide qui est déclenchée en dehors de cet intervalle, c'est-à-dire à un pH inférieur à 4, afin d'éviter un déclenchement indésirable dans les compartiments légèrement acides de la cellule. Pour rendre cette approche possible, nous devons donc concevoir un micro-environnement acide qui conservera son acidité dans l'environnement biologique fortement tamponné. Le principal défi consiste à identifier un matériau hétérogène répondant à cette exigence. Pour atteindre cet objectif ambitieux, nous allons nous intéresser à des catalyseurs de nature différente (hydrophobes, hydrophiles) et, si nécessaire, concevoir et synthétiser des catalyseurs acides solides dotés de caractéristiques adaptées.

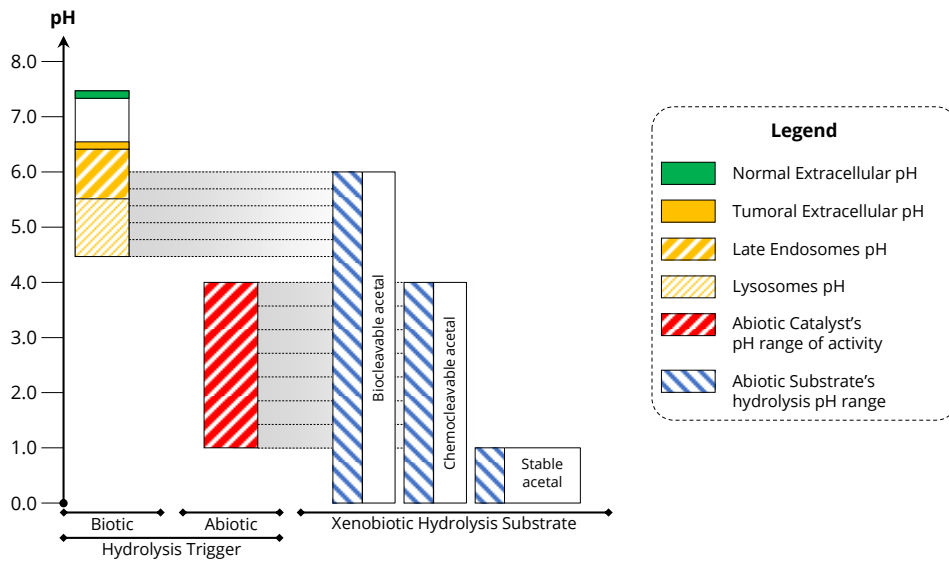
En ce qui concerne la réaction à effectuer, nous avons opté pour l'hydrolyse d'acétals cycliques. Cette réaction est catalysée par un acide, nécessite la présence d'eau et est une réaction de rupture de liaison qui peut trouver des applications dans les stratégies basées sur la libération d'une charge utile.

Les propriétés des acétals comprennent la clivabilité dans des conditions douces, la solubilité dans les solvants aqueux et une faible hydrophobicité. Les agents de liaison acétal ont été utilisés comme agents de liaison clivables pour des applications dans des domaines tels que le développement de médicaments, la protéomique, l'imagerie et le séquençage d'ADN<sup>20–22</sup>. Ainsi, les acétals ont toujours été conçus pour avoir un taux d'hydrolyse précis, soit pour s'hydrolyser sélectivement dans des organites cellulaires spécifiques (lysosomes et endosomes tardifs) à un pH voisin de 5 soit pour être stables et servir de lieurs non clivables. Dans ce travail, la relation structure-réactivité des lieurs acétal cycliques sera examinée afin d'identifier les substrats appropriés pouvant être clivés dans différentes gammes de pH. Notre objectif est de concevoir et de synthétiser des acétals qui appartiennent aux trois catégories suivantes :

- Acétals pouvant être clivés à un pH <4. Cette classe d'acétals peut être clivée dans une plage de pH qui correspond à celle du catalyseur acide approprié. Une telle combinaison d'acétal et de catalyseur constituerait un bon candidat pour un système de réaction xénobiotique qui n'interférerait pas avec les processus biologiques naturels.
- Acétals clivables entre pH = 4 et pH = 5. Ce type d'acétals peut être clivé dans la gamme de pH des lysosomes et des endosomes tardifs ; ainsi, ils seraient d'excellents candidats pour la libération de stratégies à l'intérieur de cellules.
- Acétals non clivables. Acétals qui pourraient être utilisés comme composant hydrosoluble stable dans des lieurs non clivables.

La figure suivante reprend nos objectifs à l'aide d'une échelle de pH. Les bandes représentées correspondent à i) les plages de pH naturel dans l'environnement cellulaire et extracellulaire (première bande), ii) l'activité de pH cible du catalyseur acide hétérogène approprié à la catalyse in vivo (bande rouge) et iii) les différentes plages de pH auxquelles l'hydrolyse des acétals abiotiques est déclenchée en fonction des applications souhaitées (bandes bleues).





**Figure 1.** Représentation des objectifs poursuivis. La première bande à gauche représente la plage de pH couverte par les cellules et l'environnement extracellulaire. La deuxième bande rouge représente la plage de pH couverte par le catalyseur acide abiotique. Les trois bandes bleues à droite représentent les plages de pH dans lesquelles l'hydrolyse de différents substrats abiotiques d'acétal est supposée être déclenchée. Des bandes horizontales estompées en gris sont utilisées pour montrer la correspondance entre les substrats abiotiques et les promoteurs d'hydrolyse correspondants.

La figure montre la plage de pH idéale dans laquelle un catalyseur adapté aux applications in vivo serait actif. Cette valeur correspond à la plage de pH dans laquelle le substrat d'acétal xénobiotique correspondant est hydrolysé. Les deux ne se chevauchent pas avec celui des compartiments acides de la cellule. D'autre part, l'acétal abiotique conçu pour être hydrolysé dans des conditions acides douces ( $\text{pH} > 4$ ) correspond aux plages de pH des lysosomes et des endosomes tardifs, tandis que le troisième type de substrat acétal est extrêmement stable à faible pH et n'a pas de valeur correspondante déclencheur pour son hydrolyse.

La nature chimique des acétals pouvant être clivés à  $\text{pH} < 4$  doit être étudiée en association avec celle de son catalyseur acide hétérogène abiotique correspondant. L'interaction entre le substrat acétal, le catalyseur et le milieu aqueux peut être liée à la nature hydrophobe ou hydrophile du catalyseur et de l'acétal, sans prendre en compte la liaison aux protéines plasmiques.

Quatre combinaisons possibles sont examinées :

A. Catalyseur acétal hydrophobe + hydrophobe : le catalyseur a un échange minimal avec le milieu aqueux. L'acétal a beaucoup plus d'affinité pour le catalyseur que pour le solvant, on

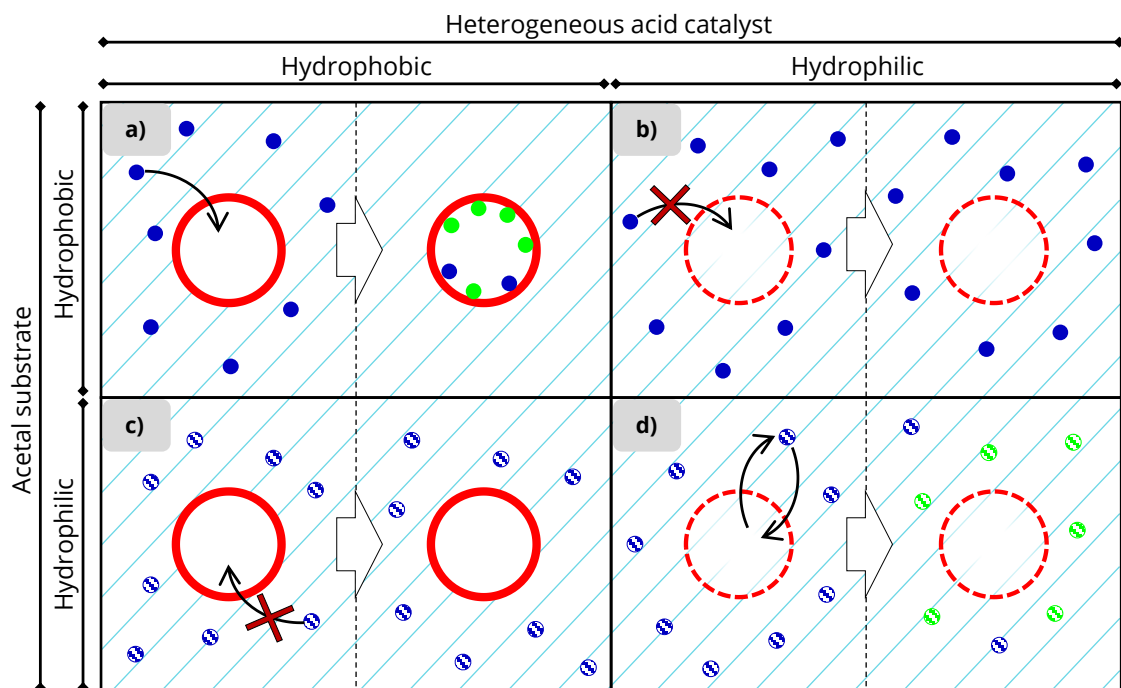
s'attend donc à ce qu'il s'adsorbe dans le catalyseur solide, où l'hydrolyse peut se produire grâce à son acidité.

B. Acétal hydrophile + catalyseur hydrophobe : l'acétal a une affinité pour l'environnement aqueux et présente donc beaucoup moins d'interaction avec le catalyseur. Ainsi, l'hydrolyse ne devrait pas avoir lieu.

C. Catalyseur acétal hydrophobe + hydrophile : dans ce cas également, l'absence d'affinité entre le substrat et le catalyseur entraînera probablement l'absence de clivage acétal.

D. Acétal hydrophile + catalyseur hydrophile : l'acétal, le catalyseur et le milieu aqueux peuvent s'échanger. Dans ce cas, le substrat peut être adsorbé par le catalyseur, hydrolysé en raison de son acidité interne, puis le produit peut être libéré grâce à l'affinité avec le solvant aqueux.

La figure 2 montre les quatre combinaisons décrites de substrat acétal et de catalyseur acide. Le catalyseur solide est représenté sous la forme d'une perle sphérique. Le contour de la sphère est simple pour le catalyseur hydrophobe (pour représenter l'absence d'interactions avec le solvant) et en pointillé pour celui hydrophile (pour représenter l'échange avec de l'eau). Le substrat est symbolisé par des points bleus, tandis que le produit de l'hydrolyse est représenté par des points verts. Les points sont lisses dans le cas de produits chimiques hydrophobes et rayés s'ils sont hydrophiles.



**Figure 2.** Représentation des quatre scénarios possibles donnés par la combinaison du substrat et du catalyseur solide. Le catalyseur hydrophobe est symbolisé par une sphère avec un contour plat, tandis que

que le symbole du catalyseur hydrophile a un contour en pointillé. Le substrat et le produit sont représentés respectivement par des points bleus et verts. Les points sont simples pour le substrat hydrophobe et rayés pour celui hydrophile. a) substrat hydrophobe + catalyseurs hydrophobes; b) substrat hydrophobe + catalyseurs hydrophiles; c) substrat hydrophile + catalyseur hydrophobe et d) substrat hydrophile + catalyseur hydrophile.

Les scénarios A et D dans lesquels le substrat et le catalyseur ont des caractéristiques correspondantes sont plus susceptibles de réaliser une hydrolyse par l'acétal. Les deux situations divergent dans l'interaction entre le substrat et le catalyseur. Nous avons émis l'hypothèse que dans le premier cas, l'interaction hydrophobe conduit à l'adsorption irréversible de l'acétal dans le catalyseur solide. L'absence de libération ni du substrat ni des produits peut sembler un inconvénient important. En réalité, dans l'optique de la mise en place d'une première preuve de concept *in vivo*, c'est exactement ce dont nous avons besoin. Afin de prouver que l'hydrolyse a été réalisée dans le système vivant, un catalyseur solide adsorbant permet de : (i) concentrer la sonde en un point, facilitant ainsi la détection de la fluorescence du produit; (ii) affirmer que l'hydrolyse n'a été réalisée que grâce au catalyseur. Dans le second cas, la nature hydrophile du substrat et du catalyseur permet au produit (= charge utile libérée) de rester en solution et d'interagir avec l'environnement biologique, mettant en œuvre sa ou ses fonctions. Étant donné le degré d'échange plus élevé entre le catalyseur et le solvant aqueux, il est encore plus difficile de trouver un catalyseur qui puisse maintenir son acidité dans le milieu tamponné que dans le cas précédent. En la matière, l'expertise des Drs Jean-Michel Becht et Lavinia Balan, chercheurs de l'Institut des matériaux de Mulhouse (IS2M, Institut de la science des matériaux, Université de Haute Alsace), partenaire de ce projet doctoral, est essentiel pour la formulation et la production de polymères solides spécialement conçus pour répondre à toutes nos exigences (biocompatibilité, hydrophilie et acidité).

La première question abordée au chapitre II concerne l'identification de l'acétal et la modification de sa structure chimique afin d'ajuster sa stabilité à l'hydrolyse. Une fois que les acétals hydrophobes et hydrophiles pouvant être clivés dans la plage de pH souhaitée, éloignée de la valeur biologique (pH <4), ont été reconnus, au chapitre III, l'attention sera concentrée sur l'identification des catalyseurs acides hydrophobes et hydrophiles correspondants actifs dans cette plage de pH. . Ensuite, les expériences *in vivo* seront définies en détail au chapitre IV et devraient prouver notre hypothèse.

Enfin, les applications possibles de ce système abiotique basé sur l'hydrolyse de l'acétal sont abordées. Comme mentionné ci-dessus, cette réaction de rupture de liaison pourrait être exploitée par des techniques de libération de charge utile, si la charge utile présente un motif diol dans sa structure chimique. Comme la plupart des xénobiotiques actuellement utilisés ne présentent pas de diol dans leur structure, nous avons postulé qu'il était possible de modifier la structure chimique complexe de molécules actives pour insérer une fonction de diol sans mettre en danger leur activité. Dans le chapitre V, nous étendons le champ d'application de l'insertion du diol à un ensemble de réactions de fonctionnalisation à un stade avancé d'agents anticancéreux dans le but de trouver des procédures modérées pouvant être appliquées à un large groupe de composés complexes afin d'améliorer leur activité et leurs performances.



## II – IDENTIFICATION AND MODULATION OF THE ACETAL SUBSTRATE

### 1. OBJECTIVES

In this chapter we aim to identify a small group of acetal substrates with tuneable reactivity towards hydrolysis.

#### 1.1 LIST OF TARGETED ACETAL SUBSTRATES ACCORDING TO THEIR STABILITY

The possible applications of cyclic acetals vary according to the range in which they can be cleaved and according to their hydrophobic or hydrophilic nature (Cf. Introduction, section 2, page 10):

- pH < 4 – hydrophobic: substrate for abiotic hydrolysis catalysed by hydrophobic heterogeneous acid catalyst.
- pH < 4 – hydrophilic: substrate for abiotic hydrolysis catalysed by hydrophilic heterogeneous acid catalyst.
- 4 < pH < 6: candidate for hydrolysis inside the cell acidic compartments (lysosomes and late endosomes)
- stable at pH < 1: exceptionally stable acetals which can find applications as the core of non-cleavable linkers for bioconjugation.

Our objective is to modulate the chemical structure of cyclic acetals to encounter the cases listed above. Additionally, we aim to mimic as much as possible the *in vitro* and *in vivo* conditions when performing experiments with the aforesaid substrates. We addressed this issue in the following section.

#### 1.2 FRET PROBES AS TOOLS TO MONITOR HYDROLYSIS AT “IN VIVO-LIKE” CONCENTRATION OF SUBSTRATES

As recently pointed out by Tamura and Hamachi,<sup>23</sup> the difficulties in passing from bench standard chemistry to *in vitro* and *in vivo* chemistry are many. One substantial restriction is related to the substrates' concentration: in classical bench procedures the concentration of the substrate is around 0.3 M while *in vitro* and more complex biological systems is of the order

of micro- and even nano-molar. Consequently, the monitoring of the reaction via the typical organic chemistry techniques is not possible, especially when in living systems.

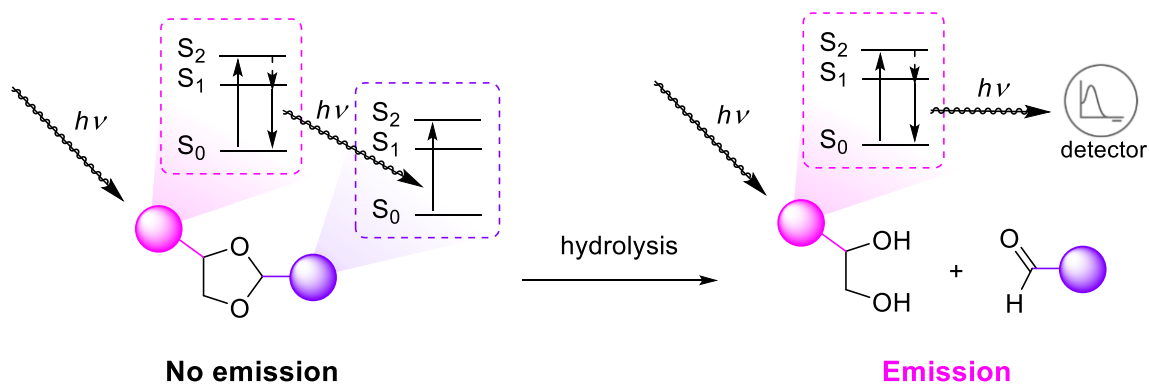
One way to circumvent the problem consists in the exploitation of fluorophores. These molecules emit photons if hit with the appropriate amount of energy to cause the excitation of electrons from the ground state to the excited singlet state.<sup>24</sup> The efficiency of the process is given by the fluorescence quantum yield. A fluorescence signal is highly detectable even when emitted from a very low concentrated solution of the fluorophore. For this reason, many strategies for the detection of low amounts of compounds have been based on fluorescence.<sup>25</sup> In some cases, the fluorescence of those molecules can be “activated” and “deactivated” by a change in their chemical structure (usually it involves several conjugated double bonds). In other cases, they can be combined with a molecule able to adsorb their emission, as in FRET probes.

FRET stands for Förster Resonance Energy Transfer, after the German physical chemist Theodor Förster for his understanding of the phenomenon in the 40s.<sup>26</sup> A FRET molecule is composed by a donor (the fluorophore) chemically linked and in close proximity to an acceptor. The acceptor can be a fluorescent molecule (“dual-dye FRET”) or a non-fluorescent molecule (“quencher FRET”). If subjected to an excitation light beam, the donor adsorbs the energy by promoting an electron from the ground state energy  $S_0$  to the excited vibrational state  $S_2$ . After vibrational relaxation ( $S_2 \rightarrow S_1$ ), the relaxation from  $S_1$  to  $S_0$  corresponds to the emission at a wavelength shorter than the excitation one. The emission is transferred to the acceptor which can undergo another fluorescence episode (in case of dual dye FRET) or not (in case of quencher FRET). In the first case there will be a fluorescence emission corresponding to the emission of the second fluorophore, while in the second case there will be no light emission.<sup>27-29</sup>

For an efficient energy transfer, donor/acceptor pairs require:<sup>30,31</sup>

- spectral overlap of the emission spectra of the donor and absorption spectra of the acceptor;
- high quantum yield of donor and high absorption coefficient of acceptor;
- very close distance (1-10 nm) between donor and acceptor: the transfer is extremely dependent on distance (6<sup>th</sup> order);
- matching orientations of the donor and acceptor dipole.

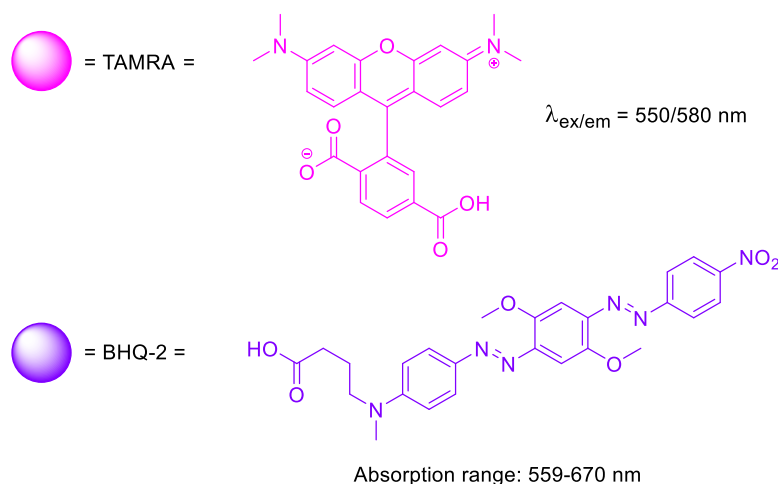
This principle can be successfully applied to monitor the acetal hydrolysis object of this work. As shown in **Figure 3** when hydrolysis of the acetal occurs, the fluorophore and the quencher are taken apart and the Energy Transfer is cancelled. Thus, the hydrolysis is directly related to the appearance of a fluorescence signal.



**Figure 3.** FRET principle applied on cyclic acetals. The acetal is the link between the donor (in fuchsia) and the acceptor (in violet). The excitation and relaxation are represented with Jablonski diagrams. When hydrolysis occurs, the donor and acceptor are no longer in close proximity and the energy transfer do not happen, allowing the detection of the donor fluorescence emission.

For this project, 6-Carboxytetramethylrhodamine (TAMRA) was chosen as fluorophore. Wavelength of excitation and emission are respectively 550 and 580 nm. Thus, Black Hole Quencher-type 2 (BHQ-2) was chosen as counterpart, with an absorption maximum of 583 nm (**Figure 4**).<sup>32</sup> The highly hydrophobic nature of BHQ-2 was also exploited to give to the acetal a sufficient degree of hydrophobicity to match that of the hydrophobic acid catalyst.





**Figure 4.** Chemical structure of the donor/acceptor pair chosen, TAMRA and BHQ-2.

In conclusion, FRET probes are particularly suitable for this project because they will allow to:

- quantify the hydrolysis by measuring the fluorescence emitted by TAMRA with the aid of a spectrofluorometer. This instrument can analyse very low concentrated samples, so allowing us to work with substrate's concentration in the order of  $\mu\text{M}$ ;
- make a quick qualitative evaluation of the hydrolysis reaction by looking at the reaction vials under a UV lamp given that the hydrolysis is directly related with the appearance of fluorescence. This advantage will come to hand when the fluorescence cannot be quantified, like in case the substrate is adsorbed by the solid catalyst;
- give the acetal a hydrophobic nature, thanks to the use of BHQ as quencher.

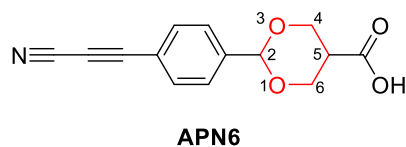
Next sections are dedicated to the identification of the above-mentioned cyclic acetals: **i)** hydrophobic and hydrophilic acetals cleavable at  $\text{pH} < 4$  (sections 2 and 3), such acetals will be used as substrates for the abiotic hydrolysis catalysed by heterogenous catalyst (Cf. Chapter 3); **ii)** acetals cleavable at  $\text{pH} > 4$  (section 4), eligible for applications as cleavable linkers in bioconjugation, will be also tested for hydrolysis *in vitro*; **iii)** acetals stable at very low pH (section 5), eligible as hydrophilic non-cleavable linkers for bioconjugation, will also be investigated for structure-reactivity relationship.

## 2. IDENTIFICATION OF HYDROPHOBIC ACETAL CLEAVABLE AT PH < 4

### 2.1 IDENTIFICATION OF ACETAL **APN6** AS CANDIDATE FOR HYDROLYSIS AT PH < 4

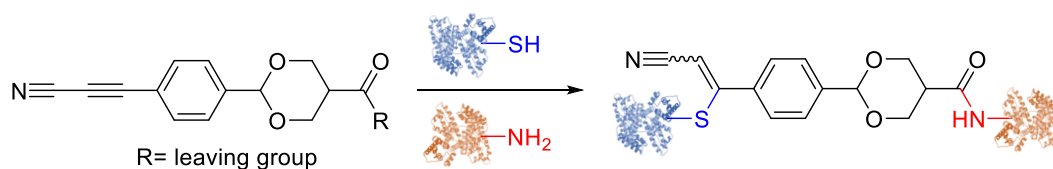
As mentioned above, the cyclic acetal is the chemical function identified as substrate for the hydrolysis. This bond breaking reaction can be exploited in biochemical applications in which a payload chemically linked to a carrier is meant to be released. The chemical structure of the acetal-containing linker has to permit the linkage between the payload and the carrier. A major class of linkers for bioconjugation are amine-to-thiol cross linkers in which two functions are designed to orthogonally react with amine and thiol functions present in the payload and carrier (often they are lysine and cysteine residues).<sup>33</sup>

Our research group investigated over the years the preparation of new amine-to-thiol linkers, especially conceived for ADC (Antibody-Drug Conjugates), with a focus on the use of arylpropionitrile moieties for the selective linkage of cysteine residues.<sup>34</sup> One of the linkers (named **APN6**, never published) contained also a 6-membered ring cyclic acetal, as shown in **Figure 5**. The code name **APN6** is conceived as follow: “**APN**” stands for “arylpropionitrile”, “**6**” is referred to the size of the acetal ring.



**Figure 5.** Chemical structure of amino-to-thiol acetal linker model **APN6**.

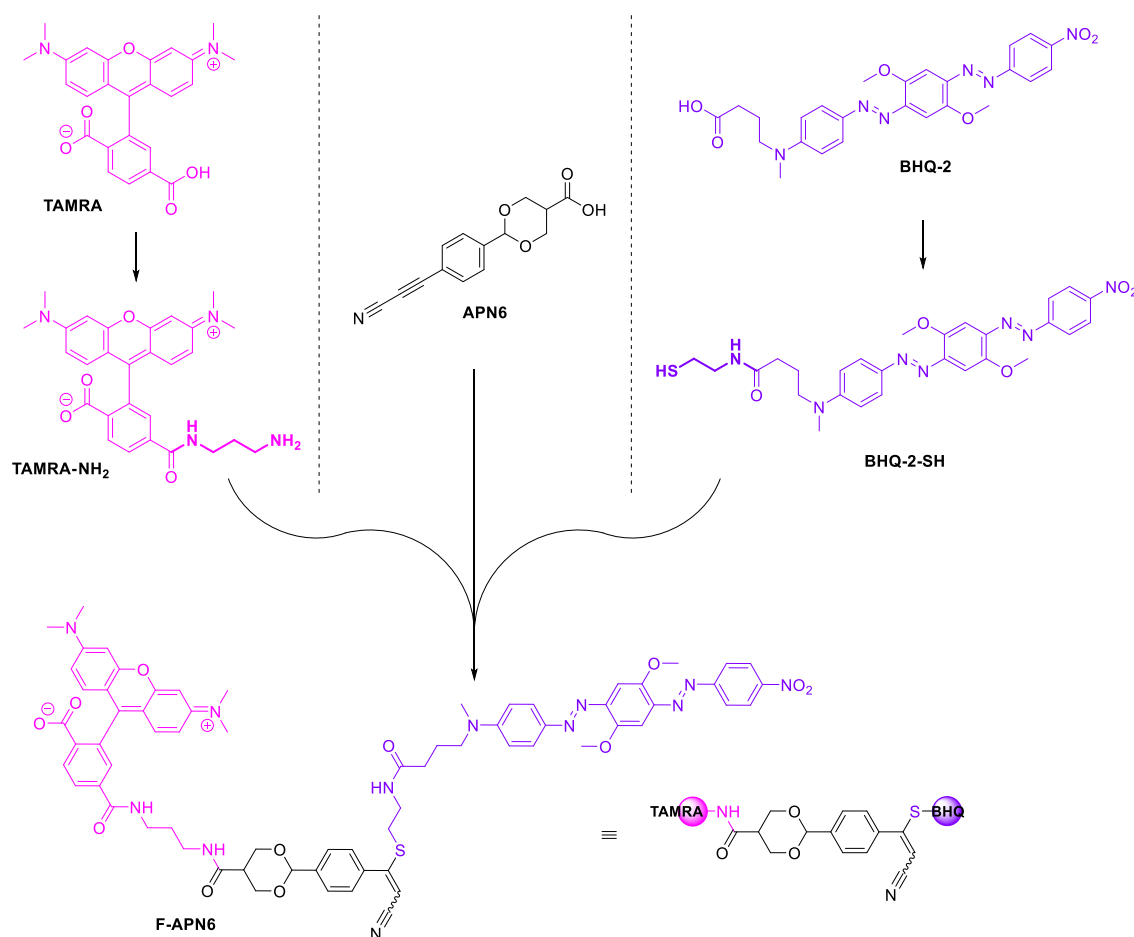
**APN6** is composed by a central 6-membered ring substituted acetal. Substitutions in position 2 and 5 of the acetal are the moieties for the linkage to, respectively, the thiol and the amino functions. The chemical linkage to amino and thiol groups is shown in **Figure 6**.



**Figure 6.** Conjugation to natural amines and thiols of activated linker **APN6**.

### 2.1.1 FRET probe of APN6

As mentioned above, FRET probe will be used to address the stability of the acetals towards hydrolysis. In this case, the FRET probe of **APN6**, named **F-APN6**, was already synthesized and ready to be tested. As previously stated, TAMRA and BHQ-2 were used as fluorophore and quencher respectively. Their chemical structure, however, doesn't present any grip for the bonding to the **APN6** linker. Hence, both TAMRA and BHQ-2 has been modified to allow the conjugation to the acetal linker. A primary amine function was added to TAMRA exploiting the carboxylic acid not involved in the fluorescence emission. BHQ-2 was equipped with a thiol function exploiting -also here- the carboxylic acid, which is not involved in its quenching properties. The following figure summarize the synthesis of **F-APN6**, performed in our laboratory by Dr. Igor Dovgan.

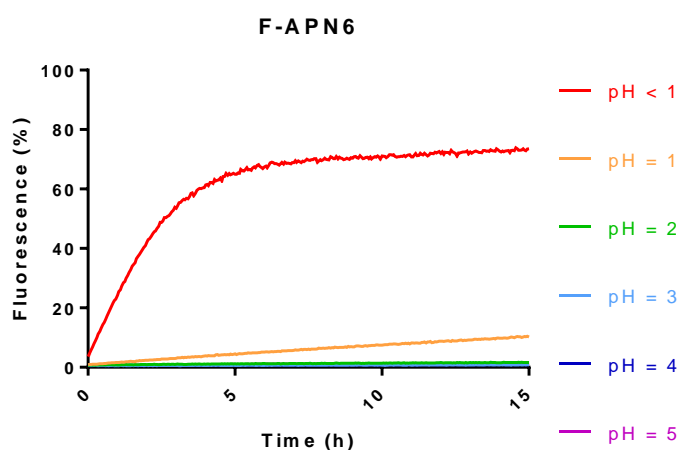


**Figure 7.** Modification of TAMRA and BHQ-2 and conjugation to **APN6** to obtain the corresponding FRET probe **F-APN6**.

### 2.2.2 Profile of APN6 stability towards hydrolysis at different pH

The FRET probe **F-APN6** was tested for stability in different acidic conditions. Aqueous solutions at different pH were prepared, as well as 40 $\mu$ M solutions in DMSO of **i)** the FRET probe **F-APN6**, **ii)** **TAMRA-NH<sub>2</sub>** and **BHQ-2-SH**, as comparison. Note that from now on in the text **TAMRA-NH<sub>2</sub>** and **BHQ-2-SH** will be mentioned just as TAMRA and BHQ, unless otherwise specified.

The 40 $\mu$ M solution were diluted in the appropriate acidic solution to a final concentration of 1 $\mu$ M, three aliquots of each solution were placed in a 96-well plate and analysed with a spectrofluorometer. The fluorescence was monitored for 15 hours at 23°C (temperature of the room); measurements were taken every 3 minutes. Since the fluorescence of TAMRA is dependent on the pH, each value of fluorescence measured for the FRET probes was normalized to the corresponding value measured for the solution of TAMRA and BHQ in the same buffer. Results are shown in **Figure 8**.

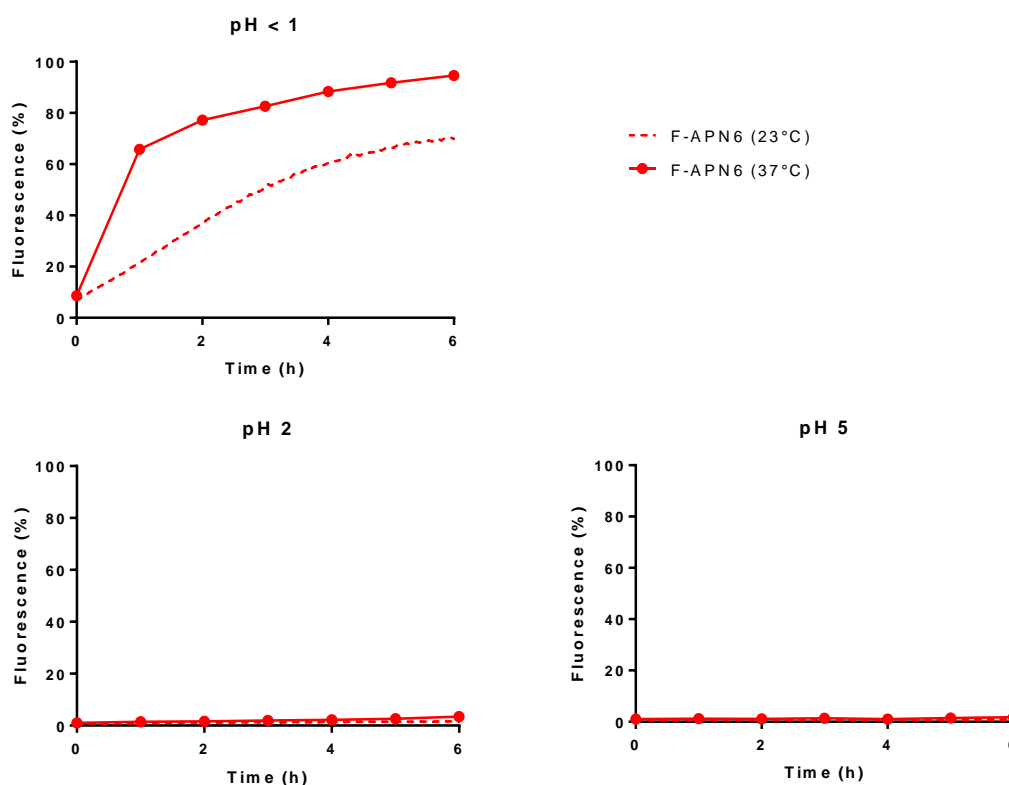


**Figure 8.** Hydrolysis profiles of acetal **F-APN6** in different concentration of proton at 23°C.

Acetal **APN6** shows a good degree hydrolysis only at pH < 1 (1M HCl aq. solution), while at pH = 1 (0.1 M HCl aq. solution) only 10% of hydrolysis is reached after 15 hours at 23°C. It is remarkably stable in all the other tested conditions.

Unfortunately, with the provided spectrophotometer it was not possible to set the temperature of the 96-well plate. Therefore, the hydrolysis was profiled manually at 37 °C also. The 1  $\mu$ M solutions were agitated at a constant temperature of 37 °C, aliquots were taken and analysed every hour for 6 hours. **Figure 16** shows a comparison between hydrolysis of **F-APN6**

at 23°C and 37 °C. As expected, at pH < 1, the hydrolysis was faster thanks to the increased temperature, while at pH = 2 -as well as at pH = 5- the hydrolysis did not occur, confirming the extraordinary stability of this acetal at high proton concentration.



**Figure 9.** Hydrolysis profiles of acetal **F-APN6** in three different acidic solutions; comparison between 23°C and 37 °C.

Despite the remarkable stability of acetal **APN6** at physiological pH, this acetal might be not enough reactive in the pH range activity which is envisaged for the abiotic solid acid catalyst (cf. **Figure 1**, page 11). For this reason, the chemical structure of **APN6** was further improved to reach a higher degree of reactivity towards hydrolysis (at least at pH > 2), while maintaining stability at physiological pH.

## 2.2 IDENTIFICATION OF **APNM5** AS SECOND CANDIDATE FOR HYDROLYSIS AT $\text{pH} < 4$

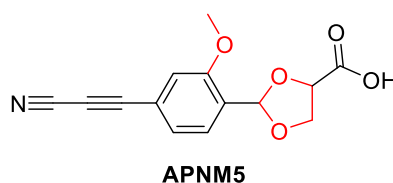
### 2.2.1 Design of **APNM5** to reach hydrolysis at $\text{pH} < 4$ and $\text{pH} > 2$

In 2016, our group described the influence of slight structural modifications on pH-sensitive linkers<sup>35</sup>. According to this work, 5-membered cyclic acetals are more prone to hydrolysis than 6-membered cyclic acetals. Also, modification to the aryl substituent can improve the hydrolysis rate: the work of Jacques *et al.* suggests that a methoxy in *para* and/or *ortho* position accelerates the hydrolysis, with a bigger effect exerted by the substitution in *para* than in *ortho*. In this case the *para* position was already occupied by the propiolonitrile moiety, only *ortho* positions were available. Conveniently, it seems that the substitution in *ortho* position brings about a better hydrolysis selectivity: at physiological pH ( $\text{pH} = 7.4$ ) the hydrolysis is much slower with the methoxy in *ortho* than in *para*. This makes the addition of the methoxy substituent an important added value to meet the target's criteria.

Thus, the central acetal core of compound **APN6** was modified as follow (**Figure 10**):

- the acetal ring was shrunk by one carbon atom to a 5-membered ring;
- a methoxy was added to the phenyl in *ortho* position with respect to the acetal.

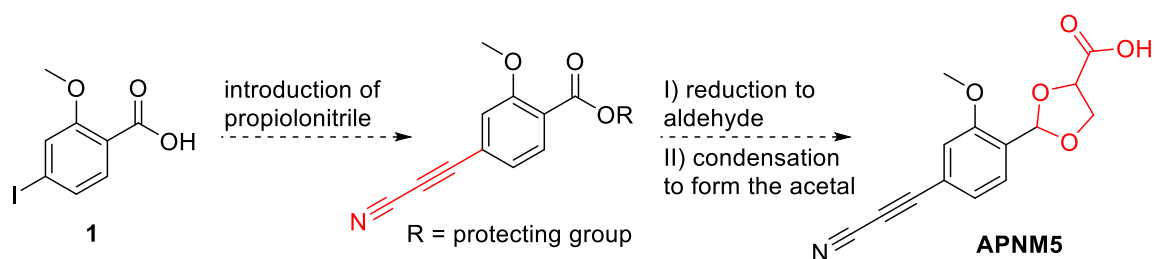
The new cyclic acetal was named **APNM5**, where **M** indicates the presence of a methoxy, while **APN** and **5** are referred respectively to the arylpropiolonitrile function and the size of the ring, as it was for **APN6**. Next section describes in detail the synthetic plan for its synthesis.



**Figure 10.** New amino-to-thiol linker model **APNM5**, designed to be more prone to hydrolysis than its parent **APN6**. “**APN**” stands for “arylpropiolonitrile”, “**M**” indicates the presence of a methoxy substituent and “**5**” accounts for the size of the acetal ring.

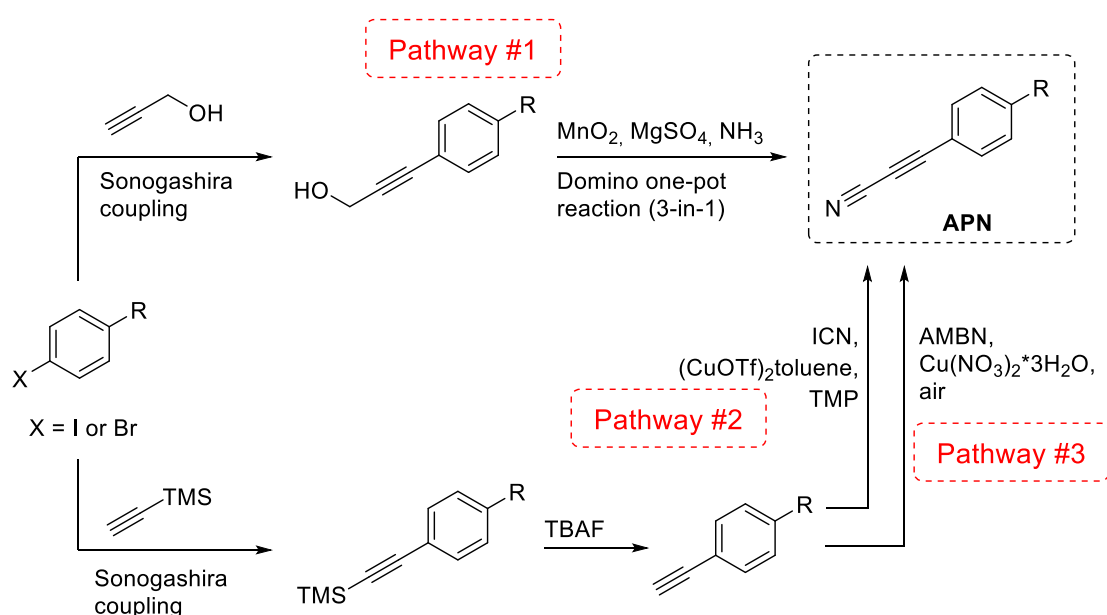
### 2.2.2 Synthesis of acetal **APNM5**

A short synthetic strategy for the synthesis of compound **APNM6** is illustrated in **Figure 11**. Starting from benzoic acid **1**, the iodine atom is exploited to insert the propiolonitrile moiety, while the acid is -in a first moment- protected and then reduced to aldehyde. The obtained aldehyde is then condensed with the suited vicinal diol (1,2 diol).



**Figure 11.** First outline of the synthetic pathway for compound **APNM5**.

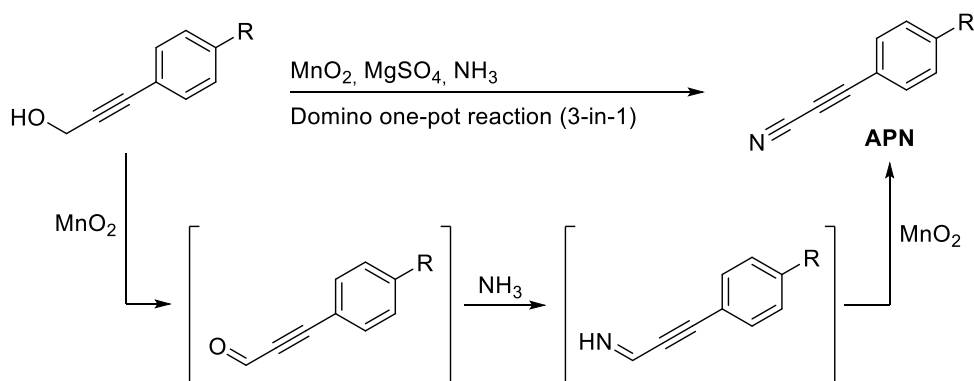
As reported in literature, the arylpropiolonitrile motif can be synthesized starting from an aryl iodide or bromide in three ways, resumed in **Scheme 1**.



**Scheme 1.** Generic scheme of the three possible synthetic pathways for the preparation of arylpropiolonitrile compounds.

The first pathway consists of two steps:<sup>36</sup>

- I. a Sonogashira coupling between the aryl halide and propargylic alcohol yielding the aryl propargylic alcohol;
- II. a domino one-pot reaction involving three subsequent transformations (**Scheme 2**):
  - i. oxidation of the primary  $\alpha,\beta$ -unsaturated alcohol to aldehyde by manganese oxide;
  - ii. formation of the imine by condensation between the aldehyde and ammonia;
  - iii. final oxidation of imine to nitrile operated by manganese oxide.



**Scheme 2.** Formation of arylpropionitrile from aryl propargylic alcohol in a one-pot domino reaction involving three transformations. Manganese oxide is used for the two oxidations, ammonia is used for the imine formation and magnesium sulphate is used as drying agent.

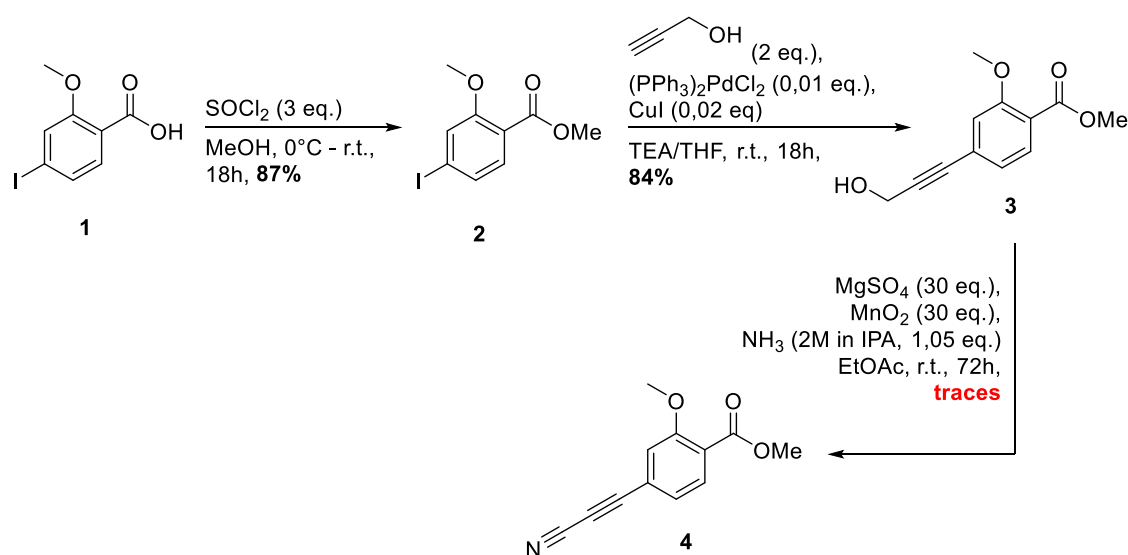
The second pathway consists of three steps:<sup>37</sup>

- I. a Sonogashira coupling between the halo-benzene and ethynyltrimethylsilane;
- II. the deprotection of the alkyne thanks in presence of fluoride anions (TBAF), yielding the substituted ethynylbenzene;
- III. copper-catalysed reaction of ethynylbenzene with cyanogen iodide (ICN) to obtain the arylpropionitrile. Tetramethylpiperidine (TMP) is used as a sterically hindered base. According to Okamoto *et al.*<sup>37</sup> the reaction involves the noncatalyzed formation of alkynyl iodides followed by copper-catalysed cyanation of the iodide.

Over the years, many similar strategies for the cyanation of terminal alkyne have been investigated. They involve the use of a metal cyanide (MCN, M = Cu, K, Na) as cyanation agent in combination with a copper catalyst.<sup>38</sup> These approaches, as well as the one involved in the above-described pathway #2, require the use of highly toxic cyanation agents. For this reason, Rong and co-workers recently described a copper-catalysed direct cyanation of the terminal alkyne with the non-toxic azobisisoamylonitrile (AMBN) as cyanation agent in presence of copper catalyst and oxygen.<sup>39</sup>

Hence, pathway #3 is preferred over pathway #2, however pathway #1 was first tried -given its apparent simplicity- starting from commercially available 4-iodo-2-methoxybenzoic acid **1** (**Scheme 3**).

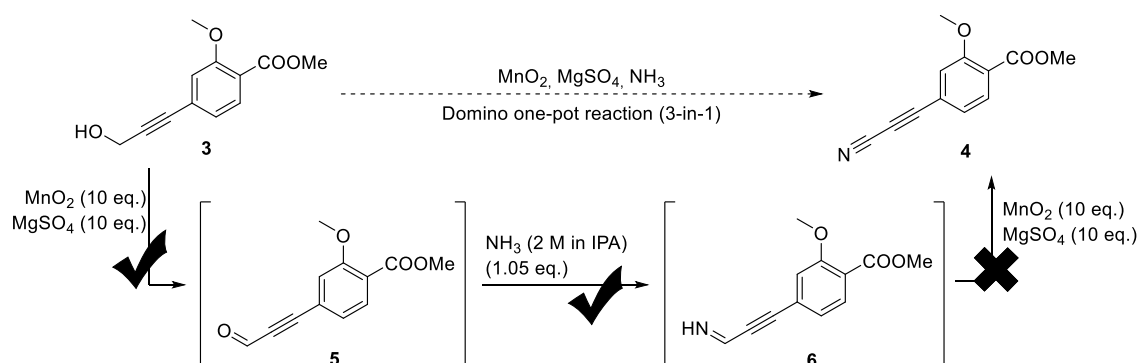




**Scheme 3.** First attempt of APN synthesis: **i**) esterification on the benzoic acid, followed by **ii**) a Sonogashira coupling to give compound **3** (isolated); **iii**) domino one-pot reaction to obtain the intermediate **4** (not successful).

The carboxylic acid is protected by esterification with methanol with a good 87% yield. Then the Sonogashira coupling with propargylic alcohol proceeded smoothly affording the desired compound **3** with 84% yield.

The last step for the formation of the arylpropionitrile -the domino one-pot reaction- revealed to be very tricky. After two unsuccessful attempts, in which only traces of the arylpropionitrile **4** were obtained within 72 hours, the one-pot reaction was carried out stepwise. Instead of mixing all the reagents together, they were added progressively, after the complete conversion of the intermediary products was confirmed by LC/MS and/or TLC (**Scheme 4**).

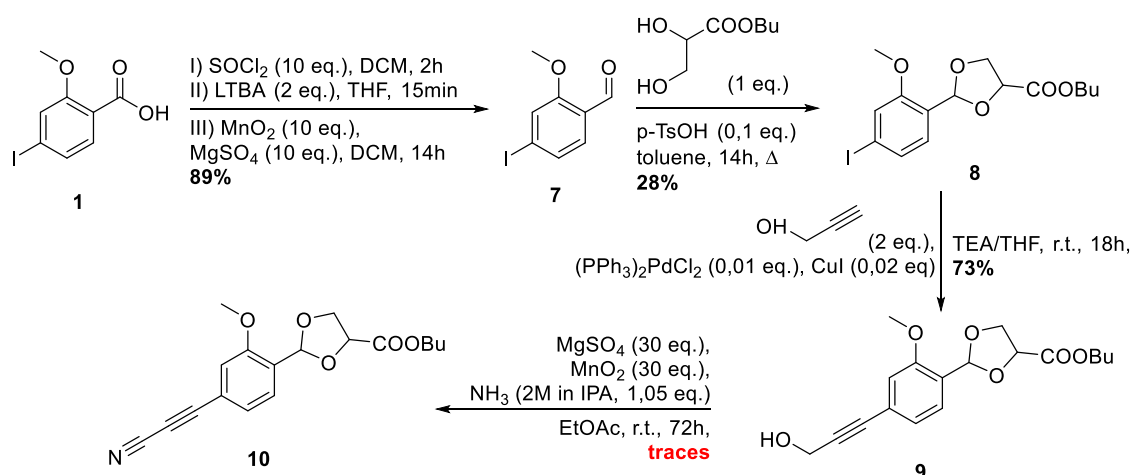


**Scheme 4.** Step-by-step formation of arylpropionitrile **4**. The reaction proceeds well till the formation of the imine, while the last oxidation does not occur.

Since the aim was to reveal which one of the three subsequent transformation was responsible for the failure of the reaction, it was not necessary to try to isolate the intermediates. We thus analysed crude reactions to reveal the formation of the desired intermediate. The three steps were analysed as follow:

- I. Oxidation of primary alcohol **3** to aldehyde **5**. Reagents: propargylic alcohol **3** (1 eq.), manganese oxide (MnO<sub>2</sub>, 10 eq.), magnesium sulphate (MgSO<sub>4</sub>, 10 eq.). The oxidation was followed by LC-MS and TLC, after 30 minutes the reaction was complete.
- II. Imine **6** formation. Reagents added to the mixture: NH<sub>3</sub> (saturated solution in isopropylalcohol, 2 M, freshly prepared by bubbling NH<sub>3</sub> into IPA). The imine formation and the disappearance of the starting aldehyde were monitored with TLC (ninhydrin staining). TLC revealed complete imine formation within 30 minutes after the addition of ammonia.
- III. Oxidation of imine **6** to nitrile **4**. Reagents added to the mixture: manganese oxide (MnO<sub>2</sub>, 10 eq.), magnesium sulphate (MgSO<sub>4</sub>, 10 eq.). Formation of the product was not observed, even after a few days.

The final oxidation is the problematic step in the one-pot reaction. Another attempt was done by changing the substrate for the formation of the propiolonitrile motif, trying to address the ineffectiveness of the imine oxidation by modifying the chemical structure of the starting material. The two steps of the synthetic strategy (Cf. **Figure 11**, page 36) were inverted: first the cyclic acetal was formed and then the propiolonitrile. In other words, in the first strategy the substrate for the APN synthesis was iodobenzene with an electron withdrawing substituent in *para* (the methyl ester), while in this second attempt, the electron withdrawing effect is weakened by the presence of an acetal in *para* position. The new synthetic pathway is shown in **Scheme 5**.



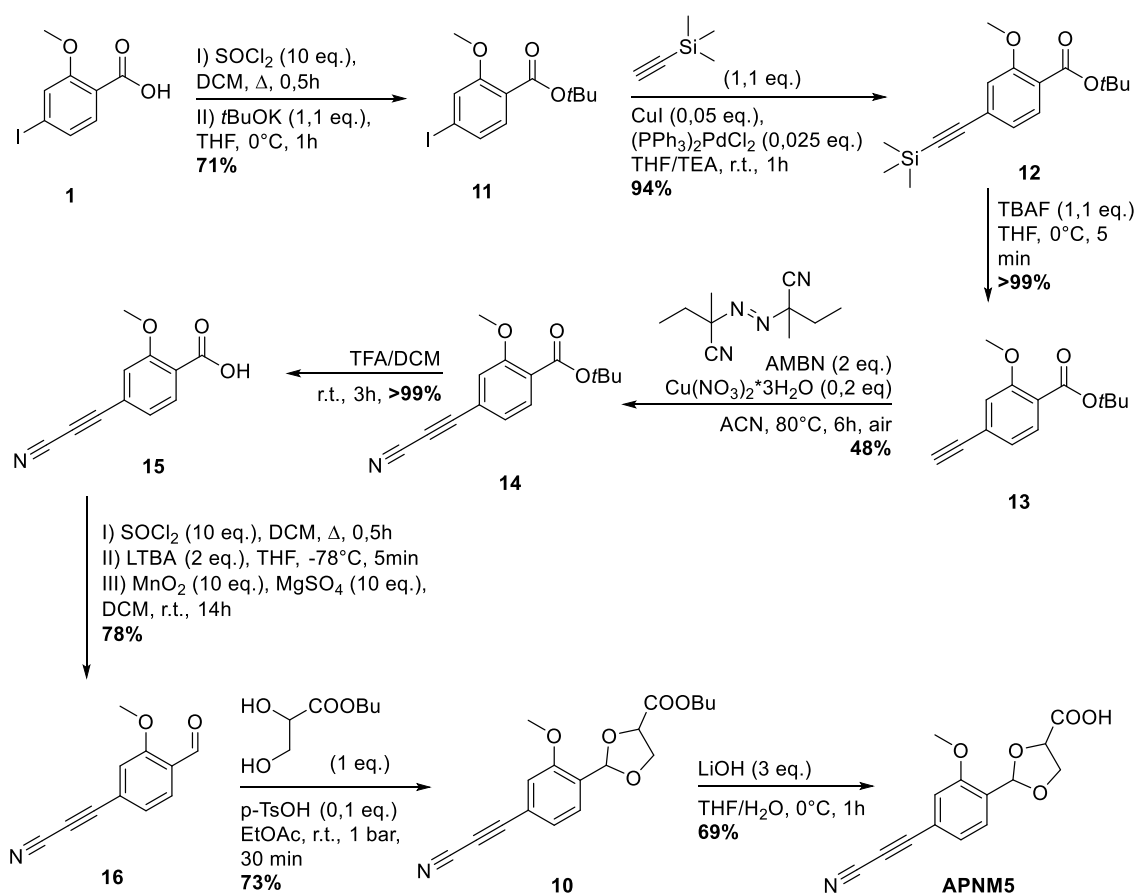
**Scheme 5.** Second strategy for the synthesis of **APNM5**.

Carboxylic acid **1** was reduced to primary alcohol and re-oxidized to aldehyde **7** with very good 89% yield (over three steps). Purification of the intermediary products was not required. The following step is the condensation between the aldehyde and the diol (butyl 2,3-dihydroxy propanoate) carried out under classical acidic conditions with *p*-toluenesulfonic acid in toluene (28% yield). Water is removed as azeotrope of toluene thanks to a Dean-Stark apparatus.

Once the acetal had been obtained, the Sonogashira coupling between the iodobenzene **8** and propargylic alcohol could be performed, yielding compound **9** in 73% yield. The one-pot domino reaction for the oxidation of the alcohol to nitrile was carried out. Unfortunately, also in this case, no product was detected, even after three days.

At this point it was decided to change strategies and try the third pathway (Cf. **Scheme 1**, page 36) which consist in the cyanation of a terminal alkyne with AMBN. According to Rong *et al.* substrates bearing electron-withdrawing groups on the benzene rings tend to achieve the reaction in much higher yields than those with electron-donating substituent.<sup>39</sup> Thus, the starting material for the new strategy was the 4-iodo-2-methoxybenzoic acid **1**.

**Scheme 6** shows the complete successful synthesis of **APNM5**.



**Scheme 6.** Complete synthesis of target compound **APNM5**.

First step is the protection of the carboxylic acid motif by esterification in two steps. 4-iodo-2-methoxybenzoic acid **1** was transformed into its reactive derivative 4-iodo-2-methoxybenzoyl chloride. The following nucleophilic substitution with potassium *tert*-butoxide gave the corresponding *tert*-butoxy ester in 71% yield (over the two steps).

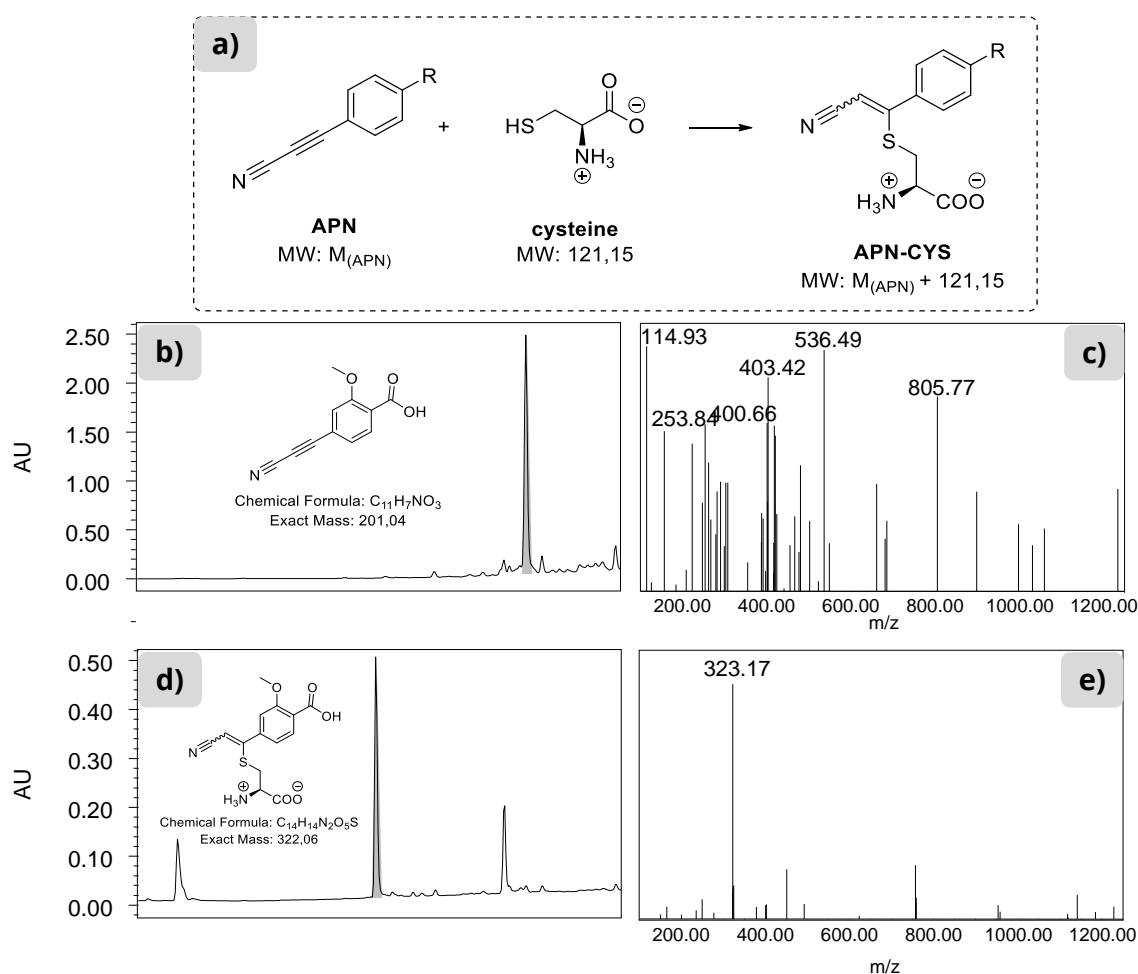
The Sonogashira coupling with protected ethynyl (ethynyltrimethylsilane) was carried out in classical conditions in presence of a strong base (triethylamine, TEA) and catalytic amount of copper iodide and palladium (II) complex. Compound **12** was isolated in excellent 94% yield. Then, the trimethyl silane protection was removed with tetrabutylammonium fluoride to yield the terminal alkyne **13** quantitatively.

Cyanation of the terminal alkyne was achieved with a moderate 48% yield applying the procedure of Rong *et al.*:<sup>39</sup> to the solution of the substrate in acetonitrile AMBN and copper nitrate were added, the reaction mixture was stirred at 80°C for 6h. The presence of oxygen - required for the reaction- was ensured by performing the reaction in normal atmosphere.



The last step is the hydrolysis of the ester with sodium hydroxide. It required special attentions since the propionitrile motif is sensible to nucleophilic attack by the hydroxyl anion. Temperature must be kept at 0°C and the solution must be neutralized as soon as the reaction is complete. Final compound **APNM5** was isolated in 69% yield after preparative HPLC purification.

About the arylpropionitrile compounds, it is noteworthy that their detection by LC-MS is quite difficult. They absorb quite well at 254 nm but they are not detected by the mass analyser, *i.e.* they are not -or weakly- ionizable by electrospray ionization (ESI), at least by the one currently in use in our laboratory (cf. Experimental procedures, section 1.2, page 162). Thus, in each reaction involving an APN compound, to be sure that the product was formed and that the APN function was still intact, a little sample treatment was necessary before running the LC-MS analysis. Being the arylpropionitrile motif conceived to react with thiols, cysteine was added to the sample for the LC-MS and the conjugation was allowed to occur before the analysis. The new derivative product is very well ionizable and its presence confirms the presence of the APN motif. An example of such analysis is shown in **Figure 13**.

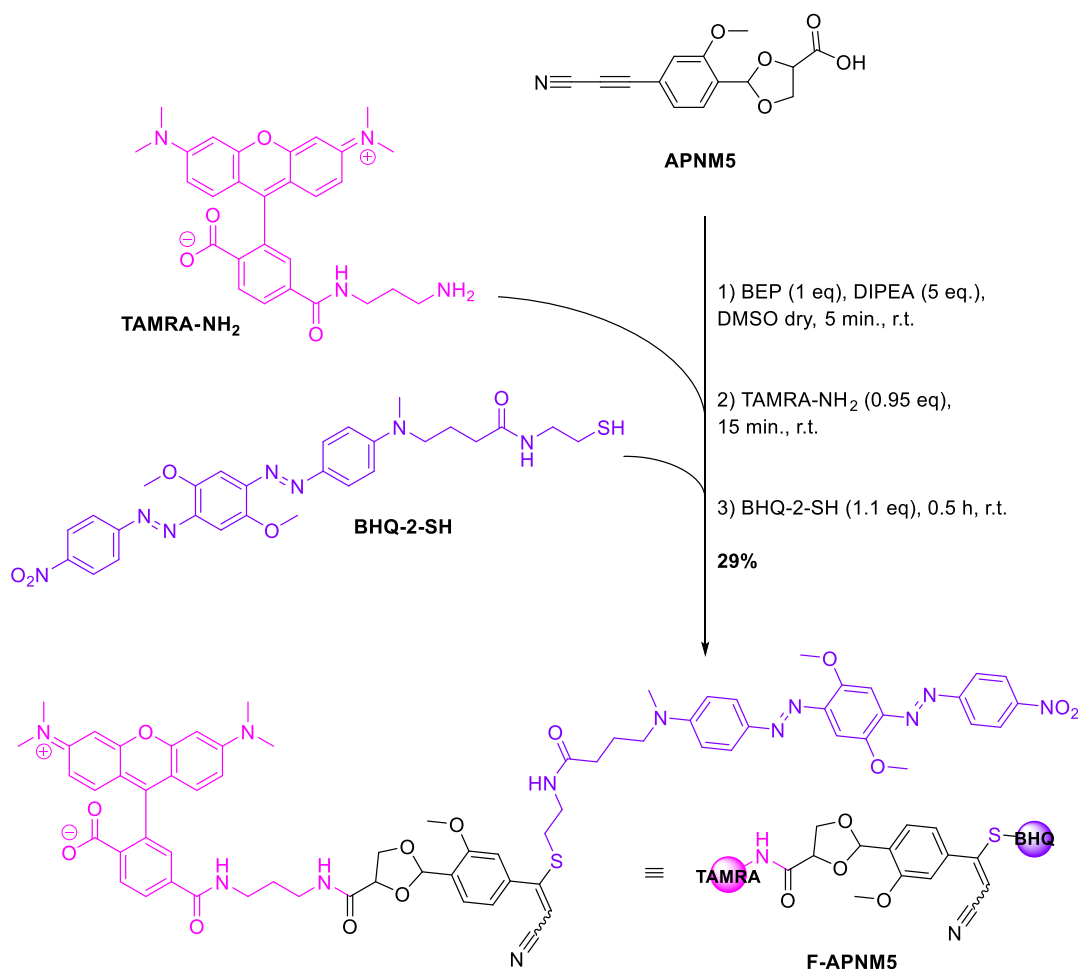


**Figure 13.** a) Generic reaction between cysteine and arylpropionitriles, the change in molecular mass is indicated. b) LC chromatogram of a sample of **APNM5** with c) the MS extract of the main peak. d) LC chromatogram of a sample of **APNM5** treated with cysteine and e) the MS extract of the corresponding peak with the expected m/z value well visible.

Once the new amine-to-thiol acetal linker **APNM5** was obtained, the corresponding FRET probe was synthesized.

### 2.2.3 Synthesis and purification of FRET probe of acetal APNM5

For the synthesis of the acetal FRET probe, the carboxylic acid and the arylpropionitrile functions were exploited to link TAMRA and BHQ respectively. **TAMRA-NH<sub>2</sub>** and **BHQ-2-SH** were used in a one-pot sequential coupling, as shown in **Scheme 7**.

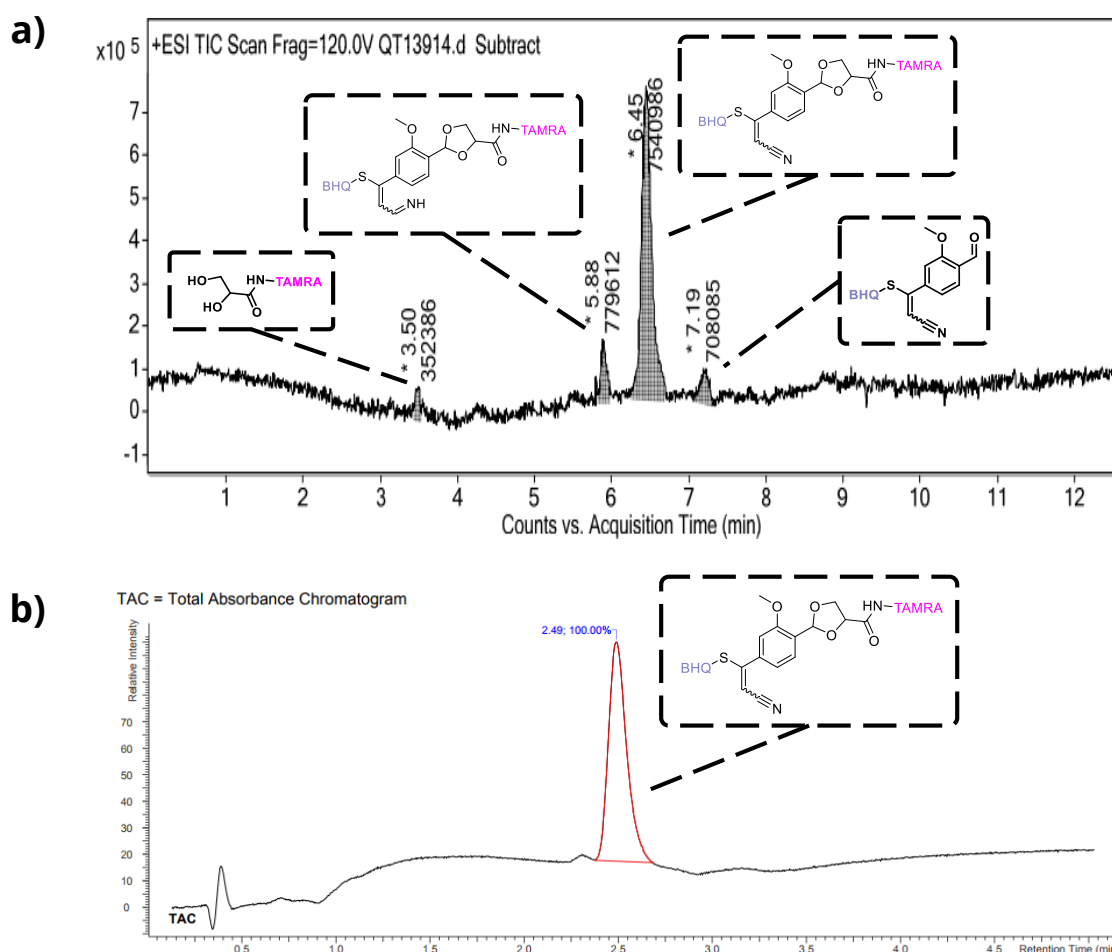


**Scheme 7.** Synthesis of the FRET probe **F-APNM5** of acetal amino-to-thiol linker **APNM5**.

2-Bromo-1-ethyl-pyridinium tetrafluoroborate (BEP) was used to activate *in situ* the carboxylic acid (step 1) and to allow the following insertion of **TAMRA-NH<sub>2</sub>** through nucleophilic acyl substitution (step 2).<sup>40</sup> The final step is the thiol conjugation to APN, for which only the presence of **BHQ-2-SH** is necessary. The yield of 29% over the three steps is calculated after the purification with preparative HPLC.

Attention must be paid during purification. Indeed, a first attempt of purification with preparative HPLC was done with a usual mobile aqueous phase with 0,05% content of trifluoroacetic acid (TFA). The acidity of the mobile phase causes a partial hydrolysis of the acetal during the run, resulting in a sample of FRET already hydrolysed at 10%. Changing the mobile phase to a neutral aqueous solution with 0,025% of ammonium formate (HCOONH<sub>4</sub>) allowed to overcome this problem, even if longer time was needed to get rid of the ammonium formate salt in the final sample. **Figure 14** shows the chromatograms of the two obtained samples.



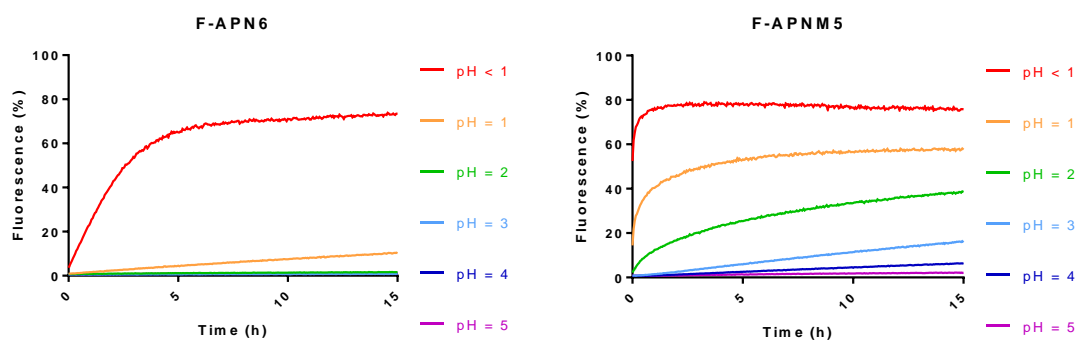


**Figure 14.** Chromatograms of the preparative HPLC outcome when using **a)** an acidic mobile phase and **b)** a neutral mobile phase. All the chemical species are detected by HR/MS and shown in the figure.

#### 2.2.4 Profile of F-APNM5 stability towards hydrolysis at different pH

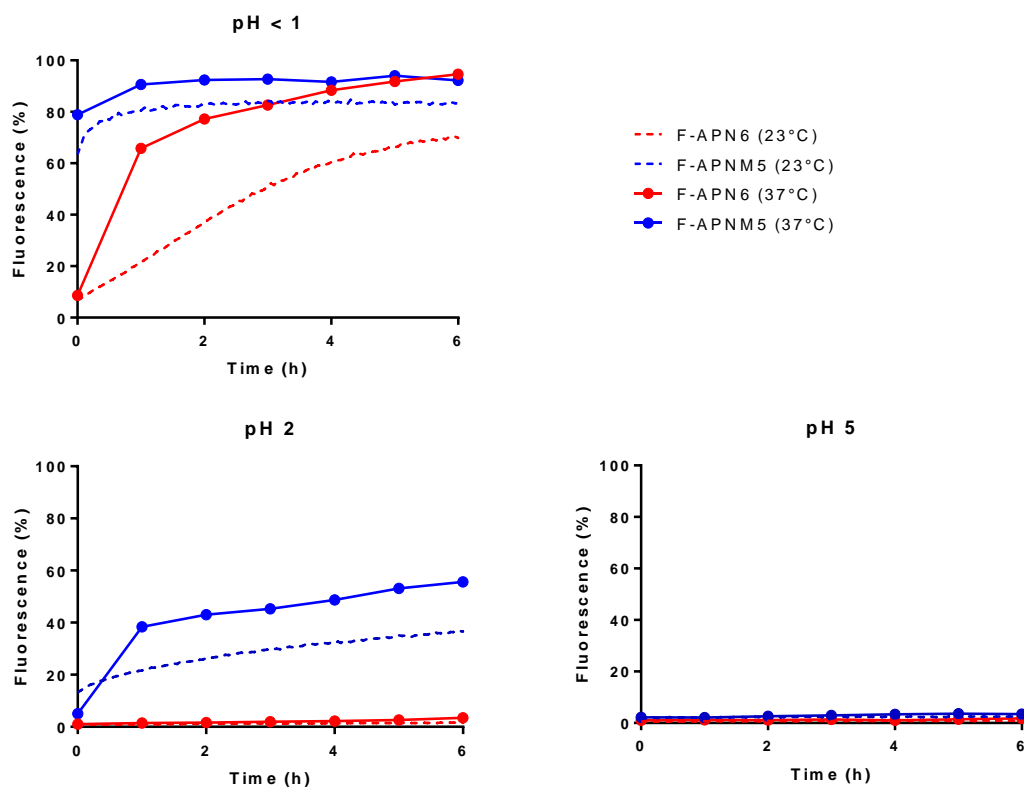
The FRET probe **F-APNM5** was tested for stability in different acidic conditions. Solutions at different pH were prepared, as well as 40 $\mu$ M solutions in DMSO of: **i)** the FRET probe **F-APNM5** and **ii)** **TAMRA-NH<sub>2</sub>** and **BHQ-2-SH**, as comparison.

The 40 $\mu$ M solution were diluted in the appropriate acidic solution to a final concentration of 1 $\mu$ M, three aliquots of each solution were placed in a 96-well plate and analysed with a spectrofluorometer. The fluorescence was monitored for 15 hours at 23°C (temperature of the room); measurements were taken every 3 minutes. Since the fluorescence of TAMRA is dependent on the pH, each value of fluorescence measured for the FRET probes was normalized to the corresponding value measured for the solution of TAMRA and BHQ in the same buffer. Hydrolysis profile of **F-APNM5** is shown in **Figure 15** and is compared to the one of **F-APN6** previously obtained.



**Figure 15.** Hydrolysis profiles of acetals **F-APN6** and **F-APNM5** in different concentration of proton at 23°C.

As predicted, the acetal **APNM5** is more prone to hydrolysis, while maintaining its stability at  $\text{pH} \geq 4$ . As previously done with **F-APN6**, also in this case the FRET probes was analysed manually at 37 °C. The 1  $\mu\text{M}$  solutions were agitated at a constant temperature of 37 °C, aliquots were taken and analysed every hour for 6 hours. **Figure 16** shows a comparison between hydrolysis of **F-APN6** and **F-APNM5** at 23°C and 37 °C. As expected, acetal **APNM5** is faster hydrolysed at higher temperature in acidic media but remains very stable at  $\text{pH} = 5$ . The results obtained confirmed that acetal **F-APNM5** was a much better candidate as abiotic substrate for the hydrolysis catalysed by a heterogeneous acidic catalyst. It is stable at physiological pH and is cleavable in the expected range of pH anticipated for the active solid catalyst.



**Figure 16.** Hydrolysis profiles of acetals **F-APN6** and **F-APNM5** in three different acidic solution; comparison between 23°C and 37 °C.

Having found a promising cyclic acetal cleavable at pH < 4 with a hydrophobic nature, **F-APNM5**'s chemical structure was modified to increase its hydrophilicity, in order make it compatible with hydrophilic heterogeneous catalysts for the abiotic acid-catalysed hydrolysis (cf. Introduction, **Figure 1**, page 11).

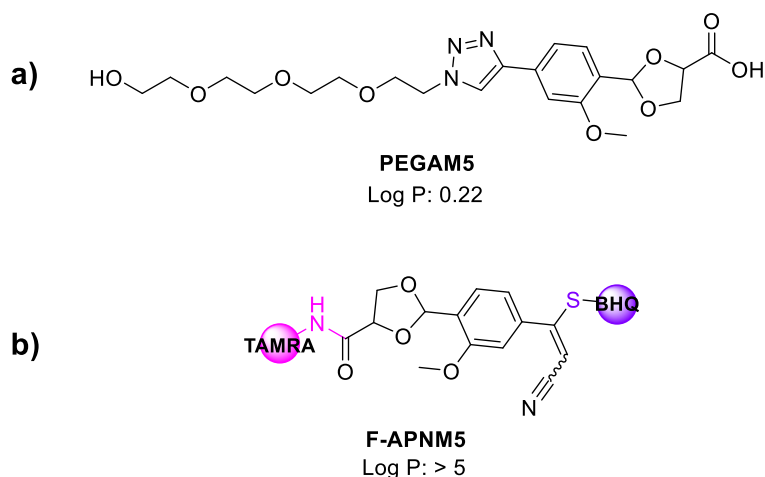
Next section will describe the design and synthesis of the hydrophilic equivalent of **F-APNM5**.

### 3. IDENTIFICATION OF HYDROPHILIC ACETAL CLEAVABLE AT PH < 4

#### 3.1 DESIGN AND SYNTHESIS OF **PEGAM5**: THE HYDROPHILIC EQUIVALENT OF **F-APNM5**

##### 3.1.1 Design of **PEGAM5**

As defined above, acetal **F-APNM5** showed to be stable in physiological pH and hydrolysable at pH < 4. Hence, its acetal core **APNM5** was used as base to design a hydrophilic equivalent. The new cyclic acetal bears a triazole -in place of the propiolonitrile motif- and a short PEG-4 chain which makes the molecule much more hydrophilic than **F-APNM5**. Its chemical structure is shown in **Figure 17a** and it is named **PEGAM5**. The code name is composed by: “**PEG**”, because of the presence of a PEG-4; “**M**” for methoxy and “**5**” for the acetal ring size. The calculated LogP value correspond to 0.22, in contrast with the LogP value estimated for the hydrophobic FRET acetal (**Figure 17b**).

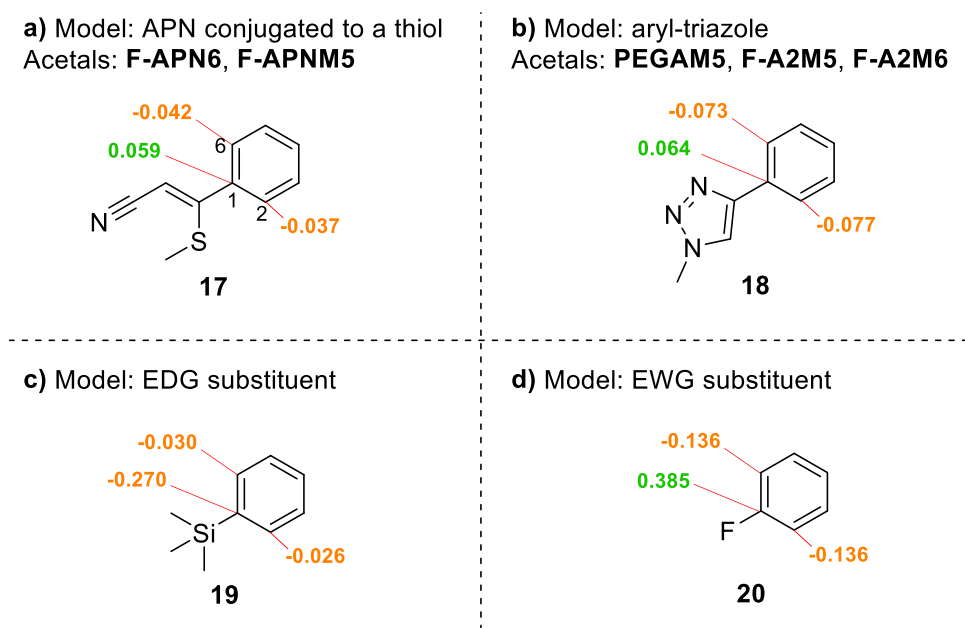


**Figure 17.** a) Structure of **PEGAM5**, the hydrophilic version of acetal model **APNM5**, and calculated LogP value; b) comparison with FRET acetal **F-APNM5** structure and estimated LogP value.

##### 3.1.2 Evaluation of Huckel charges on the new acetal model

Changing the aryl substituent at position 4 from a propiolonitrile to a triazole could affect the stability of the acetal towards hydrolysis. This issue was addressed by calculating Huckel charges for the two aryl model compounds and comparing the values obtained on the aromatic carbons close to the substituent. As additional comparison, Huckel charges were also calculated for two benzene with an electron-donating group and an electron-withdrawing group as substituent.

A strong EDG or EWG substituent, like respectively a silane and a fluorine, causes the charge on the adjacent aromatic carbon atom to raise or decrease by an absolute value of around 0.3, while both the thio-acrylonitrile (APN conjugated to a thiol) and the triazole substituents have a weak electron-withdrawing effect which raise the charge of the adjacent aromatic carbon to respectively 0.059 and 0.064 (**Figure 18**).



**Figure 18.** Calculation of Huckel charges on carbons 1, 2 and 6 of the aromatic ring in four model compounds; positive charges are enlightened in green, negative charges are in orange. Calculations were made with ChemDraw® 3D software. **a)** Model compound **17** for APN-acetals conjugated to **BHQ-2-SH**. This model applied to FRET probes **F-APN6** and **F-APNM5**. **b)** Model compound **18** for triazole-aryl compounds. This model applies to acetal **PEGAM5** and to FRET probes **F-A2M5** and **F-A2M6** (describe later in section 4 of this chapter, page 53). As comparison, Huckel charges were calculated also for **c)** trimethyl(phenyl)silane (**19**) and **d)** fluorobenzene (**20**) to give a comparison of charge values on the aromatic carbons close to respectively an electron-donating group and an electron-withdrawing group.

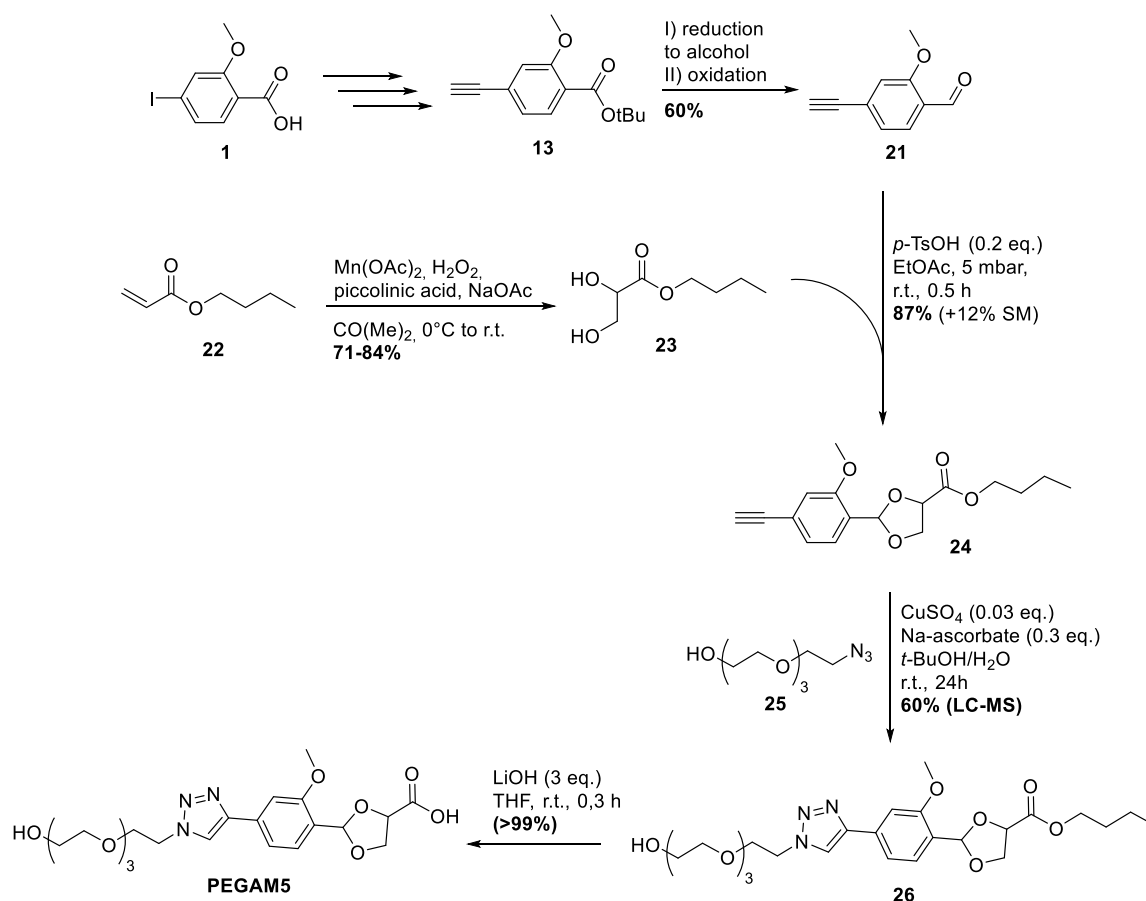
Thus, passing from APN-acetals to triazole-aryl acetals should not affect the charge distribution on the aromatic ring in a remarkable way. We thus hypothesised that the stability of the cyclic acetal towards hydrolysis will be only very slightly affected.

### 3.1.3 Synthesis of PEGAM5

The synthesis of **PEGAM5** is presented in **Scheme 8**. Starting from compound **13**, previously synthesized as intermediate in the synthesis of **APNM5**, the first steps involves the reduction of the protected acid to a primary alcohol and the subsequent partial oxidation to aldehyde,

following the same strategy previously used for **APNM5** (Cf. **Scheme 6**, page 41). Aldehyde **21** was obtained with an overall 60% yield.

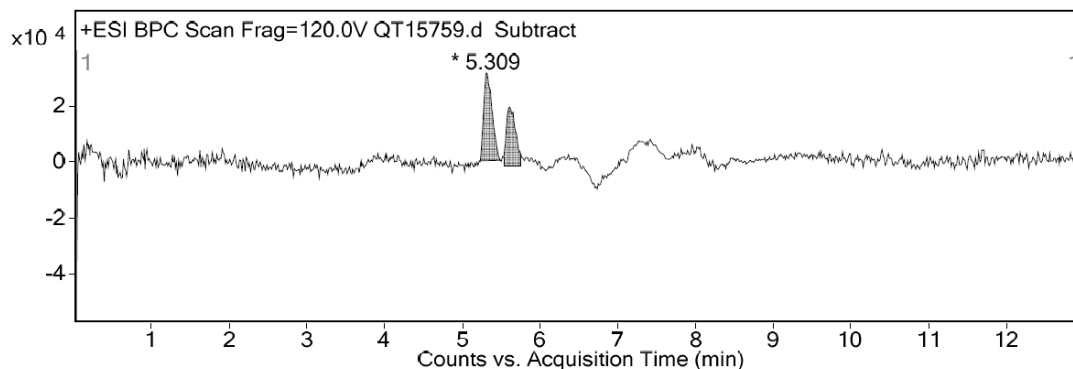
Condensation between the aldehyde **21** and the diol **23** (butyl 2,3-dihydroxypropanoate) is carried out in ethyl acetate at reduced pressure, following the procedure previously described, with a good 87% yield. Cyclic acetal **24** was obtained as a 1:1 mixture of *cis* and *trans* isomers.



**Scheme 8.** Synthesis of **PEGAM5**.

Then the obtained terminal alkyne **24** undergoes a click reaction with PEG-azide **25**, carried out in classical copper-catalysed alkyne-azide cycloaddition (CuAAC) conditions in presence of catalytic amount of copper sulphate and sodium ascorbate in *tert*-butanol/water mixture. The triazole **26** was obtained in 60% yield (calculated by LC-MS). The final step consists in the hydrolysis of the butyl ester with lithium hydroxide. Final compound **PEGAM5** was obtained in quantitative yield and purified with preparative HPLC, paying attention to the pH of the aqueous mobile phase which -as previously mentioned- must be neutral to prevent the

hydrolysis of the acetal in the column. HR-ESI-MS analysis of the isolated product revealed an isomeric ratio of 1:0.74 (**Figure 19**).



**Integration Peak List**

Peak	Start	RT	End	Height	Area	Area %	AreaSum%
1	5.219	5.309	5.492	31403.66	234541.61	100	57.39
2	5.535	5.612	5.757	20946.74	174109.19	74.23	42.61

**Figure 19.** HR-ESI-MS chromatogram of isolated **PEGAM5**. The two peaks correspond to the two stereoisomers obtained.

Having found both the hydrophobic and hydrophilic acetals cleavable at  $\text{pH} < 4$ , the reactivity of **APNM5** was further investigated in order to obtain acetals more prone to hydrolysis. Indeed, we anticipated that maintaining a  $\text{pH} < 2$  in the heterogeneous catalyst in a surrounding media buffered at  $\text{pH} = 7.4$  will be very challenging. Thus, a more labile acetal could increase our chance of success.

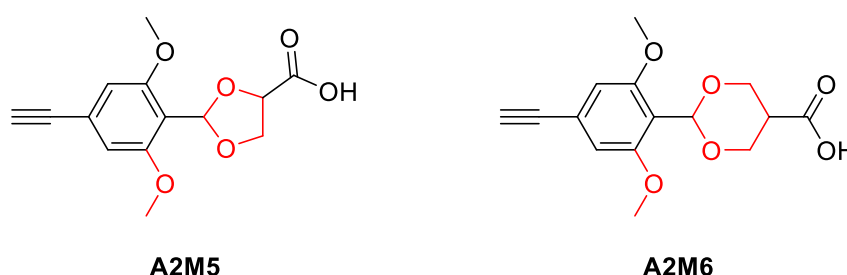
In the next section we described the design and the synthesis of two brand-new cleavable cyclic acetals, as well as the synthesis of the corresponding FRET probes, the tests for hydrolysis in acidic solutions, plasma and *in vitro*.

## 4. IDENTIFICATION OF ACETAL CLEAVABLE AT PH > 4

### 4.1 DESIGN AND SYNTHESIS OF ACETAL CLEAVABLE AT PH > 4 AND STABLE AT PH > 6

#### 4.1.1 Design of acetal A2M5 and A2M6

Two brand-new cyclic acetals were designed on the model of compound **APNM5**. Given the proved influence of the methoxy substituent in *ortho* position, a second methoxy was added in the *ortho'* position in order to weaken even further the acetal stability in acidic conditions. Moreover, the difference in the ring-size was also introduced as a variable to test towards acid stability. We expected that the 5-membered cyclic acetal would be more prone to hydrolysis than the 6-membered one, as previous studies suggested.<sup>35</sup> Regarding the propiolonitrile motif, it was substituted by a terminal alkyne, which can undergo copper-catalysed cycloaddition with an azide, generating a triazole. **Figure 20** shows the chemical structure of the two new targets **A2M5** and **A2M6**. Code names are conceived as follow: **A** = aryl; **2M** = two methoxy substituents; **5** or **6** = size of the acetal ring.



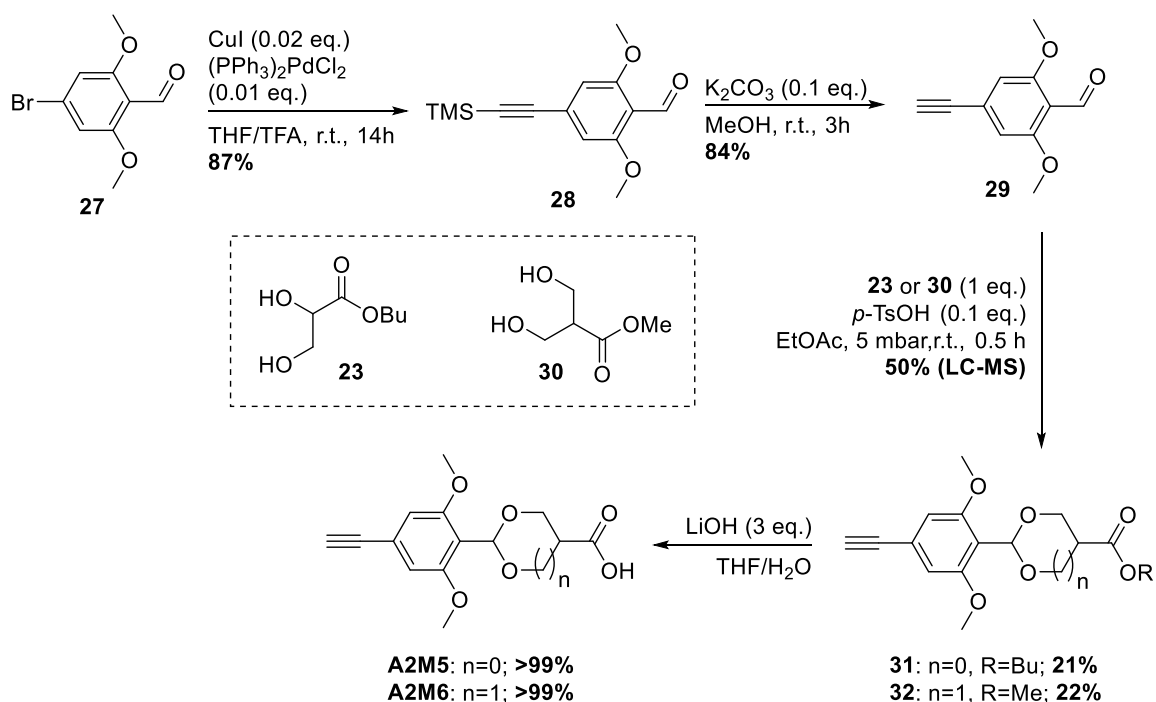
**Figure 20.** New cyclic acetal linker models **A2M5** and **A2M6**.

#### 4.1.2 Synthesis of A2M5 and A2M6

Inspired by the work on acetal linker **APNM5**, we decide to apply the same synthetic strategy. Starting from commercially available 4-bromo-2,6-dimethoxybenzaldehyde **27**, the synthesis of the acetals was straightforward and achieved in four steps (**Scheme 9**):

- I. Sonogashira coupling with protected ethyne;
- II. removal of trimethylsilyl ether protection in basic conditions;
- III. condensation with the proper diol;
- IV. hydrolysis of ester.



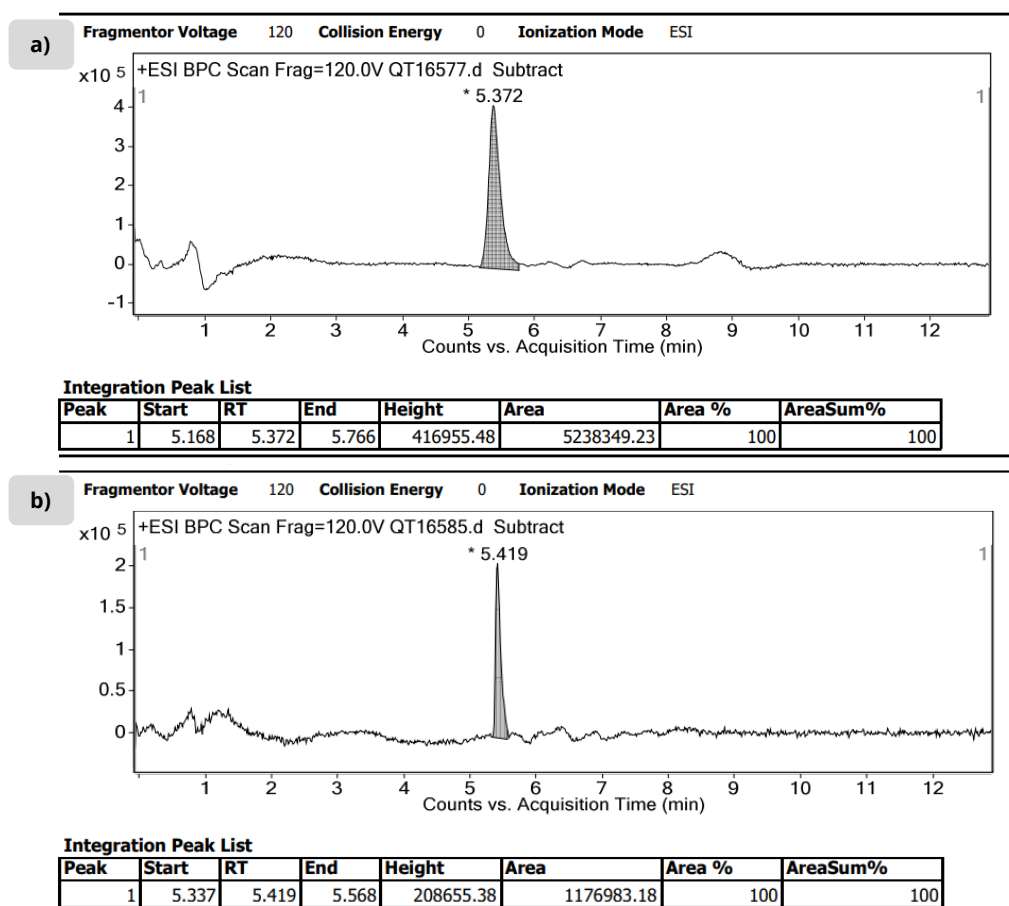


**Scheme 9.** Synthesis of compounds **A2M5** and **A2M6**.

The protected terminal alkyne **28** was obtained from starting iodo-benzaldehyde **27** through a Sonogashira coupling in good 87% yield. Given the presence of the aldehyde, the deprotection of the terminal alkyne was carried out in basic condition with 84% yield, instead of using fluoride anion (TBAF), which would lead to the formation of propargylic alcohol, as described in literature by Chintareddy *et al.*<sup>41</sup>

The condensation reaction between aldehyde **29** and the diol (**23** or **30**) afforded the acetal in 50% yield (calculated by LC-MS). The work-up of this reaction was the trickiest part of the whole synthesis. The classic work-up implies a phase extraction but the presence of a large amount of water and the *p*-toluenesulfonic acid caused the complete hydrolysis of the newly formed acetal. Consequently, the extraction was replaced with a fast purification on a silica pad of the reaction mixture to get rid of the acid, followed by a chromatographic column. Even though the initial yield was around 50%, the product fractions obtained from the chromatographic purification contained an important amount of the initial aldehyde. At a first moment, this was imputed to a bad separation since the  $R_f$  values of the starting material and of the product are very similar. After two more purification it was clear that the acidity of the silica itself was responsible for hydrolysis of the acetal. Final yields for acetals **31** and **32** were of 21% and 22% respectively. The NMR characterization revealed the presence of starting materials (< 5%).

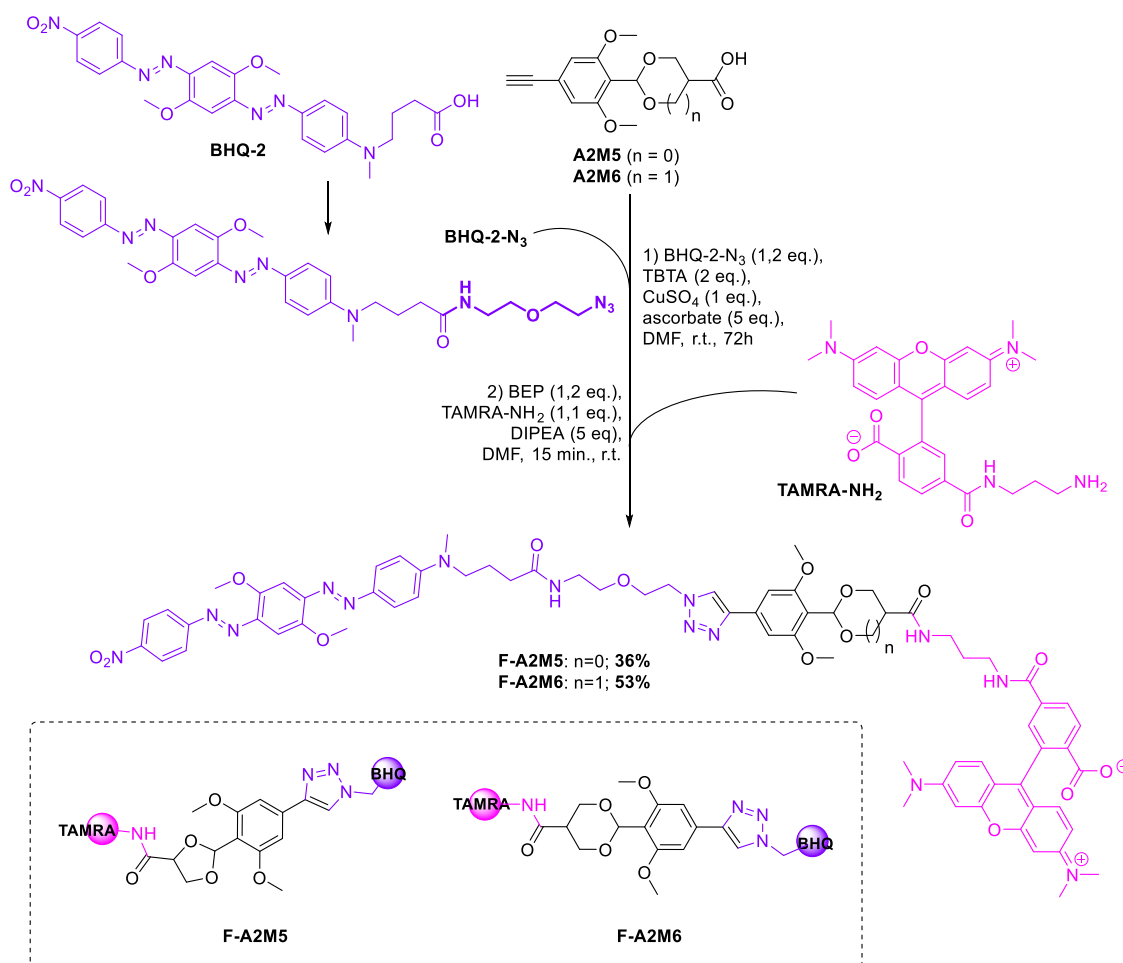
The final step was the ester hydrolysis with lithium hydroxide. The reaction gave the final products **A2M5** and **A2M6** in quantitative yield. Given their instability in acidic conditions, the final purification was done by preparative HPLC, using a neutral mobile aqueous phase (0.025 mM content of ammonium formate). HR-ESI-MS analysis showed that the two products were successfully isolated (**Figure 21**).



**Figure 21.** HR-ESI-MS chromatograms of isolated compound **A2M5** (a) and **A2M6** (b).

#### 4.1.3 Synthesis of FRET probes F-A2M5 and F-A2M6

FRET probes of the two new acetals were synthesized in order to address their stability towards hydrolysis in different proton concentrations and their cleavability in cell. **Scheme 10** shows their synthesis. In this case, the quencher BHQ-2 was modified via the addition of an azide moiety, in order to subsequently perform a copper-catalysed alkyne-azide cycloaddition (CuAAC) between the latter and the terminal alkyne of the acetals, resulting in the creation of a 1,4-disubstituted triazole.

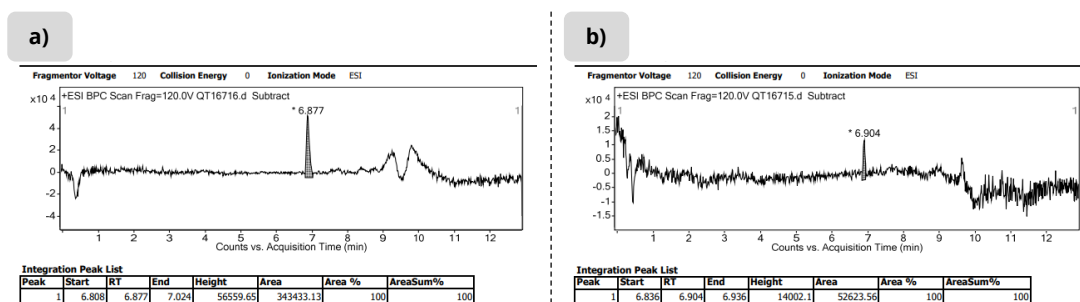


**Scheme 10.** Synthesis of FRET probes **F-A2M5** and **F-A2M6**.

The click reaction was carried out in classical conditions, in presence of copper sulphate (CuSO<sub>4</sub>) and sodium ascorbate, until complete conversion was reached (LC-MS analysis). The work-up was a fast phase extraction in water/DCM to get rid of the copper and the ascorbate salts.

The obtained mixture was used without any further purification for the second step: the amide formation. The activation of the carboxylic acid with BEP (2-Bromo-1-ethyl-pyridinium tetrafluoroborate) was followed by nucleophilic substitution by **TAMRA-NH<sub>2</sub>**.

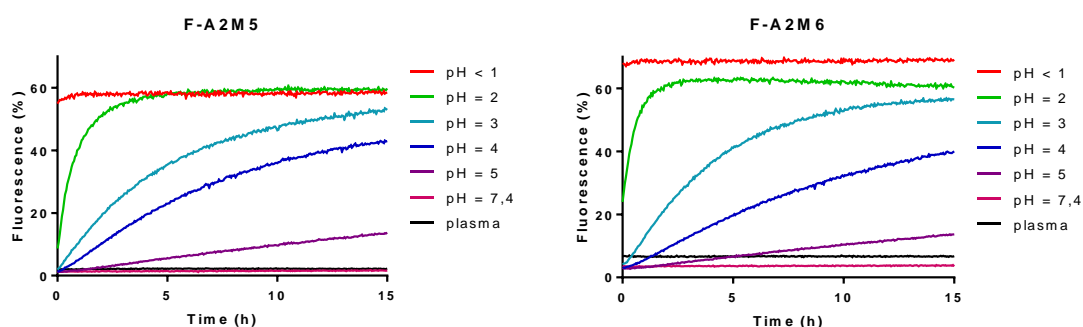
Overall the reaction proceeded well and the yield over the two steps was almost quantitative, according to LC-MS analysis. Unfortunately, the final yields obtained after the purification with preparative HPLC are 36% and 53% for **F-A2M5** and **F-A2M6** respectively, despite the use of a neutral aqueous phase for the HPLC purification. The two FRET probes were however isolated with an excellent degree of purity, as confirmed by the HR-ESI-MS chromatograms (**Figure 22**).



**Figure 22.** HR-ESI-MS chromatograms of isolated compound **F-A2M5** (a) and **F-A2M6** (b).

#### 4.2 PROFILE OF **F-A2M5** AND **F-A2M6** STABILITY TOWARDS HYDROLYSIS AT DIFFERENT PH

FRET probes **F-A2M5** and **F-A2M6** were tested for stability with the same method used for **F-APN6** and **F-APNM5**. Results are shown in **Figure 23**.



**Figure 23.** Hydrolysis profiles of acetals **F-A2M5** and **F-A2M6** in different aqueous solutions in plasma at 23°C.

Both probes have similar profiles. Hydrolysis at pH < 1 was achieved immediately, at pH = 2 maximum hydrolysis was reached within 3 hours. With increasing pH, the rates decreased, as expected. At pH = 5 hydrolysis was very slow, while at physiological pH = 7.4 and in plasma, both the acetals showed stability. Regarding the comparison between the profiles of the two acetals, they are very similar: it seems that the size of the ring does not make a significant contribution to the hydrolysis rate. As a reminder, it was expected that the 5-membered ring acetal would hydrolyse faster than the 6-membered one. Apparently, the increase in hydrolysis rate with respect to acetals **F-APN6** and **F-APNM5** is to impute mainly to the introduction of a second methoxy in *ortho* position.

The hydrolysis profiles of the new acetals **F-A2M5** and **F-A2M6** match the target. They are stable at the pH of cells and extracellular environment and are cleaved in the range of pH of the more acidic compartments of the cell (Cf. **Figure 1**, page 11). Thus, they could represent a competitive alternative to the already existing cleavable linkers. For this reason, their cleavability in cells was evaluated.

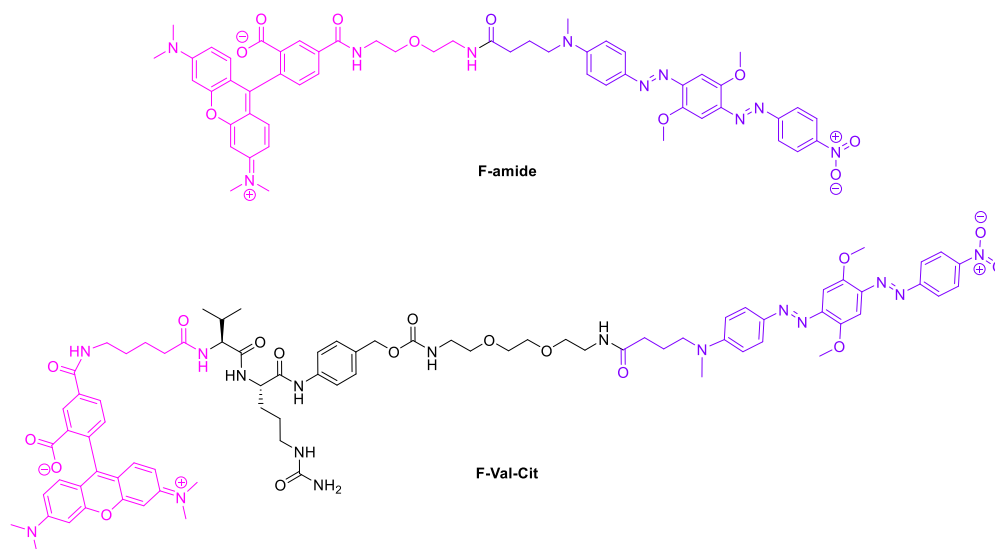
#### 4.3 *IN VITRO* EVALUATION OF **F-A2M5** AND **F-A2M6** CLEAVABILITY IN CELLS

Cell culture and flow cytometry experiments were performed by Dr. Fabien Thoreau.

**F-A2M5** and **F-A2M6** are incubated with five cell lines (**Table 1**, next page). After 1.5 hour incubation at 37 °C, solution was removed, cells were washed with PBS, trypsinized (5 min, 37 °C) and resuspended in PBS. Fluorescence was assessed through flow cytometry and was compared to the one of two other FRET probes:

- **F-amide**, in which the fluorophore **TAMRA-NH<sub>2</sub>** and the quencher **BHQ-2** are connected through an amide bond;
- **F-Val-Cit**, in which the fluorophore and the quencher are linked via **Val-Cit** (valine and citrulline), a cleavable linker currently used in the FDA approved antitumoral ADC *brentuximab vedotin* (trade name: Adcetris®).<sup>42,43</sup>

Chemical structure of the two FRET probes are showed in the following figure.

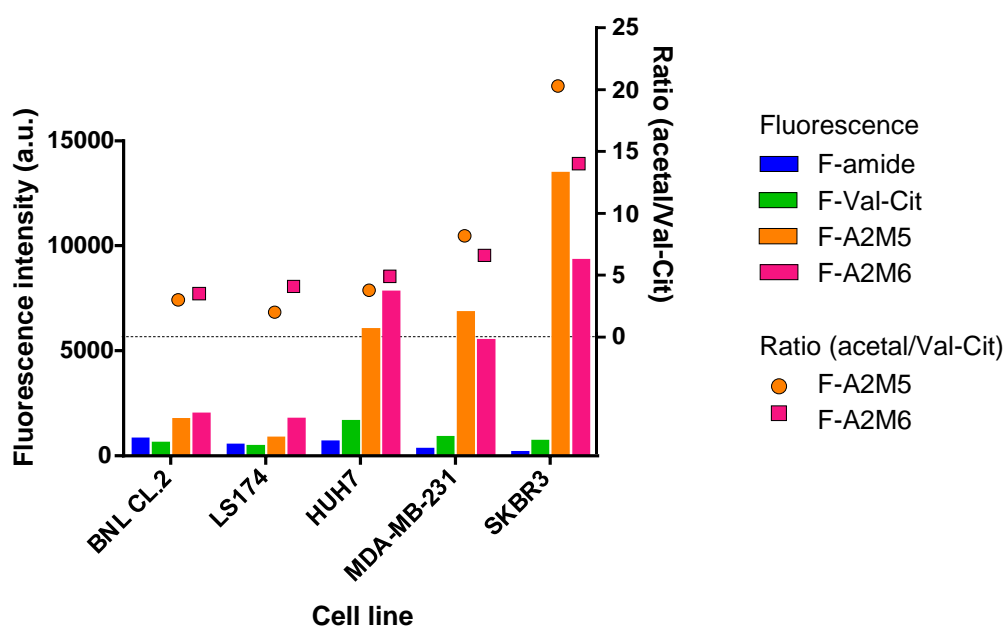


**Figure 24.** Chemical structure of FRET probes **F-Val-Cit** and **F-amide**.

Cell line	Description
BNL CL.2	Mouse healthy liver cell line
LS174	Human Dukes' type B, colorectal adenocarcinoma cell line
HUH7	Human well differentiated hepatocyte derived cellular carcinoma cell line
MDA-MB-231	Human breast adenocarcinoma, derived from metastatic site: pleural effusion
SKBR3	Human breast adenocarcinoma, derived from metastatic site: pleural effusion

**Table 1.** Cell lines tested for the acetal cleavage.

All the tests are conducted in triplicates. The values of fluorescence obtained have been subtracted of the values obtained from the control (cells incubated just in the media) of the corresponding cell line. Results are shown in **Figure 25** and are represented as fluorescence intensity (bars, left scale) and as ratio between the fluorescence given by the acetals (**F-A2M5** and **F-A2M6**) and that given by **F-Val-Cit** (squared dots, right scale) for each cell line. This gives a better understanding of the relative stability of the acetals on the different cell lines with respect to the **Val-Cit** cleavable linker.



**Figure 25.** Cell viability of **F-amide**, **F-Val-Cit**, **F-A2M5** and **F-A2M6** on five cell lines. Two set of data are showed: plain bars indicate the value of fluorescence calculated trough flow cytometry (scale on the left); dots represent the relative cleavability of the new two acetals **F-A2M5** and **F-A2M6** with respect to the cleavable probe **F-Val-Cit** (scale on the right). All values are subtracted of the corresponding values obtained from the control (cells incubated only in presence of the media).

For cell lines BNL CL.2, LS174 and HUH7, the fluorescence observed for **F-A2M5** and **F-A2M6** is from 2 to 5 times higher than that measured for **F-Val-Cit**, with the 6-membered cyclic acetal **F-A2M6** showing faster hydrolysis over its 5-membered ring analogue. This trend is inverted for the two breast cancer cell lines MDA-MB-231 and SKBR3: **F-A2M5** is more prone to hydrolysis than **F-A2M6**. With SKBR3 cell line, the ratio between the fluorescence measured for the acetals and for the **Val-Cit** linker is greater than with the other cell lines. Fluorescence from **F-A2M6** hydrolysis is 14 times higher, while fluorescence from **F-A2M5** hydrolysis is 20.3 times higher.

Overall, both the acetals show better cleavability *in vitro* than **F-amide** and **F-Val-Cit**, confirming that the cyclic acetals **A2M5** and **A2M6** are good candidates as cleavable motifs for payload-release bioapplications.

## 5. IDENTIFICATION OF ACETAL STABLE TOWARDS HYDROLYSIS AT VERY LOW PH

### 5.1 INTRODUCTION

The biochemical characteristics of hetero-bifunctional cross-linker used in bioconjugates are of essential importance to the desired features of the final adduct. These include stability in biological media, chemical and biological reactivity, cleavability in defined conditions and solubility.<sup>33</sup> In a work previously conducted in our group, we introduced a new amine-to-thiol acetal linker -maleimidomethyl dioxane (**MD**, **Figure 27b**, page 62)- as an alternative to classical maleimide conjugation, with increased hydrophilicity and remarkable stability in very acidic solutions.<sup>44</sup> Hence, such cyclic acetal linker falls into the class of non-cleavable amine-to-thiol linker with the advantage of improved solubility due to the presence of two oxygen atoms.

Inspired by the significant qualities showed by **MD** linker, we investigated the generality of cyclic acetal amine-to-thiol linkers containing maleimide as bioconjugation site for thiol linkage. Results of this investigation were published in 2017 in *Organic and Biomolecular Chemistry* journal.<sup>45</sup>

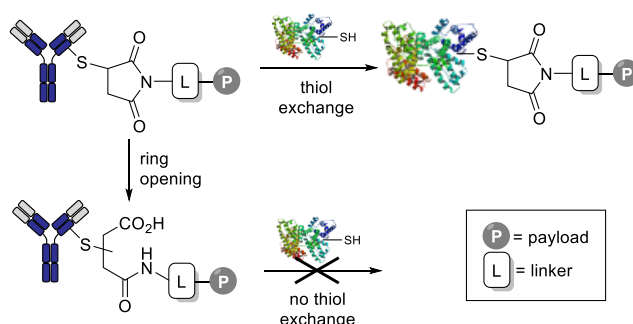
#### 5.1.1 Maleimide group in bioconjugation

The maleimide group is one of the most used chemoselective moieties for bioconjugation because it reacts quickly and selectively with a sulfhydryl group through Michael addition forming a thioether. Maleimide is thus present in many amino-to-thiol heterobifunctional coupling agents, such as succinimidyl 4-(N-maleimidomethyl)-cyclohexane-1-carboxylate (**SMCC**).

Maleimide-containing reagents are used for numerous applications, from the preparation of hapten-carrier conjugates,<sup>46-48</sup> protein nanoparticles,<sup>49</sup> or antibody-nanoparticle conjugates,<sup>50</sup> to the advanced and growing field of antibody-drug conjugates (ADCs).<sup>51,52</sup> For instance, **SMCC** is used in Kadcyła®, an antibody-drug conjugate currently used in the treatment of metastatic breast cancer.<sup>53</sup> The resulting thiosuccinimidyl linkage is however not without drawbacks, especially concerning the tendency of maleimide-based ADC to lose their drug during prolonged circulation.<sup>54-56</sup>



Indeed, it is now well known that the maleimide-thiol adduct is prone to retro-Michael reactions and exchanges with other thiol-bearing molecules<sup>57</sup> present in biological media such as albumin, reduced glutathione and free cysteine,<sup>54</sup> leading to the premature release of the payload. In competition with this process, the succinimidyl ring can undergo a favourable ring-opening hydrolysis,<sup>58</sup> leading to a linear structure<sup>59</sup> which does not undergo further thiol exchange (**Figure 26**), thus enhancing the stability and the pharmacological properties of ADCs.<sup>60,61</sup>

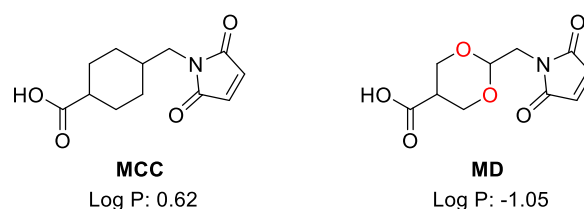


**Figure 26.** Illustration of the two reaction pathways of the ADC containing the thiosuccinimidyl linkage. In human plasma, the ADC can undergo either thiol exchange with thiol-bearing biomolecules (human serum albumin for example in the figure), or succinimidyl ring-opening, which precludes thiol exchange.

### 5.1.2 SMCC vs MD amine-to-thiol heterobifunctional linkers

Probably the most famous amine-to-thiol linker, 4-(N-maleimidomethyl)-cyclohexane-1-carboxylate (**MCC**) is composed by a central cyclohexane ring with two substituents in para position, the first is an activated acid for linkage to amines, the second is a maleimide ring for linkage to thiols (**Figure 27a**).

The previously presented 2-(maleimidomethyl)-1,3-dioxane (**MD**) has two oxygen atoms which substitute carbons 1 and 3 in the central ring, thus giving an acetal function (**Figure 27b**).



**Figure 27.** Molecular structure of **MCC** and **MD** and relative LogP values.

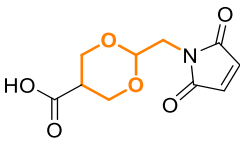
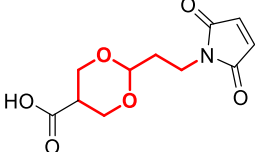
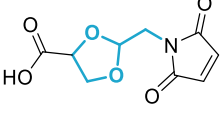
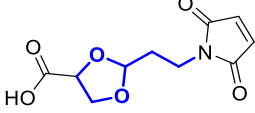
**MD** is a potent alternative to the classical **MCC** linker. The two intra-cyclic oxygen atoms increase the hydrophilicity of both the heterobifunctional coupling reagent and its resulting conjugates, circumventing potential problems related to the poor water solubility of **MCC**-based bioconjugates, like aggregation and precipitation. Moreover, the succinimidyl ring in **MD**-based conjugates underwent fast self-stabilization via ring-opening hydrolysis.<sup>44</sup>

Interestingly, despite the presence of an acetal moiety, **MD** linker was remarkably stable in aqueous media even at pH < 1, thus maintaining all the desired characteristics of a non-cleavable linker. This feature, combined with the high solubility in aqueous media and the stability resulting from the succinimidyl ring-opening, makes the maleimide dioxane an excellent heterobifunctional reagent for the building of stable amine-to-thiol bioconjugates. In this section we wanted to investigate these surprising phenomena (acidic stability/auto-catalysed ring-opening) and decipher what, in terms of chemical structure, influences the peculiar reactivity of the maleimide dioxane motif.

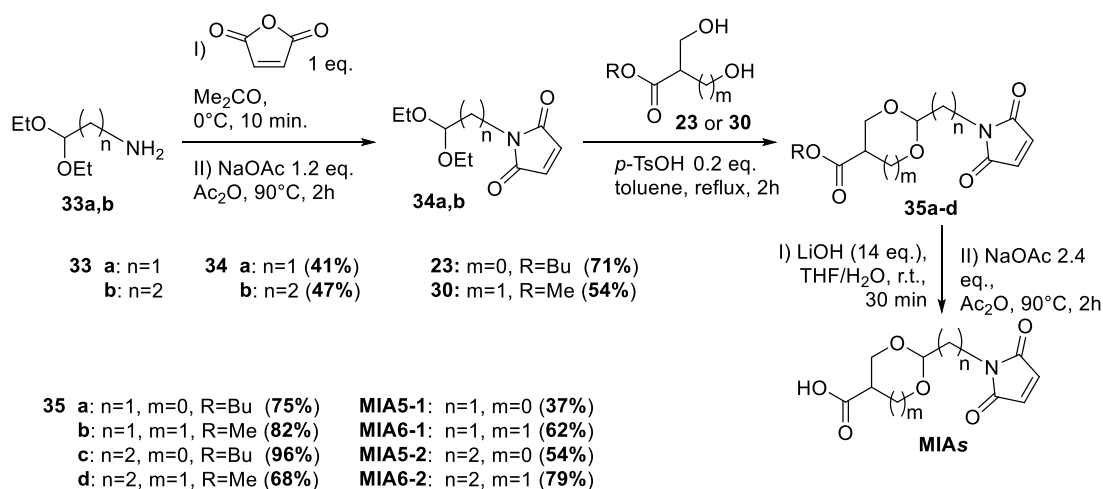
## 5.2 STRUCTURAL INVESTIGATION OF MALEIMIDE-ACETAL LINKERS FOR ACID AND SERUM STABILITY

### **5.2.1 Design and synthesis of MD linker analogues**

New analogues of **MD** linker were designed and synthesized. They differ in ring size (5 and 6 membered cyclic acetals) and carbon-chain length (1 and 2 aliphatic carbons). Chemical structures are pictured in **Table 2** and their synthesis is resumed in **Scheme 11**. Code-names are assigned to all the linkers, including the original **MD**. For the sake of clarity and easy comparison with its analogues, from this point **MD** will be named “**MIA6-1**”, where “**MI**” stands for “maleimide”, “**A**” for “acetal”, “**6**” for the ring size and “**1**” for the carbon-chain length.

		Carbon-chain length	
		1 aliphatic C	2 aliphatic C
Ring-size	6-membered ring	 <p><b>MD or MIA6-1</b></p>	 <p><b>MIA6-2</b></p>
	5-membered ring	 <p><b>MIA5-1</b></p>	 <p><b>MIA5-2</b></p>

**Table 2.** Chemical structures of **MD** and three new amine-to-thiol cross-linkers based on **MD**. Code names are given on the following base: “**MI**” for “maleimide”, “**A**” for “acetal”, “**5**” or “**6**” for the ring size and “**1**” or “**2**” for the carbon-chain length. So **MD** will be named also “**MIA6-1**” to help the reader quickly identifying its structural composition.



**Scheme 11.** Synthesis of **MIA** linkers.

Syntheses of compounds **34a,b** were achieved in two steps:

- I. a nucleophilic ring-opening reaction of maleic anhydride with amines **33a,b**;
- II. a cyclisation reaction in the presence of acetic anhydride and sodium acetate.

Noteworthy, the second step was the most challenging and required to be performed at 90°C. Under these conditions, the cyclisation reactions had to be carefully monitored since

prolonged reaction time led to decomposition. Compounds **34a** and **34b** were obtained in 41% and 47% yield respectively.

Then, the key step of the synthetic procedure was the condensation between the synthons **34** and **23** or **30**, which was carried out in refluxing toluene in the presence of a catalytic amount of *para*-toluenesulfonic acid. The two acetals **34a** and **34b** were used in different combinations with the diols **23** and **30** to obtain four different linkers **35a-d** in moderate to good yields (68-96%).

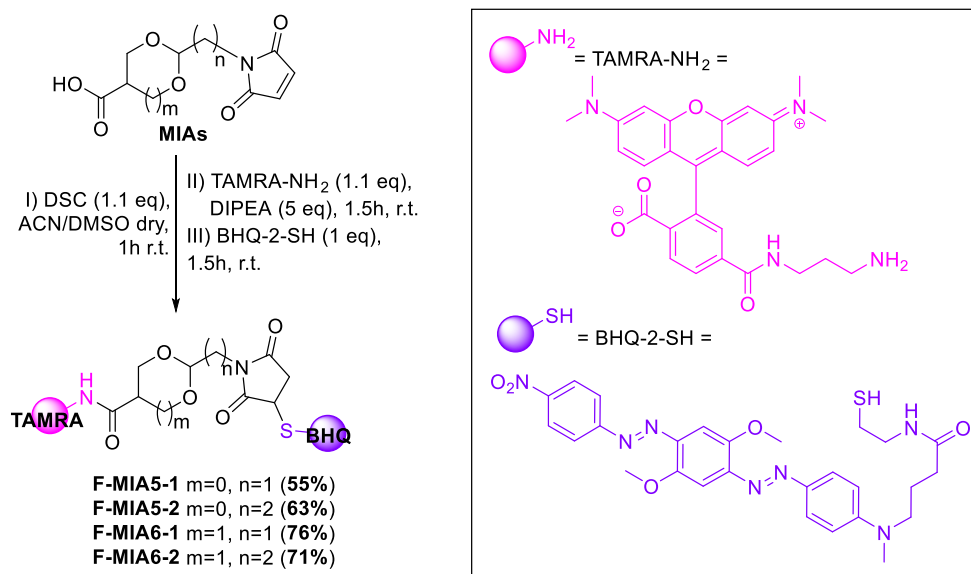
Finally, the saponification of esters **35a-d** with LiOH in THF/H<sub>2</sub>O gave the corresponding carboxylates but hydrolysed the maleimide ring concomitantly. Thus, a second cyclisation reaction under the conditions previously described was necessary to reform the maleimide ring and deliver the final products in 37-79% yield.

It is worth mentioning that the syntheses of linkers **MIA5-1** and **MIA5-2** took less steps compared to those of linkers **MIA6-1** and **MIA6-2** as diol **30** was prepared in one step, while **23** was prepared in four (Cf. Experimental Procedures, section 1.7, page 194). As for the cyclic linkers previously described, the final compounds were obtained as an almost equimolar mixtures of *cis* and *trans* diastereomers.

### 5.2.2 Synthesis of FRET probes of MIA linkers

For each linker, Fluorescence Resonance Energy Transfer (FRET) probes were prepared. As a reminder, FRET strategy allows to address the stability of the dioxo-ring and to study the maleimide ring-opening and the thiol-exchange processes by means of detecting and measuring the generation of fluorescence. Indeed, cleavage of the linkage between the two moieties (*i.e.* via acetal hydrolysis, complete hydrolysis of the succinimidyl ring, or thiol exchange of **BHQ-2-SH**) leads to the appearance of a strong fluorescence signal.

Their synthesis was achieved via a one-pot three-step procedure consisting of the in-situ activation of the acid with disuccinimidyl carbonate (DSC) followed by coupling with the fluorophore **TAMRA-NH<sub>2</sub>** and subsequent reaction with the quencher **BHQ-2-SH** (**Scheme 12**). All the reactions were carried out on a 2.5 mg scale. Successive transformations were controlled by LC-MS and the final products purified by preparative HPLC with good overall yield (55-76%) of the isolated product. Stock solutions were then prepared in DMSO-d<sub>6</sub> and the concentrations were determined by <sup>1</sup>H-ERETIC NMR.



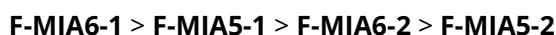
**Scheme 12.** One-pot three-step synthesis of the FRET probes.

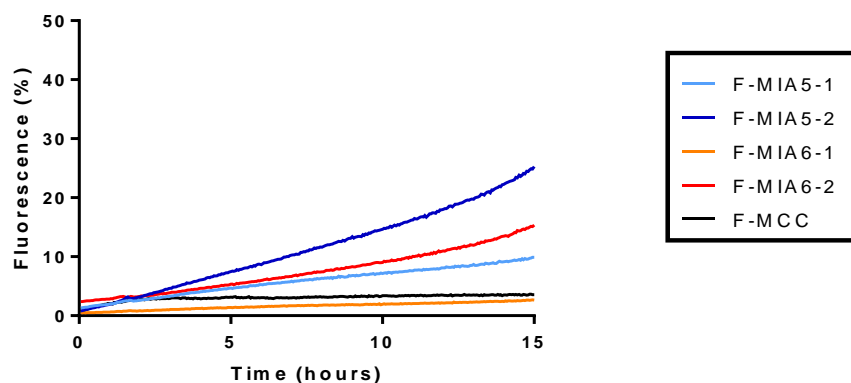
### 5.3.3 Profile of MIAs stability towards acetal hydrolysis at various pH.

With these versatile tools in hand, the stability of the FRET probes (1  $\mu$ M) in different buffers (PBS, TRIS) at various pH (5.0 - 9.0), as well as in HCl solutions (1 M and 0.01 M in water) was tested. The fluorescence was monitored for 15 hours at 25 °C and was normalized against that of a 1  $\mu$ M solution of an equimolar mixture of TAMRA and BHQ recorded under the same conditions. The FRET probe of **MCC (F-MCC)**, bearing the same quencher and fluorophore, was used as a control in order to address the appearance of fluorescence as the result of the acetal ring hydrolysis.

Results show that in a pH range from 2 to 9, including biological conditions, the fluorescence did not exceed 10% (See Experimental Procedure, section 2.2, page 217), proving the stability of the linkers despite the presence of an acetal moiety. Only under strong acidic conditions significant acetal hydrolysis could be observed (1 M aq. HCl, **Figure 28**).

It is notable that in such non-physiological conditions, it was possible to discriminate between the different linkers and reveal a pattern for the acetal relative stability. The stability of the probes increases following the order:





**Figure 28.** Stability assay in 1 M HCl aqueous solution (pH<1).

Under the experiment conditions (1  $\mu$ M solution of acetal in 1 M HCl aq.), and given that the concentration of one of the reactants ( $H^+$ ) is  $10^6$  times greater than the other (acetal), the reaction follows a pseudo-first order kinetic, with the following rate constants:

- **F-MIA5-2**       $k_{5-2} = 4,61 \cdot 10^{-6} \text{ s}^{-1}$
- **F-MIA6-2**       $k_{6-2} = 2,28 \cdot 10^{-6} \text{ s}^{-1}$
- **F-MIA5-1**       $k_{5-1} = 1,59 \cdot 10^{-6} \text{ s}^{-1}$
- **F-MIA6-1**       $k_{6-1} = 3,80 \cdot 10^{-7} \text{ s}^{-1}$
- **F-MCC**           $k_{MCC} = 3,06 \cdot 10^{-7} \text{ s}^{-1}$

The two probes with five-membered rings proved to be slightly less stable than the six-membered ones, while increasing the distance between maleimide and acetal resulted also in decreased stability in both series.

These experimental results appear to be consistent with several studies on stereo-electronic effects on acetal hydrolysis and may serve as a basis for explanation. First, it has been reported that acetal hydrolysis rate is decreased by increased steric hindrance from the substituents<sup>62</sup> and by the presence of electron-withdrawing substituent.<sup>63,64</sup> In this case, the acetal ring in **MIA5-1** and **MIA6-1** seems more hindered because of the maleimidomethyl substituent, thus accounting for the decrease in reactivity. In addition, the electron-withdrawing maleimide residue is closer to the acetal in **MIA5-1** and **MIA6-1** than in **MIA5-2** and **MIA6-2**. These factors may account for the observed hydrolysis-rate trend.

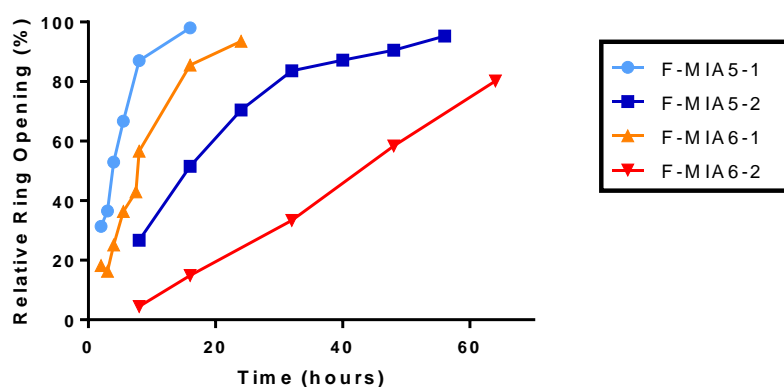
Regarding the size of the dioxo-ring, it is already known that a 5-membered cyclic acetal is more prone to hydrolysis than a 6-membered one,<sup>35,65</sup> which is confirmed by our experimental results: **MIA5-2** and **MIA5-1** are hydrolysed faster than **MIA6-2** and **MIA6-1** respectively.

These two factors are both in accordance with the obtained experimental trend. Thus, the original linker **MIA6-1** (previously presented as **MD**)<sup>44</sup> proved to be the most stable under acidic conditions, even though all four probes showed to be equally stable under physiological conditions.

### 5.3.4 Profile of succinimide ring-opening in PBS

Attention was then focused on the succinimide part which, through auto-catalysed ring-opening, prevents the thiol-exchange process, contributing in this way to the overall stability of the probe.

In order to measure the relative abundance of the closed and opened succinimidyl forms, 50  $\mu\text{M}$  solutions of FRET probes in PBS buffer (pH 7.4, 10% DMSO) were prepared and incubated at 37 °C. Aliquots were taken at various time points and were analysed by LC-MS. Comparison of the peak-area of the probe itself (of mass [M]) with the peak-area of the opened molecule (of mass [M+18]) enabled calculation of the transformation rate. In this way, ring-opening profiles for all the probes were determined, by plotting values of opened form percentage against time (**Figure 29**).



**Figure 29.** Ring-opening rate of the succinimidyl ring in PBS for the four probes (50  $\mu\text{M}$  solution).

The reaction follows a pseudo-first order kinetics, rate constants of all the probes were calculated:

- **F-MIA5-1**       $k_{5-1} = 7,29 \cdot 10^{-5} \text{ s}^{-1}$
- **F-MIA6-1**       $k_{6-1} = 3,43 \cdot 10^{-5} \text{ s}^{-1}$
- **F-MIA5-2**       $k_{5-2} = 1,53 \cdot 10^{-5} \text{ s}^{-1}$
- **F-MIA6-2**       $k_{6-2} = 6,81 \cdot 10^{-6} \text{ s}^{-1}$

Interestingly, probes **F-MIA6-1** and **F-MIA5-1** with a methylene spacer are hydrolysed much faster than the corresponding probes **F-MIA6-2** and **F-MIA5-2** bearing an ethylene spacer. Consequently, for the desired ring opening, the one-carbon spacer is preferable to the two-carbon spacer.

Addressing the effect of the ring size in both series, 5-membered rings proved to have faster ring opening reactions than their corresponding 6-membered analogues: **F-MIA5-1** > **F-MIA6-1** and **F-MIA5-2** > **F-MIA6-2**.

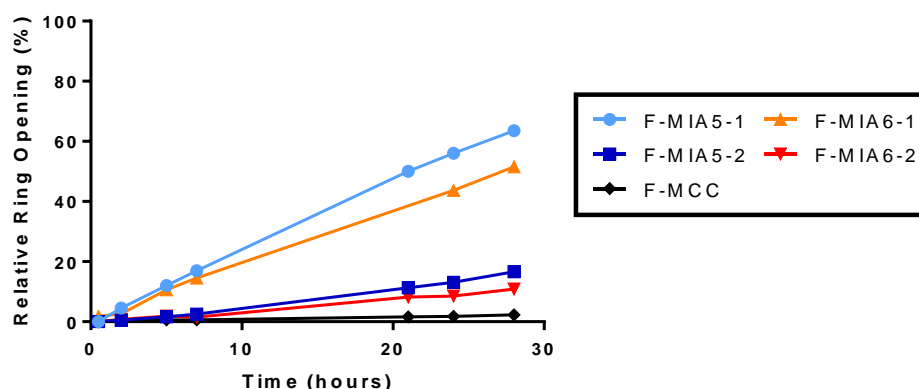
The data obtained clearly indicate that both the distance between the dioxane ring and the succinimide and the ring size are crucial for the rate of the ring-opening reaction in aqueous media. According to these data, **MIA5-1** appears potentially superior to the original **MIA6-1**.

### ***5.3.5 Profile of succinimide ring-opening in plasma.***

In order to validate this result under relevant physiological conditions the ring-opening rate was measured in human plasma at 37 °C. As in previous experiments, the **F-MCC** probe served as a comparison point. Aliquots were taken at appropriate intervals of time, proteins were precipitated with acetonitrile, the resulting solutions were centrifuged and the supernatants were analysed as described above for PBS solutions. The results are plotted as the ring-opening percentage versus time (**Figure 30**).

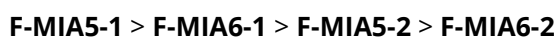
Interestingly, the process seems to be slower in human plasma than in PBS solution. Again, the probes with one-carbon spacer are more prone to hydrolytic succinimide ring opening than their homologues.





**Figure 30.** Ring-opening rate of the succinimidyl ring in plasma for the four probes and for **F-MCC** (1  $\mu$ M solution).

As proven by Fontaine and co-workers in 2015<sup>58</sup> in a study on the effects of the N-substituent on the succinimidyl ring opening rate, if the substituent is an electron-withdrawing group, the reaction is faster. Moreover, the closer the group is to the maleimide, the faster is the reaction. On the other hand, variation of the ring size had less impact on the kinetics even though the overall ranking of the probe was the same in PBS and plasma:



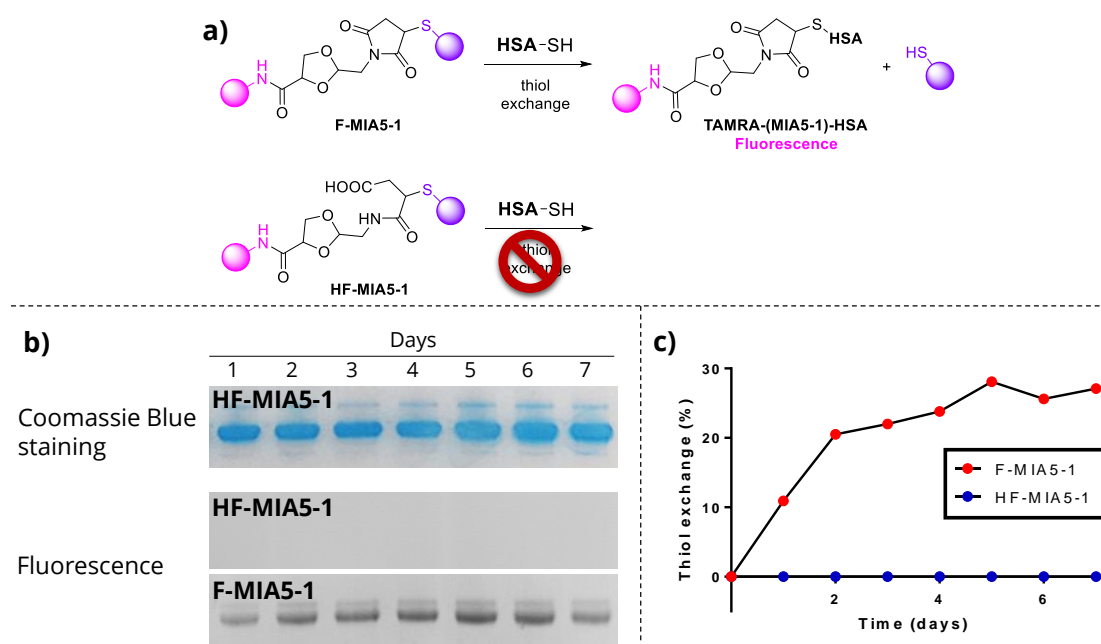
It is important to consider that, during the protein precipitation prior to LC-MS analysis, the probe undergoing thiol exchange with albumin also precipitated and was therefore not detected. As proven by thiol-exchange experiment (**Figure 32**, next section), within the timeframe of our experiment, the thiol exchange was less than 15% and the qualitative information coming from the experiment about the structure-reactivity relationship is still valid and confirms the results obtained in PBS.

### 5.3.6 Assessment of thiol exchange with HSA in plasma.

The fastest self-hydrolysable probe **F-MIA5-1** was pre-incubated in PBS until a complete ring opening could be observed. This pre-hydrolysed probe **HF-MIA5-1** was incubated along with its non-hydrolysed equivalent **F-MIA5-1** in plasma (50  $\mu$ M) at 37 °C. Fluorescence of **HSA-(MIA5-1)-TAMRA** could be detected upon thiol exchange between proteins (mainly HSA) and BHQ (**Figure 32a**). Aliquots were taken every day over a period of one week and were analysed by SDS-PAGE (**Figure 31b**). The fluorescence intensity of the HSA bands was measured and converted to a percentage of thiol exchange (**Figure 31c**).

For probe **HF-MIA5-1** no fluorescence was detected, while for the native probes **F-MIA5-1**, the fluorescence of the HSA band gradually increased over time. The appearance of fluorescence in case of **F-MIA5-1** and the lack of it in **HF-MIA5-1** account for complete inhibition of the thiol exchange process thanks to maleimide ring opening.

Along with this predicted result, even the non pre-hydrolysed native probe **F-MIA5-1** hydrolyses in situ fast enough to give only 12% of thiol exchange after 24 hours and to stop at <30% of exchange in 7 days.



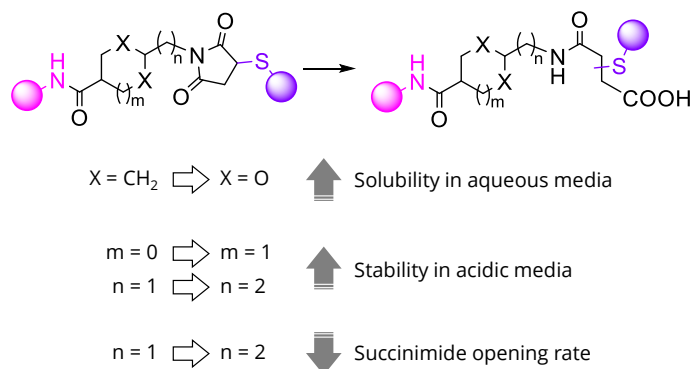
**Figure 31. a)** Illustration of thiol-exchange reaction with human serum albumin (HSA). **b)** HSA bands revealed by Coomassie Blue staining of gel with **HF-MIA5-1** probe and fluorescence of HSA bands on gel with **HF-MIA5-1** and **F-MIA5-1** probes (for a complete illustration, see Experimental Procedures, section 2.4, page 208). **c)** Analysis of fluorescence intensity reported as percentage of thiol exchange.

### 5.3 CONCLUSION: OVERVIEW OF MALEIMIDE-ACETAL LINKERS' STRUCTURE-REACTIVITY RELATIONSHIP

In conclusion, from this study an improved linker emerged: 2-(maleimidomethyl)-1,3-dioxolane (**MIA5-1**) linker is somewhat more efficient for self-stabilizing than **MIA6-1** (or **MD**), the amine-to-thiol linker that we originally presented. It showed a faster hydrolysis in human plasma, which is the most wanted feature in maleimide-bearing linkers, while keeping all the improved characteristics of **MD** and being easier to synthesize. **Figure 32** summarise the

information obtained from the investigation on maleimide-acetal linkers' chemical structure:

- i)** the presence of a cyclic acetal instead of a cyclohexyl increases the hydrophilicity of the linker itself and of its adduct;
- ii)** the acetal ring size and the distance between the acetal and the maleimide is correlated to the stability in acidic media, with the most stable acetal being the one with a 6-member cycle and the maleimide just one aliphatic carbon apart from the acetal;
- iii)** the succinimide opening rate is higher when acetal is closer to the maleimide.



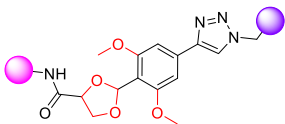
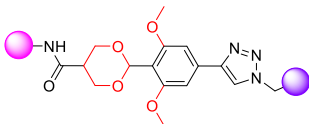
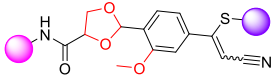
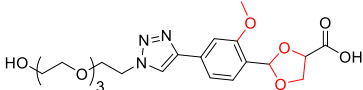
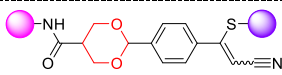
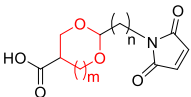
**Figure 32.** Summary of the investigation on maleimide-acetal linkers for hydrophilicity and stability in acidic media -towards acetal hydrolysis- and in serum towards thiol exchange.

## 6. CONCLUSION

As stated in the introduction of this thesis (chapter I.2, page 6), we aim to define a reaction setup for the acid-catalysed hydrolysis of cyclic acetals which is abiotic in every part: the cyclic acetal substrate and the acidic heterogeneous catalyst.

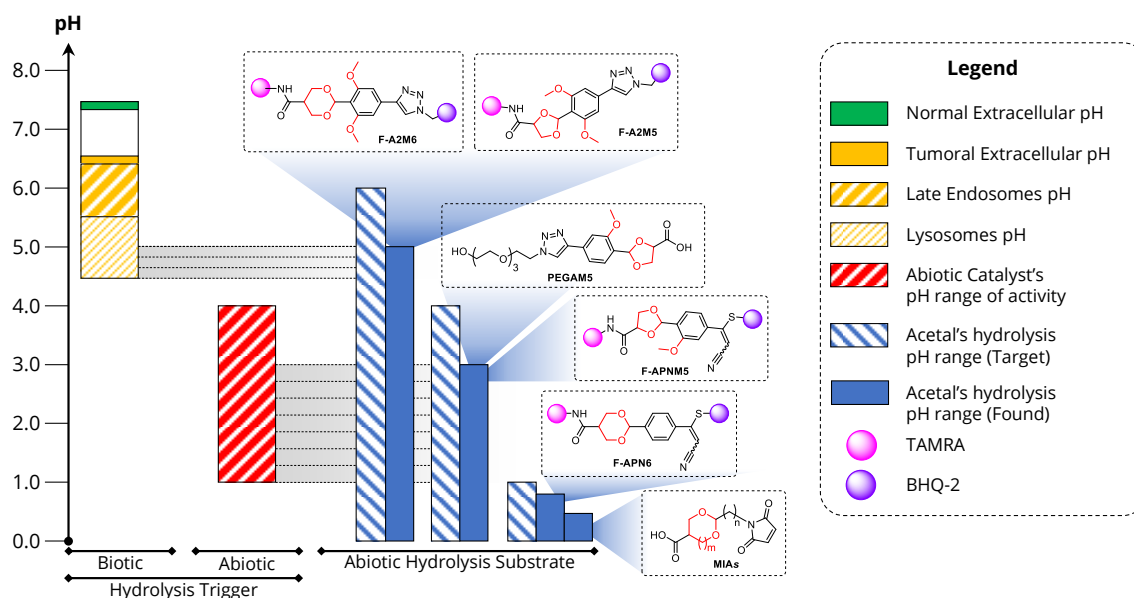
In this chapter we investigated the reactivity of different cyclic acetals towards hydrolysis. Our objective was to identify a little group of cyclic acetals hydrolysable at different pH ranges and with a different chemical nature (hydrophobic or hydrophilic) to match the nature of the abiotic catalyst.

Our investigation led to the identification of nine cyclic acetals. Their structure, reactivity, nature and envisaged applications are listed in the following table.

Acetal	Structure	Hydrolysis pH range	Nature	Applications
F-A2M5		pH < 6	Hydrophobic LogP > 5	Cleavable linkers for bioconjugation techniques
F-A2M6				
F-APNM5			Hydrophobic LogP > 5	Match with an abiotic hydrophobic acid catalyst
PEGAM5		pH < 4	Hydrophilic LogP = 0.22	Match with an abiotic hydrophilic acid catalyst
F-APN6		pH < 1	Hydrophobic LogP > 5	Match with an abiotic extremely acidic hydrophobic catalyst
MIAs (4 acetals)		Stable	Hydrophilic -1.21 < LogP < -0.78	Stable amine-to-thiol linkers for bioconjugation

**Table 3.** Synopsis of the cyclic acetals investigated. The table includes: denomination; chemical structure (acetal and significant motifs are enlightened in red, fuchsia sphere represents the fluorophore TAMRA and violet spheres represents BHQ-2 quencher); pH in which hydrolysis occurs; hydrophobic or hydrophilic nature of the acetal (with calculated and estimated LogP values) and the contemplated applications.

The following figure depicts all the acetals and the pH range in which they are cleaved in comparison to the objectives described in the introduction (Cf. **Figure 1**, page 11). With some neglectable differences, all the objectives described have been successfully achieved.



**Figure 33.** Representation of the objectives pursued and achieved. The first band on the left represent the range of pH covered by cells and extracellular environment. The second red band in the centre represents the range of pH covered by the abiotic acid catalyst. The three striped blue bands on the right represent the pH ranges in which the hydrolysis of different abiotic acetal substrates is supposed to be triggered. Plain blue bands represent the pH ranges in which the hydrolysis of the identified acetals actually occurs, with the corresponding chemical structures. Grey faded horizontal bands are used to show the matching between the pH activity ranges of xenobiotic substrates and the corresponding hydrolysis promoters.

In the next chapter, we will inquire into the abiotic hydrolysis trigger, by identifying two kind of heterogeneous catalysts that could maintain an acidic environment in the buffered fluids: one hydrophobic (to combine with the hydrophobic **F-APN6** and/or **F-APNM5**) and one hydrophilic (to combine with the hydrophilic **PEGAM5**).

# III – IDENTIFICATION OF THE BIOCOMPATIBLE ACID CATALYST

## 1. INTRODUCTION

### 1.1 OBJECTIVES

After describing the synthesis of acetals showing a panel of acido-lability profiles, we will now discuss the constraints and modalities linked to the development of a heterogeneous acidic catalyst which can maintain acidic activity in a highly buffered environment.

To reach this goal, we screened a pool of acidic catalysts for the hydrolysis of the cyclic acetal stable at physiological pH (**F-APN6**, **F-APNM5** and **PEGAM5**) in close-to-*in vivo* reaction conditions, in order to mimic as much as possible the biological environment. As mentioned above when introducing the advantages of the use of FRET probes (Cf. chapter II.1.2, page 27) carrying out a chemical reaction in conditions which are far from classical synthetic chemistry presents many limitations. Concentration of the substrate must be very low, in the order of macro-molar, *i.e.* close to possible plasmatic concentration obtained after injection in mice. Likewise, temperature is fixed to 37 °C, as the normal body temperature and there is no possibility to change parameters like solvent (biofluids), pressure (1 atm) and atmosphere (reactions requiring absence of oxygen and/or water are banned). These limitations are likely to affect the efficiency of many acidic catalysts known to work very effectively for the acetal hydrolysis.

Given the constraints arising from the reaction setup, we did not restrict our investigation to solid Brønsted acid catalysts. We took into consideration acid catalysts falling into the following categories:

- ***Homogeneous catalysts.*** Homogeneous catalysts of different nature (Brønsted acids, Lewis acids) were tested. In case some of them revealed to be able to hydrolyse the acetal in the above-mentioned conditions, the following step would be to chemically bind, immobilise or disperse them into a support. For example, grafting, co-polymerization, absorption and other techniques can be used to make, in other words, an heterogenous version of the homogeneous catalyst.

- **Heterogeneous catalysts.** Heterogeneous catalysis, by definition, includes all the cases where the catalyst and the substrate are in different phases. In this case the catalysts are in solid form, whereas the substrate is in solvated liquid phase, thus the catalysts are referred both as “heterogeneous” and as just “solid”. The catalysis takes place at the surface between the solution and the solid material.<sup>66</sup> This class can be divided into two subcategories:
  - **Hydrophobic catalysts,** in which the solid matrix has a hydrophobic nature (it would adsorb hydrophobic substrates). This kind of catalysts can be combined with the hydrophobic acetals **F-APN6** and **F-APNM5**.
  - **Hydrophilic catalysts,** in which the solid matrix has a hydrophilic nature. Solid catalysts belonging to this class can exchange with the aqueous biofluids used as solvent. Such interaction presents two consequences: the first is that -if paired with an hydrophilic substrate like **PEGAM5**- both substrate and products can diffuse in and out from the polymer matrix; the second is that also ionic exchange can occur between the cations present in the solvent and the protons of the acidic functions supported by the solid, causing an acidification of the biological media and a decrease of the catalyst’s activity. To address the obstacle presented by hydrophilic solid catalysts, we turned to our collaborators Dr. Becht and Dr. Balan at the Institute of Material Science (Institut de Sciences des Matériaux, IS2M, Université Haute-Alsace, Mulhouse). Thanks to their expertise, we could explore the development of a hydrophilic solid catalyst specifically tailored to meet the needs of this project (acidity kept in buffered media and ability to hydrolyse the acetals and release the products).

In view of all the variables and limitations herein described, the catalyst’s screening requires a precise setup and meticulous planning, which is described in the following section.

## 1.2 SETUP OF THE CATALYST’S SCREENING

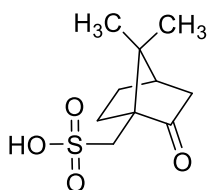
Before starting the actual screening, three points required optimization.

- I. ***The positive and comparison control.*** In the previous tests for the stability in different acidic solutions, an equimolar solution of TAMRA and BHQ was used as positive control, as a measure of a 100% hydrolysis value. In the screenings, there will be a

comparison control in addition. It is an equimolar solution of the reaction substrate (FRET probe) in the presence of a homogeneous strong acid catalyst. The catalyst must be soluble in both aqueous and organic solvents, not interfere with the detection of fluorescence, be easily handled and hydrolyse the acetal within one to three hours. It will be used as comparison of 100% efficiency for the acidic catalysts screened (section 1.2.1)

- II. *The solvent.*** Solvent plays a major role in the outcome of the reaction, especially when dealing with the solubility of hydrophobic acetal substrates in aqueous media. For this reason, the first series of screenings was done in organic protic non-anhydrous solvent (methanol) and then we moved stepwise to the use of biofluids (plasma) as solvent. Intermediate steps include first the use of water as solvent and then in phosphate-buffered saline (PBS) solution (isotonic with biological systems) and finally in plasma (much more complex media, closer to the *in vivo* condition). To facilitate the solubility of the substrate in aqueous solvents water and PBS, a co-solvent (5% of the total reaction volume) was selected (section 1.2.2). Regarding the solubility in plasma, this rich medium can solubilize hydrophobic acetals at low concentration without any further support.
- III. *Experiment conditions.*** Standard concentration of the starting material and of the catalyst, volume of the solutions, preparation of aliquots and method of control will be carefully set up (sections 1.2.4 and 1.2.5).

### 1.2.1 Definition of camphor sulfonic acid as positive control



**Camphor Sulfonic Acid (CSA)**

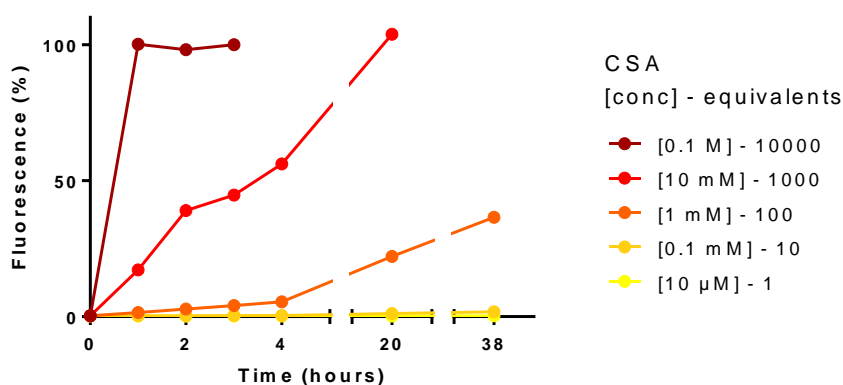
**Figure 34.** Chemical structure of camphor sulfonic acid (CSA).

Camphor sulfonic acid (CSA, **Figure 34**) was chosen as catalyst of comparison for complete hydrolysis after a given time. It is a strong organic acid, soluble in both the solvents of choice for the screening (methanol and water). Since it is a homogeneous catalyst the reaction course can be checked by measuring the fluorescence of the solution.



A screening of various CSA concentrations was performed in order to find the amount to be used as comparison. Reactions were carried out at 37 °C in methanol, under mechanical agitation in plastic Eppendorf tubes, in a volume of 0.3 mL and with a FRET probe (**F-APN6**) concentration equal to 10  $\mu$ M. CSA amount is given both as molar concentration and as number of equivalents with respect to the FRET probe. Indeed, when solid catalysts are used, the molar concentration cannot be used to describe their quantity, while the number of acidic sites can be calculated and related to the weight and composition of the solid. Thus, it appears an interesting information to define CSA concentration also as number of equivalents with respect to the substrate, although this may seem unusual.

At given time, aliquots of 30  $\mu$ L were taken, diluted ten times with water and analysed with a spectrofluorometer (final concentration of the probe = 1  $\mu$ M). The fluorescence values obtained were compared to those on an equimolar solution of TAMRA and BHQ treated the same way. **Figure 35** shows the CSA concentration dependence on the hydrolysis of **F-APN6**. With a CSA concentration of 0.1 M (10K equivalents), the hydrolysis is almost immediate, while at 10 mM, almost 50% of hydrolysis is reached after three hours. This last may be too slow to serve as comparison, while the in the first case is way too fast. For this reason, a 50 mM CSA solution (5K equivalents), was chosen as the one to relate to.



**Figure 35.** Graph of the hydrolysis of **F-APN6** in MeOH in the presence of different amount of camphor sulfonic acid.

### 1.2.2 Identification of the co-solvent for tests in aqueous media

As mentioned in the first section of this chapter, the hydrophobicity of the FRET probes is likely to cause solubility problems even at 10  $\mu$ M concentration. To avoid such issue, the presence of a co-solvent is required for tests in water and in PBS. The test of possible co-solvents was

done using CSA (50 mM) as acid promoter. Reactions were carried out using **F-APNM5** as substrate (10  $\mu$ M) in different combinations of water/5% co-solvent, at 37 °C for one hour. At this point, aliquots were taken, diluted ten times and the emission of fluorescence was measured. Hydrolysis was calculated by comparing the fluorescence given by the reaction mixtures to that of an equimolar solution of TAMRA and BHQ treated the same way. Results are shown in **Table 4**. In the first line the percentage of hydrolysis of **F-APNM5** in methanol (37 °C, 1h) is given as comparison (75%).

Solvent: MeOH		Hydrolysis (%)	
		75%	
Solvent: ultrapure water			
Co-solvent:	Hydrolysis (%)	Co-solvent:	Hydrolysis (%)
DMSO (5%)	40	CDX <sup>(2)</sup> (5wt%)	40
MeOH (5%)	45	CDX (10wt%)	33
BSA <sup>(1)</sup> (5wt%)	25	CDX (5%wt) + PBS (5%)	33

<sup>(1)</sup> BSA = Bovine Serum Albumine

<sup>(2)</sup> CDX =  $\beta$ -Cyclodextrin

**Table 4.** Screening of possible co-solvents. Percentage of hydrolysis is calculated from fluorescence measured after 1h at 37 °C and normalised to the fluorescence given by an equimolar solution of TAMRA and BHQ treated in the same conditions.

Organic co-solvents DMSO and MeOH showed 40% and 45% hydrolysis respectively. Bovine serum albumin was less performant (25% hydrolysis), while  $\beta$ -cyclodextrin used in different percentage showed hydrolysis between 33% and 40%. As expected, the yield was much lower than that obtained in 100% organic solvent methanol (75%). However, MeOH was chosen as co-solvent since it showed the higher degree of hydrolysis and it modifies only marginally the reaction medium.

### 1.2.3 Setup of catalyst's screening general conditions

Once a control catalyst was found and tested and the best mixture water/co-solvent was chosen, the following points regarding the set-up of the acid catalysts screening were addressed.

- **Concentration of the FRET probe and reaction volume.** A concentration of 10  $\mu$ M of the FRET probe was chosen. This concentration allows to easily prepare the 1  $\mu$ M aliquot sample for the spectrophotometer with a dilution of ten times. Moreover, the

reaction solution is sufficiently coloured so that appearance of fluorescence can be spotted by human eye if the sample is put under UV light. The concentration stock solutions of FRET probe in DMSO is between 1 and 2 mM, thereby -with a dilution of around 100 times- the final DMSO content in the reaction mixture is less than 2%. The volume of the reaction used for the previous test of CSA (0.3 mL) was enough to have good manipulation of the reaction vials so it was kept all along the screening.

- **Concentration of the catalyst.** As previously mentioned, the concentration of the acid was chosen according to the profile obtained testing different concentration on the comparison control CSA. For homogeneous catalysts such as CSA, the concentration is 50 mM. For solid catalysts, this amount corresponds to 5000 equivalents of protons, the amount of catalyst will be calculated with respect to the distribution of active acidic sites. Sometimes it was not possible to know the exact composition of the heterogeneous catalyst and so an amount of 10 mg was used.
- **Reaction monitoring (homogeneous catalysts).** The reaction conditions are applied on the positive control (10  $\mu$ M solution of TAMRA and BHQ), on the comparison control (10  $\mu$ M FRET probe and 0.05 M CSA) and on the catalysts subjected to screening (10  $\mu$ M FRET probe and 5000 eq. of catalyst). Aliquots of 35  $\mu$ L were taken from all the samples and diluted ten times with water. 300  $\mu$ L of the obtained solutions were transferred to a 96-well plate (two replicates of 150  $\mu$ L each) and fluorescence was measured with a spectrofluorometer. Obtained values are normalized to the fluorescence of the positive control and the efficiency of the catalysts is compared to the one of CSA.
- **Reaction monitoring (heterogeneous catalysts).** There are three possible scenarios when using heterogeneous catalysts, which impact the monitoring procedures. They will be described in the following paragraph.

#### **1.2.4 Heterogeneous catalysts: reaction monitoring**

As anticipated, the screening revealed that many solid catalysts are adsorbent: they act by sorption of the hydrophobic substrate in a non-specific way, without releasing it.<sup>67</sup> As a consequence, there can be three possible case scenario when an heterogeneous catalyst is tested. Each scenario requires a different approach for the monitoring of the reaction.

- In the first case, the catalyst is not adsorbent and both the FRET probe and the eventual products remain in solution. The hydrolysis could be checked with a

spectrofluorometer as in the case of homogeneous catalysts, but the presence of solid particles should be considered in the preparation of the sample for spectrophotometer. Hence, the aliquots can be either filtrated and then diluted, either centrifugated and the supernatant is taken and diluted.

- In the second case, the catalyst adsorbs completely the probe without releasing it. Given the variety of catalysts tested, from powders to gels, from clays to polymeric beads, from transparent to coloured, the monitoring of the reaction was qualitative. The reaction vial was put under a UV source and the eventual fluorescence of the polymer given by the hydrolysed FRET-acetal was evaluated by comparison with the fluorescence emitted by the same catalyst soaked with an equimolar amount of TAMRA and BHQ. This qualitative method was accurate enough for the screenings. Once one or more catalysts were selected, an effort was put to find a quantitative or semi-quantitative way to analyse the efficiency of the catalysts (section 2.5, page 96).
- The third case is a mix of the previous two: the catalyst adsorbs only partially the probe. In this case, both the monitoring methods are applied and reaction outcomes are interpreted accordingly.

Once every aspect of the catalyst's screening was analysed, we proceed with the identification of a hydrophobic and a hydrophilic solid catalysts which fulfil our requirements. Section 2 of this chapter describes the route which led to the identification of a heterogeneous catalyst with a hydrophobic matrix, while section 3 is dedicated to the development of the hydrophilic solid catalyst in collaboration with the Institute of Material Science. Ultimately, in section 4 we dealt with a more accurate investigation of the core acidity of the selected catalysts.

## 2. IDENTIFICATION OF A HYDROPHOBIC HETEROGENEOUS ACID CATALYST

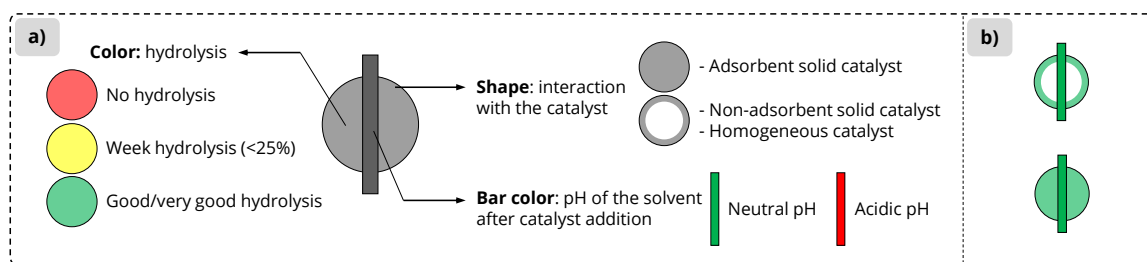
The first three sections of this chapter are devoted to the screening of homogenous and heterogeneous catalysts (both commercial and synthesized in laboratory). For a comprehensive table of all the catalyst screened, see Appendix A (page 247). The following sections focus on **i)** the adsorbing properties of selected catalysts; **ii)** the efforts to quantify the hydrolysis in adsorbent solid catalysts; **iii)** the deeper investigation of the selected catalyst (pre-treatment and different forms); **iv)** the test of the selected hydrophobic catalyst with the hydrophilic acetal **PEGAM5**.

### 2.1 SCREENING OF HOMOGENEOUS CATALYSTS

The first homogeneous catalysts were tested in the early stage of the project only with the parent acetal probe **F-APN6** (**Table 5**, entries 1-11), while the latter were tested also with **F-APNM5** (**Table 5**, entries 12-15). Their performance was compared to that of CSA in the chosen solvents (**Table 5**, entries 0a, 0b). Reactions were conducted in the conditions settled previously. As a reminder: [substrate] = 10  $\mu$ M, [catalyst] = 0.05 M, T = 37 °C, V = 0.3 mL, solvent = methanol *or* water+5%MeOH *or* PBS+5%MeOH *or* plasma. Hydrolysis was monitored by measuring the fluorescence of the solution.

**Table 5** (next page) shows the results obtained after 3 hours. For the sake of clarity and fast visualization of such an amount of data, the results are presented in a simple way. As elucidated in **Figure 36a**, the symbol used in the table is the graphical depiction of three separate information: **(i)** the degree of hydrolysis at 3 hours (colour of the sphere), **(ii)** the interaction of the FRET probe with the catalyst (shape of the sphere), **(iii)** the pH value of the aqueous solutions after addition of the catalyst, measured with pH paper (colour of the vertical bar).

The starting pH values are: pH  $\approx$  6,5 for ultrapure water and pH = 7,4 for PBS and plasma. Ionic exchange with the catalyst can modify the proton initial concentration. Indeed, an acidification of the reaction media was expected for all the tested homogeneous strong acid catalysts. Ideally, the perfect catalyst would be represented by the symbols in **Figure 36b**. Beside the kind of interaction with the probe, we look for a catalyst that hydrolyses the acetal (green sphere = good hydrolysis) without affecting the pH of the solvent (green bar: neutral pH).



**Figure 36.** **a)** Legend of the symbol used to describe the efficiency of a catalyst, its interaction with the FRET probe and with the proton concentration of the solvent. **b)** Representation of the wanted reaction outcome.

Entry	Catalyst	FRET probe	Solvent			
			MeOH	Water	PBS	Plasma
0a	CSA	F-APN6	○	⊗	⊗	⊗
0b		F-APNM5	○	⊗	⊗	⊗
1	AlCl <sub>3</sub>	F-APN6	○	X	X	X
2	CeCl <sub>3</sub> /NaI	F-APN6	○	X	X	X
3	CAN <sup>(1)</sup>	F-APN6	○	X	X	X
4	CuCl <sub>2</sub>	F-APN6	○	X	X	X
5	FeBr <sub>3</sub>	F-APN6	○	X	X	X
6	FeCl <sub>3</sub>	F-APN6	○	X	X	X
7	ZnBr <sub>2</sub>	F-APN6	○	X	X	X
8	Zn(OTf) <sub>3</sub>	F-APN6	○	X	X	X
9	Sc(OTf) <sub>3</sub>	F-APN6	○	X	X	X
10	In(OTf) <sub>3</sub>	F-APN6	○	X	X	X
11	Yt(OTf) <sub>3</sub>	F-APN6	○	X	X	X
12	PAASA <sup>(2)</sup>	F-APN6	○	⊗	⊗	X
13		F-APNM5	○	⊗	⊗	X
14	PacMA <sup>(3)</sup>	F-APN6	○	X	X	X
15		F-APNM5	○	⊗	X	X

<sup>(1)</sup> CAN = Cerium Ammonium Nitrate;

<sup>(2)</sup> PAASA = Poly(2-acrylamido-2-methyl-1-propanesulfonic acid);

<sup>(3)</sup> PacMA = Poly(acrylic acid-co-maleic acid)

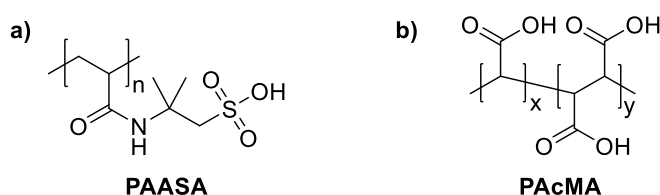
**Table 5.** Screening of homogeneous acidic catalysts. Reactions were monitored after 3 hours. pH value is determined with a universal indicator a few minutes after the addition of the catalyst, there are no changes in pH after 3 hours. "X" is for "not tested".

Comparison control homogeneous acid CSA (entries 0a, 0b) showed very good hydrolysis in methanol for both the acetals **F-APN6** and **F-APNM5**, as previously observed (section 1.2.1 of this chapter). Clearly, when the solvent was shifted to aqueous (water, PBS) the proton concentration was affected (acidic pH, red bar), the performance though was not the same for the two substrates, only **F-APNM5** was hydrolysed in such conditions. Evidently, proton concentration was not enough high for the more stable **F-APN6**. When CSA is used in plasma it causes the precipitation of the protein content, which lowered also the hydrolysis yield of **F-APNM5**, the acetal is probably trapped in the precipitate.

Regarding all the Lewis acid tested (entries 1-11), none of them showed hydrolysis when the reaction was carried in organic solvent methanol, thus their investigation was stopped at this stage.

**PAASA** (entries 12-13), a commercial linear soluble polymer bearing sulfonic acid as active moiety (**Figure 37a**) showed a very good degree of hydrolysis, slightly better than that of CSA. Eventually, it was chosen as acidic motif to be supported on a solid material. Design, synthesis and results are presented and discussed on the sections dedicated to the screening of synthesised heterogeneous catalysts (Section 2.2.5, page 91) and to the hydrophilic catalysts (Section 3, page 116).

**PAcMA** (entries 14-15) is a commercial soluble linear polymer bearing acrylic and maleic acid functions (**Figure 37b**). This weak organic acid was able to hydrolyse the acetal **F-APNM5** only partially. When tested in water, it did not alter the pH of the water solution, unfortunately in this case hydrolysis was not achieved as well.



**Figure 37.** Chemical structure of **a) PAASA** and **b) PAcMA** linear polymers.

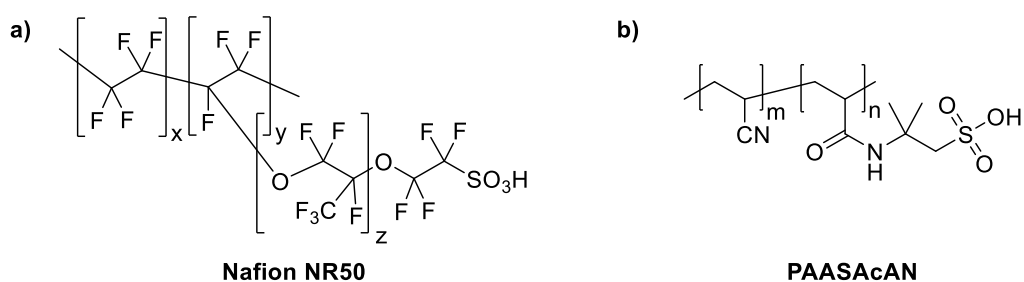
In conclusion, we identified **PAASA** as acid to be supported on a solid material and, given the poor results obtained with almost all the homogeneous catalysts, we decide to focus on heterogeneous solid catalysts.

## 2.2 SCREENING OF HETEROGENEOUS CATALYSTS

Reactions were conducted in the conditions settled previously. As a reminder: [substrate] = 10  $\mu$ M, [catalyst] = 0.05 M, T = 37 °C, V = 0.3 mL, solvent = methanol *or* water+5%MeOH *or* PBS+5%MeOH *or* plasma. Hydrolysis was monitored according to the interaction of the solid solvent with the substrate, as described previously in section 1.2.4.

### 2.2.1 Screening of commercial catalysts

A variety of commercial solid acid catalysts were screened, starting from some well-known ionic exchange resins and clays. Some solid Lewis acids were tested, as well as perfluorinated resin Nafion NR50 (acidic function: sulfonic acid, **Figure 38a**) and poly(2-acrylamido-2-methyl-1-propanesulfonic acid-co-acrylonitrile) (**PAASAcAN**, **Figure 38b**).



**Figure 38.** Chemical structure of heterogeneous catalysts **a)** Nafion NR50 and **b)** PAASAcAN.

To recall the possible monitoring methods (cf. section 1.2.4, page 71), at this stage of the project the fluorescence emitted by the solid is qualitatively evaluated by comparing it with the fluorescence emitted by the same solid catalyst soaked with an equal amount of TAMRA and BHQ. Thus, for the colour code here used (cf. **Figure 36a**), a plain green circle means that the fluorescence observed under the UV lamp is comparable to that of the positive control, while a plain yellow circle stands for a level of fluorescence much lower than that of the positive control but still well detectable by human eye.



Entry	Catalyst	FRET probe	Solvent			
			MeOH	Water	PBS	Plasma
16	Amberlyst A-15	F-APN6	●	●	●	X
17		F-APNM5	●	●	●	●
18	Amberlyte	F-APN6	●	X	X	X
19	CG-50	F-APNM5	●	X	X	X
20	Dowex	F-APN6	●	X	X	X
21	50WX8-200	F-APNM5	●	●	●	X
22	Montmorillonite	F-APN6	●	X	X	X
23	KSF	F-APNM5	●	X	X	X
24	Montmorillonite	F-APN6	●	X	X	X
25	K10	F-APNM5	●	X	X	X
26	Ti(IV) silicate	F-APN6	○	X	X	X
27	Nb <sub>2</sub> O <sub>5</sub>	F-APN6	○	X	X	X
28	Nafion NR-50	F-APN6	●	●	●	X
29		F-APNM5	●	●	●	●
30	PAASAcAN <sup>(1)</sup>	F-APN6	●	●	X	X
31		F-APNM5	●	●	●	X

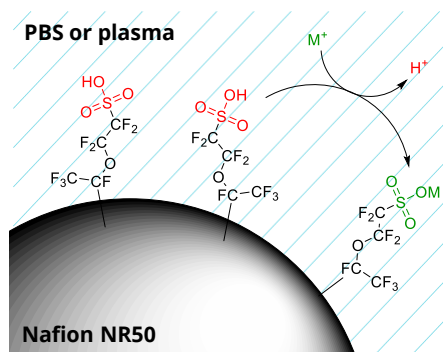
<sup>(1)</sup> PAASAcAN = Poly(2-acrylamido-2-methyl-1-propanesulfonic acid-co-acrylonitrile)

**Table 6.** Screening of commercial heterogeneous catalysts. “X” stands for “not tested”.

Heterogeneous catalysts Amberlyte, Montmorillonite KSF, Montmorillonite K10, Titanium(VI) silicalite and Niobium Oxide (**Table 6**, entries 18, 19, 22-27) do not trigger hydrolysis in the applied conditions. Dowex 50WX8-200 (entries 20, 21) and **PAASAcAN** (entries 30, 31) have somewhat good results in methanol, especially with the **F-APNM5** substrate but they are not strong enough in aqueous solvents.

Amberlyst A15 (entries 16, 17) and Nafion NR50 (entries 28, 29) have similar profiles. They show very good hydrolysis in methanol as well as in water and PBS: fluorescence of the solid is comparable to that of the corresponding positive control for both catalysts. Regarding the value of pH in solution, it was observed that Nafion NR50 and Amberlyst A-15 do not change the pH of ultrapure water, while buffered PBS and plasma solutions were acidified. We

theorized that the sulfonic acid motifs undergo cationic exchange with the metal cations present in solution, generating a sulfonate motif and releasing  $H^+$  in solution (**Figure 39**).



**Figure 39.** Representation of the cationic exchange between the proton of the sulfonic acid and metal ion present in the buffered solutions.

This could explain the observed acidification of PBS and plasma and the precipitation of the protein content observed in plasma. We also hypothesized that the massive precipitation of proteins in plasma obstructs the progress of hydrolysis by preventing the acetal to come in contact with the catalyst. According to our hypothesis, the absence of metal ions in ultrapure water ("mQ water") prevents the cationic exchange, resulting in unchanged proton concentration in solution. This applies to all the heterogeneous catalysts herein tested.













The results obtained till this point suggest that the sulfonic acid (present in CSA, **PAASA**, **PAAcMA**, Amberlyst A-15 and Nafion NR50) is the most efficient acid among those tested, but in order to be useful it is important to find a way to avoid acidification of the buffered media. This work will be described in section 2.6 (page 104). In the next three paragraphs we describe the screening of synthetic catalysts. We divided the paragraphs according to the nature and origin of the catalysts.

### **2.2.2 Screening of synthetic catalysts: modified silica**

Many examples of easily-prepared supported acids are present in literature, since the use of heterogenous catalysts in organic synthesis has many advantages in terms of sustainability.<sup>68</sup> They include examples of adsorption of the acid into a porous material, functionalization through weak bonding (hydrogen bond, Wan der Waals interactions), strong ionic interactions and covalent bonding. The last category is the finest for this project since the release of the active species in salt solutions (PBS and plasma) must be avoided.

Among the described synthetic supported acids, four procedures have been selected. All of them are functionalization of silica ( $\text{SiO}_2$ ) achieved in one step. The acids are both Brönsted and Lewis acids: phosphomolybdic acid ( $\text{H}_3\text{PMo}_{12}\text{O}_{40}$ , PMA),<sup>69</sup> sulfuric acid ( $\text{H}_2\text{SO}_4$ ),<sup>70,71</sup> perchloric acid ( $\text{HClO}_4$ )<sup>72-74</sup> and boron trifluoride ( $\text{BF}_3$ ).<sup>75</sup> Their preparation is described in chapter VI (Experimental procedures, section 1.8.1, page 209).

The following table shows the results obtained with FRET probe **F-APN6** as substrate; the screening was performed before the completion of **F-APNM5** synthesis.

Entry	Catalyst		Solvent			
			MeOH	Water	PBS	Plasma
0a	CSA					
32	PMA/SiO <sub>2</sub>	fresh <sup>(1)</sup>		X	X	X
33	HClO <sub>4</sub> /SiO <sub>2</sub>	fresh <sup>(1)</sup>		X	X	X
34		fresh <sup>(1)</sup>		X	X	X
35	BF <sub>3</sub> /SiO <sub>2</sub>	washed <sup>(2)</sup>		X	X	X
36		washing sol. <sup>(3)</sup>		X	X	X
37		fresh <sup>(1)</sup>		X	X	X
38	H <sub>2</sub> SO <sub>4</sub> /SiO <sub>2</sub>	washed <sup>(2)</sup>		X	X	X
39		washing sol. <sup>(3)</sup>		X	X	X

<sup>(1)</sup> "fresh" = the catalyst is used without any treatment after its synthesis;

<sup>(2)</sup> "washed" = the catalyst is washed in methanol/water mixture 9:1 for 1 hour, separated from the washing solution, let to dry and tested;

<sup>(3)</sup> "washing sol." = the FRET probe is added to the washing solution recovered from the above-mentioned washing;

**Table 7.** Screening of functionalized silica with FRET probe **F-APN6**. PMA/SiO<sub>2</sub> (entry 34) and H<sub>2</sub>SO<sub>4</sub>/SiO<sub>2</sub> (entry 37) gave a good level of hydrolysis, unfortunately this was due to leaking of the acid from the support material, as proved by the results obtained after catalyst's washing (entries 35, 36, 38, 39). "X" is for "not tested".

PMA/SiO<sub>2</sub> and HClO<sub>4</sub>/SiO<sub>2</sub> did not work in methanol (entries 32-33), while BF<sub>3</sub>/SiO<sub>2</sub> and H<sub>2</sub>SO<sub>4</sub>/SiO<sub>2</sub> showed very good hydrolysis in the same solvent, 48% and 83% respectively at t = 4 hours (green circle, entries 34, 37). For those two, it was investigated if the hydrolysis came from the acidity of the catalyst itself or if it was due to a leak of the acid from the support. The catalysts were washed with a 9:1 methanol/water mixture ("washing solution") for 1 hour, separated from the washing solution, let to dry and tested again in methanol to see if their

performance didn't change after washing (entries 36, 39). Also, the recovered washing solutions were tested in the presence of the substrate only, in order to see if they were acidified by interaction with the supported acid (entries 35, 38). The washed supported silica showed less hydrolytic activity than the original catalyst (cf. entries 35 vs 34, 38 vs 37), while the washing solution were clearly enough acidified during the washing treatment to deliver the hydrolysis of the acetal: 23% and 60% after 4 hours for  $\text{BF}_3/\text{SiO}_2$  and  $\text{H}_2\text{SO}_4/\text{SiO}_2$  washing solutions respectively (entries 36, 39).

Such acidification could be due to **i)** cationic exchange with the washing solution or **ii)** release of the acid caused by an incomplete reaction with silica. At this point of the screening we decided to not investigate the nature of such phenomenon and we pursued with the test of other synthetic catalysts.

### 2.2.3 Screening of synthetic catalysts from IS2M



















As previously mentioned, the collaboration with Dr. Jean-Michel Becht from the Institute of Materials in Mulhouse (IS2M, Université Haute-Alsace) allowed us to test three acid supported catalysts of different nature prepared in the groups of Dr. Camelia Ghimbeu (**HASG-400-ox** and **Lignine-400**) and Prof. Jocelyne Brendle (**ALA014**, **Table 8**).

Catalyst	Description
<b>HASG-400-ox</b>	Obtained by oxidation treatment of <b>HASG-400</b> (porous commercial graphite) using concentrated nitric acid ( $\text{HNO}_3$ ) at 60°C for 1 hour, then at 100°C for 30 minutes. <sup>76</sup>
<b>Lignine-400</b>	Lignin alkali (low sulphonate content) was pre-carbonized at 400 ° C for 1 h under Argon. Heating at low temperature (400 ° C) ensures the decomposition of lignin to obtain a carbon rich in oxygen and sulfur compounds.
<b>ALA014</b>	Information not available. Aspect: white powder.

**Table 8.** Heterogeneous catalysts provided by Dr. Becht (IS2M, Université Haute-Alsace, Mulhouse).

Results of the screening are shown in **Table 9**. As comparison, also the commercial **HASG-400** was tested. All the catalysts are adsorbent and unfortunately almost all of them were not able to trigger the hydrolysis of both **F-APN6** and **F-APNM5** acetals. Only **ALA014** showed some hydrolysis when the reaction was carried out in methanol with the less stable **F-APNM5**.

Unfortunately, no fluorescence was detected when the reaction was performed in aqueous solvents (water and PBS); the pH of the solution was maintained neutral.

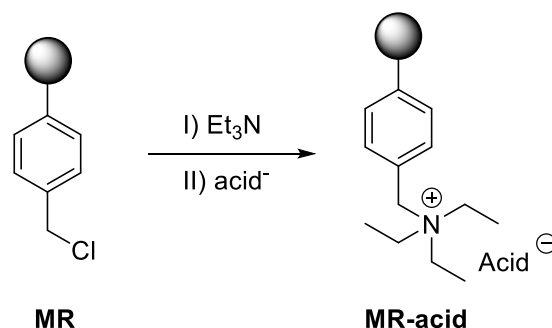
Entry	Catalyst	FRET probe	Solvent			
			MeOH	Water	PBS	Plasma
0a	CSA	F-APN6				
0b		F-APNM5				
40	HASG-400	F-APN6		X	X	X
41		F-APNM5		X	X	X
42	HASG-400-ox	F-APN6		X	X	X
43		F-APNM5		X	X	X
44	ALA014	F-APN6		X	X	X
45		F-APNM5				X
46	Lignine 400	F-APN6		X	X	X
47		F-APNM5		X	X	X

**Table 9.** Screening of synthetic acid catalysts provided by IS2M.

#### 2.2.4 Screening of synthetic catalysts: modified Merrifield resin

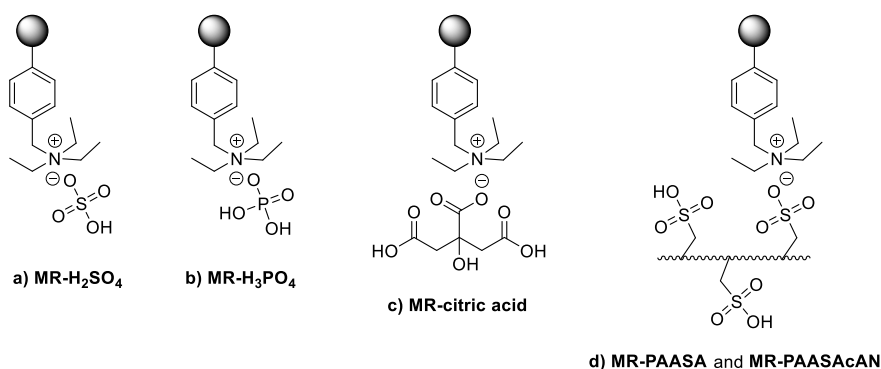
Inspired by the good results obtained with Amberlyst A-15, a polystyrene cross-linked polymer functionalized with aryl sulfonic acids, we used Merrifield resin as base for functionalization. MR is a polystyrene cross-linked with 4-vinylbenzyl chloride, probably the most frequently employed resin in solid-phase synthesis.<sup>77,78</sup>

The functionalization was performed by Dr. Sébastien Dautrey in our laboratory, it is described in the experimental section (section 1.8.2, page 209) and illustrated in **Figure 40**.



**Figure 40.** Representation of the modification of Merrifield resin. **MR** = Merrifield resin; **MR-acid** = Merrifield resin functionalized with acid.

The acid chosen are: sulfuric acid ( $\text{H}_2\text{SO}_4$ , **Figure 41a**), phosphoric acid ( $\text{H}_3\text{PO}_4$ , **Figure 41b**), citric acid **Figure 41c**) and the two linear sulfonic acid polymers **PAASA** and **PAASAcAN** (**Figure 41d**). The first three are ionically bounded through one of the acidic protons, while the other(s) is let free for the hydrolysis of the acetal. **PAASA** and **PAASAcAN** linear polymers are supposed to be ionically bounded to the resin through some of the sulfonic acid moieties, leaving a major part of them free to interact with the acetal substrate. The following table shows the results obtained by testing them in methanol and water.



**Figure 41.** Chemical structures of Merrifield resin modified with **a)**  $\text{H}_2\text{SO}_4$ , **b)**  $\text{H}_3\text{PO}_4$ , **c)** citric acid, **d)** **PAASA** and **PAASAcAN**.

Entry	Catalyst	FRET probe	Solvent			
			MeOH	Water	PBS	Plasma
0a	CSA	F-APN6				
0b		F-APNM5				
48	MR-PAASA <sup>(1)</sup>	F-APN6			X	X
49		F-APNM5			X	X
50	MR-PAASAcAN <sup>(2)</sup>	F-APN6			X	X
51		F-APNM5			X	X
52	MR- $\text{H}_3\text{PO}_4$	F-APN6			X	X
53		F-APNM5			X	X
54	MR- $\text{H}_2\text{SO}_4$	F-APN6			X	X
55		F-APNM5			X	X
56	MR-Citric Acid	F-APN6			X	X
57		F-APNM5			X	X

MR = Merrifield resin; <sup>(1)</sup> **PAASA** = Poly(2-acrylamido-2-methyl-1-propanesulfonic acid)

<sup>(2)</sup> **PAASAcAN** = Poly(2-acrylamido-2-methyl-1-propanesulfonic acid-co-acrylonitrile)

**Table 10.** Screening of modified Merrifield resins.

None of the modified resins worked, even if it is worthy to mention that MR-**PAASA** promoted some degree of hydrolysis in methanol with **F-APNM5** as substrate (entry 49), confirming that sulfonic acids are the most performing acidic agents for the hydrolysis of these cyclic acetals.

### 2.3 SCREENING'S RESULTS: SYNOPSIS

**Table 11** gathers the homogeneous and heterogeneous catalysts among those screened that showed promising activity in both the aqueous solvents (water+5%MeOH and PBS+5%MeOH). Interestingly, they all have in common the sulfonic acid as acidic function.

Entry	Catalyst	FRET probe	Solvent			
			MeOH	Water	PBS	Plasma
0a	CSA	F-APN6				
0b		F-APNM5				
12	PAASA	F-APN6				X
13		F-APNM5				X
16	Amberlyst A-15	F-APN6				X
17		F-APNM5				
28	Nafion NR50	F-APN6				X
29		F-APNM5				

**Table 11.** Recall of the acidic catalysts who showed good hydrolysis in water and PBS.

The soluble linear polymer **PAASA** showed a similar outcome to CSA. They both discriminated between the cleavability of the two substrates tested, with **F-APNM5** being hydrolysed, while **F-APN6** remained intact.

Amberlyst A-15 and Nafion NR50 showed a good degree of hydrolysis for both the acetals. As a reminder, the hydrolysis is related to the fluorescence emission. In the case of Nafion NR50 and Amberlyst A-15, the fluorescence emitted by the solid is comparable to that emitted by the corresponding catalyst soaked with an equimolar amount of TAMRA and BHQ.

All the catalysts listed in **Table 11** presented the same drawback when tested in buffered PBS and plasma: they caused acidification of the media, which we supposed was due to cationic exchange (cf. paragraph 2.2.1, page 85).

We addressed this issue in different ways according to the nature of the catalyst. The homogeneous ones could be bind to a solid support (cf. Merrifield resins described above and section 3.2.1, page 117), while the heterogeneous ones were object of further studies, exposed in the following sections.

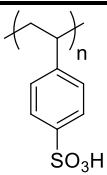
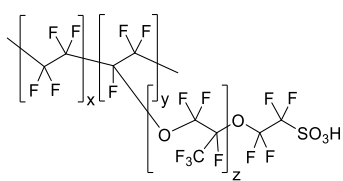
- Section 2.4 will focus on the investigation of the adsorbance rate of Nafion NR50 and Amberlyst A-15, in order to identify the catalyst with faster adsorption.
- Section 2.5 will investigate three different approaches for the quantification of the fluorescence. Indeed, at this point of our work, we wanted to find a method to quantify the degree of hydrolysis more precise than the qualitative check of fluorescence appearance under UV lamp.
- In section 2.6 we addressed the Nafion cationic exchange in solution which cause the pH of PBS and plasma to lower (cf. section 2.2.1, page 85). This is probably the most important investigation described in this chapter because it addresses the main challenge arising from this project, related to the preservation of the catalyst acidity in buffered media.
- Sections 2.7 and 2.8 are dedicated to the investigation of other commercially available forms of Nafion and on the test with the hydrophilic probe **PEGAM5**, respectively.

#### 2.4. INVESTIGATION OF THE ADSORBANCE RATE OF NAFION NR50 AND AMBERLYST A-15

As explained in the introduction (chapter 1.2, page 10) for a first *in vivo* proof of concept it is essential to be able to detect the fluorescence of the probe coming from the acid abiotic material. For this reason, the rate of substrate adsorbance of Nafion NR50 and Amberlyst A-15 was compared.

**Table 12** shows the chemical structures of the two ion-exchanging resins and compares some characteristics such as surface area, pore volume and capacity.<sup>79</sup>

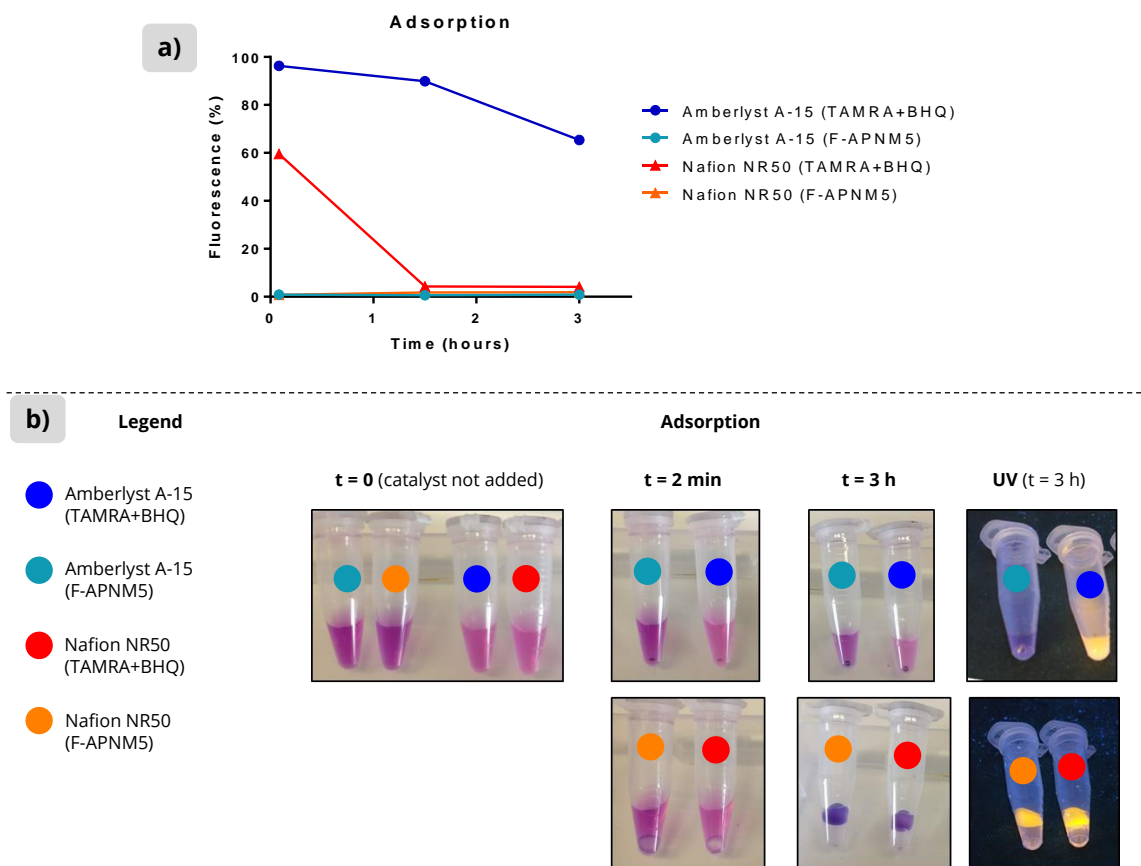


	Amberlyst A-15	Nafion NR50
<b>Structure</b>	 <p>PS + 20% DVB</p>	
<b>Surface area</b>	0.35 m <sup>2</sup> /g	0.02 m <sup>2</sup> /g
<b>Pore volume</b>	4.8 mL/g	non porous
<b>Capacity</b>	120 meq(H <sup>+</sup> )/g	0.9 meq(H <sup>+</sup> )/g

PS = polystyrene; DVB = divinylbenzene

**Table 12.** Comparison between Amberlyst A-15 and Nafion NR50.

To quantify the adsorption, a 10  $\mu\text{M}$  solution of FRET-acetal probe **F-APNM5** and an equimolar solution of TAMRA and BHQ (0.3 mL) were treated with 1 bead of the catalyst at 37  $^{\circ}\text{C}$ . The coloured solutions allowed to follow the adsorbance phenomenon in real time: the solution turned from violet to transparent and the transparent Nafion NR50 beads became coloured. The solution of TAMRA and BHQ allowed to quantify the adsorption by measuring the fluorescence of the solution, which decreased over time, as the chemicals were adsorbed. At given times, aliquots of the solutions were taken, diluted with water (final concentration: 1  $\mu\text{M}$ ) and analysed at the spectrophotometer. The fluorescence emission was related to that of a 1  $\mu\text{M}$  solution of TAMRA and BHQ in the same solvent, in order to obtain values as percentage of the initial quantity (**Figure 42a**). Pictures of the reaction vials were taken before the catalyst addition, at  $t = 2$  minutes and at  $t = 3$  hours under artificial light and at  $t = 3$  hours under UV light (**Figure 42b**).



**Figure 42. a)** Adsorption profiles of Nafion NR50 and Amberlyst A-15 by means of fluorescence emitted by TAMRA remained in solution. **b)** Pictures of the samples taken at  $t = 0$ ,  $t = 2$  minutes and  $t = 3$  hours under artificial light and at  $t = 3$  hours under UV light (using a laboratory UV lamp). The vials are identified by coloured dots. Blue and light blue dots identify Amberlyst A15 samples, red and orange dots identify Nafion NR50 samples.

According to the profile obtained and the real-time monitoring of the coloured solutions, Nafion NR50 completely adsorb the FRET probe, TAMRA and BHQ in less than 1.5 hours, while Amberlyst A15 do not show complete adsorption even after 3 hours.

Pictures taken under artificial and UV light at  $t = 3$  hours revealed that:

- BLUE DOT. Solution of TAMRA and BHQ in presence of Amberlyst A-15 is still coloured and fluorescent: the adsorption was not complete;
- LIGHT BLUE DOT. Solution of **F-APNM5** in presence of Amberlyst A-15 is still coloured (the adsorption was not complete) and little fluorescence is emitted by the bead (the part of FRET acetal adsorbed is hydrolysed);
- RED DOT. Solution of TAMRA and BHQ in presence of Nafion is clear, the bead is coloured and fluorescent: all the TAMRA and BHQ were adsorbed;

- ORANGE DOT. Solution of **F-APNM5** in presence of Nafion NR50 is transparent and the bead is coloured and fluorescent: the acetal was completely adsorbed and hydrolysed inside the bead.

Given the results obtained, Nafion NR50 was the catalyst of choice and it was object of further investigations listed above (cf. page 93). In particular, in the next section we investigate three methods for the quantification of hydrolysis in solid adsorbent catalysts, with a focus on Nafion NR50. Note that from now on in the text, Nafion NR50 will also be referred simply as Nafion, and Amberlyst A-15 as Amberlyst, unless otherwise specified.

## 2.5 APPROACHES TOWARDS THE QUANTIFICATION OF HYDROLYSIS IN SOLID ADSORBENT CATALYSTS

During the screening, given the variety of catalyst's forms and nature, the hydrolysis was qualitatively assessed through the spotting of fluorescence under UV light. The pictures showed in the previous paragraph (**Figure 42b**) are an example of what we observed when analysing the catalysts under UV lamp. This method revealed to be fast and accurate enough to distinguish among a total of 60 reactions involving adsorbent heterogeneous catalysts (see Appendix A for a comprehensive table of all the catalysts' screening, page 247). At this stage, being the investigation focused only on Nafion, it would be suitable to develop a method for the quantification of the hydrolysis in solid Nafion beads. A total of three approaches were studied and they are presented in the following sections.

### **2.5.1 First quantitative hydrolysis evaluation method: wash out of reaction products**

A first attempt to quantify the yield of the reaction was to try to extract the products of the hydrolysis from the polymer at a given time. Their release in solution would allow the quantification through fluorescence measurement.

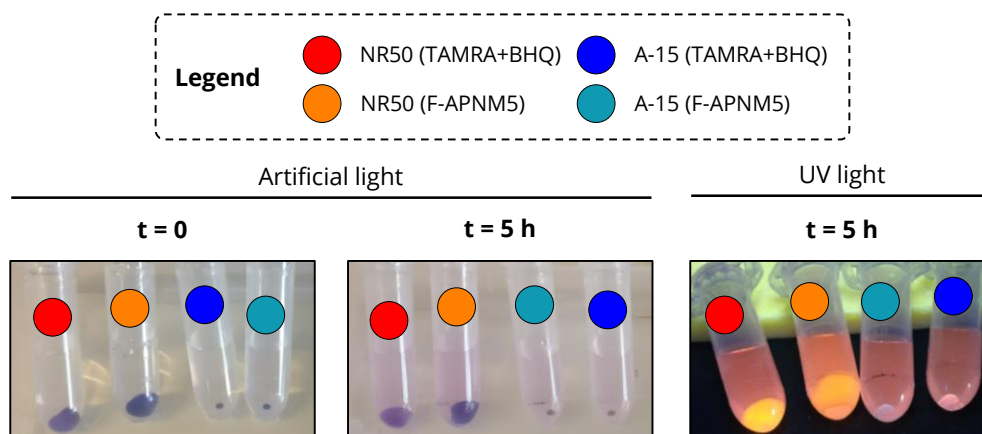
Two beads of the polymer were added to a 10  $\mu$ M solution of the FRET probe **F-APNM5** and of the mixture **TAMRA+BHQ** in methanol. The reaction vials were left at 37 °C under mechanical agitation for 3 hours. Within this time the bead turned fluorescent, as in the previous experiment. Then the beads were separated from the solvent and put in a 1 mL mixture 1:1 of DMSO and HCl (3 M aq.) under agitation at room temperature. This mixture allowed the slow release of the chemicals in solution, the colour of the solvent turned to light violet and emits fluorescence. After 24 hours, an aliquot of the solvent mixture was taken, diluted and analysed

at the spectrophotometer. Values obtained are related to those of an equimolar mixture of TAMRA and BHQ in the same solvent mixture.

The two percentage values obtained indicate how much of **TAMRA-NH<sub>2</sub>** and **TAMRA-NHCO-diol** (product of the hydrolysis) was released within 24 hours. Assuming that the non-specific interaction between the polymer and the two forms of TAMRA is almost the same, the amount of the two chemicals in solution can be compared to determine the yield of the reaction, according to the following equation:

$$\text{Yield of Hydrolysis (\%)} = \frac{\% \text{ of TAMRA - NHCO - diol released from bead}}{\% \text{ of TAMRA - NH}_2 \text{ released from bead}} * 100$$

This method was tested on commercial Nafion NR50 and Amberlyst 15. **Figure 43** shows picture taken under UV light at t = 0 and t = 5 h of the release process. Fluorescence was measured after 24 hours and the percentages of the chemical released are reported on **Table 13**.



**Figure 43.** Pictures of Nafion NR50 and Amberlyst A15 in the releasing solvent mixture at t = 0 (under artificial light) and at t = 5 hours (under artificial and UV light). Vials are identified by coloured dots according to the legend.

Entry	Catalyst	Probe(s)	Release (%)	Ratio
1	Amberlyst A15	TAMRA+BHQ	21,64	<b>0,987</b>
2		<b>F-APNM5</b>	21,36	
3	Nafion NR50	TAMRA+BHQ	34,84	<b>1,57</b>
4		<b>F-APNM5</b>	54,69	

**Table 13.** Fluorescence values measured after 24 hours are reported as percentage of the positive control (equimolar solution of **TAMRA** and **BHQ** in 1 mL of the releasing solvent mixture. Ratio between the values of **TAMRA+BHQ** and **F-APNM5** are reported.

**TAMRA-NH<sub>2</sub>** and **TAMRA-NHCO-diol** are released from Amberlyst almost at the same rate (~21% of releasing after 24 hours in DMSO/HCl). 35% of **TAMRA-NH<sub>2</sub>** was extracted from Nafion after the same time, while **TAMRA-NHCO-diol** released was 55% (1.57 times more than **TAMRA-NH<sub>2</sub>**). These discordant values suggested that our hypothesis about the similar rate of extraction between the two chemicals was probably incorrect. According to the ratio between the fluorescence values (= 1.57) **TAMRA-NHCO-diol** is released faster than **TAMRA-NH<sub>2</sub>**.

Therefore, a comparison between the amount of **TAMRA-NH<sub>2</sub>** released and the amount of **TAMRA-NHCO-diol** released under the same conditions cannot be used to quantify the hydrolysis. Moreover, this approach takes too much time and requires removing the bead from plasma at a given time, so the reaction can't be monitored over a period with multiple checks.

Consequently, it was endeavored to establish the quantification of hydrolysis by resorting to imaging techniques, which would allow a simpler monitoring of the reaction.

### **2.5.2 Second quantitative hydrolysis evaluation method: imaging with UV transilluminator**

UV transilluminators are used in life-science laboratories to spot proteins and nucleic acids in agarose and polyacrylamide gels stained with a fluorescent dye after electrophoresis. The UV transilluminator works by emitting high levels of UV radiation generated by a lamp through the viewing surface. An image is registered which can be analysed with a software to quantify the intensity of fluorescence spots.

Our hypothesis is that if the fluorescence intensity of each bead is proportional to the amount of TAMRA soaked in, it would be possible to build a calibration curve in function of the fluorophore concentration. The calibration curve shall be used to extrapolate the yield of the

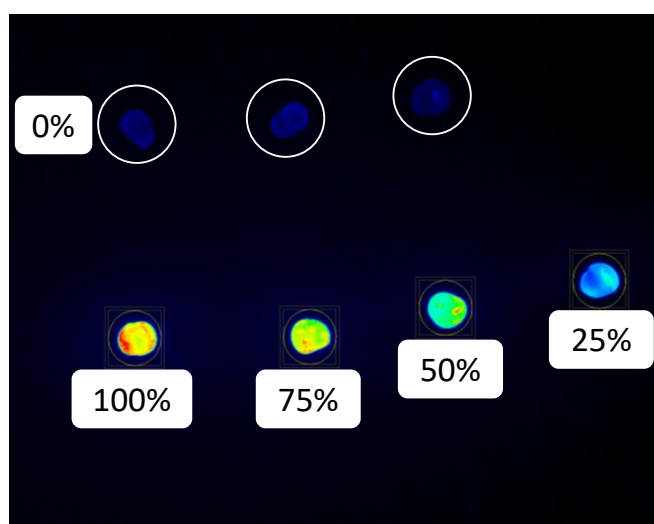
hydrolysis when analysing the Nafion beads used in the reaction with the UV transilluminator under the same conditions.

Several Nafion beads were soaked with 0.3 mL solutions of TAMRA and BHQ at different concentration, ranging from 1  $\mu\text{M}$  to 10  $\mu\text{M}$  (**Table 14**). The bead soaked with 0.3 mL of 10  $\mu\text{M}$  TAMRA+BHQ will emit a fluorescence signal corresponding to a theoretical conversion of 100%, while the bead soaked with the 2.5  $\mu\text{M}$  solution represents a reaction yield of 25%.

Entry	Volume	[TAMRA+BHQ]	Theoretical conversion
1	0.3 mL	//	0%
2	0.3 mL	1 $\mu\text{M}$	10%
3	0.3 mL	2.5 $\mu\text{M}$	25%
4	0.3 mL	5 $\mu\text{M}$	50%
5	0.3 mL	7.5 $\mu\text{M}$	75%
6	0.3 mL	10 $\mu\text{M}$	100%

**Table 14.** List of solutions used to build the calibration curve. For each solution, a Nafion bead was added and let to soak all the TAMRA and BHQ (37 °C, agitation, 15 minutes), then analysed.

The beads were placed on the viewing surface of the transilluminator and several snapshot were taken. An example in shown in **Figure 44**. The fluorescence intensity for each bead is measured with a specific software.



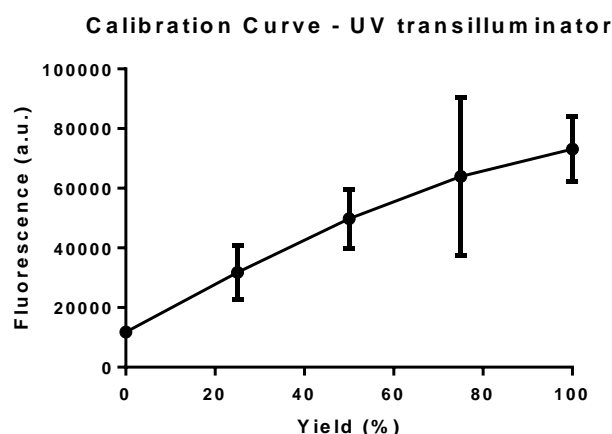
**Figure 44.** Sample of images taken at the UV transilluminator. Beads are identified by the corresponding percentage of conversion. Colour is modified according to the intensity (red = high intensity, blue = low intensity).

Beads not soaked (0% theoretical conversion) show a little autofluorescence. Beads soaked with TAMRA and BHQ (from 25% to 100% theoretical conversion) show increasing emission intensity, as expected.

Various variables were considered when analysing the beads with the transilluminator:

- Change in intensity within beads. Nafion beads are not identical one to another. The fluorescence intensity for each concentration was measured in triplicates (3 different beads).
- Change in intensity within the bead's rotation. Since the Nafion beads are not perfectly spherical, each bead was analysed in 3 different orientations (the change in intensity is indeed very small).
- Change in intensity within the bead's position in the viewing surface. Unfortunately, the UV radiation emitted is not uniform through the viewing surface of the transilluminator. Thus, each probe was photographed in 8 different fixed spots in the trans-illuminated surface. Unlike previous cases, here the difference between the intensities for each position is remarkable. By using the same fixed spots for each bead, the differences in intensity caused by this variable are reduced to the minimum.
- Change in intensity within time. All the images are taken on the same day within one hour to eliminate variations in the lamp emission due to its usage.

Hence, each point on the calibration curve is the result of the analysis of 72 images. The obtained calibration curve is reported in the following figure.



**Figure 45.** Calibration curve built with the aid of UV transilluminator.

It can be observed that:

- The curve does not intersect at the origin: a small degree of auto-fluorescence is observed for untreated Nafion beads.
- Even with all the above described efforts to reduce the external errors to the minimum, the values of standard deviation for the point corresponding to 75% conversion is way too high to consider the calibration curve statistically valid.
- The calibration curve is not linear after the point corresponding to 50% of conversion but it seems to tend to a plateau. This can be attributed to appearance of FRET effect due to the increased spatial proximity of BHQ to TAMRA and of two molecules of TAMRA.<sup>80</sup>

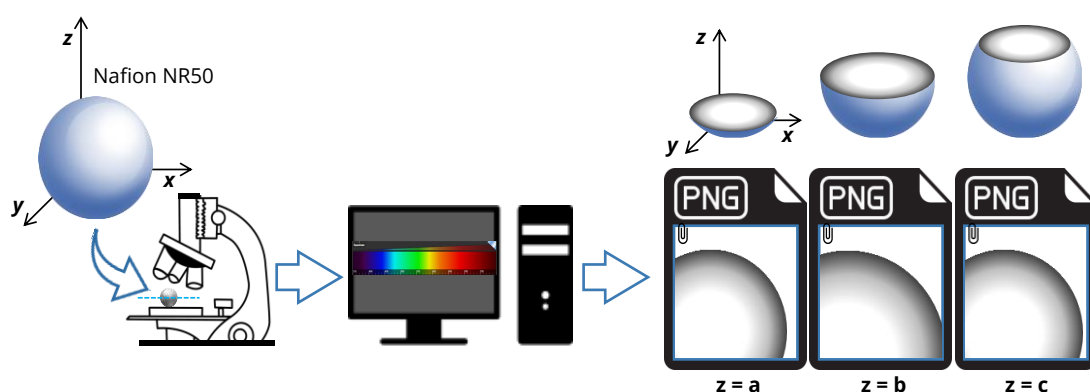
Overall, the first calibration curve obtained with this method is quite good, especially in the first part (0% to 50% conversion) which is the range of conversion in which most of the reaction outcome would fall. It is, though, susceptible of major improvements, especially regarding the values of standard deviation.

However, this method relies too much on the power of the UV lamp of the transilluminator which varies with time. A new calibration curve should be built each time a Nafion bead from a reaction has to be analysed. For this reason, we abandoned this method and we turned to a more reliable instrument for bioimaging: a Confocal Laser Scanning Microscope.

### ***2.5.3 Third quantitative hydrolysis evaluation method: imaging with Confocal Microscope***

Confocal laser scanning microscopy (CLSM), often shorten as “confocal microscopy”, is an optical imaging technique for capturing multiple two-dimensional images at different depths in a sample, enabling the reconstruction of three-dimensional structures of the analysed object.<sup>81,82</sup> **Figure 46** illustrates the kind of images that are expected from the scanning of the bead at various depths (along **z** dimension). The objective used applies a 20X magnification, so -given the bead’s dimension (diameter  $\approx$  3 mm)- it is not possible to catch the bead in its entirety. The images obtained are just a part of a circle, as represented in the figure. Moreover, given the dimension of the solid beads (diameter =  $\sim$ 3 mm, that is  $\sim$ 150 times bigger than a mammalian HeLa cell) the confocal microscope cannot record the core of the solid, so we take into consideration that information about the core of the catalyst is not available.

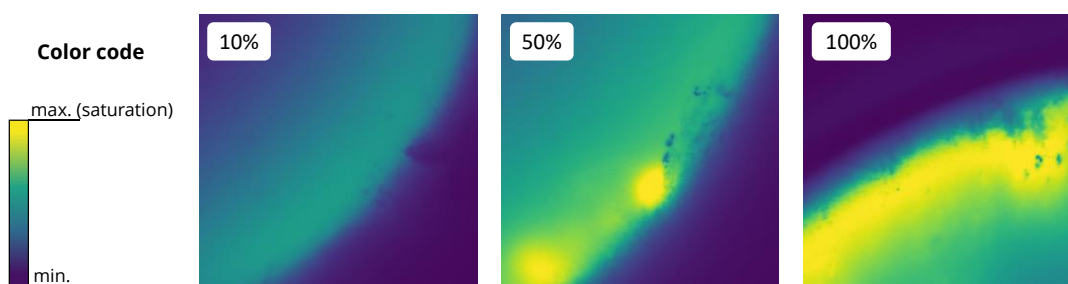




**Figure 46.** Confocal laser scanning microscopy applied on Nafion beads. The microscope records images of the bead by scanning it at different depths ( $z$  dimension). The grey area represent the external part of the bead, the core is not scanned by the microscope because of the bead dimension.

Confocal microscopy is widely used to image cells in biology, but its applications are not limited to that.<sup>83,84</sup> Here it was used to take images of the Nafion beads soaked with increasing concentration of TAMRA+BHQ to build a calibration curve, as in the previous section. A laser emitting at 561 nm was used as source if the excitation wavelength and the recording channel was set at  $580 \pm 10$  nm (570-590).

In this case, it is very important to fix the photomultiplier intensity (PMI), since the intensity emission will be directly related to the amount of TAMRA. The main trouble given by such approach is that emission intensities can be recorded on a scale going from 0 (= no emission) to a maximum. Above the maximum the signal is saturated. Nafion beads soaked with an amount of TAMRA corresponding to 10% of yield will require a certain PMI to see fluorescence; this PMI must be applied to all the beads of the calibration. Images of beads with an increasing amount of TAMRA will have more and more saturated areas, which will alter the real intensity values. **Figure 47** shows some of the images obtained. They are coloured according to an intensity scale which allows to easily spot the areas which are saturated (in yellow).



**Figure 47.** Images of Nafion beads soaked with solutions of TAMRA and BHQ at different concentrations. The colour code applied highlights the saturated areas.

As expected, images of beads corresponding to 50% and 100% conversion present expanding saturated areas. In these cases, ratiometric approaches are usually preferred: a second probe emitting at a wavelength different from that of TAMRA should be soaked in the polymer as standard and the two emission intensities should be compared. Even if more precise, this ratiometric approach would require stopping the reaction and soaking the Nafion bead with another chemical in order to quantify the hydrolysis. The introduction of another probe would impede to continue the reaction after monitoring the first time. For this reason, a ratiometric approach was not investigated.

#### ***2.5.4 Conclusion on quantitative hydrolysis evaluation methods***

We investigated three different methods for the quantification of hydrolysis in solid catalyst. First method is based on the release of the hydrolysis product **TAMRA-NHCO-diol** from the solid catalyst into a solution of DMSO/HCl aq. 3M. This method requires very long time for the probe to be released (more than 24 hours), the risk of alteration of the results is very high.

Second method is based on the measure of the fluorescence emitted by the beads with a UV transilluminator. The use of this instrument requires the construction of a new calibration curve at each analysis.

Third method involves measuring the fluorescence with confocal microscope. Limitations arose from signal saturation would require applying a ratiometric approach which does not fit with the possibility of monitoring the reaction multiple times.

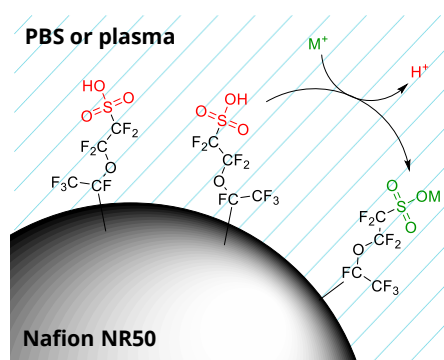
In conclusion, a method for the quantification of hydrolysis conversion happening inside a solid material was not found. Nevertheless, the confocal microscope was still used to confirm the presence of fluorescence since it is more reliable than the UV lamp, given that the excitation laser and the emission channel are specific for TAMRA.

In the next section we investigate the cationic exchange of Nafion beads in buffered solutions and we address the issue of media acidification.

## 2.6 INVESTIGATION OF NAFION NR50 ACIDIFICATION OF BUFFERED MEDIA

As we previously observed, commercial Nafion acidifies the buffered PBS and plasma solutions (cf. section 2.2.1, page 85). Hence, to be considered as candidate for the abiotic hydrolysis in biological media, the acidification of the buffered environment must be avoided.

We previously speculate that such acidification is due to the cationic exchange with metal ions present in the media. We report again **Figure 39** as a recall.

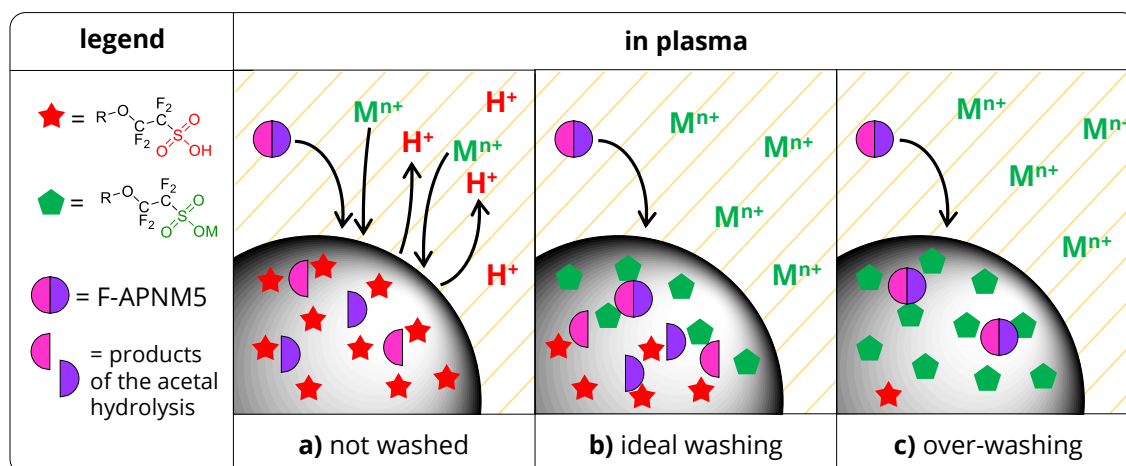


**Figure 39.** Representation of the cationic exchange between the proton of the sulfonic acid and metal ion present in the buffered solutions.

Herein we hypothesize that a smoother cationic exchange pre-treatment could be used to neutralize the sulfonic acid moieties of the external layers of the beads, while keeping untouched the inner ones. In this way, the FRET probe adsorbed into the bead can still be hydrolysed while the cationic exchange with the buffered media is reduced to the minimum. A first attempt was done by pre-treating Nafion beads in plasma. A bead was left at 37 °C in plasma for enough time to cause the precipitation of the proteins and reach the equilibrium. Then the bead was removed from the solution and put in 0.3 mL of fresh plasma, the acetal **F-APNM5** was added (10 μM) and the vial was left at 37 °C for 24 hours. With this pre-treatment the reaction media maintained its normal pH (7.4) and no precipitation was observed but the Nafion revealed to be completely neutralized since no fluorescence was observed.

So, we envisaged to pre-treat the beads by washing them with sodium salt solutions, with the hope that only surface sulfonic acid motif will exchange protons (H<sup>+</sup>) for cations (Na<sup>+</sup>).

In **Figure 48** we illustrate the three cases that will be encountered by applying a washing pre-treatment.



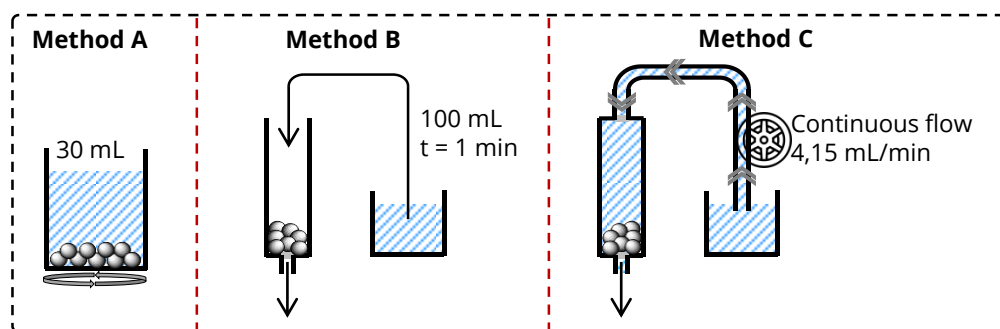
**Figure 48.** Representation of possible scenarios of acetal hydrolysis triggered by three different Nafion beads: **a)** commercial or not washed enough, **b)** partially neutralized (ideal-washing) and **c)** almost completely neutralized (over-washing).

The washing pre-treatment has to be adjusted to find the balance between the complete neutralization of the catalyst (**Figure 48c**) -whose hydrolytic activity is lowered too much- and not enough neutralization (**Figure 48a**) which, despite showing high hydrolytic activity, leads to acidification of plasma. We hope to find the conditions to reach the ideal case illustrated in **Figure 48b** in which a partial neutralization of the acid functions prevents acidification of the media while not impeding to trigger the hydrolysis.

To this end, Nafion beads were washed with different dilutions of **i)** a saturated sodium chloride solution:  $[\text{NaCl}] = 6,57 \text{ M}$ ; or **ii)** a PBS solution of composition:  $[\text{NaCl}] = 137 \text{ mM}$ ,  $[\text{KCl}] = 2,7 \text{ mM}$ ,  $[\text{Na}_2\text{HPO}_4] = 10 \text{ mM}$ ,  $[\text{KH}_2\text{PO}_4] = 1,8 \text{ mM}$ . Dilutions of the mentioned salt solutions allowed to have a range of NaCl concentration from 6,57 M to 6,57  $\mu\text{M}$ .

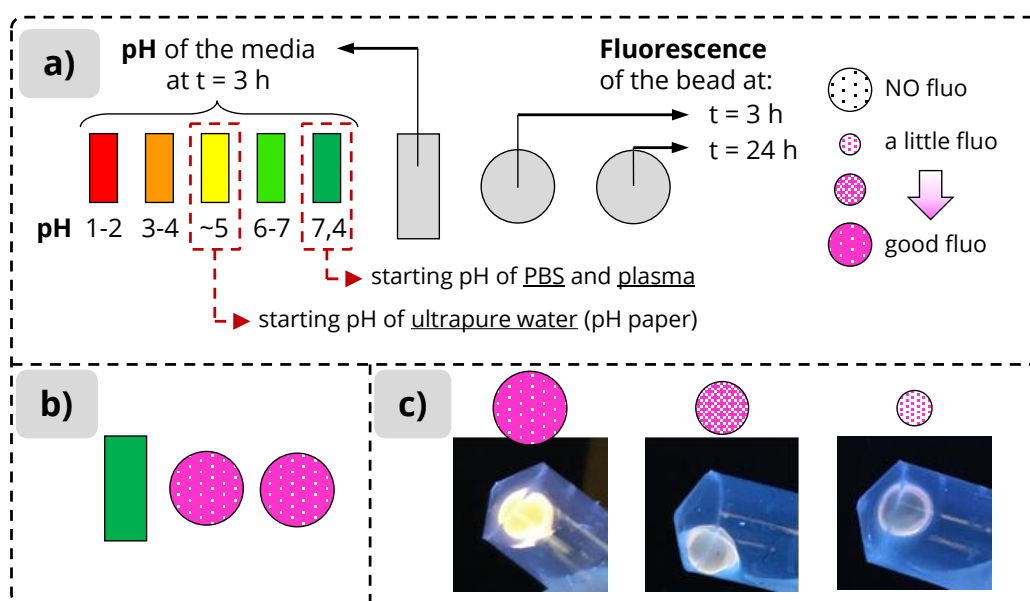
Three different methods are employed (**Figure 49**, cf. Experimental procedures, section 3.3.1, page 224):

- A.** beads were added to 30 mL of the washing solution and let under magnetic stirring at room temperature for 18 hours;
- B.** 100 mL of the washing solution was used to flush the Nafion beads (1 minute);
- C.** the beads were continuously washed in flow at a rate of 4,5 mL/min for a chosen amount of time.



**Figure 49.** Schematic representation of the three different methods employed for the pre-treatment of Nafion beads.

The substrate used for the screening was **F-APNM5**, applying the usual reaction conditions: [substrate] = 10  $\mu\text{M}$ ; solvent: 0.3 mL; 37 °C. As for the previous screenings, the data are shown in a *ready-to-catch* form, explained in detail in the following figures, along with the ideal outcome.



**Figure 50. a)** Legend of the symbols used to represent the pH of the reaction media and the hydrolysis (= fluorescence) at given times. **b)** Symbol of the ideal reaction outcome. **c)** Examples of fluorescence emission level detected under UV lamp related to the corresponding symbol.

The bar colour indicates the pH of the media measured at reaction time  $t = 3$  hours. Starting pH of PBS and plasma is 7.4 (dark green bar), while the pH of mQ water (measured with pH paper) was around 5. The shift of pH value in solution from the starting one is the most important parameter here since we look for a pre-treatment conditions which does not affect the proton concentration and, at the same time, maintains the catalyst's hydrolytic activity. The


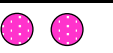

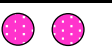













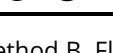

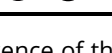
hydrolysis of **F-APNM5** is checked after 3 hours and 24 hours and is depicted by the two spheres on the right (first one for  $t = 3$  h, second for  $t = 24$  h). White dotted sphere represents the absence of fluorescence, while a fuchsia dotted sphere represents the appearance of fluorescence in different degrees according to the size and colour intensity (**Figure 50a**). Pictures of some Nafion beads having different levels of fluorescence emission are showed in **Figure 50c** and related to the corresponding symbol. Ideally the catalyst shows good fluorescence within three hours (**Figure 50b**), but also catalysts showing low fluorescence are well accepted if they do not alter the pH of the solvent.

The following table groups the various pre-treatment tested according to the method used for the pre-washing and are organized as follow:

- *Columns on the left* give information about the washing solution (water, PBS, NaCl sat.) and the dilution of the latter expressed as concentration of NaCl. Ex.: entry 8, Nafion beads are washed with a PBS solution diluted 100 times: actual concentration of NaCl is 1.37 mM.
- *Columns on the right* give information about the outcome of the hydrolysis reaction in different solvents (three columns: water, PBS, plasma).

Method A							
Entry	Washing Solution	Dilution - [NaCl]	Reaction Solvent				
			Water	PBS	Plasma		
1	Water	// - //			X		
2	NaCl sat.	// - 6.57 M			X		
3		100 - 65.7 mM			X		
4		10K - 657 μM			X		
5		1M - 6.57 μM			X		
6		// - 137 mM					
7	PBS	10 - 13.7 mM					
8		100 - 1.37 mM					
9		1K - 137 μM					
10		10K - 13.7 μM					

**Table 15.** Screening of washing procedures of Nafion – Method A. Fluorescence of the bead is checked under UV light at  $t = 3$ h, 24h. pH is checked with pH paper at  $t = 3$ h. “X” is for “not tested”.

Method B							
Entry	Washing Solution	Dilution - [NaCl]	Reaction Solvent			Plasma	
			Water	PBS			
11	Water	// - //					X
12		// - 6.57 M					X
13	NaCl sat.	100 - 65.7 mM					X
14		10K - 657 μM					X
15		1M - 6.57 μM					X

**Table 16.** Screening of washing procedures of Nafion – Method B. Fluorescence of the bead is checked under UV light at t = 3h, 24h. pH is checked with pH paper at t = 3h. "X" is for "not tested".

Overall, for reactions in water, the proton concentration is not changed too much and the acetal is always hydrolysed inside the solid catalyst in good yield. This is not surprising, since the absence of ions in ultrapure water prevents the cationic exchange. So, only results in PBS and plasma must be taken into consideration since they represent better the biological conditions.

Some quite good results have been obtained with method A:

- unchanged neutral pH was obtained in PBS when the concentration of NaCl was higher than 50 mM (entries 2, 3, 6);
- in plasma a concentration equal to 13.7 mM was sufficient to maintain a pH around 6-7 (entry 7). Despite the pH being neutral, ion concentration of 137 mM and above (entries 2 and 6) neutralize the catalysts too much. Consequently, no fluorescence was observed. For entries 3 and 7, with a pH in solution around 6-7, a little fluorescence is spotted in PBS and plasma respectively.

Method B does not insure enough neutralization of the acidic catalysts (pH in PBS always turned very acidic).

Method C (Washing Solution: PBS)						
Entry	Dilution - [NaCl]	Minutes	Reaction Solvent			
			Water	PBS	Plasma	
16	// - 137 mM	5			X	
17		15				
18		30				
19		60				
20	10 - 13,7 mM	15	X			
21		30	X			
22		45	X			
23		75	X			
24		90	X			
25		120	X			

**Table 17.** Screening of washing procedures of Nafion – Method C. Fluorescence of the bead is checked under UV light at t = 3h, 24h. pH is checked with pH paper at t = 3h. “X” is for “not tested”.

The third method allows to modulate the degree of ionic exchange in a more controllable way by modifying the time of washing and by constantly renewing the washing solution (washing in flow). In this case, the washing solutions assayed were **i**) PBS solution not diluted ([NaCl] = 137 mM) and **ii**) PBS solution diluted ten times ([NaCl] = 13.7 mM). Washing time went from 5 to 90 minutes (this information is given in the left part of the table). On the right part of the table, the outcome of the hydrolysis reaction with the corresponding pre-treated beads is depicted as before.

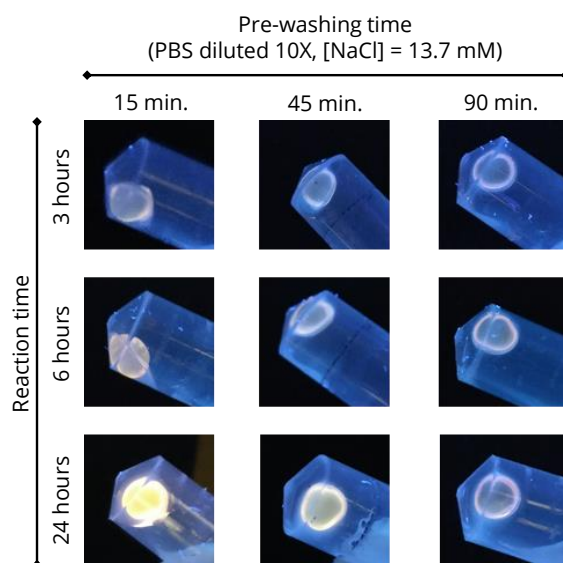
Results in water (first column in the right part of the table) are the same obtained with the previously used washing methods: pH of ultrapure water is constant and the hydrolysis takes place. As mentioned above, PBS and plasma constitute a much real portrait of biological conditions.

When PBS is used as solvent (second column in the right part of the table), its ionic strength always causes cationic exchange with the catalyst, resulting in the increase of proton concentration. The only exception is represented by the catalysts washed with a non diluted PBS solution for 60 minutes (entry 19). This pre-washing, though, neutralizes too much the solid catalyst, since no fluorescence is detected after 24 hours.



When beads washed with PBS solution are used as catalyst in plasma (third column in the right part of the table), the cationic exchange is mitigated passing from beads washed for 15 minutes (entry 17, pH ~5) to beads washed for 60 minutes (entry 19, pH = 7.4). Such a stepwise variation was not observed when PBS was the solvent. Unfortunately, a little fluorescence was detected at  $t = 24$  hours only when the pH of plasma was almost neutral (entry 18, 30 minutes washing, pH = 6-7). Fluorescence of Nafion was also detected for washing time = 15 minutes, but the change in pH was still not acceptable (entry 17, pH ~5).

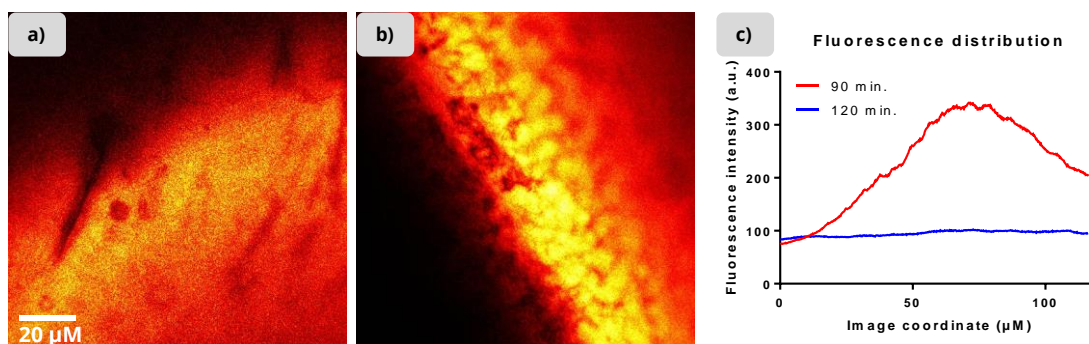
Washing with a PBS solution diluted ten times ( $[\text{NaCl}] = 13.7 \text{ mM}$ , entries 20-25) allows to finely tune the cationic exchange in plasma. Passing from a 15-minutes pre-washing to a 120-minutes one results in a cationic exchange of the beads with plasma inversely proportional to the washing time. For 15-minutes washed beads, the final pH in plasma was around 3-4, fluorescence was spotted (entry 20); for 30-minutes and 45-minutes washed beads, pH of plasma was ~5 and hydrolysis occurred also in this case (entries 21-22); for 75-minutes washed Nafion beads, the pH was more close to the natural one (pH = 6-7, entry 23) and fluorescence was observed, even if it was less than in the previous case. With beads washed for 90 minutes, the pH of plasma stayed neutral: the neutralization given by the washing was enough to not disturb the buffered biofluid but not too much to prevent hydrolysis, since a little fluorescence is observed within three hours. Finally, beads washed for 120 minutes did not affect the pH of plasma but fluorescence was not spotted after 24 hours, probably the acidic functions of the beads were neutralized too much. **Figure 51** shows a selection of photos of the beads taken under UV light at  $t = 3$  hours, 6 hours and 24 hours.



**Figure 51.** Photos of Nafion beads used in the hydrolysis of acetal **F-APNM5** (cf. **Table 17**, entries 20-24). Nafion beads are pre-washed with a PBS solution diluted 10 times for different amount of time (Method C). Pictures are taken under a UV lamp at given reaction times.

The Nafion bead pre-washed for 90 minutes (named “Nafion-90” from now) and treated with **F-APNM5** in plasma for 24 hours was also analysed at the confocal laser scanning microscope and compared to a bead pre-washed for 120 minutes (“Nafion-120”) and treated the same way. The intensity of fluorescence of TAMRA detected at the confocal microscope is measured thanks to a software for image treatment (ImageJ®) and can be directly correlated to the hydrolysis (**Figure 52**).

We expected Nafion-90 to show a higher degree of hydrolysis (*i.e.* higher fluorescence emission) than Nafion-120 since the prolonged washing time was supposed to cause a higher neutralization of the acidic sulfonic functions of the catalyst.



**Figure 52.** **a)** Nafion-120 and **b)** Nafion-90 analysed at confocal microscope after 24 hours reaction with **F-APNM5** in plasma. **c)** Fluorescence intensity of the whole images measured with ImageJ®.

Images obtained confirmed our theory about the higher neutralization of the catalyst reached after 120 minutes of pre-washing.

Regarding the washing pre-treatment, other variables were tested:

- Reactivated beads: Beads which were completely neutralized by cationic exchange were reactivated by a further cationic exchange (beads were put in a 3 M HCl solution and stirred for 1 to 3 hours). These “re-activated” beads were washed with the optimized method and tested in plasma. Results in terms of hydrolysis and pH values of the media are similar to those obtained with the pre-washed Nafion. This shows that the cationic exchange is not irreversible.
- Pre-equilibration in plasma: Pre-treated beads were let to equilibrate in plasma at 37 °C prior to the addition of the FRET substrate. Equilibration time was ranging from 20 minutes to 3 hours. In all the cases, the Nafion bead was still working.

See Appendix B for a comprehensive table of all the washing tests (page 251).

In conclusion, Nafion-90 has all the searched characteristics: hydrophobicity and hydrolytic activity towards hydrophobic acetal substrate **F-APNM5** in buffered media, without affecting the proton concentration of biofluids. The main constraint relative to the use of acidic solid catalyst in buffered media has been successfully addressed.

At this point we took into consideration the bead's dimension. The 3 mm diameter beads had many advantages, including easy-handling, transparency and the possibility to detect fluorescence by human eye. It is also true that it may be too big for *in vivo* tests and applications in mice of average weight ~30 g. For this reason, other forms of Nafion were taken into consideration, as described in the following section.

## 2.7 INVESTIGATION OF OTHER COMMERCIAL FORMS OF NAFION NR-50

**Table 18** gathers other types of Nafion, either commercial or derivatives of Nafion NR50. Indeed, it is possible to chop the “big” beads into three or four pieces with a less regular spherical shape but with an average diameter of around one millimetre. Except for Nafion SAC-13, the other types were purchased (entries 2-4) or made (entry 1).

Entry	Denomination	Dimensions	Notes
1	Nafion NR50 CH	d = ~1 mm	Nafion beads manually chopped
2	POWDion™	40-60 mesh <sup>(1)</sup>	Transparent/white colour
3	POWDion™ sol.	40-60 mesh <sup>(1)</sup>	Soluble in MeOH, brown colour
4	POWDion™ sol.	200 mesh <sup>(2)</sup>	Soluble in MeOH, brown colour
5	Nafion SAC-13	Nanoparticles	10-20% polymer on amorphous silica <sup>(3)</sup>

<sup>(1)</sup> 40-60 mesh = 420-250 µM in diameter; <sup>(2)</sup> 200 mesh = 74 µM in diameter

<sup>(3)</sup> Not commercially available at the time of this work

**Table 18.** Different types of acidic resin Nafion.

Regarding Nafion NR50 CH, Nafion NR50 beads commercially available (d = ~3mm, weight = ~40 mg) are manually chopped into 4 pieces of diameter ~1 mm and weight ~10 mg.

Tests are conducted with these other forms of Nafion in plasma and are resumed in the following table. Washing pre-treatments are conducted using method C (washing in flow) and PBS diluted 10 times as washing solution. Results are visualized with the help of the symbol-code used previously (**Figure 50**, page 106).

Entry	Catalyst	Quantity	Pre-treatment	Hydrolysis in Plasma
1			//	
2	Nafion NR50 CH	1 bead	45 min. washing	
3			75 min. washing	
4			//	
5	POWDion™	2.5 mg	20 min. washing	
6	POWDion™ sol. (40-60 mesh)	2.5 mg	//	
7	POWDion™ sol. (200 mesh)	2.5 mg	//	

**Table 19.** Hydrolysis of FRET acetal **F-APNMS** in plasma carried out by different forms of Nafion. Conditions: [substrate] = 10 µM, T = 37 °C, V = 0.3 mL, t = 24 hours. pH is measured at t = 3 h (pH paper).

The chopped Nafion beads show less acidification of plasma (pH ~5) as well as less hydrolysis than original Nafion (entry 1). When pre-washed for 45 minutes, the proton concentration of plasma remains unaltered, but fluorescence is observed only after 24 hours (entry 2), a result comparable to that of Nafion-90 (**Table 17**, entry 24). A pre-washing of 75 minutes resulted in the complete neutralization of the bead (entry 3). Commercial POWDion™ shows the appearance of some fluorescence but acidifies the media (entry 4). A pre-washing of 20 minutes neutralizes the acidity of the catalyst (entry 5). The two soluble POWDion™ (40-60 and 200 mesh) did not show any fluorescence, as well as any induced increasing of the proton concentration in plasma.

The results obtained suggested that the washing procedure should be optimized for each type of catalyst. At this point we decided to prioritize our research into gain insight on how the acidity of the solid catalysts changes with the pre-treatment. This aspect will be deeply investigated on section 4 of this chapter, after a second hydrophilic catalyst has been identified (section 3).

Meanwhile, since in the definition of the objectives of this project, we theorized that a hydrophobic adsorbent acid catalyst would have not shown hydrolytic activity towards an hydrophilic substrate because of the lack of interactions due to their different nature, in the next section we addressed our statement by testing Nafion with the hydrophilic acetal substrate **PEGAM5**.

## 2.8 INVESTIGATION OF NAFION NR50 ACTIVITY IN COMBINATION WITH HYDROPHILIC ACETAL

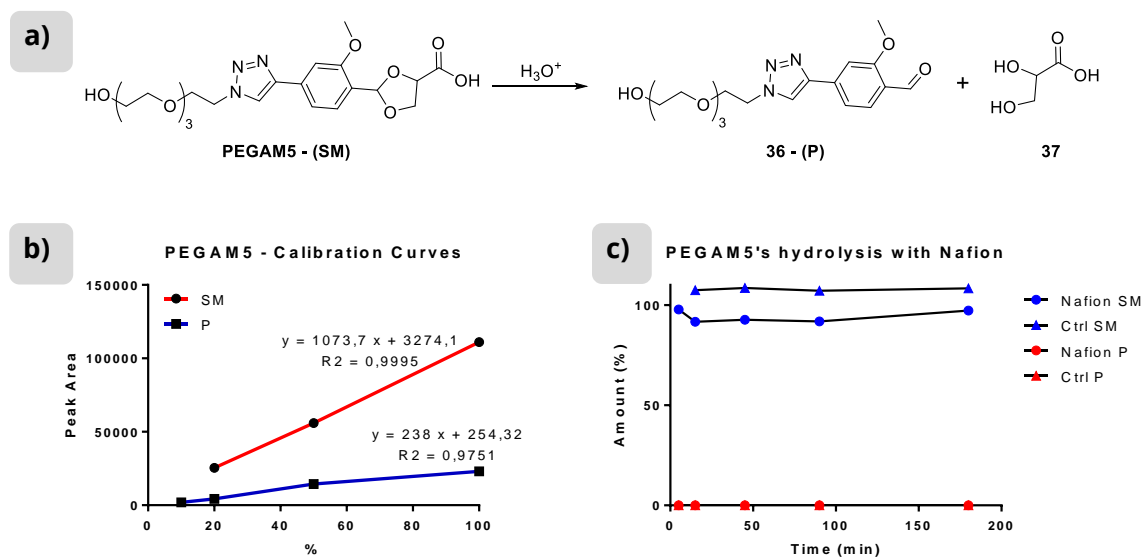
### **PEGAM5**

As a reminder, **PEGAM5** (introduce in chapter II.3.1, page 49) is the hydrophilic version of acetal **F-APNM5**. In this case we cannot exploit the FRET effect to monitor the hydrolysis via fluorescence appearance, thus the reaction has to be monitored via LC-MS.

Two calibration curves were built for **PEGAM5** and its hydrolysis product **36** (**Figure 53a**). Solutions of the two compounds at different concentrations were prepared in plasma and kept under agitation at 37 °C for one hour, in order to reproduce the reaction conditions as accurately as possible. Then, they were analysed with LC-MS and the values of peak area were plotted as function of the concentration (**Figure 53b**).

**PEGAM5** was then tested for hydrolysis with Nafion beads. A pre-treated bead was put in 0,3 mL plasma and **PEGAM5** was added (final concentration in plasma: 0,28 mM). A control

solution was prepared, it contained only the substrate and it is supposed to always have a constant concentration of starting material **PEGAM5 (SM)** and the absence of hydrolysis product **36 (P)**. Aliquots of the reaction mixtures were taken, treated with acetonitrile to cause protein precipitation and centrifugated. The supernatant is analysed with LC-MS at given times; the amount of starting material (**SM**) and product (**P**) was extrapolated from the calibration curves and reported in percentage (**Figure 53c**).



**Figure 53.** **a)** Hydrolysis reaction of **PEGAM5**. Of the two products, only the aldehyde is visible at the LC-MS, the diol does not adsorb at 254 nm. **b)** Calibration curves for the starting material (**SM**) and the product (**P**). **c)** Hydrolysis reaction of **PEGAM5** catalyzed by pre-treated Nafion and control (**Ctrl**).

Over three hours, the amount of starting material did not decrease and no product was detected at LC-MS. As expected, the reaction did not take place because the substrate is not adsorbed by the Nafion bead and remains in solution.

In conclusion to this first part about the identification of a hydrophobic heterogeneous catalyst, Nafion NR50 has been identified among all the catalysts screened. Upon pre-treatment with a washing solution (13.7 mM content of NaCl, continuous flow washing, rate: 4.15 mL/min,  $t = 90$  min) it shows all the wanted characteristics: hydrolytic activity in biofluid without affecting the highly buffered surroundings. Its acidity will be further investigated in section 4 of this chapter (page 126). Now we describe the identification of a hydrophilic heterogeneous catalyst with the same performances in buffered media.

### 3. IDENTIFICATION OF A HYDROPHILIC HETEROGENEOUS ACID CATALYST

As a reminder, in this chapter we aim to identify two kind of heterogeneous acidic catalyst (hydrophobic and hydrophilic). In section 2 we explored among a pool of catalysts of different nature to find a hydrophobic catalyst able to hydrolyse the hydrophobic substrate in a buffered aqueous environment. In this section our objective is to identify a hydrophilic solid catalyst to pair to a hydrophilic substrate.

With respect to the previous case, a major constraint is represented by the affinity between the hydrophilic catalyst's backbone and the aqueous solvent of the reaction. We hypothesized that their interaction is more significant than in case of the hydrophobic catalyst so it could cause a faster and uncontrollable cationic exchange between the acid motifs and the buffered media, resulting in the neutralization of the catalyst.

We addressed this issue by trying two approaches: **i)** the encapsulation of an organic sulfonic acid into a hydrophilic matrix; **ii)** the co-polymerization of the sulfonic acid monomer with a hydrophilic monomer. For both the strategies, the sulfonic acid moiety was chosen according to the outcome of the screening of homogeneous catalysts (Section 2.1, page 82).

To test the catalysts, we used the same conditions as before: 10  $\mu\text{M}$  concentration of the substrate, 0.3 mL of reaction volume, normal body temperature (37 °C) and plasma as solvent. The acetal substrate used in a first place was **F-APNM5**. Even if the hydrophobic nature of the FRET probe could slow down the hydrolysis rate because of the diminished interaction with the hydrophilic catalyst, we chose it because of the great advantage given by the FRET effect: the possibility to **i)** work at very low close-to-*in vivo* concentration and **ii)** monitor the reaction by measuring the fluorescence. Moreover, **iii)** the violet-coloured solution allows to easily assess if the polymer has adsorbent capacity or not.

Eventually, we tested the catalyst also with the less stable acetals **F-A2M5** and **F-A2M6** and with the hydrophilic acetal **PEGAM5**. For the latter we used a higher concentration (0.28 mM instead of 10  $\mu\text{M}$ ) and we checked the progression of hydrolysis by LC-MS.

### 3.1 ENCAPSULATION OF PAASA INTO ALGINATE BEADS

Among all the acids tested, **PAASA** (Poly(2-acrylamido-2-methyl-1-propanesulfonic acid)), a linear polymer soluble in water, was by far the best candidate for encapsulation, even better than CSA used as 100% comparison.

Alginate is a naturally occurring linear polysaccharide extracted from brown algae, it can be crosslinked by the addition of divalent cations (such as calcium) in aqueous solution to form a hydrogel which is biocompatible, biodegradable and non-toxic. Moreover, during the gelation process biomacromolecules and even cells can be incorporated in the matrix, making the alginate gels a great tool for a variety of bio applications.<sup>85,86</sup> Following the reported procedure, calcium alginate gel beads incorporating the linear sulfonic polymer **PAASA** were produced (~2 mm diameter).<sup>87</sup> Different amount of beads (from 1 up to 10) were tested in plasma for the hydrolysis of **F-APNMS** (10  $\mu$ M) at 37 °C for at least 24 hours. After 24 hours no fluorescence was detected and it was observed that the alginate beads fused one to another to create a unique big sphere. The experiments were repeated, each time the beads' fusion was observed. We decided to abandon this strategy and we preferred to design a hydrophilic solid catalyst which could meet our needs (next section).

### 3.2 DESIGN AND TEST OF A TAILORED HYDROPHILIC HETEROGENOUS CATALYST

Thanks to the collaboration with Dr. Lavinia Balan and her group at the Institute of Material Science (IS2M) of Mulhouse, a tailored acid solid catalyst has been conceived. The polymer is formulated to meet the following requirements:

- I. non-toxicity;
- II. affinity with protic solvents (hydrophilic scaffold)
- III. compatibility with plasma;
- IV. presence of a sulfonic motif;
- V. possibility to modulate the number of acidic sites.

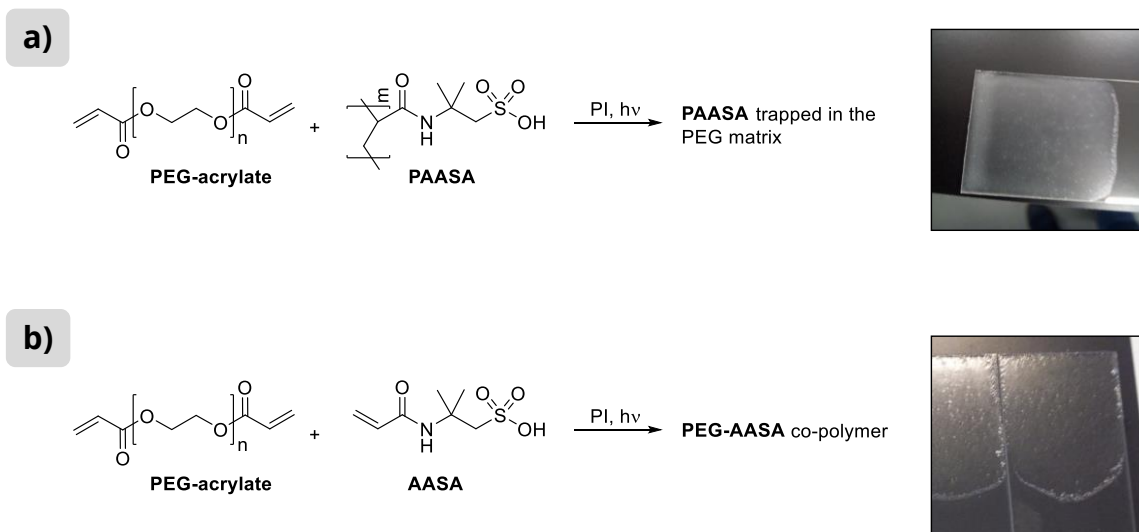
The first three points were addressed by identifying polyethylene glycol (PEG) as the main component of the new solid acid catalyst. PEG has been known for its low toxicity and it has been widely used in pharmaceutical applications, as well as in cosmetology.<sup>88-90</sup> The second component of the polymer was identified in linear polymer **PAASA** for the motivation explained above.



The formulation of the new polymer can be done using two forms of the acid:

- A. PAASA.** In this case the linear polymer will be mixed with the PEG monomer and imprisoned in the matrix during the polymerization.
- B.** 2-acrylamido-2-methyl-1-propanesulfonic acid (**AASA**), monomer of **PAASA**. The monomer can be co-polymerized with PEG-acrylate monomer, that is be covalently bonded to the matrix.

**Figure 54** shows the two processes of polymerization by photoionization, as well as pictures of the obtained films. The thickness of the films was set to 100  $\mu\text{M}$ .



**Figure 54.** **a)** Synthesis and photo of **PEG-PAASA** film: polymerization of PEG-acrylate with encapsulation of **PAASA** within the matrix. **b)** Synthesis and photo of the co-polymer **PEG-AASA**.

The amount of the sulfonic acid in the polymer and co-polymer can be modulated. A screening of the composition is described in the next paragraph.

### 3.2.1 Formulation of PEG-acid polymer composition

Different formulations of **PEG-PAASA** and **PEG-AASA** provide by Dr. Balan were tested in plasma with **F-APNM5** (10  $\mu\text{M}$ ,  $V = 0.3 \text{ mL}$ ,  $T = 37 \text{ }^\circ\text{C}$ ). The percentage of PAASA and AASA varied from 1wt% to 30wt%. The amount of catalyst tested was of 80 mg or 40 mg, corresponding, respectively, to a whole sample or half a sample of the films provided (thickness: 100  $\mu\text{M}$ , surface area =  $\sim 6 \text{ cm}^2$ ). The polymers were provided on a glass support, each film was detached from the support by wetting it with 3 mL of plasma. This procedure was indeed a

pre-washing of the catalyst. In some case the polymer detached spontaneously from the support, so the pre-washing was not performed.

In the definition of this project, we supposed that a hydrophilic catalyst (such as PEG-based polymers here tested) would not have a significant interaction with hydrophobic substrates (such as **F-APNM5**). Thus, we expect longer reaction times than those observed with Nafion. Moreover, during the tests, we observed that the **F-APNM5** substrate is not irreversibly adsorbed by the PEG-based catalysts, so the reaction can be monitored by measuring the fluorescence of an aliquot and the degree of hydrolysis can be calculated by relating the fluorescence to an equimolar solution of TAMRA and BHQ (positive control) treated at 37 °C for an equal amount of time. Results are shown in **Table 20**.

Entry	Polymer	[Acid]	Quantity	Pre-Washing	pH (24h)	Yield (t = 7 d)
1		1%	80 mg	No	7,5	//
2		10%	80 mg	Yes	7,5	4.5%
3	PEG-PAASA	10%	80 mg	Yes	6	10%
4		20%	80 mg	Yes	7,5	19%
5		20%	40 mg	Yes	7,5	9.7%
6		10%	40 mg	No	7,5	//
7		20%	80 mg	No	4,5/5	30%
8	PEG-AASA	20%	80 mg	Yes	7,5	33%
9		30%	80 mg	Yes	1,5	//
10		30%	40 mg	Yes	3	//

**Table 20.** Test of the different compositions of **PEG-PAASA** and **PEG-AASA**. The composition giving the highest yield is enlightened in red. pH of the solution is measured after 24 hours with pH paper.

As expected, the hydrolysis rate was slower than with the hydrophobic Nafion. Fluorescence was detected after few days. PEG-PAASA with only 1% content in acid didn't show any fluorescence after a week (entry 1), when the percentage of **PAASA** was increased to 10%, the highest hydrolysis observed was of 4.5% and 10% (entries 2, 3). The highest yield (19% hydrolysis) was achieved with a **PAASA** content equal to 20% (entry 4). Using half of the amount lowered this value to 9.7% (entry 5).

PEG-AASA co-polymer with a content in acid of 10% did not hydrolyse the acetal in 7 days (entry 6), while doubling the percentage of **AASA** in the formulation allowed to get a 30-33% hydrolysis (entries 7, 8), a better result than that obtained with PEG-PAASA.

Given this promising result, the acid content was increased to 30%. Unfortunately, it caused acidification of the solvent followed by a massive protein precipitation in plasma and so invalidation of acetal hydrolysis (entries 9, 10).

Overall, despite the long reaction time, the tests with **F-APNM5** allowed to discriminate between the different formulations and to identify PEG-AASA-20% as the one which gave the highest hydrolysis.

Moreover, tests conducted with PEG-AASA-20% revealed also that pre-washing in plasma is essential for the maintenance of the buffer. Indeed, without the pre-washing the polymer lowered the pH of plasma to 4.5-5 (entry 7), while it did not affect the buffer if previously treated (entry 8). Regarding the quantity and the form of catalyst used, 80 mg is too much for tests in such a small volume of solvent (0.3 mL). Thus, the following experiments with PEG-AASA-20% in form of film were conducted with a lower quantity of catalyst (20 mg, cf. paragraph 3.2.3 below).

Having identified the right formulation, the researchers of the group of Dr. Lavinia Balan at IS2M synthesized PEG-AASA-20% in form of little beads of diameter = ~0.5 mm.

The process is much longer than that used to produce the glass supported films (cf. experimental procedures, section 1.8.5, page 211), thus a limited number of beads was provided for first tests, which are described in the next paragraph.

### **3.2.2 Tests of PEG-AASA-20% beads with F-APNM5**

Acetal **F-APNM5** was tested with different quantities of PEG-AASA beads. For the reasons explained above, the amount of catalyst used was much lower (0.5 – 5 mg) compared to previous tests. Reactions were carried out and monitored in the same conditions described above, results are reported in the following table.

Entry	Polymer	[Acid]	Quantity	Pre-Washing	pH (24h)	Yield (t = 7 d)
1	PEG-AASA beads	20%	0.5 mg	No	7,5	2.5%
2		20%	1.5 mg	No	5	9.5%
3		20%	5 mg	Yes	7	2.0% (t=3days)

**Table 21.** Test of different amount of PEG-AASA-20% in form of beads with acetal **F-APNM5**. pH of the solution is measured after 24 hours with pH paper.

Using 0.5 mg of catalyst (corresponding to 3 beads) hydrolysis was not observed within a week (2.5% at t = 7 days, entry 1). Less than 10% of hydrolysis was observed when using 3 mg of catalyst (corresponding to 9 beads, entry 2). For these two experiments the beads were used as provided, without any washing. We observed that 1.5 mg of catalyst was enough to lower the pH of plasma to 5 (entry 2). The lowered pH probably cause the 9.5% hydrolysis of FRET in solution observed after 7 days.

Hence, 5 mg of catalyst were pre-washed by using 1 mL of plasma as washing solution (r.t., few seconds of vial manual agitation, washing plasma is then replaced by 0.3 mL of fresh plasma). The pre-washing proved to be effective in terms of preservation of the buffered media but at t = 3 days hydrolysis was basically not observed (2%, entry 3).

Probably this amount of catalyst is not enough or the catalyst acidity is not enough strong for the substrate used. To answer to this uncertainty we tested PEG-AASA-20% in form of film (20 mg) and in form of beads (5 mg) with the less stable acetals F-A2M5 and F-A2M6.

### 3.2.3 Tests of PEG-AASA-20% co-polymer with F-A2M5 and F-A2M6

**F-A2M5** and **F-A2M6** were tested with PEG-AASA-20% in form of film and in form of beads. According to the values of pH of plasma reported above (**Table 20**, entries 7; **Table 21**, entry 2), both the catalysts were pre-washed to avoid acidification of plasma. A suspension of the co-polymer and plasma (1 mL) is manually agitated at room temperature for 15 seconds (precipitation of protein was not observed, pH of plasma was ~5). Then plasma is removed, 0.3 mL of fresh plasma are added, followed by the acetal (10  $\mu$ M). Reaction vials were put at 37 °C under mechanical agitation (750 rpm). At given times aliquots were taken, diluted ten times and the fluorescence emitted was measured with a spectrophotometer.

Obtained values are related to those of an equimolar solution of TAMRA and BHQ in plasma in the presence of the same amount of catalyst kept at 37 °C under mechanical agitation for the same amount of time (positive control).

The following table displays the results obtained with **F-A2M5** and **F-A2M6** after 3 days in comparison with those obtained with the more stable **F-APNM5**.

Catalyst	Form	Quantity	pH of plasma <sup>(2)</sup>	Hydrolysis (t = 3 days)		
				F-APNM5	F-A2M5	F-A2M6
PEG-AASA-20% <sup>(1)</sup>	film	20 mg	6	7.8%	63.2%	65.3%
PEG-AASA-20% <sup>(1)</sup>	bead	5 mg	7.5	2.0%	11.3%	10.3%

(1) the catalyst is pre-treated with a "fast washing"

(2) pH is measured with pH paper at t = 1 day

**Table 22.** Test of PEG-AASA-20% in form of film and beads with the cleavable hydrophobic probes **F-A2M5** and **F-A2M6**. Results obtained with the more stable **F-APNM5** are listed as comparison.

After 3 days in presence of 20 mg of PEG-AASA-20% (film) only 7.8% of **F-APNM5** hydrolysis was reached, while the more cleavable **F-A2M5** and **F-A2M6** showed a major improvement (by a factor of ~8), with a hydrolysis of 63% and 65% respectively. pH of plasma was equal to 6 after one day. An improvement by a factor of ~5.4 was also observed with PEG-AASA-20% in form of beads (5 mg) when passing from **F-APNM5** (2% hydrolysis) to **F-A2M5** and **F-A2M6** (11.3% and 10.3% of hydrolysis).

These results suggest that the nature of the substrate plays a major role in the catalyst's performance. Consequently, we tested PEG-AASA-20% catalyst with acetal **PEGAM5**, a hydrophilic substrate with higher affinity to the PEG-based catalyst than the FRET probes previously tested.

### 3.2.4 Tests of PEG-AASA-20% beads with PEGAM5

**PEGAM5** was introduced as the hydrophilic alternative to FRET probe **F-APNM5** and was unsuccessfully tested with Nafion NR50 beads (cf. section 2.8, page 114). In this case, the hydrophilic nature of **PEG-AASA** and the hydrophilicity of **PEGAM5** constitute a promising combination for abiotic acetal hydrolysis, according to our initial hypothesis.

**PEG-AASA-20%** beads (5 or 10 mg) were pre-washed with plasma in three different ways:

- A.** *Fast washing.* A suspension of beads and plasma (1 mL) is manually agitated at room temperature for 15 seconds. Then plasma is removed.
- B.** *10 minutes washing.* A suspension of beads and plasma (1 mL) is agitated at 37 °C (750 rpm) for 10 minutes. Then plasma is removed.

- C.** 30 minutes washing. A suspension of beads and plasma (1 mL) is agitated at 37 °C (750 rpm) for 30 minutes. Then plasma is removed.

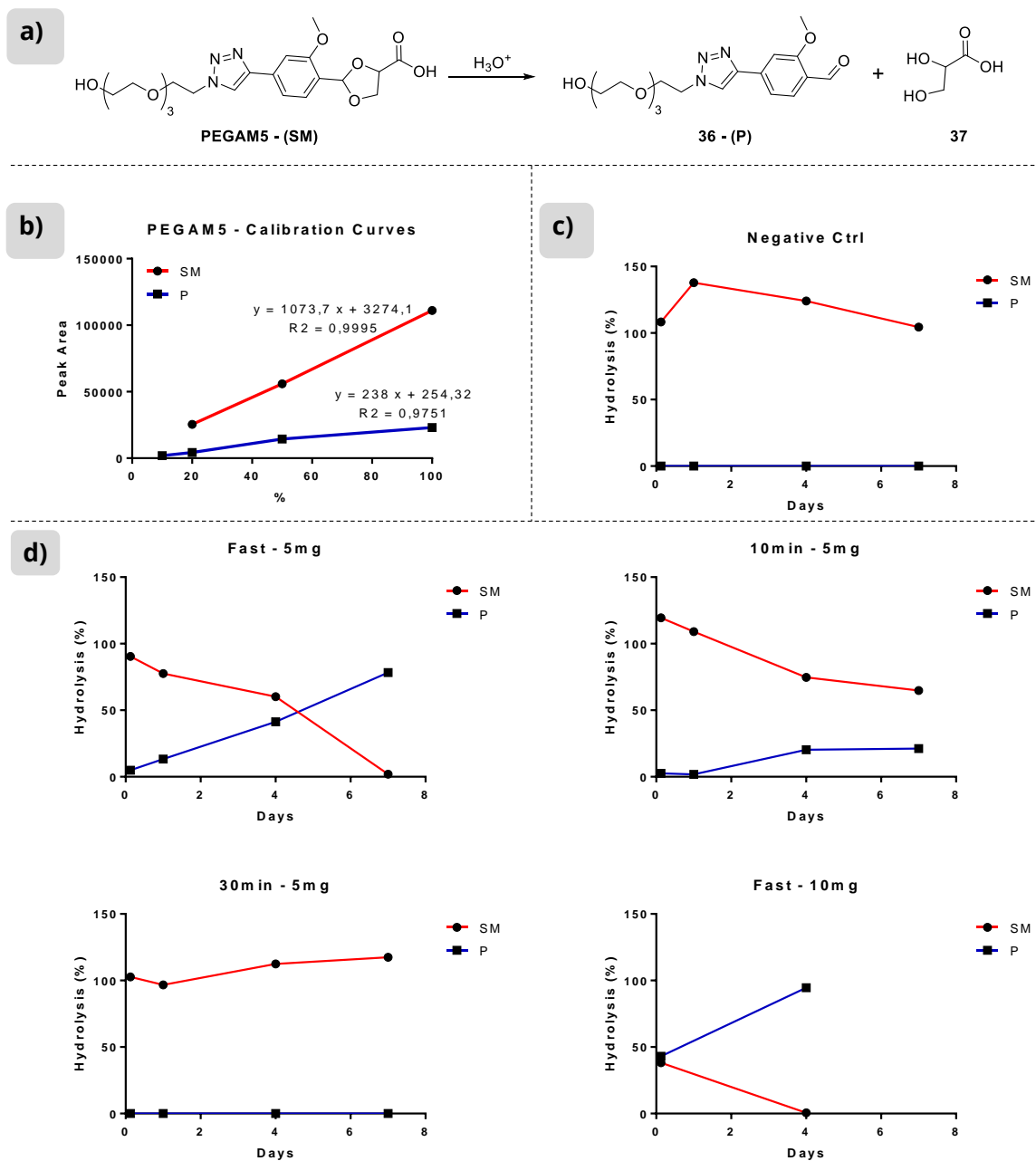
After the pre-washing, 0.3 mL of fresh plasma and **PEGAM5** were added (substrate concentration: 0.28 mM). Reaction vials were put at 37 °C under mechanical agitation (750 rpm). Negative control solution contains only the substrate and it is supposed to always have a constant concentration of starting material **PEGAM5 (SM)** and the absence of hydrolysis product **36 (P)**. Tested conditions are resumed in **Table 23**.

Entry	Name	Catalyst quantity	Pre-washing
1	<i>Negative Ctrl</i>	//	//
2	<i>Fast - 5mg</i>	5 mg	Fast, r.t.
3	<i>10min - 5mg</i>	5 mg	10 min, 37 °C
4	<i>30min - 5mg</i>	5 mg	30 min, 37 °C
5	<i>Fast - 10mg</i>	10 mg	Fast, r.t.

**Table 23.** Reaction condition for **PEGAM5** hydrolysis carried out by PEG-AASA beads.

The negative control consists in 0.28 mM solution of **PEGAM5** in plasma. It is expected that the amount of **PEGAM5** remains constant over the days and, more important, that the product is not formed in the absence of the catalyst.

Aliquots of the reaction mixtures were taken at given times, treated with acetonitrile to cause protein precipitation and centrifugated. The supernatant is analysed with LC-MS; the amount of starting material (**SM**) and product (**P**) was extrapolated from the calibration curves and reported in percentage in the following graphs (**Figure 55**). pH of plasma after addition of catalysts is neutral in all the cases.



**Figure 55.** a) Hydrolysis reaction of **PEGAM5 (SM)** gives aldehyde **36 (P)** and diol **37** as products. b) Calibration curves for the starting material (**SM**) and the aldehyde product (**P**) of the reaction in plasma. c) Negative control: no auto-hydrolysis is detected over 7 days. d) Acetal hydrolysis with PEG-AASA beads in different conditions.

The negative control showed no formation of the product over 7 days (**Figure 55c**). When 5 mg of beads are subjected to a “fast washing”, almost complete hydrolysis is reached after 7 days (78%), while with the “10 minutes washing” only 20% of hydrolysis is observed within 7 days. If the catalyst is washed for 30 minutes, any product is detected in the same timeframe.

When the amount of catalyst is doubled (10 mg) and subjected to the fast washing, complete hydrolysis is reached within 4 days and almost 50% of hydrolysis was reached within the first hours.

From the reaction profiles it can be deduced that:

- the washing procedure has a great impact on the catalyst's performances. The "30 minutes washing" procedure causes complete neutralization of the catalyst.
- as expected, **PEGAM5** works better as substrate than the hydrophobic FRET acetals.

### 3.3 CONCLUSION ON THE IDENTIFICATION OF THE HYDROPHILIC HETEROGENEOUS ACID CATALYST

Thanks to the expertise of Dr. Lavinia Balan (IS2M) we were able to design a tailored PEG-based polymer crosslinked with a sulfonic acid of our choice (**AASA**, monomer of **PAASA**) which showed hydrolytic activity in early screenings.

We identified the formulation of PEG-AASA-20% as the one with the right amount of acid to avoid acidification of the buffered media while showing hydrolytic activity. Such polymer was produced in form of glass-supported films or beads. The latter are preferred because of much easier handling.

Thus, PEG-AASA-20% beads were tested with PEGAM5, the hydrophilic acetal specifically designed to be paired with a hydrophilic catalyst. Complete hydrolysis and no change of plasmatic pH was observed within 4 days when 10 mg of the catalyst are pre-treated with a "fast washing". This first results are very promising and there is probably some margin of improvement about the reaction time.

At this point of the project, we focused our attention on gaining insight on the inner acidity of the catalysts selected till now. Such investigation is described in the next section.



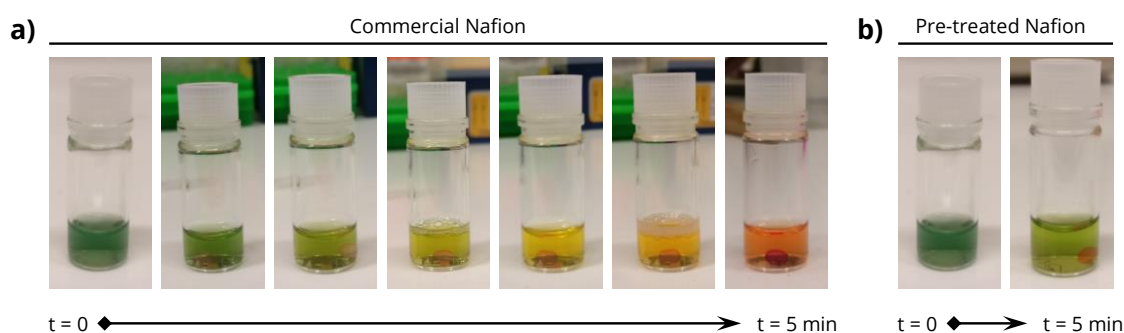
## 4. INVESTIGATION OF CATALYSTS INNER ACIDITY

In this section we aim to investigate the modification in the acidity of the hydrophobic solid catalyst Nafion and of the hydrophilic PEG-AASA operated by the washing procedures. Our aim is to make a comparison between pre-treated and non-treated catalysts as well as to demonstrate that the pre-washed catalysts Nafion-90 and PEG-AASA-20% are actually preserving their activity.

First (section 4.1) we addressed the matter in a qualitative way with the aid of a pH universal indicator. Later (section 4.2) we exploited the confocal laser scanning microscope in combination with a pH-sensitive ratiometric probe.

### 4.1 QUALITATIVE INVESTIGATION OF ACIDITY WITH PH UNIVERSAL INDICATOR

Nafion beads (commercial Nafion NR50 and pre-washed Nafion-90) are put in a PBS solution of a universal pH indicator. Colour varies from red for acidic pH to violet/blue for basic pH, passing by green for neutral pH, thus the PBS solution is coloured in green (pH = 7.4). The beads adsorb part the pH indicator resulting in the colouring of the bead. The colour of the PBS solution changes according to the degree of cationic exchange with the probe and it will shift to red if the Nafion bead acidifies the buffer. Pictures of the solutions are taken in a time frame of 5 minutes and are shown in **Figure 56**. The solutions obtained at  $t = 5$  minutes are representative of the equilibrium and after storage at room temperature for several months they look unchanged.



**Figure 56.** A fast, qualitative proof of Nafion's acidity in buffered media. **a)** Commercial Nafion in a PBS solution. The cationic exchange kills the buffer within minutes. **b)** Washed Nafion in a PBS solution. The buffer is maintained while the bead keeps its acidity (light red colour). The solution remains the same even after months.

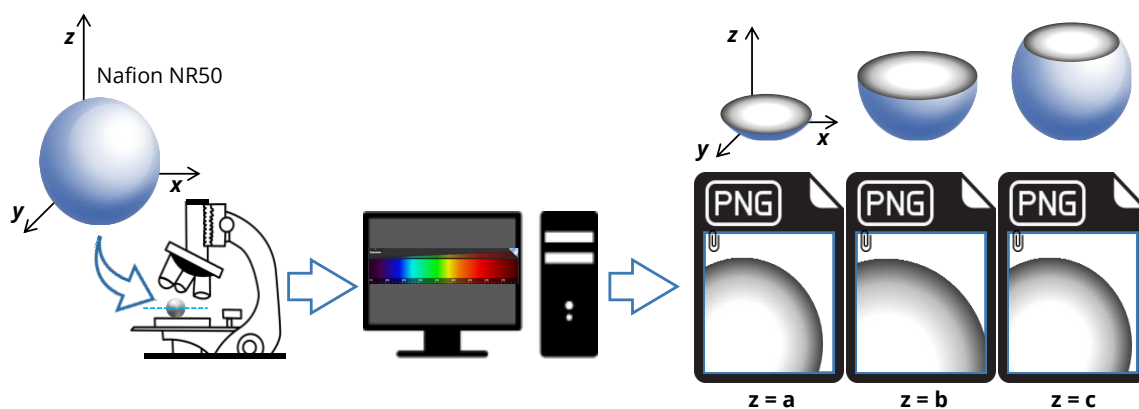
As expected, acidic commercial Nafion NR50 (red bead) acidify the PBS solution, which quickly turns from green to red. Nafion-90 (which showed catalytic activity in plasma, cf. **Table 17**, entry24) does not affect significantly the pH of the buffer (the solution is still green) while the dark orange colour of the adsorbed pH indicator demonstrates that a good part of the sulfonic acid moieties is preserved.

With these results in hand, we decided to move forward and to try to determine the inner acidity of the Nafion beads in a quantitative way. The next section will describe the investigation of beads' acidity through a combination of confocal laser scanning microscopy and ratiometric imaging with a pH-sensitive probe.

## 4.2 QUANTITATIVE DETERMINATION OF ACIDITY WITH CONFOCAL MICROSCOPE

### **4.2.1 Identification of ratiometric probe for confocal microscope**

As a reminder, confocal laser scanning microscopy is an optical imaging technique for capturing multiple two-dimensional images at different depths in a sample. The following image resume the kind of image we expect to obtain by analysing Nafion beads.

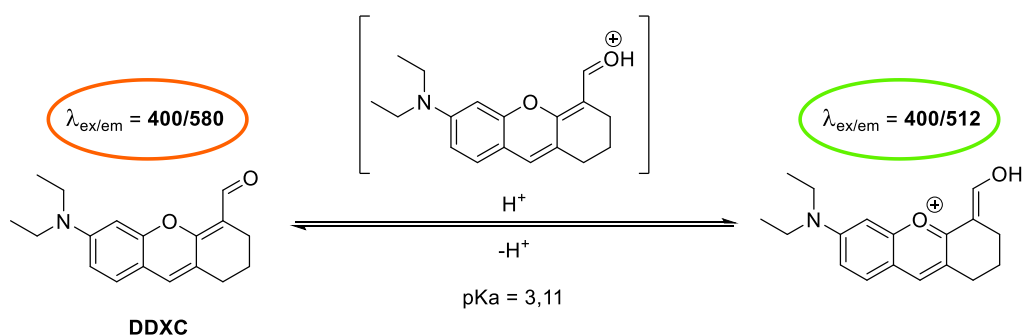


**Figure 46.** Confocal laser scanning microscopy applied on Nafion beads. The microscope records images of the bead by scanning it at different depths ( $z$  dimension). Given the bead's dimension it is possible to take image of only a portion.

To quantify the inner acidity, we coupled the confocal microscope technique with a ratiometric fluorescence strategy. Ratiometric fluorescence is the method where the ratio between the emission intensities at two (or more) wavelengths is related to the change of a parameter. Typically, a fluorescent probe specifically sensitive to an environmental parameter such as ion

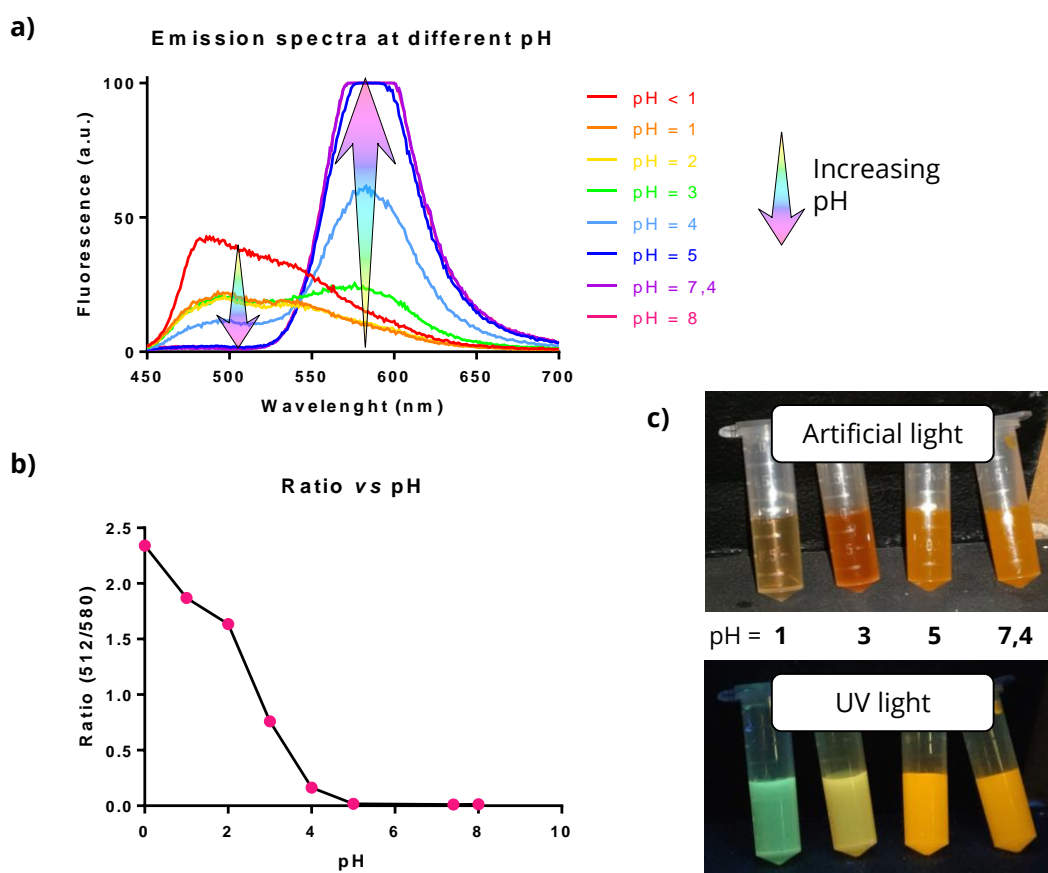
concentration, pH, viscosity, polarity is used.<sup>91,92</sup> Usually the fluorescence excitation spectra of the mentioned probe has two peaks, the intensity of which changes as the probe reacts to changes in the parameter, like pH in our case. Many ratiometric pH-sensitive fluorescent probes have been designed for pH detection in living system, but they are mostly sensitive in a range of pH slightly acidic, not far from the biological one ( $3 < \text{pH} < 8$ ).<sup>93-95</sup>

In 2017, Tong *et al.* introduced a ratiometric pH-sensitive fluorescent probe called **DDXC** which changes its fluorescence properties in the range of acidic pH ( $1 < \text{pH} < 5$ ) thanks to the keto-enol tautomerization (**Figure 57**).<sup>96</sup> **DDXC**'s most important characteristic is that it can be used with confocal microscopy. Indeed, this powerful instrument uses laser sources of fixed wavelength, including  $\lambda = 405 \text{ nm}$  which fits perfectly with the excitation wavelength of the ratiometric probe ( $\lambda = 400 \text{ nm}$ ).



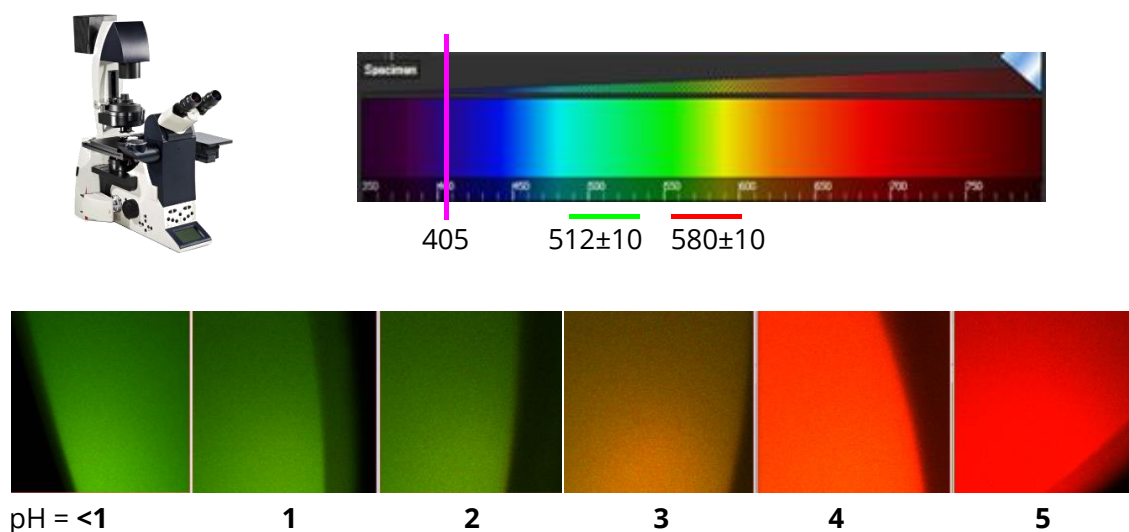
**Figure 57.** DDXC probe keto-enol tautomerization, with excitation and emission wavelengths.

**DDXC** was easily synthesized in two steps and its spectra in aqueous solutions at different pH were recorded using a UV spectrofluorometer. With increasing pH, the emission at 580 nm decreases as that at 512 nm increases **Figure 58a**. The ratio between the two maxima (512/580) was calculated and plotted against pH, resulting in a curve which can be used to calculate the value of pH by extrapolation. As described by Tong *et al.* the  $\text{Em}_{512}/\text{Em}_{580}$  ratio changes only in a range of acidic pH. At  $\text{pH} > 5$  all the DDXC is converted in his enol form (**Figure 58b**). **Figure 58c** shows pictures of the different solution under artificial and UV light.



**Figure 58.** **a)** Emission spectra recorded with a UV spectrophotometer at excitation wavelength of 400 nm. The arrows indicate the change in relation to the pH. **b)** The ratio between the emission at 512 nm and at 580 nm are plotted in function of the pH. The graph can be used to determine the pH of a solution by extrapolation. **c)** DDXC probe dissolved in aqueous solution of pH = 1; 3; 5; 7.4. Picture are taken under artificial and UV light to show the change in colour related to the proton concentration.

To use the obtained graph as calibration curve for the extrapolation of the pH value, it has to be reproduced with the same instrument which will be used to analyse the solid Nafion beads, *i.e.* the confocal microscope. Drops of DDXC solutions at various acidic pH were analysed with confocal microscope, using the 405 nm laser and recording images at the two emission wavelengths ( $512 \pm 10$  and  $580 \pm 10$ ). For each drop of DDXC solution, two digital images are obtained. The first one (512 nm) is coloured in green and its intensity will decrease with increasing pH, while the second (580 nm) is coloured in red and its intensity will increase with pH (Cf. **Figure 58**). The two images can be merged with a dedicated software to give a superimposed image whose colour will vary from greenish (low pH) to reddish (high pH). **Figure 59** shows the settings of the laser and the collection channels on the confocal microscope as well as the image of the drops obtained with the merging of the two channels.

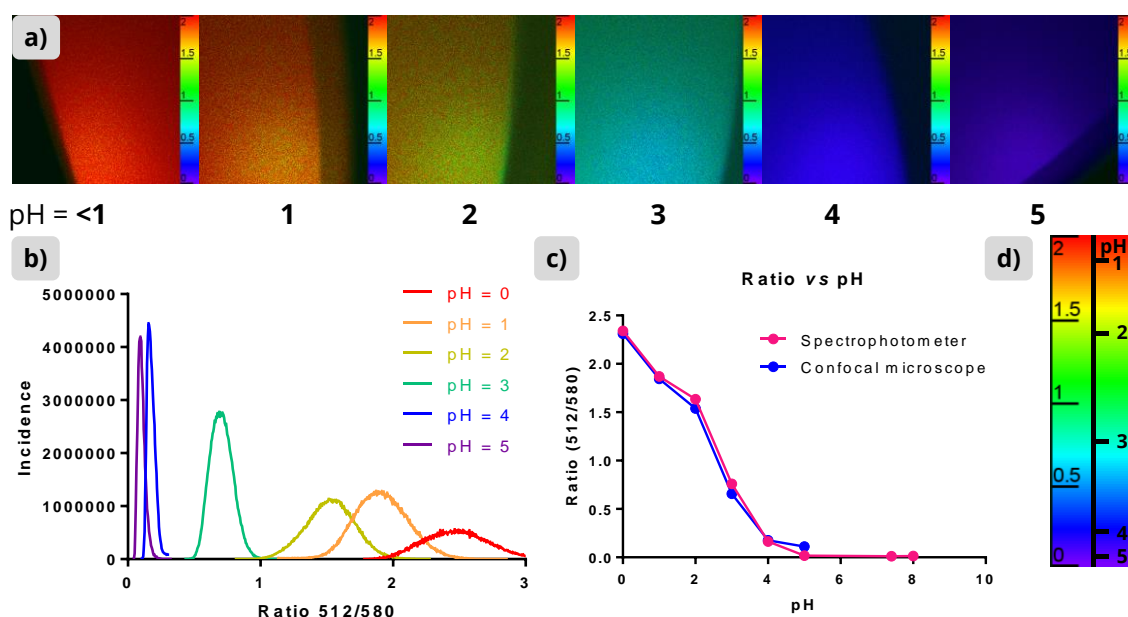


**Figure 59.** Above: confocal microscope settings for excitation (laser at 405 nm) and emission (two channels at  $512\pm 10$  and  $580\pm 10$ ). Below: merged images of **DDXC** solutions' drop from acidic pH < 1 (on the left end) to pH = 5 (on the right end).

A dedicated ImageJ software plug-in, especially conceived at the University of Strasbourg by Romain Vauchelles, allows us to process the obtained images. In each point the ratio between the intensity of the emission at 512 nm and at 580 nm is calculated and the obtained value is related to the colour of the said point. We set the images colouring to a rainbow scale going from purple (ratio = 0, pH = 5) to red (ratio = 2, pH < 1). **Figure 60a** shows the same images presented above (**Figure 59**) processed with the software, the rainbow scale indicates the value of the ratio  $em_{512}/em_{580}$  in function of the colours.

Moreover, it is possible to quantify the distribution of each value of ratio in the picture. The incidence of a certain value of ratio can be plotted in a graph, resulting in a representation of the ratio distribution. **Figure 60b** cumulates the ratio distribution curves of all the analysed images in one graph. For each curve, the ratio value corresponding to the maximum of the curve is representative of the pH at which the image was taken. The values of ratio obtained from all the maxima in the picture are plotted against the corresponding pH to obtain a curve of pH vs ratio, as it was done for the spectra recorded at the spectrofluorometer. The two obtained curves match perfectly one with each other (**Figure 60c**).

Regarding the rainbow scale, for the sake of clarity, we will use from this point a scale which correlates the colour directly with the pH value (**Figure 60d**).

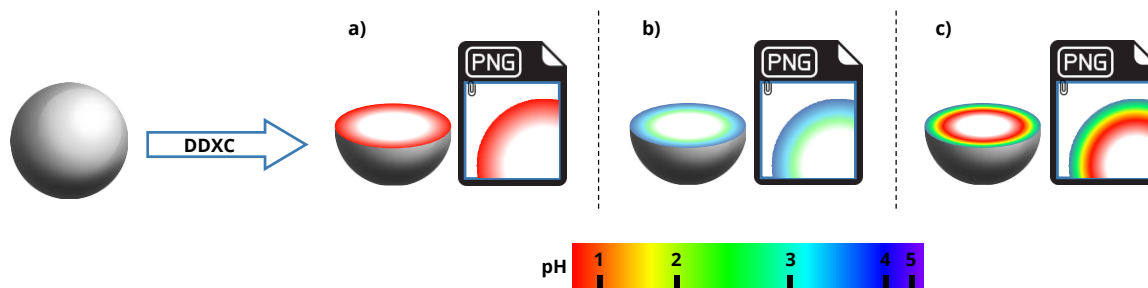


**Figure 60.** **a)** Processed images of DDXC solutions' drops. The colour is in function of the ratio between the intensities of fluorescence recorded at 512 nm and 580 nm. **b)** Graph of the population of each image according to the value of the ratio. The value of ratio corresponding to the maximum incidence is attributed at the corresponding value of pH, allowing to build the calibration curve. **c)** Calibration curve obtained with the confocal microscope, compared to the one obtained with the spectrophotometer (Cf. **Figure 58**). **d)** Colour scale in function of the ratio  $E_{m512}/E_{m580}$  and of the corresponding pH values.

Once the calibration curve has been acquired, the imaging of Nafion beads and PEG-AASA co-polymer can follow.

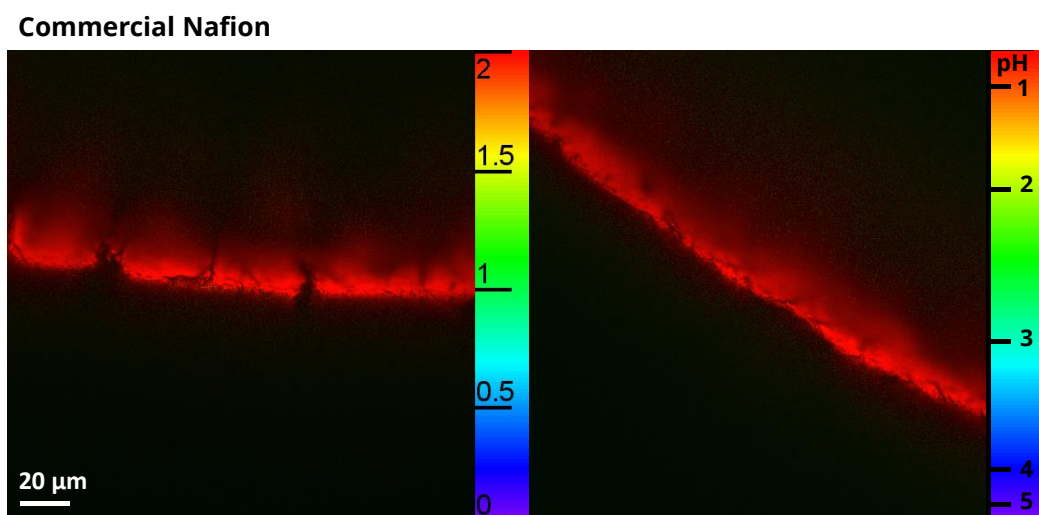
#### 4.2.2 Determination of acidity of Nafion

Nafion beads are soaked with the ratiometric pH-sensitive probe **DDXC** (in aqueous solution) and are analysed at the confocal microscope. The images obtained are processed with the software for ratiometric analysis and, depending on the degree of neutralization of the acidic sites, we expected them to fall into the casuistry illustrated in **Figure 61**. Nafion-90, which gave the best combination of fluorescence and buffer preservation in plasma (**Table 17**, entry 24, page 109) is meant to have an increasing proton concentration from the external layers to the inner part (**Figure 61**, case c).



**Figure 61.** Confocal microscopy images of Nafion soaked with DDXC expected with **a)** commercial untreated acidic Nafion, **b)** neutralized Nafion and **c)** partially deactivated Nafion-90 keeping inner acidity. pH colour scale is the same derivate from the processed images of **DDXC** at different pHs (Cf. **Figure 60**).

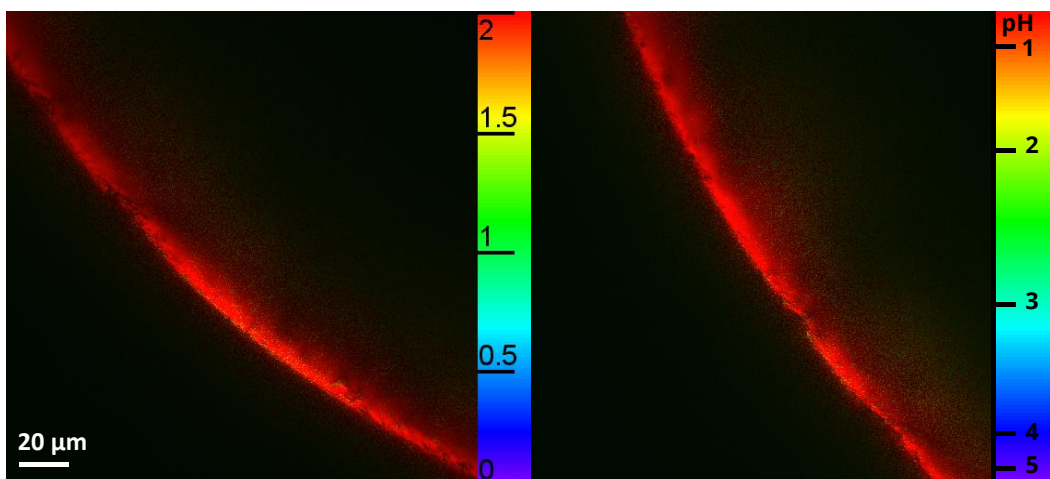
Non-treated commercial Nafion beads and beads washed in flow with a PBS solution for different amount of time (**Table 17**, page 109) are soaked with 0.5 mL of a 0.5 mM **DDXC** solution in ultrapure water. Images are taken at the confocal microscope with the same excitation/emission setting used to build the calibration curve. Two images are recorded for each bead at a given depth, one for each emission channel. Then they are processed with the ratiometric software to give an image coloured according to the ratio between the two emission intensities ( $em_{512}/em_{580}$ ). Processed images are reported in the following figures.



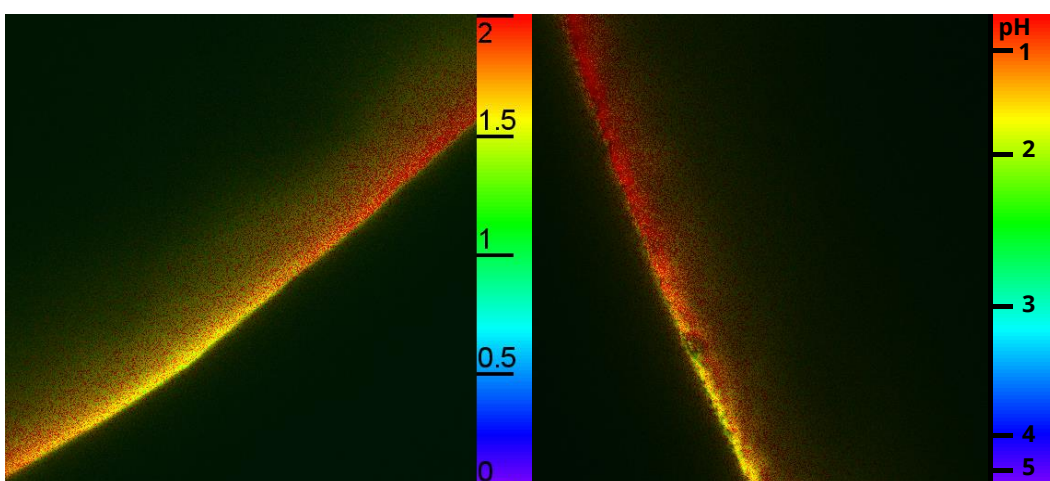
**Figure 62.** Ratiometric images of commercial Nafion NR50. Colour code is represented both as in function of the ratio and of the pH.



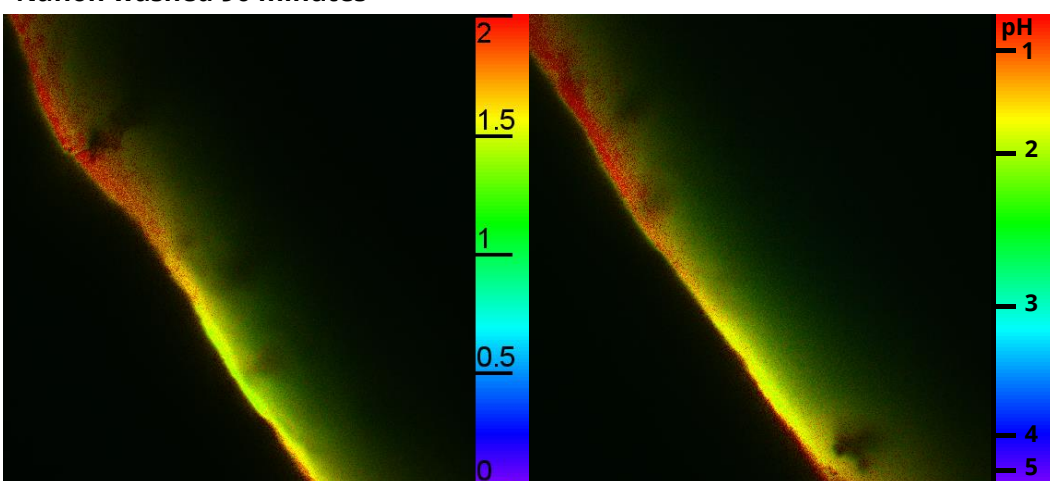
**Nafion washed 30 minutes**



**Nafion washed 60 minutes**



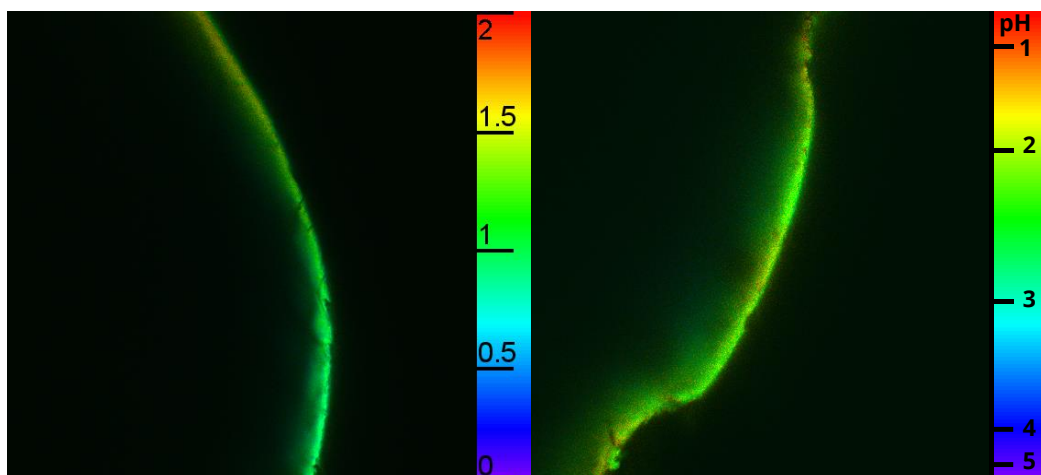
**Nafion washed 90 minutes**



**Figure 63.** Ratiometric images of Nafion NR50 washed for 30, 60, and 90 minutes. Colour code is represented both as in function of the ratio and of the pH.

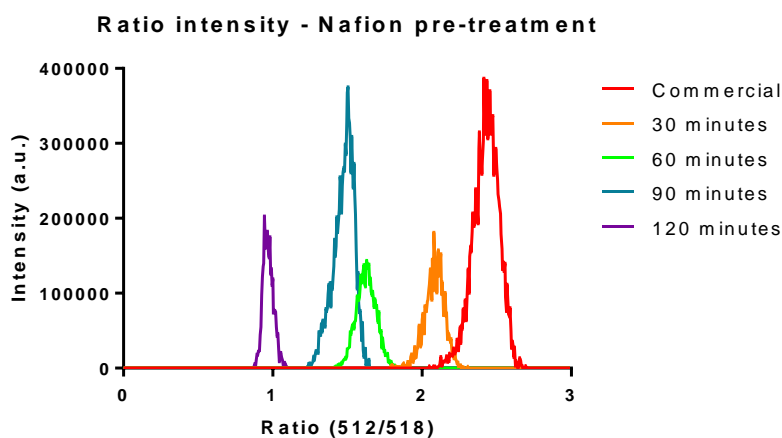


## Nafion washed 120 minutes

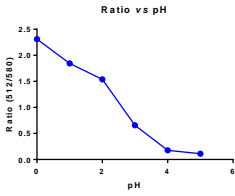


**Figure 64.** Ratiometric images of Nafion NR50 washed for 120 minutes. Colour code is represented both as in function of the ratio and of the pH.

Intensity of all the above images were plotted in function of the ratio, resulting in the graph showed below (**Figure 65**). The value of ratio corresponding to the maxima is correlated to the value of pH, according to the ratiometric curve previously built (**Table 24**).



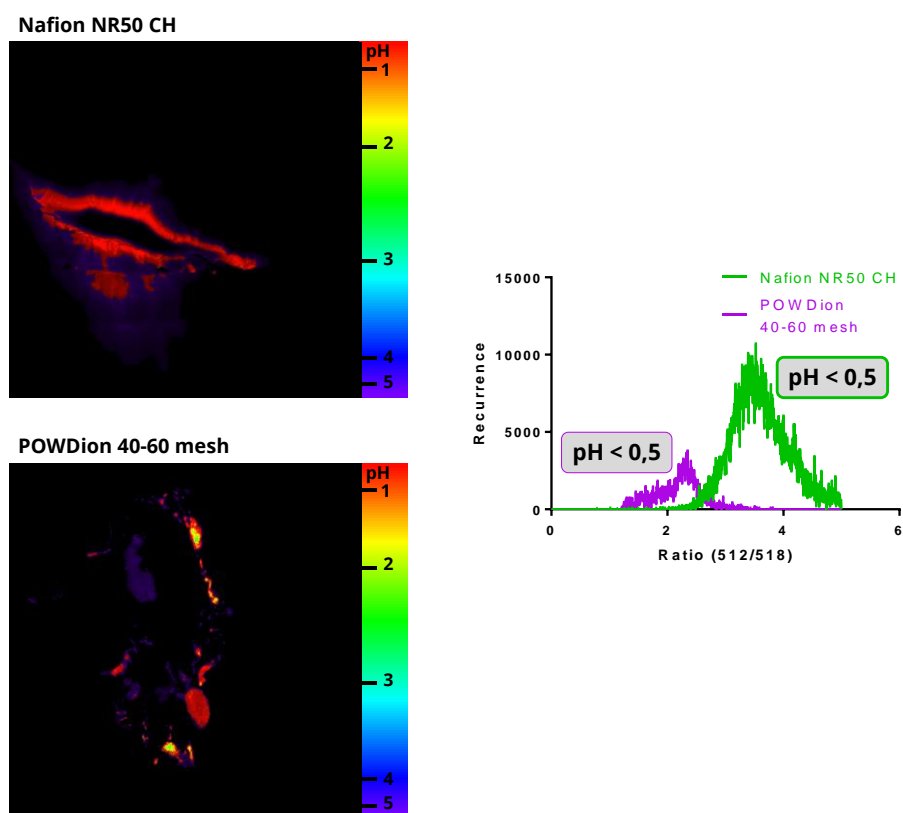
**Figure 65.** Graph of the ratio intensities of different Nafion beads. The maxima correspond to a value of ratio which is directly correlated to the proton concentration (Cf. **Figure 60**).

Ratio vs pH graph	Entry	Nafion	Ratio(max)	pH
	1	Commercial	2.4	<0.5
	2	30 minutes	2.1	~0.5
	3	60 minutes	1.65	~1.9
	4	90 minutes	1.5	~2.1
	5	120 minutes	0.95	~2.7

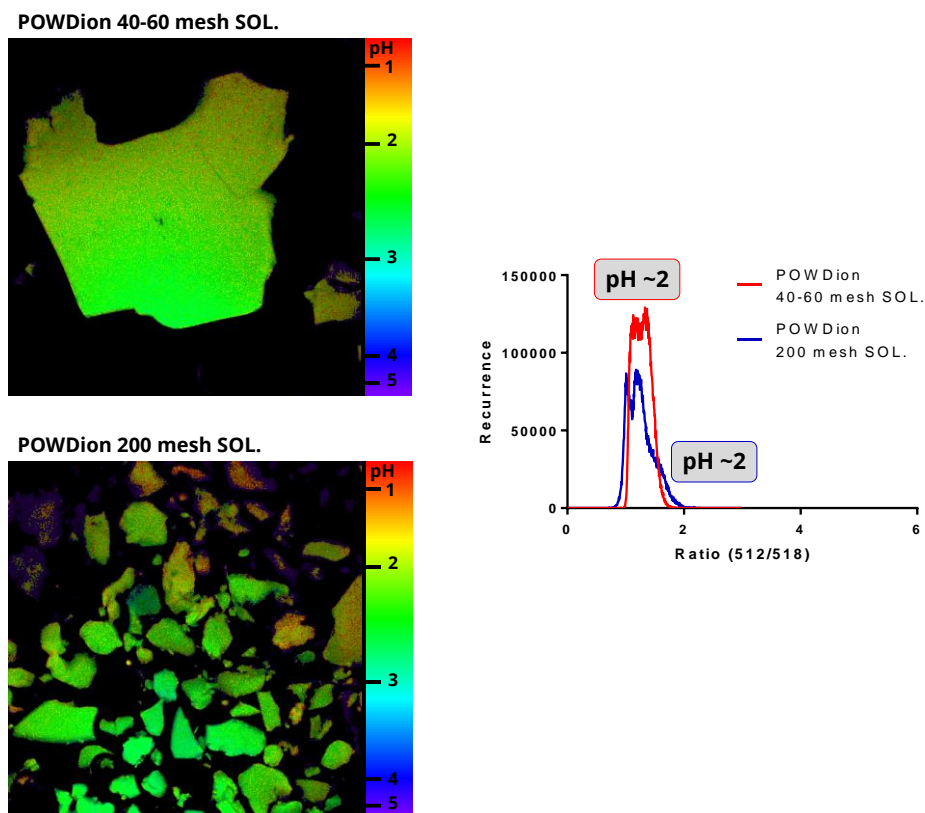
**Table 24.** Acidity of solid catalyst Nafion NR50 according to the ratiometric analysis.

According to the pH values extrapolated from the ratio vs pH curve, the acidity of Nafion decreases with the increase of the pre-washing time. In particular, Nafion-90 presents a pH of ~2.1 and, as we observed during the screenings, it is able to preserve its acidity (and hydrolytic activity) in plasma.

Ratiometric analysis with DDXC and confocal microscope was also conducted on other commercially available forms of Nafion. The following figures show a selection of the processed ratiometric images and the corresponding ratio distribution.



**Figure 66.** Nafion NR50 - CH and POWDion™ 40-60 mesh soaked with DDXC and analysed at confocal microscope; the graph shows the ratiometric distribution and extrapolated pH values.

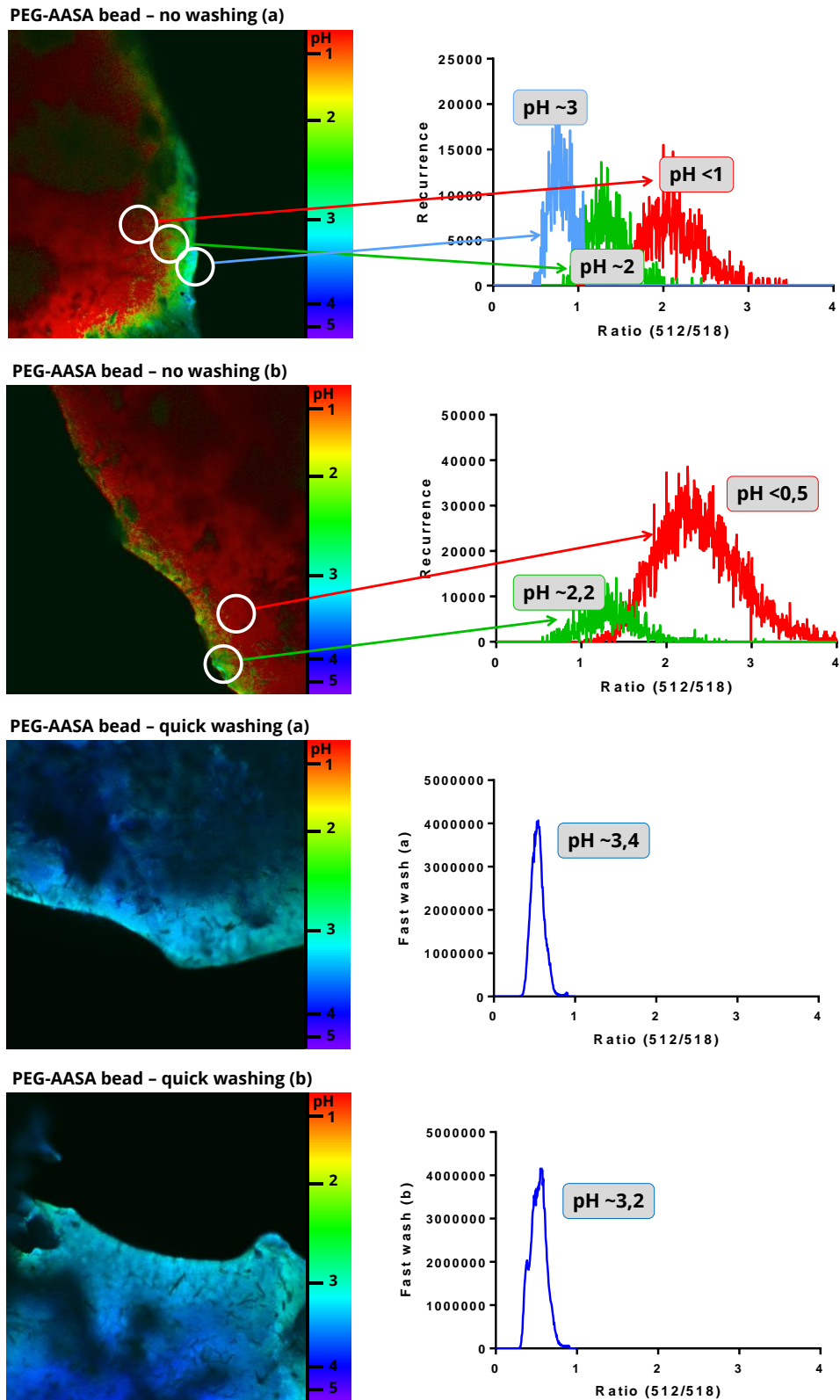


**Figure 67.** POWDion™ 40-60 mesh SOL. and POWDion™ 200 mesh SOL. soaked with DDXC and analysed at confocal microscope; ratiometric distribution and extrapolated pH values.

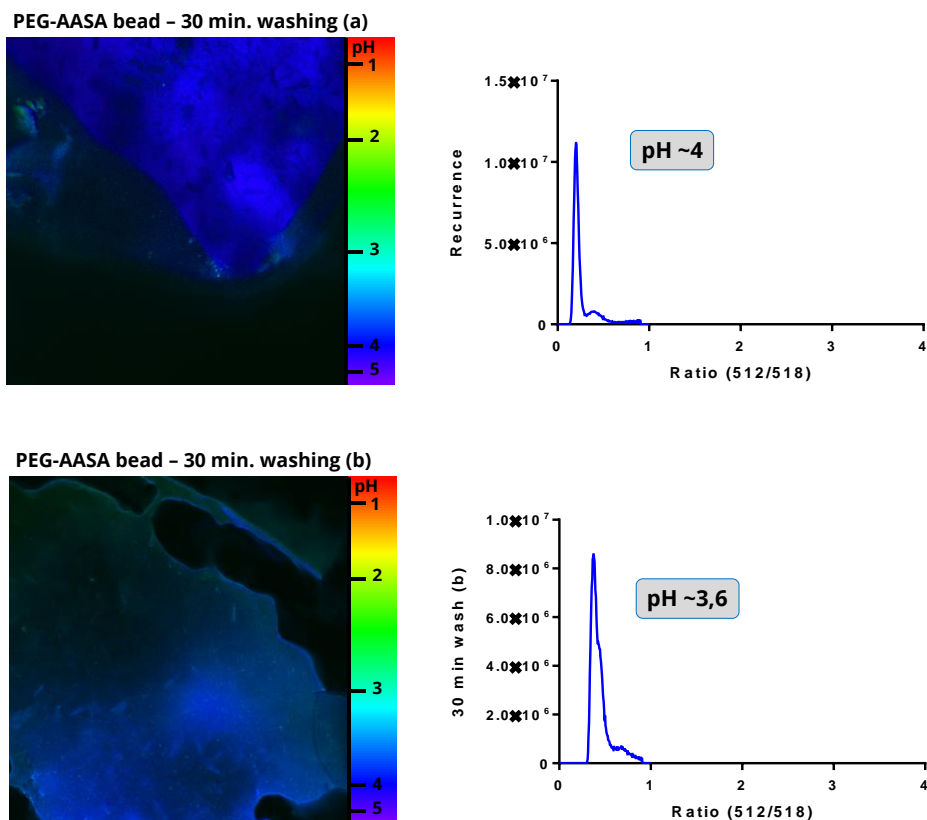
Nafion chopped beads (Nafion NR50 CH) and POWDion™ 40-60 mesh are very acidic, as confirmed by the results obtained when tested with acetal **F-APNM5** in plasma (cf. **Table 19**, page 113). On the contrary, the ratiometric analysis of the two commercial “soluble” Nafion powders revealed that their acidity is close to that of Nafion-90 but when tested in plasma, no hydrolysis was observed in 24 hours. This may be imputed to the different formulation of the two polymers -with respect to Nafion NR50- which makes them soluble in organic solvents. Information about the chemical composition and synthetic procedures is not provided by the supplier, so our hypothesis could not be verified.

#### 4.2.3 Determination of acidity of PEG-AASA beads

The ratiometric analysis of **PEG-AASA** beads was also performed. Given the susceptibility of the co-polymer to the time of pre-washing in plasma (cf. **Figure 55**, page 124), three kind of beads were analyzed: **i)** not washed; **ii)** quickly washed in plasma; **iii)** washed for 30 minutes at 37 °C in plasma (cf. page 122). Images obtained are reported in **Figure 68** and **Figure 69**, as well as the ratio distribution graph and the extrapolated pH value.



**Figure 68.** Ratiometric images, ratio distribution and extrapolated pH value for **PEG-AASA** beads not washed (first two images) and quickly washed in plasma (last two images).



**Figure 69.** Ratiometric images, ratio distribution and extrapolated pH value for **PEG-AASA** beads washed in plasma for 30 minutes.

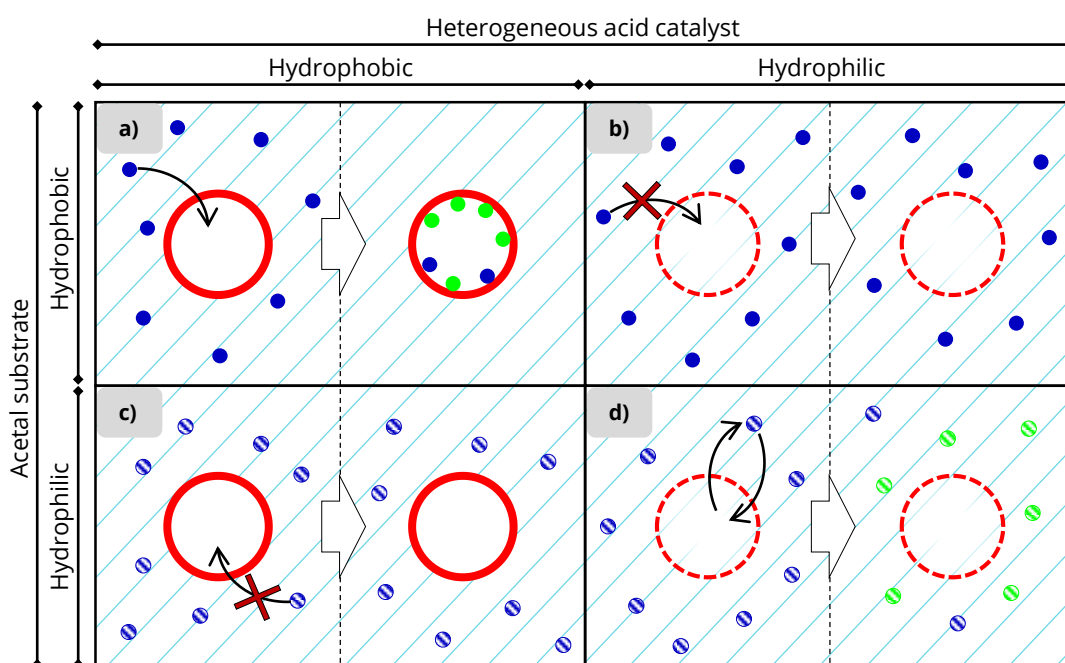
The ratiometric analysis reveal that even a short contact with a buffered solution can significantly affect the acidity of the PEG-based co-polymer, probably because of its porosity and affinity with the biofluid.

In the next section we related the calculated pH of Nafion and PEG-AASA beads to the degree of hydrolysis with different acetal substrate observed above (sections 2 and 3 of this chapter).

## 5. CORRELATION BETWEEN OBSERVED HYDROLYTIC ACTIVITY AND CALCULATED ACIDITY OF NAFION NR50 AND PEG-AASA-20% WITH DIFFERENT ACETAL SUBSTRATES

The acidity of the solid catalysts calculated through ratio-metric analysis should match the results obtained in terms of hydrolysis with acetal substrates of different nature.

According to our premises exposed in the early definition of the project, the hydrophobic or hydrophilic nature of the heterogeneous catalyst is responsible to the delivery of different degree of hydrolysis according to the nature of the acetal used as substrate. As a reminder, here we report again **Figure 2**.



**Figure 2.** Representation of the four possible scenarios given by the combination of the substrate and the solid catalyst. Hydrophobic catalyst is symbolized by a sphere with a plain contour, while the hydrophilic catalyst's symbol has a dotted contour. The substrate and the product are represented as, respectively, blue and green dots. Dots are plain for the hydrophobic substrate and striped for the hydrophilic one. **a)** Hydrophobic substrate + hydrophobic catalysts; **b)** hydrophobic substrate + hydrophilic catalysts; **c)** hydrophilic substrate + hydrophobic catalyst and **d)** hydrophilic substrate + hydrophilic catalyst.

We speculated that scenarios **a)** and **d)** in which the substrate and catalyst have matching natures are more likely to carry out acetal hydrolysis, unlike cases **b)** and **c)** in which the lack of affinity between the catalysts and the substrate would give a negative outcome.

In the following table we collected all the results obtained in plasma with the two selected catalysts Nafion NR50 and PEG-AASA-20% in combination with acetal substrates cleavable at pH < 4 (**F-APM5** and **PEGAM5**). We took into consideration only the type of catalyst which, thanks to the right washing pre-treatment, do not lower the proton concentration in plasma more than 1.5 unit:

- “Nafion-90”. Nafion NR50 beads washed with a PBS solution ([NaCl] = 13.7 mM) in continuous flow for 90 minutes;
- “PEG-AASA-20%”. PEG-AASA co-polymer with a 20% content of the acid, pre-washed for few seconds with plasma (“fast washing”).

Entry	Catalyst	Substrate	pH of plasma <sup>(1)</sup>	Time	Hydrolysis
1	Nafion-90	F-APNM5	7.5	24 hours	Low fluorescence detected in beads <sup>(2)</sup>
2	Nafion-90	PEGAM5	7.5	7 days	0% <sup>(3)</sup>
3	PEG-AASA-20% (film-20 mg)	F-APNM5	6	3 days	7.8% <sup>(4)</sup>
4	PEG-AASA-20% (bead-5 mg)	F-APNM5	7.5	3 days	2.0% <sup>(4)</sup>
5	PEG-AASA-20% (bead-5 mg)	PEGAM5	7.5	7 days	78% <sup>(3)</sup>
6	PEG-AASA-20% (bead-10 mg)	PEGAM5	7.5	4 days	94% <sup>(3)</sup>

(1) pH of plasma measured with pH paper after catalyst addition

(2) Fluorescence of TAMRA detected under UV lamp and with confocal microscope (ex<sub>561</sub>/em<sub>580</sub>)

(3) Calculated by LC-MS peak area of the product

(4) Fluorescence of TAMRA measured with spectrophotometer (ex<sub>550</sub>/em<sub>580</sub>)

**Table 25.** Condensed collection of results obtained by treating acetals **F-APNM5** and **PEGAM5** in plasma with heterogeneous catalysts Nafion-90 and PEG-AASA-20% (in form of film and beads). Entries in which the hydrophobic or hydrophilic nature of the substrate and the catalyst matches are enlightened in grey.

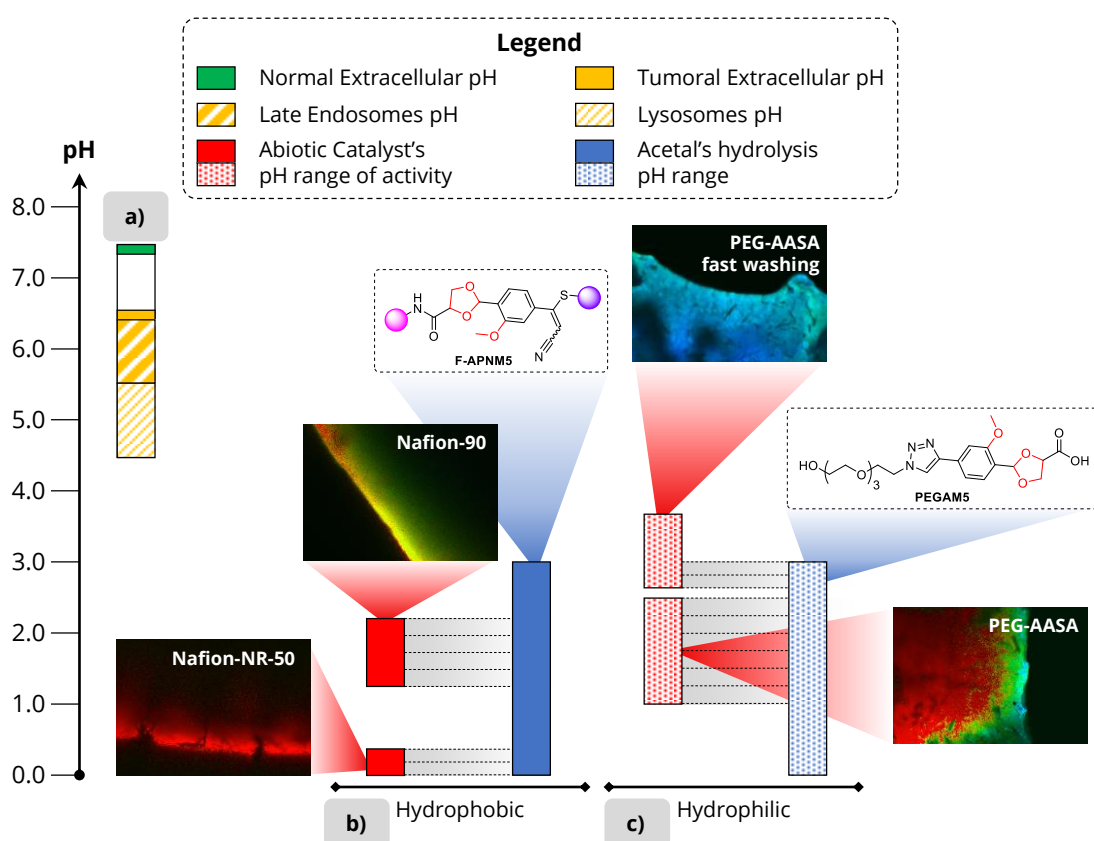
Nafion-90 catalyse the hydrolysis of the hydrophobic FRET acetal **F-APNM5** (fluorescence due to the TAMRA product is detected after 24 hours, entry 1), while when the hydrophilic **PEGAM5** is used, the solid catalyst does not adsorb the acetal, so no hydrolysis is observed over 7 days (entry 2).

PEG-AASA-20% in form of film and beads do not catalyse the hydrolysis of **F-APNM5** with an appreciable rate: less than 10% hydrolysis is reached after a week (entries 3, 4). On the contrary, the affinity with the hydrophilic **PEGAM5** cause an increment of hydrolysis rate such

that 78% of hydrolysis is observed after 7 days (entry 5) and 94% is observed after 4 days if the quantity of the catalyst is raised to 10 mg (entry 6).

Overall, the two catalyst-substrate couples of similar nature (highlighted in grey on the table) revealed to be more performing than the others. These results confirm our hypothesis about the importance of the interaction between the substrate and the solid catalyst in the hydrolysis rate.

Such catalyst-substrate couples are depicted in the following figure according to the range of pH in which the catalyst is active and the substrate is hydrolysable. pH values for the catalysts are those obtained by the ratiometric analysis, while pH values of the substrate are in accordance with the profile obtained in different acidic solution (cf. **Figure 33**, page 74)



**Figure 70.** **a)** biological pH values; **b)** pH ranges of hydrolytic activity of commercial and pre-treated Nafion NR50 related to the pH range of **F-APNM5** cleavability; **c)** pH ranges of hydrolytic activity of PEG-AASA-20% washed and not-washed related to the pH range of **PEGAM5** cleavability.

In conclusion we can positively affirm that we meet our objective. We defined two different systems for a bond-breaking reaction in biological environment. Both the systems involve the use of an abiotic heterogeneous acid catalyst and a xenobiotic substrate of matching nature



(hydrophobic or hydrophilic). Both the acidic catalysts work in biofluid (plasma) without affecting the highly buffered media. Both the substrates are not cleaved in the normal biological environment, since the pH of extracellular fluid and of cell organelles is not enough low to trigger the hydrolysis. Indeed, we can think of the heterogeneous catalysts as some extremely acidic organelles which can maintain a high proton concentration inside them, selectively hydrolyse the substrate and -in case of PEG-AASA- release the product.

At this point of the project we defined the first *in vivo* proof of concept in mice, which will be described on the next chapter.

## IV – TOWARDS *IN VIVO* PROOF OF CONCEPT

### 1. OBJECTIVES

In the work described previously we responded to some issues pertinent to the transposition of a chemical reaction from the bench to close-to-biological conditions. In our tests we used a concentration of the substrate in the order of micromolar (when possible) and we optimized the hydrolysis in a complex and rich biofluid (plasma).

In this chapter we aim to proceed one step further and apply our abiotic hydrolysis system *in vivo*. Such experiments are carried in a much more complex biological system in which factors like the multi-molecular crowding, the distribution and excretion of the xenobiotic substrate and its pharmacokinetic play a major role.

Our objective here is to get a first indication that acetal hydrolysis -triggered in a range of pH lower than the biological one- can be carried out *in vivo*, thanks to an heterogenous biocompatible acidic catalyst able to maintain inner high proton concentration in a buffered environment.

To this end, we planned a *proof of concept* in mice, in collaboration with Dr. Wojciech Krezel and Joanna Sobska (IGBMC, Illkirch), described in the following section.

## 2. IN VIVO PROOF OF CONCEPT SETUP

### 2.1 CHOICE OF CATALYST AND SUBSTRATE

In the previous work we identified two catalyst-substrate couples that proved to work in plasma:

- Nafion-90 and hydrophobic FRET probe F-APNM5. The catalyst is in form of beads of ~3 mm diameter and adsorbs the FRET probe. The acetal substrate is hydrophobic and allows to monitor the hydrolysis through the fluorescence emission given by the TAMRA product.
- PEG-AASA-20% and hydrophilic PEGAM5. The catalyst is produced in form of beads or film and is not adsorbent. The acetal substrate is hydrophilic and its hydrolysis cannot be detected via imaging techniques.

For the first application and proof of concept *in vivo* we chose the first system because **i)** the adsorbent catalyst allows to concentrate the substrate in one spot, so the appearance of fluorescence inside the catalyst can be related only to the hydrolysis operated by the catalyst; **ii)** the FRET substrate should allow to monitor the hydrolysis by appearance of a fluorescence signal located within the beads.

In the next section, the setup of the *in vivo* experiment will be described in detail and the major constraint coming from the use of Nafion and **F-APNM5** will be addressed.

### 2.2 IN VIVO PROOF OF CONCEPT: CHALLENGES AND PLANNING

#### **2.2.1 Constraint relative to the use of Nafion beads**

The relatively big dimension of Nafion beads constitute a constraint that has to be taken into consideration in the experiment planning. We decided to implant the Nafion beads ( $d \approx 3$  mm) under the skin of the mice. This arose a major challenge: since the acetal substrate will be injected in the blood stream, the vascularization of the bead must be insured. Hence, before implantation, Nafion beads were pre-washed for 90 minutes in flow (following the procedure previously described, cf. section 2.6, page 104) and then soaked with human Fibroblast Growth Factor, which promotes endothelial cell proliferation and the physical organization of endothelial cells into tube-like structures. It thus promotes angiogenesis, the growth of new blood vessels from the pre-existing vasculature.<sup>97</sup>

After implantation, we will wait for the angiogenesis to occur, at which point the mice is ready for injection of the substrate (cf. section 2.2.4 on experiment planning).

The soaked bead to be implanted (called “Nafion-hFGF”) was tested to check that it still triggers the acetal hydrolysis (cf. paragraph 2.2.3, below in this page).

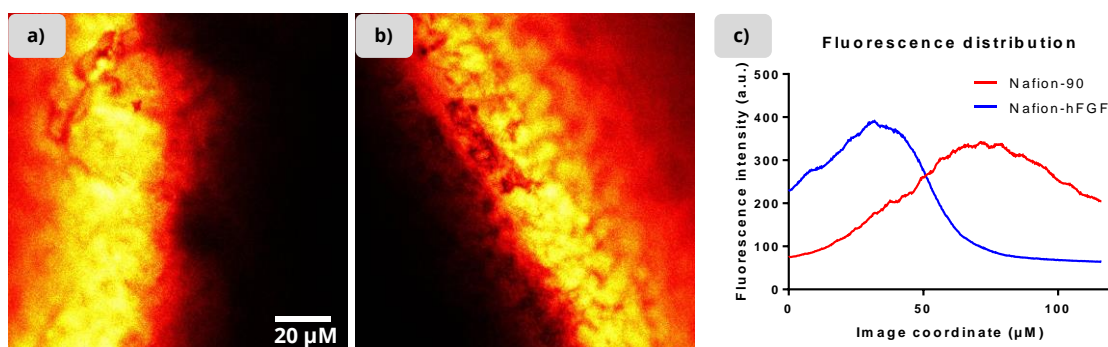
### **2.2.2 Constraint relative to the use of F-APNM5**

Despite the great advantage that the use of FRET probes gives in terms of the monitoring of the hydrolysis, its hydrophobicity constitutes a major constraint in the formulation of the solution for injections in mice. Indeed, a solution of concentration from 10 to 30 mM has to be used to reach a plasmatic concentration high enough to allow the hydrolysis to be detected. At such concentration **F-APNM5** is not soluble neither in water nor PBS, nor in a mixture of DMSO/water with a percentage of DMSO tolerated by the living organism (up to 50% if only one IV injection is given).

We addressed this issue to Dr. François Daubeuf (UMR7200, Université de Strasbourg), expert in formulations for *in vivo* experiments. He suggested that one possibility would be to exploit the hydrophobicity of the BHQ extremity of the molecule and the charged TAMRA extremity to create micelles in which the charged TAMRA is in contact with the aqueous solution and the hydrophobic BHQ is in the inside of the micelle. To help the formation of micelle, **F-APNM5** was solubilized in a PBS solution with 10wt% content of Kolliphor® EL, also known as Cremophor®. Kolliphor® is a derivative of castor oil and it is commonly used to emulsify and solubilize oils and other water-insoluble substances. Thanks to this emulsifying agent, it was possible to obtain a 10 mM solution of **F-APNM5** ready to be injected intravenously. Such formulation should still enable the acidic catalysis to occur (cf. next paragraph).

### **2.2.3 Test of Nafion-hFGF beads with F-APNM5 from Kolliphor® solution**

Nafion bead soaked with hFGF were tested for hydrolysis in plasma in presence of **F-APNM5** from the stock solution in PBS-10wt%Kolliphor®, using the procedure previously described for the catalyst screening ([**F-APNM5**] = 10  $\mu$ M, V = 0.3 mL, T = 37 °C, t = 24h, agitation at 750 rpm). At t = 24 hours, the bead was taken and analysed at the confocal microscope. The image of fluorescence emission obtained was compared to that obtained with a Nafion-90 (not soaked with hFGF) bead tested with **F-APNM5** from the stock solution in DMSO (**Figure 71**).



**Figure 71.** a) Nafion-hFGF and b) Nafion-90 analysed at confocal microscope after 24 hours reaction with **F-APNM5** in plasma. c) Fluorescence intensity of the whole images measured with ImageJ®.

The fluorescence distribution measured with ImageJ® software reveals that fluorescence emission of Nafion-hFGF bead is comparable to that of the Nafion-90 bead. Hence, it can be deduced that the soaking of the bead with human Fibroblast Growth Factor does not affect the outcome of the hydrolysis. Also, the presence of the emulsifying agent seems to not affect the reactivity of the acetal. In conclusion, both the catalyst and the acetal solution prepared for the *in vivo* experiment maintain the same activity observed previously.

In the next section we describe the setup of the *in vivo* proof of concept.

### 2.2.4 *In vivo* experiments planning

To prove our concept, we planned a series of experiments listed in **Table 26** and below, with the description of the expected outcome.

1. **Catalyst alone.** First, we need to confirm the vascularization of the implanted bead on mice. We expect also to confirm its biocompatibility.
2. **F-APNM5 alone.** Then we need to follow the pharmacokinetic of the probe. We check if hydrolysis can be induced *in vivo* in the absence of the trigger by monitoring the appearance of fluorescence. After some time, we expect to observe fluorescence emission in the liver and kidneys, where the acetal may accumulate, as part of the usual metabolism of xenobiotics.
3. **Catalyst in presence of acetal F-APNM5.** Then we can test our system *catalyst + probe*. We expect that the acetal is adsorbed by the solid catalyst which triggers its hydrolysis, resulting in the emission of fluorescence from the bead.
4. **TAMRA-NHCO-diol alone.** In this case the starting acetal **F-APNM5** is pre-hydrolysed into the diol (linked to TAMRA, named **TAMRA-NHCO-diol**) and the aldehyde (linked to BHQ-2, named **BHQ-2-aldehyde**). A solution of **TAMRA-NHCO-diol** is injected in a

mouse with Nafion-hFGF implanted. We want to follow the pharmacokinetic of the hydrolysis product through imaging of the fluorescence emitted. We expect to see accumulation on liver and kidney.

5. Catalyst in presence of TAMRA-NHCO-diol. We want to follow the pharmacokinetic of the product of hydrolysis (**TAMRA-NHCO-diol**) -in presence of the implanted catalyst- by imaging the fluorescence emitted by TAMRA. We expect that a part of the product is adsorbed by the catalyst and the rest is metabolized as any xenobiotic (accumulation on liver and kidney is expected).

Entry	Nafion-hFGF	F-APNM5	TAMRA-NHCO-diol
1	X		
2		X	
3			X
4	X	X	
5	X		X

**Table 26.** List of the planned experiments. Each entry line corresponds to one kind of experiment (to be reproduced in triplicates) and displays if the catalyst is implanted (marked with X) and which chemical is injected into the mice (marked with X).

A comparison between experiment #4 (Nafion-hFGF + **F-APNM5**) and experiment #1 (**F-APNM5** alone) should prove that the appearance of fluorescence in the implanted bead is to impute only to the activity of the solid catalyst, therefore proving our concept.

The experiment's procedures were planned as follow:

- I. Preparation of the catalyst, the acetal and TAMRA-diol. Nafion-hFGF is prepared right before the implantation in mice (cf. Experimental Procedures, section 5.3, page 218). **F-APNM5** and **TAMRA-NHCO-diol** solutions in PBS-10wt%Kolliphor® can be prepared before and stored at -20°C.
- II. Implantation of beads in mice. If required by the experiment (cf. **Table 26**), Nafion-hFGF is implanted under the skin of the mouse. After the formation of new blood vessels (angiogenesis) around the bead occurs, we can proceed with the next step.
- III. Intravenous injection. According to the type of experiment performed, 60 µL of a 10 mM solution of **F-APNM5** or **TAMRA-diol** are injected intravenously.

- IV.** Live Imaging. After 24 hours, the mouse is monitored for fluorescence emission, using excitation and emission wavelengths of TAMRA ( $\lambda_{\text{ex}}$ : 550/ $\lambda_{\text{em}}$ : 580). One day should be enough to spot some fluorescence. If this is not the case, a second IV injection (60  $\mu\text{L}$ ) is performed and the mouse is controlled every 24 hours for some days.

Our system is ready to be tested *in vivo*, but presently authorization for animal experiments is pending.

### 3. CONCLUSION

The *in vivo* proof of concept was planned in detail. Beads were prepared for implantation and tested to control that their hydrolytic activity was not decreased by the presence of hFGF adsorbed. A formulation of the hydrophobic acetal substrate **F-APNM5** was found and a solution ready to be injected was prepared. A series of different experiments to confirm our premises was listed, as well as all the steps of the experiments were described.

Unfortunately, within the time of this doctoral project, it was not possible to start with the implantation of the beads in mice, thus the proof of concept *in vivo* will be performed after the presentation of this thesis.





## V – LATE STAGE FUNCTIONALIZATION OF ANTICANCER AGENTS

In this chapter we address the possible applications of this abiotic system based on acetal hydrolysis. As mentioned in the introduction, this bond-breaking reaction could be exploited by payload-releasing techniques, if the payload presents a diol motif in its chemical structure. Since most of the currently used xenobiotics do not present a diol in their structure, we postulated that it is possible to modify the complex chemical structure of active molecules to insert a diol function without endangering their activity. In this chapter we broaden the scope from diol insertion to a pool of late-stage functionalization reactions of anticancer agents with the aim to find mild procedures which can be applied to a wide group of complex compounds to enhance their activity and performance.

### 1. INTRODUCTION

A part of the never-ending search of more powerful anticancer agents is usually done investigating how a little modification in the structure of a lead-compound can increase (or decrease) its activity.<sup>98,99</sup> These new molecules are often obtained by de novo synthesis (time and money consuming)<sup>100,101</sup> or by natural compound screening.<sup>102,103</sup> Such high-risk approaches are known to meet many failures at all stage of development. Late stage functionalization of anticancer agents is an alternative strategy which lead to patentable and highly active anticancer drugs with a higher success rate.<sup>104-107</sup>

Exploiting the newest chemo-selective and mild procedures for the late stage functionalization of complex compounds, it will be tried to modify the structure of readily available FDA-approved (often out of patent) anticancer drugs in order to empower their activity. Using these novel chemical transformations, it may be possible to obtain novel chemical structures that could not have been obtained using classical approaches. Some of these novel structures may present improved biological activity and safety profile while not subjected to patents limitations.

## 2. PROJECT PLANNING

### 2.1 SELECTION OF PROCEDURES

The first step of this project consists of a deep and detailed bibliographic research about late stage functionalization and C-H activation techniques and procedures suitable for being applied to complex anticancer drugs.

To be more specific, scrutinized procedures are either slight modifications of the molecule's structure –such as isomerization, oxidation, reduction, rearrangements<sup>-108,109</sup> and addition of functions –such as halogenation,<sup>110-113</sup> azidation,<sup>114-116</sup> amination,<sup>117</sup> trifluoromethylation,<sup>118-122</sup> trifluorothiomethylation,<sup>123,124</sup> cyanation,<sup>125</sup> amidation<sup>126</sup>- in order to obtain a better activity or to exploit the newly introduced function for bioconjugation.

A first set of selected procedures contains those who meet the following qualities:

- **“simple”**, that is involving the use of up to maximum three reactants and avoiding complex work up;
- **“direct”**, in other words: protection and deprotection steps of reactive moieties (mainly hydroxyl and amine groups) must be avoided;
- **selective** and **tolerant** so that can be used on molecules containing many reactive sites (*i.e.* double bonds, hydroxyl groups, primary amines and others);
- **mild conditions**: harsh conditions, such as high reaction temperature, must be avoided because of the delicacy of complex substrates. Also reaction will be carried out on a scale of 0.2 – 0.5 mg and with cytotoxic substrates, thus complex reaction set ups be better avoided.

In the last decades, more and more researches worked in the field of LSF and direct C-H activation, producing a huge amount of publications to scrutinize in order to find the more promising reactions.<sup>127-131</sup>

## 2.2 REACTION CONDITIONS

Because expensive and highly cytotoxic molecules will be used as reaction substrates, it is not possible to work in the classical organic chemistry bench set-up. The protocol for the handling of cytotoxic material must be employed. Cytotoxic substrates can be handled only in a dedicated fume hood where reaction solutions can be prepared in vials which must be sealed before moving out from the hood. Therefore, normal reaction procedures cannot be applied. These includes, but it is not limited to: bubbling inert gas into the reaction mixture once the vial is sealed, refluxing solvents, creating dry and/or inert atmosphere before adding the substrate, adding other reagents after the vial is sealed.

Moreover, it will be used a very low amount of starting material in each reaction vial (0.2 – 0.5 mg) in order to permit to run systematic campaign on more than 20 reaction conditions. As a consequence, reactions will be monitored by HPLC/MS. Each product will be purified using an HPLC instrumentation specific for cytotoxic compounds.

## 2.3 EXPERIMENTAL PLANNING

A plan will be applied as follow:

- I.** Test the stability of the molecules in a panel of temperatures and solvents (including but not limited to the one selected for screening) in order to determine for each molecule which are the temperature limits and the forbidden solvents.
- II.** Carry out the screening campaign in all the selected procedures on a micro-scale (0.2 – 0.5 mg, 20 - 50  $\mu$ L reaction volumes), controlling the reactions through HPLC-MS.
- III.** Evaluation of the reaction outcomes. In other words, seek for a reaction procedure which cause the appearance -in the HPLC-MS chromatogram- of new peak(s) at > 30%, in a mixture containing no more than three peaks > 10%. Peak of the target compound should of course be associated to a mass value in the range that would be expected for a modified drug.
- IV.** In such a case -in which we obtain a sharp and clean peak in the LC, with an interesting molecular weight- the synthesis will be scaled up a bit (2 – 5 mg of substrate) in order to isolate enough compound to run preliminary biological assays.
- V.** Ideally, the cytotoxicity assay shows a better activity with respect to the original drug, so the following step would be the structure determination of the new compound.

- VI.** Once the molecular structure and the cytotoxicity profiles are obtained, the new molecule could be used to run complementary biological assay and/or use it as payload in the preparation of model ADC. This will require a scale up of the reaction to 10 - 20 mg in the first place.
- VII.** The best drugs will be benchmarked with the parent compound on *in vivo* model to compare ADME profile, TMD, therapeutic windows. Possibly if the parent drug is subject to resistance phenomenon by receptor mutation, assay on resistant tumour model will be performed.

Since such new anticancer candidates are engineered from a scaffold that is already in clinic, the chance to come up with a favourable ADME profile and toxicity profile are likely increased by comparison with classical natural compound screening. These new drugs known mechanism of action and improved toxicity might trigger renewed interest especially if being used as payload in targeted therapy (for which highly active compound are of paramount interest).

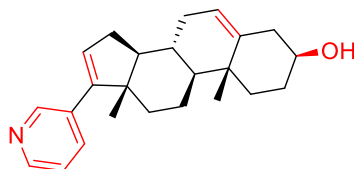
#### 2.4 SELECTION OF ANTICANCER AGENTS AS SUBSTRATES

As already said, substrates will be anticancer drugs already approved by the Food and Drug Administration, currently clinically used in human patients and whose activity is well known. A complete list of all the approved drugs was drawn up and two little groups of five and three compounds were selected.

The first group, selected for method validation purpose, consists of molecules that are relatively cheap (less than 10€ per mg) and with a chemical structure that has a good number of functionalization sites. The first screening of all the selected procedures will be done on this group of model drugs.

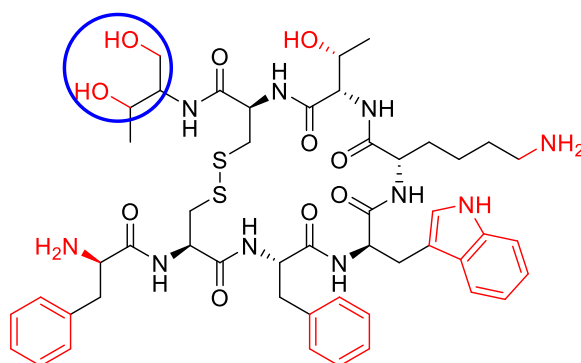
The second group consists of more expensive drugs (often more complex molecules) which are not practical for wide screening. Only the procedures that will give the best results with the first group will be performed on this second group. If the selected procedures show promising results also with the second group of drugs, then a quite larger number of compounds will be bought, functionalized and tested.

Here the list of the selected anticancer drugs: the possible sites of functionalization are enlightened in red color, except for the inactivated C-H sites (for direct C-H activation) and other interesting hydrogen atoms (i.e. allylic H, acidic H, aromatic H).

**FIRST GROUP MOLECULES****ABIRATERONE<sup>132,133</sup>****Figure 72.** Chemical structure of Abiraterone.

Brand names: Zytiga®, Abiratas®, Abretone®, Abirapro®; approved in 2011.

Abiraterone is mainly used for treatment of metastatic castration-resistant prostate cancer in combination with Prednisone. It blocks the biosynthesis of androgens by inhibiting the CYP17A1 enzyme. It has only one secondary hydroxyl group, two double bonds and a pyridine moiety.

**OCTEOTRIDE<sup>134,135</sup>****Figure 73.** Chemical structure of Octeotride.

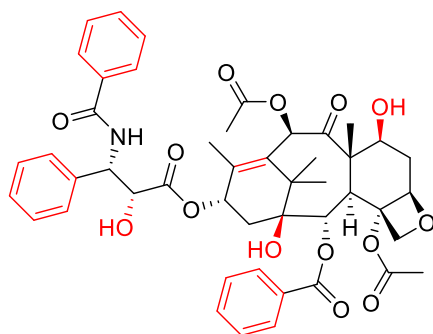
Brand name: Sandostatin®; approved in 1998.

Octeotride is an analog of natural somatostatin (growth hormone-inhibiting hormone) with a longer half-life. It is used for the treatment of growth hormone producing tumors, such as acromegaly and gigantism, and for pituitary tumors.

Concerning our project, Octeotride will be the model molecule for the peptide drugs, it has primary and secondary alcohols, primary and secondary amines and three aromatic moieties (two benzyl and one indole).

It presents a diol (enlightened by the blue circle) suitable for the condensation with an appropriate aldehyde to give a 6-membered acetal ring with tunable stability in acidic media, according to the chosen aldehyde.

*PACLITAXEL*<sup>136-138</sup>



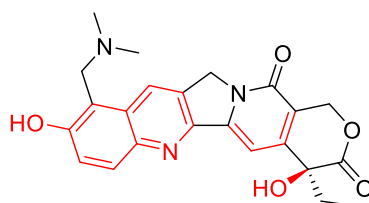
**Figure 74.** Chemical structure of Paclitaxel.

Brand names: Taxol®, Abraxane®; approved in 1998.

Paclitaxel is used to treat ovarian, breast, lung, pancreatic and other cancers. Its mechanism of action involves interference with the normal breakdown of microtubules during cell division, thus progression of mitosis is blocked.

Paclitaxel has three phenyl rings to be functionalized, as well as three hydroxyl groups and a double bond.

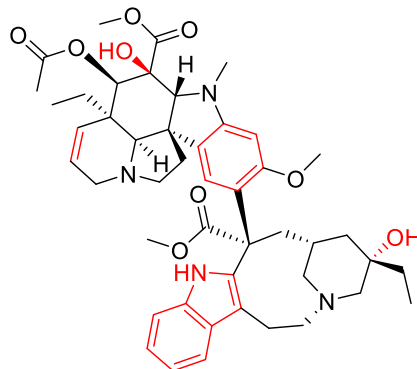
*TOPOTECAN*<sup>139,140</sup>



**Figure 75.** Chemical structure of Topotecan.

Brand name: Hycamtin®; first approval in 1996.

It is used for treatment of ovarian cancer, lung cancer and other cancers. Topotecan activity consists in the inhibition of DNA topoisomerase I, leading to DNA damage. Besides two hydroxyl groups, Topotecan has a big conjugated part which includes two fused aromatic rings and a ketone conjugated to two double bonds.

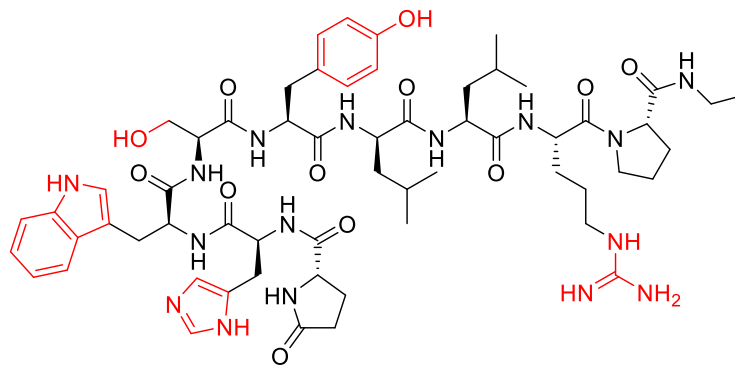
VINBLASTINE<sup>141,142</sup>

**Figure 76.** Chemical structure of Vinblastine.

Brand names: Velban®, Velsar®; approved in 1961.

Vinblastine is a mitotic inhibitor and its mechanism of action is the same as paclitaxel. It has a double bond, two not oxidable alcohols, a substituted phenyl and an indole.

## SECOND GROUP MOLECULES

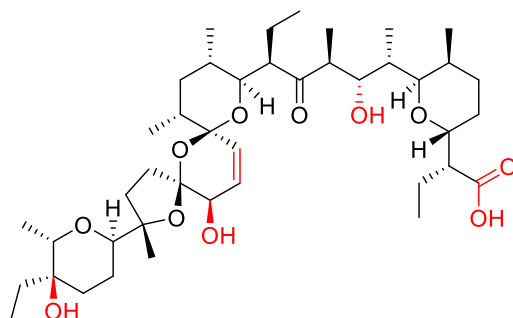
LEUPRORELIN<sup>143</sup>

**Figure 77.** Chemical structure of Leuprorelin

Brand name: Lupron®, Viadur®, Eligard®; approved in 1996.

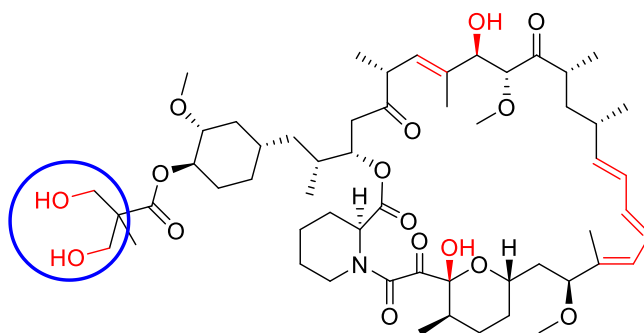
It is a potent gonadotropin-releasing hormone (GnRH) analog with a better affinity for the GnRH receptor and a longer half-life than the natural GnRH. Leuprorelin is currently used to treat prostate cancer and other diseases. This peptide has a phenolic moiety, as well as a primary alcohol, an indol, a guanidine and an imidazole ring.



*SALINOMYCIN*<sup>144–146</sup>

**Figure 78.** Chemical structure of Salinomycin.

Salinomycin is an antimicrobial drug in the first place and it functions as a ionophore. It has shown interesting anticancer activity on its own and in combination with other drugs (synergistic activity), but the mechanism of action is still unknown. It has only a double bond, a free acidic moiety and three different alcohols: a secondary, a tertiary and an allylic one.

*TEMSIROLIMUS*<sup>147,148</sup>

**Figure 79.** Chemical structure of Temsirolimus.

Brand name: Toricel®; approved in 2007.

Temsirolimus is an ester analog of natural rapamycin with antifungal, antitumor, and immunosuppressive activities. It inhibits the mTOR kinase activity leading to cell cycle arrest. It has four hydroxyl groups (two primary, one allylic and one emiketalic), an isolated double bond and three conjugated double bonds. It also presents a diol suitable for the formation of a cyclic acetal (blue circle).

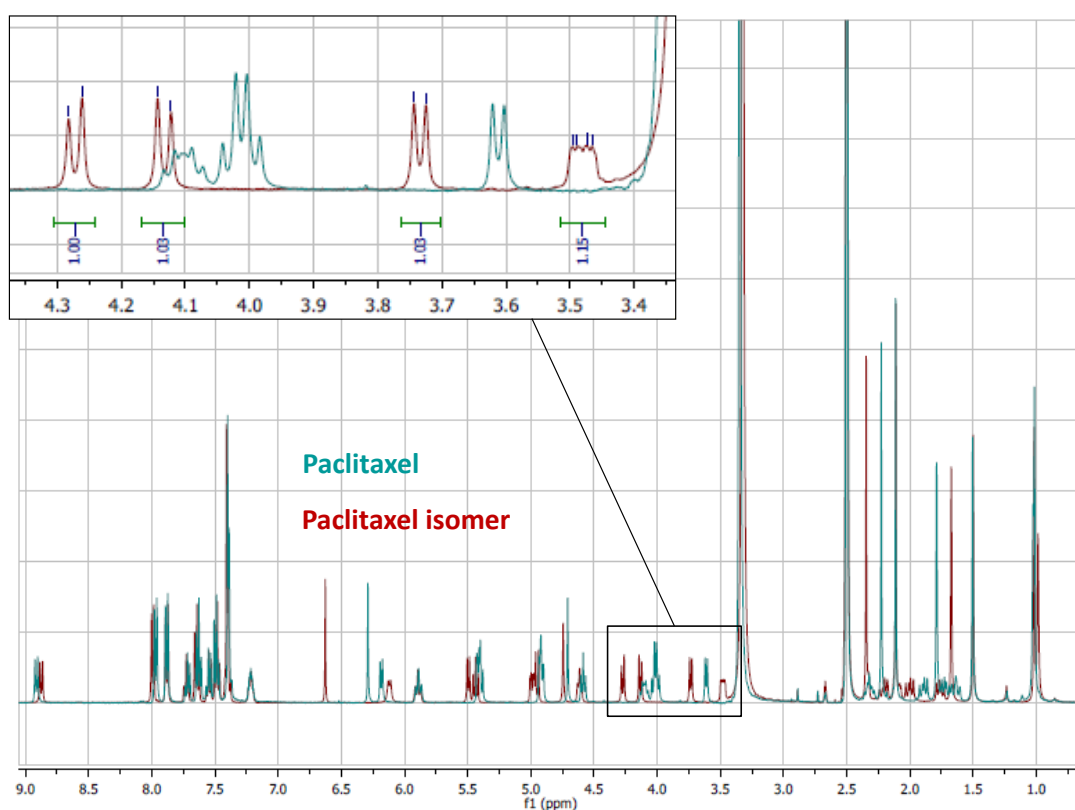
### 3. PRELIMINARY RESULTS

#### 3.1 ISOMERIZATION OF PACLITAXEL

While trying a late stage metal-free azidation on Paclitaxel,<sup>115</sup> an isomer of the drug was obtained and the procedure was repeated on a bigger scale (20 mg). Proton NMR and high-resolution mass analyses of Paclitaxel and its isomer are shown below (Cf. also Experimental Procedures, section 1.9, page 213).

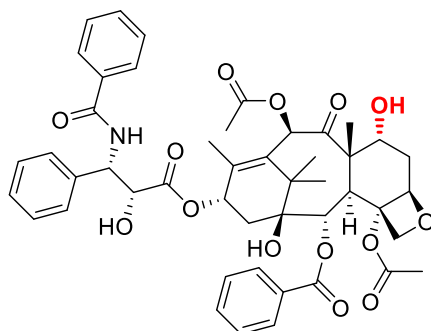
Chemical Formula	Exact Mass	Compound	HR-MS Analysis
C <sub>47</sub> H <sub>51</sub> NO <sub>14</sub>	853.33096	Paclitaxel	853.33135
		Paclitaxel isomer	853.32930

**Table 27.** HR-MS Analysis outcome of Paclitaxel and obtained Paclitaxel isomer.



**Figure 80.** NMR spectra of Paclitaxel (in green) and its isomer (in red), with an interesting region enlightened (ppm 3,4 - 4,35).

In first assay, cytotoxicity was found to be very similar:  $IC_{50} = 80$  nM, compared to 40 nM of native paclitaxel, enough to continue the investigation and determine the structure of the isomer. Eventually, thanks to Dr. Jean-Marc Nuzillard (CNRS, Reims) it was found that the isomer obtained was the well-know 7-epi-paclitaxel (**Figure 81**), resulting from epimerization in acetonitrile/water mixture.<sup>149-151</sup> The  $IC_{50}$  value found for the isomer corroborates the structure-activity relationship study of paclitaxel and its modifications.<sup>136</sup>



**Figure 81.** Chemical structure of 7-epi-paclitaxel.

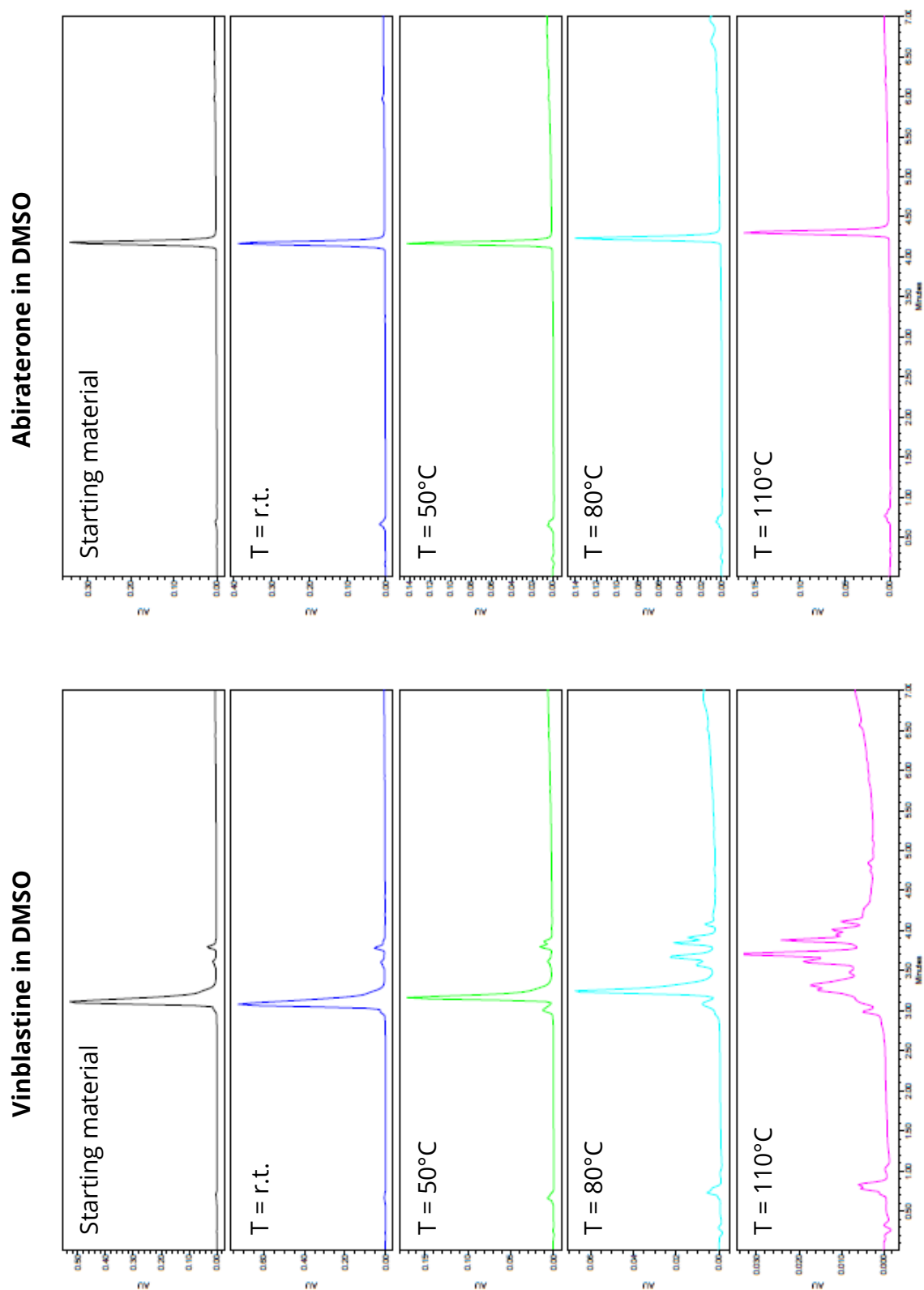
Despite this not exciting result, it was assumed that the exposure to a solvent, combined with high temperature, could cause interesting changes in the structure of a complex molecule, like isomerization in the case of paclitaxel. These may also include rearrangement, solvent addition, oxidation, reduction and others depending on the solvent used.

### 3.2 STABILITY TESTS FOR SOLVENTS AND TEMPERATURES

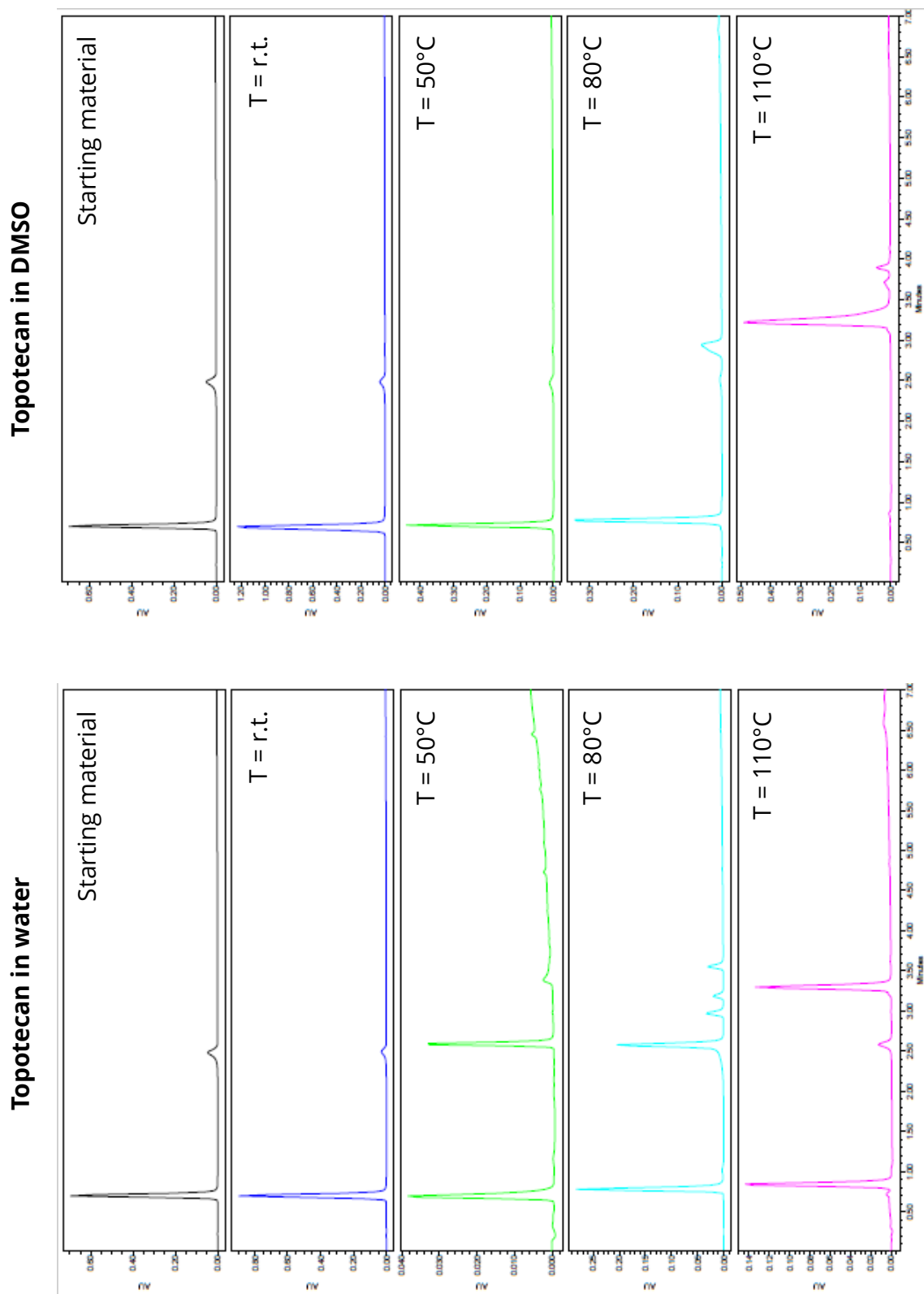
Cytotoxic drugs of the first group (Abiraterone, Octeotride, Paclitaxel, Topotecan and Vinblastine) were solubilized in different solvents at increasing temperatures to:

- D.** check their stability in the solvent-temperature conditions which will be used for the functionalization (*i.e.* if a drug is not stable under certain conditions required for a certain procedure, the drug will not be tested);
- E.** find out if the exposure to a certain solvent and temperature is sufficient to promote chemical transformation, as speculated above.

Solvents are chosen according to those required by the selected procedures: water, methanol (MeOH), pyridine (py), dimethyl sulfoxide (DMSO). Temperatures varies from room temperature ( $\sim 23^{\circ}\text{C}$ ) to  $110^{\circ}\text{C}$ . Solutions were kept at the chosen temperature for one hour and then LC-MS was run (**Figure 82** and **Figure 83**).



**Figure 82.** Selection of chromatograms of cytotoxic drugs. Vinblastine in DMSO shows degradation with increasing temperature, so procedures in DMSO at  $>70^{\circ}\text{C}$  are discouraged. Abiraterone in the same solvent is stable even at  $120^{\circ}\text{C}$ .



**Figure 83.** Selection of chromatograms of cytotoxic drugs. The appearance of new interesting peaks is observed with Topotecan in both water and DMSO: profile changes remarkably with increasing temperature. For all the obtained chromatograms, see Appendix C, page 261)

#### **4. CONCLUSION ON LATE STAGE FUNCTIONALIZATION**

An exhaustive bibliographic research for the newest and mildest procedures for the modification and/or functionalization of complex molecules has been done (updated to April 2016), as well as a meticulous planification for the late stage functionalization of anticancer agents.

A first test for stability in different solvents at increasing temperature has been carried out. At this point the project was paused and it will be likely resumed soon (Cf. next chapter)

The late stage functionalization of anticancer agents as tool for the discovery of new improved drugs, as conceived herein, has all the features to be successful and to bring to the identification of at least one new molecule with improved anticancer activity and interest in the field of antibody-drug conjugates.



## VI. CONCLUSIONS AND PERSPECTIVES

The project presented in this thesis concern acid-catalysed abiotic reactions in biological system. Our aim was to design and test in mice an abiotic system for *in vivo* applications composed by **i)** a xenobiotic cyclic acetal substrate stable in biological conditions and cleavable at abiotic acidic pH, **ii)** a corresponding biocompatible heterogeneous acid catalyst active in a buffered media.

We started from the design of the cleavable cyclic acetal substrate with the objective to define an acetal model which, by slight modifications of its structure, shows tuneable reactivity towards acid catalysed hydrolysis. Moreover, we wanted also to present one hydrophobic and one hydrophilic acetals with the same core and acido-lability profile in order to use them to explore different combination with hydrophobic and hydrophilic heterogeneous catalysts.

Keeping in mind that we were going to perform reactions in biologically relevant conditions, we identified FRET probes as the hydrophobic substrate which would allow us to monitor the formation of the product in low concentrated solutions.

Thus, we identified a total of nine 5- and 6-membered cyclic acetals showing a panel of acido-lability, from very stable acetals (to be employed as non-cleavable linkers) to acetals cleavable at pH > 4.5 in cells (to be employed as cleavable linkers). Acetals named **F-APNM5** and **PEGAM5** were found to be stable in the physiological pH range and hydrolysable at pH < 4, they are hydrophobic and hydrophilic, respectively, and were thus identified as the substrates for the abiotic reaction system.

The most challenging and ambitious part of this project was the search for a heterogeneous acid catalyst which was able to maintain its acidity confined in a micro-environment and to not affecting the buffered pH of biological media. We wanted to identify two catalyst of different nature: **i)** a hydrophobic catalyst, which would have been paired with the hydrophobic FRET acetal substrate **F-APNM5**; **ii)** a hydrophilic catalyst, which would have been paired with the hydrophilic acetal **PEGAM5**.

In the first case we identified Nafion NR50 as the hydrophobic catalyst and we developed a washing pre-treatment consisting in a partial neutralization of the sulfonic acid functions by cationic exchange. This pre-washing allowed to mitigate the acidity of the resin without however totally inhibiting its hydrolytic activity. We demonstrated that "Nafion-90" (pre-treated Nafion NR50) in plasma was able to adsorb the FRET probe and catalyse the hydrolysis without



changing the pH of plasma. A confocal microscopy analysis using pH-sensitive ratiometric probe confirmed that the washing pre-treatment affects the inner acidity of the catalyst.

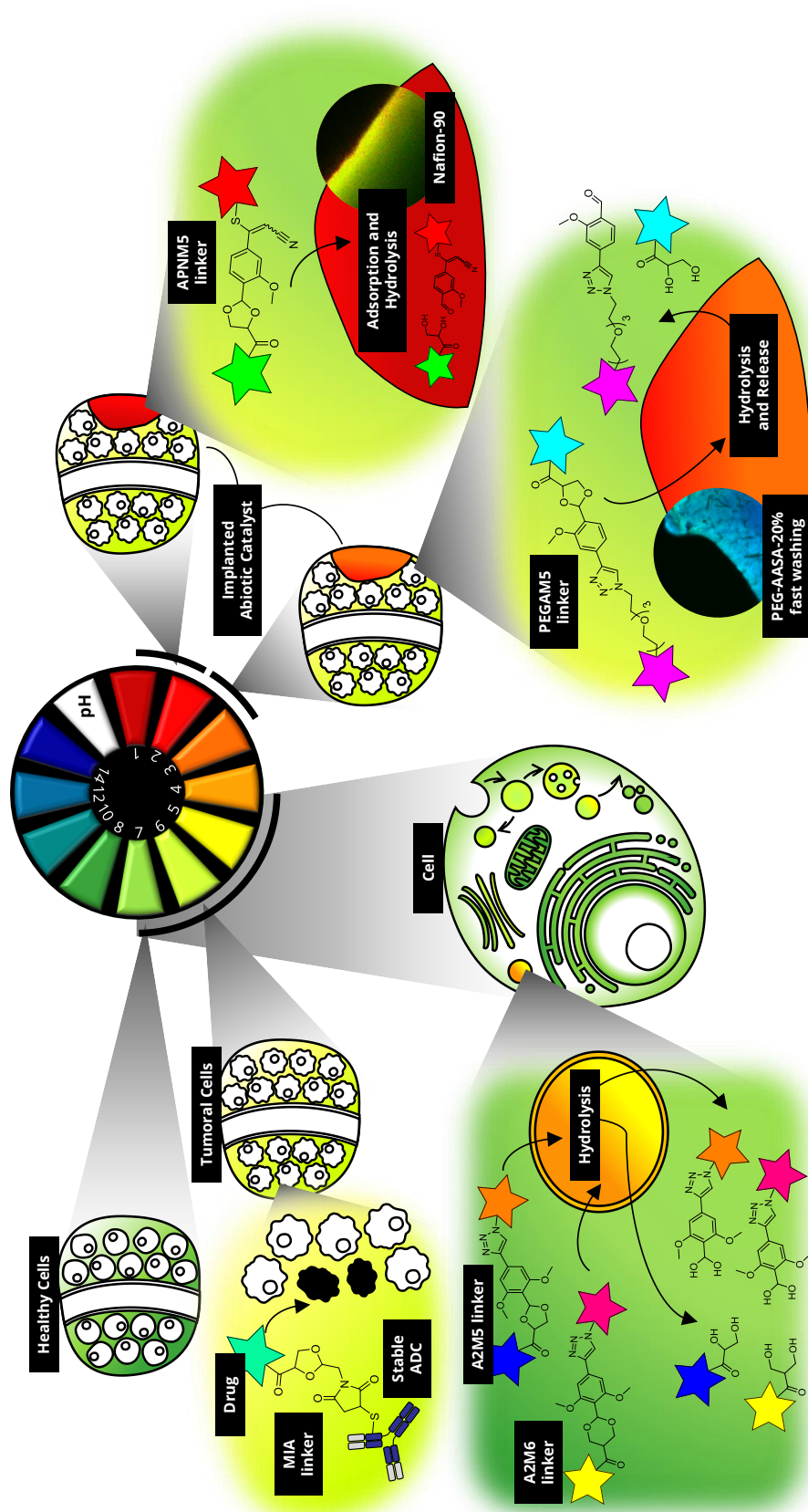
Regarding the hydrophilic catalyst, Dr. Becht and Dr. Balan of the Institute of Materials of Mulhouse, collaborated with us in the design and production of a tailored PEG-based polymer cross-linked with a sulfonic acid of our choice. We tested different formulations and forms and we found that a 20 wt.% content of **AASA** was the right balance between a too high content of acid (that would acidify the biofluid) and not enough acidic content to promote the reaction. Preliminary results were promising and we could work on the further optimization of the catalyst performances. Unfortunately, at the time of this thesis, the collaboration with Dr. Balan was interrupted. We hope that we will have the possibility to work again for the improvement of the catalyst.

Regarding the first *in vivo* proof of concept of our system, we planned the experiments, prepared both the catalyst and the FRET substrate and we were ready to start the experiment. Regrettably, the authorization to perform surgery on mice (*i.e.* the implantation of Nafion-90 beads) is currently pending. However, with the *in vivo* experiment being already planned, we will perform it as soon as we get all the permissions.

Finally, we thought also about possible applications in cancer therapy. Since the reaction catalysed is a bond breaking reaction, the acetal model could be applied to anticancer drugs presenting a suitable diol in their chemical structure. By condensation with the proper aldehyde, we could generate a pro-drug which could be selectively cleaved by our catalyst. The latter would be implanted on a chosen site, *i.e.* next to tumoral tissue.

Toward this goal, at the beginning of this thesis project we laid the foundations for a systematic late stage functionalization of anticancer agents, during which we selected two anticancer drugs with a diol function exploitable for the condensation with the suitable aldehyde. This project was, in fact, stopped at its very beginning because it consisted in the repetitive screening of late-stage functionalization procedures and we thought that it was not suited as PhD project.

We condensed the results obtained by this research and envisaged applications in the next figure.



**Figure 84.** Final overview of the thesis work and perspectives. The different scenarios hypothesized in the introduction are depicted and related to a pH scale (in the centre up part of the image). Xenobiotics are depicted as the acetal linker bearing two star-symbols (colour of the star is random), unless otherwise specified. The abiotic solid catalyst is depicted as a plain form. The colour of the catalyst, extracellular environment and cell's compartments corresponds to their pH value, according to the pH scale in the centre. Confocal ratiometric images of Nafion-90 and PEG-AASA-20% are also inserted.

## VI. CONCLUSIONS ET PERSPECTIVES

Le projet présenté dans cette thèse concerne les réactions abiotiques catalysées par un acide dans les systèmes biologiques. Notre objectif était de concevoir et de tester chez la souris un système abiotique pour applications *in vivo* composé de i) un substrat acétal cyclique xénobiotique stable dans des conditions biologiques et clivable à pH acide abiotique, ii) un catalyseur acide hétérogène correspondant biocompatible, actif dans un milieu tamponné.

Nous avons commencé par la conception du substrat acétal cyclique clivable dans le but de définir un modèle acétal qui, par de légères modifications de sa structure, montre une réactivité ajustable à l'hydrolyse catalysée par un acide. De plus, nous voulions également présenter un acétal hydrophobe et un acétal hydrophile ayant le même noyau et le même profil d'acidolabilité afin de les utiliser pour explorer différentes combinaisons avec des catalyseurs hétérogènes hydrophobes et hydrophiles.

Gardant à l'esprit que nous allions effectuer des réactions dans des conditions biologiquement pertinentes, nous avons identifié les sondes FRET comme substrat hydrophobe, ce qui nous permettrait de surveiller la formation du produit dans des solutions faiblement concentrées.

Ainsi, nous avons identifié un total de neuf acétals cycliques à 5 et 6 chaînons présentant un panel d'acidolabilité, allant d'acétals très stables (à utiliser comme agents de liaison non clivables) à des acétals clivables à un  $\text{pH} > 4,5$  dans les cellules (à éliminer). utilisés comme agents de liaison clivables). Les acétals nommés F-APNM5 et PEGAM5 se sont révélés stables dans la gamme de pH physiologique et hydrolysables à  $\text{pH} < 4$ , ils sont hydrophobes et hydrophiles, respectivement, et ont donc été identifiés comme les substrats du système de réaction abiotique.

La partie la plus difficile et ambitieuse de ce projet a été la recherche d'un catalyseur acide hétérogène capable de maintenir son acidité confinée dans un micro-environnement et de ne pas affecter le pH tamponné des milieux biologiques. Nous voulions identifier deux catalyseurs de nature différente : i) un catalyseur hydrophobe, qui aurait été couplé avec le substrat d'acétal hydrophobe FRET F-APNM5; ii) un catalyseur hydrophile, qui aurait été couplé avec l'acétal hydrophile PEGAM5.

Dans le premier cas, nous avons identifié le Nafion NR50 comme catalyseur hydrophobe et nous avons mis au point un prétraitement de lavage consistant en une neutralisation partielle des fonctions acide sulfonique par échange cationique. Ce pré-lavage a permis d'atténuer

l'acidité de la résine sans toutefois inhiber totalement son activité hydrolytique. Nous avons démontré que «Nafion-90» (Nafion NR50 prétraité) dans le plasma était capable d'adsorber la sonde FRET et de catalyser l'hydrolyse sans modifier le pH du plasma. Une analyse par microscopie confocale utilisant une sonde ratiométrique sensible au pH a confirmé que le prétraitement de lavage affecte l'acidité interne du catalyseur.

En ce qui concerne le catalyseur hydrophile, MM. Becht et Balan de l'Institut des matériaux de Mulhouse ont collaboré avec nous à la conception et à la production d'un polymère sur mesure à base de PEG réticulé avec un acide sulfonique de notre choix. Nous avons testé différentes formulations et formes et nous avons constaté qu'une teneur de 20% en poids d'AASA constituait le bon équilibre entre une teneur trop élevée en acide (qui acidifierait le biofluide) et une teneur en acide insuffisante pour favoriser la réaction. Les résultats préliminaires étaient prometteurs et nous pourrions travailler sur l'optimisation ultérieure des performances du catalyseur. Malheureusement, au moment de cette thèse, la collaboration avec le Dr. Balan a été interrompue. Nous espérons que nous aurons la possibilité de travailler à nouveau pour l'amélioration du catalyseur.

En ce qui concerne la première preuve de concept in vivo de notre système, nous avons planifié les expériences, préparé le catalyseur et le substrat de FRET, et nous étions prêts à commencer l'expérience. Malheureusement, l'autorisation de procéder à une intervention chirurgicale sur des souris (c'est-à-dire l'implantation de billes de Nafion-90) est en attente. Cependant, l'expérience in vivo étant déjà planifiée, nous la réaliserons dès que toutes les autorisations seront obtenues.

Enfin, nous avons également réfléchi aux applications possibles du traitement du cancer. Comme la réaction catalysée est une réaction de rupture de liaison, le modèle acétal pourrait être appliqué à des médicaments anticancéreux présentant un diol approprié dans leur structure chimique. Par condensation avec l'aldéhyde approprié, nous pourrions générer un pro-médicament pouvant être clivé sélectivement par notre catalyseur. Ce dernier serait implanté sur un site choisi, c'est-à-dire à côté du tissu tumoral.

Dans ce but, nous avons, au début de ce projet de thèse, jeté les bases d'une fonctionnalisation systématique des agents anticancéreux à un stade avancé, au cours de laquelle nous avons sélectionné deux médicaments anticancéreux ayant une fonction diol exploitable pour la condensation avec l'aldéhyde approprié. En fait, ce projet a été arrêté à ses débuts, car il

consistait en un filtrage répétitif des procédures de fonctionnalisation en phase finale et nous avons pensé que ce n'était pas un projet de thèse.

Nous avons condensé les résultats obtenus par cette recherche et les applications envisagées dans la figure 84 (page 167).

## VIII. EXPERIMENTAL PROCEDURES

### DETAILED INDEX

<b>1. CHEMICAL SYNTHESSES</b>	<b>173</b>
1.1 GENERAL EXPERIMENTAL PROCEDURES	173
1.2 MATERIALS AND METHODS	173
1.3 SYNTHESIS OF <b>APN6</b> AND <b>APNM5</b>	174
1.3.1 <b>APN6</b>	174
1.3.2 First attempts of <b>APNM5</b> synthesis	175
1.3.2 Final strategy for <b>APNM5</b> synthesis	181
1.4 SYNTHESIS OF <b>A2M5</b> AND <b>A2M6</b>	187
1.5 SYNTHESIS OF <b>PEGAM5</b>	191
1.6 SYNTHESIS OF <b>MIA5</b>	194
1.6.1 Synthesis of linker <b>MIA5-1</b>	194
1.6.2 Synthesis of linker <b>MIA5-2</b>	196
1.6.3 Synthesis of linker <b>MIA6-1</b>	199
1.6.4 Synthesis of linker <b>MIA6-2</b>	199
1.7 SYNTHESIS OF FRET PROBES	201
1.7.1 General procedures for synthesis of FRET probes	201
1.7.2 <b>F-APN6</b>	202
1.7.3 <b>F-APNM5</b>	203
1.7.4 <b>F-A2M5</b>	204
1.7.5 <b>F-A2M6</b>	205
1.7.6 <b>F-MIA5-1</b>	206
1.7.7 <b>F-MIA5-2</b>	206
1.7.8 <b>F-MIA6-1</b>	207
1.7.9 <b>F-MIA6-2</b>	208
1.8 SYNTHESIS OF SUPPORTED ACIDS AND SOLID CATALISTS	209
1.8.1 Silica supported acids	209
1.8.2 Modified Merrifield resins	209
1.8.3 Catalysts provided by Dr. Camelia Ghimbeu (IS2M)	210
1.8.4 <b>PAASA</b> encapsulated in alginate beads	210
1.8.5 PEG-PAASA and PEG-AASA provided by Dr. Lavinia Balan (IS2M)	211
1.9 SYNTHESIS OF <b>DDXC</b>	211
1.10 ISOMERIZATION OF PACLITAXEL	213
1.10.1 Azidation attempt on micro scale	213
1.10.2 Paclitaxel isomerization on 20 mg scale	213
<b>2. STABILITY OF FRET PROBES IN AQUEOUS MEDIA</b>	<b>216</b>

2.1 MATERIALS AND METHODS	216
2.2 STABILITY TESTS IN AQUEOUS BUFFERS	216
2.2.1 FRET probes <b>F-APN6, F-APNM5, F-A2M5, F-A2M6</b>	216
2.2.2 FRET probes <b>F-MIA5-1, F-MIA5-2, F-MIA6-1, F-MIA6-2</b>	217
2.2.3 FRET probes <b>F-APN6</b> and <b>F-APNM5</b> at 37 °C	218
2.3 RATE OF SUCCINIMIDE RING-OPENING	218
2.3.1 Rate of succinimide ring-opening in PBS buffer	218
2.3.2 Rate of succinimide ring-opening in human plasma	218
2.4 STABILITY OF <b>F-MIA5-1</b> AND <b>HF-MIA5-1</b> IN PLASMA	220
<b>3. SCREENING OF CATALYSTS AND HYDROLYSIS TESTS</b>	<b>221</b>
3.1 MATERIALS AND METHODS	221
3.2 GENERAL SCREENING PROCEDURES	221
3.2.1 Screening of CSA and homogeneous catalysts	221
3.2.2 Screening of heterogeneous catalysts	222
3.2.3 Screening of PEG-based catalysts	222
3.2.4 <b>PEGAM5's</b> hydrolysis monitoring	223
3.3 WASHING PRE-TREATMENT	224
3.3.1 Washing pre-treatment for Nafion	224
3.3.2 Washing pre-treatment for PEG-AASA (beads)	225
3.4 NAFION NR50 AND AMBERLYST A-15 ADSORBANCE AND RELEASING RATE	225
3.5 DETECTION OF HYDROLYSIS WITH UV TRANSILLUMINATOR AND CONFOCAL MICROSCOPE	226
3.5.1 Preparation of Nafion beads for the calibration curve	226
3.5.2 Fluorescence detection at UV transilluminator	226
3.5.3 Fluorescence detection at confocal microscope	226
<b>4. RATIOMETRIC ANALYSIS</b>	<b>227</b>
4.1 MATERIAL AND METHODS	227
4.2 PREPARATION OF THE SOLID CATALYSTS, IMAGE ACQUISITION AND EDITING	227
<b>5. IN VITRO AND IN VIVO EXPERIMENTS</b>	<b>228</b>
5.1 CELL VIABILITY WITH <b>F-A2M5</b> AND <b>F-A2M6</b>	228
5.2 CELL VIABILITY WITH PACLITAXEL AND 7-EPI-PACLITAXEL	229
5.3 IN VIVO EXPERIMENT: SAMPLES PREPARATION	229
<b>6. LATE STAGE FUNCTIONALIZATION</b>	<b>230</b>
6.1 SOLVENTS AND TEMPERATURES STABILITY TESTS	230

## 1. CHEMICAL SYNTHESSES

### 1.1 GENERAL EXPERIMENTAL PROCEDURES

Unless otherwise indicated, reactions were carried out under an atmosphere of argon in flame-dried glassware with magnetic stirring. Air and/or moisture-sensitive liquids were transferred via syringe. When required, solutions were degassed by bubbling of argon through a needle. Organic solutions were concentrated by rotary evaporation at 25-60 °C at 15-30 torr. Analytical thin layer chromatography (TLC) was performed using plates cut from glass sheets (silica gel 60F-254 from Merck). Visualization was achieved under a 254 or 365 nm UV light and by immersion in an appropriate revelation solution. Column chromatography was carried out as "Flash Chromatography" using silica gel G-25 (40-63  $\mu\text{m}$ ) from Macherey-Nagel and using a mixture cyclohexane-ethyl acetate in a gradient from 100% cyclohexane to 100% ethyl acetate, unless otherwise specified.

Reactions with cytotoxic substrates were carried out using standard protocol for cytotoxic material handling, monitored with LC-MS and purified by preparative HPLC.

### 1.2 MATERIALS AND METHODS

All reagents were obtained from commercial sources and used without any further purifications. Anhydrous solvents used in experiments were obtained from Sigma-Aldrich or Alfa Aesar. Cytotoxic drugs were purchased from Selleckchem and used without further purification.

LC-MS analyses were performed on a Water alliance 2695 Separation Module coupled with a Waters 2487 Dual  $\lambda$  Absorbance Detector and a Waters Acquity QDa Detector (ESI ionization). Water/ACN (containing 0.05% TFA) was used as eluent system. The gradient applied was 5% to 95% ACN in 5 minutes and 2 minutes of re-equilibration. Detection was done at 254 nm and 210 nm.

$^1\text{H}$  and  $^{13}\text{C}$  NMR spectra were recorded respectively at 400 MHz and 100 MHz with a Bruker 400 spectrometer at 23 °C. Chemical shifts are reported in parts per million ( $\delta$ ) and calibrated using residual non-deuterated solvent. Data are represented as follows: chemical shift, multiplicity (s = singlet, d = doublet, t = triplet, q = quartet, quint = quintet, m = multiplet, br = broad or a combination of the above), coupling constant (J, Hz) and integration.

High resolution mass spectra were obtained using an Agilent Q-TOF (time of flight) 6520. Low resolution mass spectra were obtained using an Agilent MSD 1200 SL (ESI/APCI) with a Agilent HPLC1200 SL and a Waters Acquity QDa (ESI) with a Waters Alliance 2695 HPLC.

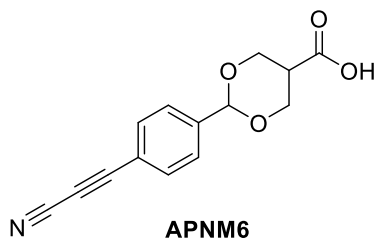
Preparative HPLC procedures were performed on semi-preparative HPLC Shimadzu Auto-injector SIL-10A (pump: Shimadzu LC-8A, UV-Vis detector: Shimadzu SPD-10A, collector: Shimadzu fraction collector FRC-10A) using a Sunfire C18 (150 mm  $\times$  19 mm i.d., 5  $\mu\text{m}$ , Waters) at a flow of 17 mL/min. 1 mL of sample was injected and water/ACN (containing 0.05% TFA or



0.025 mM ammonium formate) was used as eluent system, unless otherwise specified. The gradient applied was 5% to 95% ACN in 40 minutes and 10 minutes of re-equilibration. Detection was done at 550 nm for TAMRA derivatives.

### 1.3 SYNTHESIS OF APN6 AND APNM5

#### **1.3.1 APN6**



**APNM6**  
Chemical Formula: C<sub>14</sub>H<sub>11</sub>NO<sub>4</sub>  
Exact Mass: 257,0688

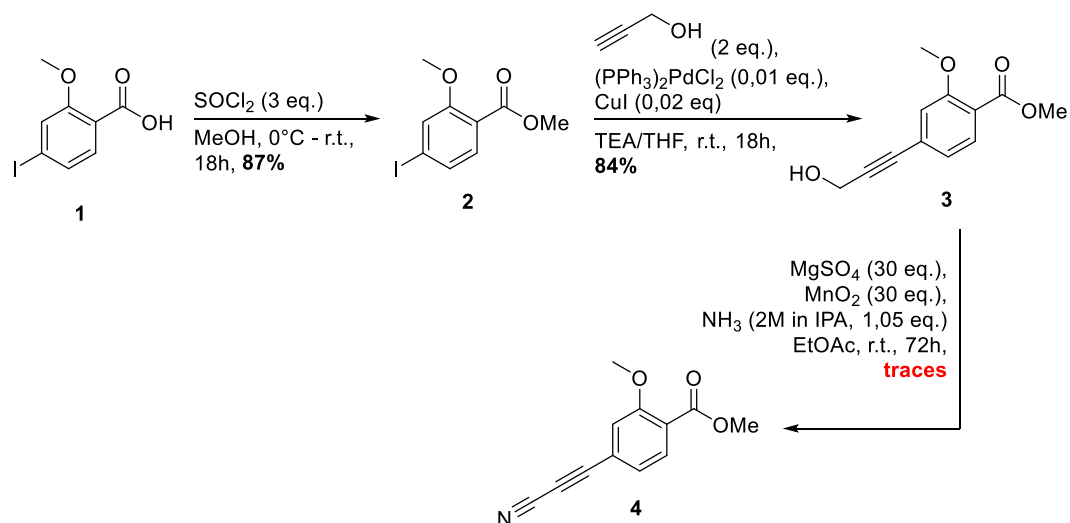
**APNM6** was synthesized by Dr. Igor Dovgan.

**<sup>1</sup>H NMR (400 MHz, MeOD-d<sub>4</sub>, δ ppm):** 7.55 - 7.67 (m, J = 8.3 Hz, 2 H), 7.41 - 7.52 (m, J = 8.3 Hz, 2 H), 5.42 (s, 1 H), 4.32 (dd, J = 11.8, 4.8 Hz, 2 H), 3.92 (t, J = 11.5 Hz, 2 H), 2.87 - 3.07 ppm (m, 1 H).

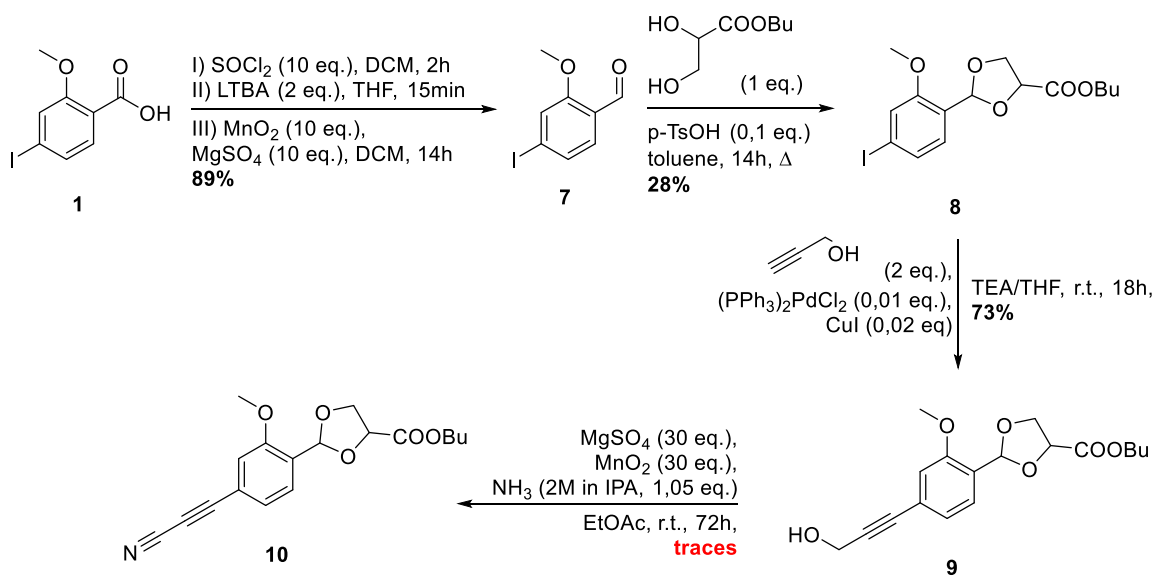
**<sup>13</sup>C NMR (101 MHz, MeOD-d<sub>4</sub>, δ ppm):** 171.5, 142.3, 133.1, 126.6, 117.4, 104.6, 99.8, 82.4, 67.8, 61.9, 39.8.

## 1.3.2 First attempts of APNM5 synthesis

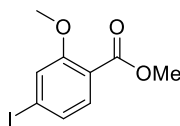
## First attempt



## Second attempt



Scheme EP 1. Failed attempts of synthesis of APNM5.

**methyl 4-iodo-2-methoxybenzoate, 2**

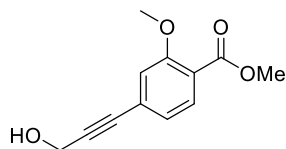
Chemical Formula:  $C_9H_9IO_3$   
Exact Mass: 291,9596

A 25 mL two-necked round bottom flask equipped with nitrogen inlet adapter was charged with 4-iodo-2-methoxybenzoic acid **1** (1 eq., 200 mg, 0.719 mmol) in MeOH (5 mL) to give a colourless solution. The reaction mixture was cooled at about 0 °C for about 20 min. Thionyl chloride (3 eq., 256 mg, 156  $\mu$ L, 2.16 mmol) was added slowly via syringe. The resulting solution was allowed to stir at r.t. for about 18 h.

The mixture was concentrated and re-dissolved in EtOAc (20 mL). The solution was washed with saturated  $NaHCO_3$  solution (1 x 20 mL) and saturated NaCl solution (1 x 20 mL). The organic phase was dried over  $MgSO_4$ , filtered and concentrated to give a brown oil. Purification through a short silica column gave compound **2** (183 mg, 0.627 mmol, 87%) as a yellow oil.

**$^1H$  NMR (400 MHz,  $CDCl_3$ ,  $\delta$  ppm):** 7.50 (d,  $J = 8.1$  Hz, 1H), 7.34 (d,  $J = 8.2$  Hz, 1H), 7.31 (s, 1H), 3.89 (s, 3H), 3.87 (s, 3H).

**$^{13}C$  NMR (101 MHz,  $CDCl_3$ ,  $\delta$  ppm):** 166.10, 159.26, 132.78, 129.57, 121.65, 119.62, 99.97, 56.33, 52.14.

**methyl 4-(3-hydroxyprop-1-yn-1-yl)-2-methoxybenzoate, 3**

Chemical Formula:  
 $C_{12}H_{12}O_4$   
Exact Mass: 220,0736

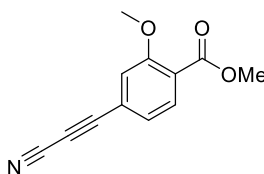
Methyl 4-iodo-2-methoxybenzoate **2** (1 eq., 210 mg, 0.719 mmol) and 2-propyn-1-ol (2 eq., 80.6 mg, 85  $\mu$ L, 1.44 mmol) were dissolved in a 1:1 amount of THF and TEA (6 mL in total). The solution was degassed and purged with argon. Dichlorobis (triphenylphosphine) palladium (0.01 eq., 5.05 mg, 0.00719 mmol) and CuI (0.02 eq., 2.74 mg, 0.0144 mmol) were added and the solution was degassed again. The reaction mixture was stirred at 25°C under argon for 14 hours.

Then the mixture was diluted with DCM, washed with sat.  $NH_4Cl$ , and deionized water. The organic phase was dried over  $MgSO_4$ , filtered and concentrated under reduced pressure to give methyl 4-(3-hydroxyprop-1-yn-1-yl)-2-methoxybenzoate (133 mg, 0.604 mmol, 84%) as an orange solid.

**$^1\text{H}$  NMR (400 MHz,  $\text{CDCl}_3$ ,  $\delta$  ppm):** 7.97 (d,  $J = 7.9$  Hz, 1H), 7.39 (d,  $J = 85.3$  Hz, 1H), 7.26 (s, 1H), 4.74 (s, 2H), 4.13 (s, 3H), 4.12 (s, 3H).

**$^{13}\text{C}$  NMR (101 MHz,  $\text{CDCl}_3$ ,  $\delta$  ppm):** 166.13, 158.85, 131.73, 127.70, 123.44, 120.10, 115.10, 89.62, 84.93, 56.11, 52.15, 51.59.

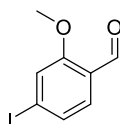
#### methyl 4-(cyanoethynyl)-2-methoxybenzoate, **4**



Chemical Formula:  $\text{C}_{12}\text{H}_9\text{NO}_3$   
Exact Mass: 215,0582

To the solution of methyl 4-(3-hydroxyprop-1-yn-1-yl)-2-methoxybenzoate (1 eq., 120 mg, 0.545 mmol) in THF (15 mL) was added  $\text{MgSO}_4$  (30 eq., 1967 mg, 16.3 mmol),  $\text{NH}_3$  (1.05 eq., 2 M in isopropanol, 0.286 mL, 0.572 mmol) and  $\text{MnO}_2$  (30 eq., 1421 mg, 16.3 mmol). After stirring the mixture at  $25^\circ\text{C}$  for 48 hours, TLC (EtOAc/Cy : 1/9) showed only traces of the starting compound, the intermediary imine as main compound and no traces of the product.

#### 4-iodo-2-methoxybenzaldehyde, **7**



Chemical Formula:  $\text{C}_8\text{H}_7\text{IO}_2$   
Exact Mass: 261,9491

**I)** Thionyl chloride (10 eq., 2010 mg, 1.225 mL, 16.9 mmol) was added to a solution of 4-iodo-2-methoxybenzoic acid **1** (1 eq., 470 mg, 1.69 mmol) in DCM (10 mL). The mixture was refluxed for 2 hours and the completeness of reaction was controlled by TLC.

Residual  $\text{SOCl}_2$  and DCM were evaporated, 4-iodo-2-methoxybenzoyl chloride was obtained as a crude brown oil and was used in the next step without further purification. If needed to be stored, special precaution should be taken to avoid moisture.

**II)** A solution of 4-iodo-2-methoxybenzoyl chloride (1 eq., 500 mg, 1.69 mmol) in THF (25 mL) was cooled to  $-78^\circ\text{C}$ . Lithium tri-tert-butoxyaluminum hydride (2 eq., 1 M in THF, 3.37 mL, 3.37 mmol) was added dropwise in 10 minutes. The solution was stirred for another 5 minutes, then saturated  $\text{NaHCO}_3$  (20 mL) was added. The obtained reaction mixture was left stirring for several minutes to let all aluminium salt to precipitate and organic phase was decanted. The aqueous phase was extracted with  $\text{Et}_2\text{O}$ . United organic phases were washed with saturated

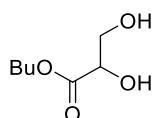
NaHCO<sub>3</sub> and brine, dried over MgSO<sub>4</sub> and evaporated to give (4-iodo-2-methoxyphenyl)methanol as crude product.

**III)** The crude product was resolubilized in DCM, then MnO<sub>2</sub> (10 eq., 1466 mg, 16.9 mmol) and MgSO<sub>4</sub> (10 eq., 2029 mg, 16.9 mmol) were subsequently added. The obtained reaction mixture was left stirring overnight at room temperature, then filtered through celite (washed thoroughly with three portions of DCM), evaporated and purified by flash chromatography to give 4-iodo-2-methoxybenzaldehyde (393 mg, 1.50 mmol, 89 %) as a white solid.

**<sup>1</sup>H NMR (400 MHz, CDCl<sub>3</sub>, δ ppm):** 10.40 (s, 1H), 7.51 (d, J = 8.1 Hz, 1H), 7.41 (d, J = 8.1 Hz, 1H), 7.36 (s, 1H), 3.93 (s, 3H).

**<sup>13</sup>C NMR (101 MHz, CDCl<sub>3</sub>, δ ppm):** 189.07, 161.46, 130.33, 129.52, 124.33, 121.37, 103.37, 56.01.

### butyl 2,3-dihydroxypropanoate, **23**



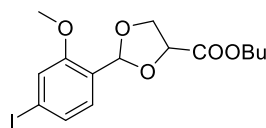
Chemical Formula: C<sub>7</sub>H<sub>14</sub>O<sub>4</sub>  
Molecular Weight: 162,19

A solution of picolinic acid (0.018 eq., 18 mM, 15.6 mL) in acetone and a solution of manganese (II) acetate (0.003 eq., 3 mM, 15.6 mL) in acetone were added subsequently to a solution of butyl acrylate (1 eq., 2 g, 15.6 mmol) in acetone (50 mL) at r.t. Then a solution of sodium acetate (0.03 eq., 0.6 M, 0.78 mL) in water was added to the reaction mixture and the temperature was lowered to 0 °C. 3.54 mL of 30% aqueous solution of H<sub>2</sub>O<sub>2</sub> (2 eq., 31.2 mmol) was added using a syringe pump at a rate of 0.5 mL/h. The resulting mixture was stirred for 16 h allowing the temperature to raise to r.t. After the reaction was complete, the mixture was poured in saturated aqueous solution of NaHCO<sub>3</sub>, the aqueous layer was extracted with DCM, the combined organic layers were dried over Na<sub>2</sub>SO<sub>4</sub> and the solvent was evaporated under reduced pressure. The residue was filtrated on a silica pad using cyclohexane to remove the remaining starting material and then using ethyl acetate to obtain **23** as a dense transparent-white liquid in 71% yield.

**<sup>1</sup>H NMR (400MHz, CDCl<sub>3</sub>, δ ppm):** 4.25 (t, J = 3.4 Hz, 1H), 4.20 (t, J = 6.7 Hz, 2H), 3.85 (ddd, J = 15.6, 11.7, 3.5 Hz, 2H), 3.58 (br. s., 1H), 2.78 (br. s., 1H), 1.70 – 1.56 (m, 2H), 1.45 – 1.31 (m, 2H), 0.92 (t, J = 7.4 Hz, 3H).

**<sup>13</sup>C NMR (100MHz, CDCl<sub>3</sub>, δ ppm):** 173.13, 71.72, 65.93, 64.14, 30.53, 19.00, 13.62.

**HR-ESI-MS** C<sub>7</sub>H<sub>14</sub>O<sub>4</sub> 162.08921 found 162.08853

**butyl 2-(4-iodo-2-methoxyphenyl)-1,3-dioxolane-4-carboxylate, 8**

Chemical Formula: C<sub>15</sub>H<sub>19</sub>IO<sub>5</sub>  
Exact Mass: 406,0277

To a mixture of butyl 2,3-dihydroxypropanoate **23** (1 eq., 92.8 mg, 0.572 mmol) and 4-iodo-2-methoxybenzaldehyde (1 eq., 150 mg, 0.572 mmol) in toluene (5.72 mL), p-toluenesulfonic acid monohydrate (0.1 eq., 10.9 mg, 0.0572 mmol) was added. The mixture was refluxed overnight, water was removed as azeotrope with toluene.

Solvent was evaporated under reduced pressure and the residue was re-dissolved in EtOAc, washed with a saturated solution of NaHCO<sub>3</sub> and brine. The organic phase was dried over Na<sub>2</sub>SO<sub>4</sub>, evaporated and the residue purified by flash chromatography (EtOAc/cyclohexane 1:9) to give butyl 2-(4-iodo-2-methoxyphenyl)-1,3-dioxolane-4-carboxylate (65 mg, 0.16 mmol, 27.95 %) as clear liquid in a 1:1 mixture of *cis* and *trans* isomers. 100 mg of starting material (iodo-2-methoxy benzaldehyde) were recovered.

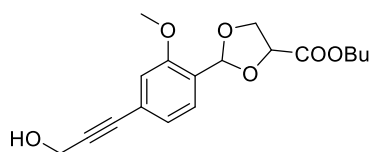
A portion of *cis* and *trans* isomers were separated for the NMR characterization.

**(trans)****butyl (2S,4R)-2-(4-iodo-2-methoxyphenyl)-1,3-dioxolane-4-carboxylate + enantiomer (2R, 4S)**

**<sup>1</sup>H NMR (400 MHz, CDCl<sub>3</sub>, δ ppm):** 7.39 (d, J = 8.6 Hz, 1H), 7.36 (s, 1H), 7.30 (d, J = 8.1 Hz, 1H), 6.34 (s, 1H), 4.80 (t, J = 6.4 Hz, 1H), 4.43 (t, J = 7.9 Hz, 1H), 4.26 (t, J = 6.6 Hz, 2H), 4.11 (dd, J = 8.0, 5.9 Hz, 1H), 3.89 (s, 3H), 1.76 – 1.68 (m, 2H), 1.51 – 1.39 (m, 2H), 0.99 (t, J = 7.4 Hz, 3H).

**(cis)****butyl (2S,4S)-2-(4-iodo-2-methoxyphenyl)-1,3-dioxolane-4-carboxylate + enantiomer (2R, 4R)**

**<sup>1</sup>H NMR (400 MHz, CDCl<sub>3</sub>, δ ppm):** 7.59 (d, J = 8.1 Hz, 1H), 7.40 (d, J = 8.1 Hz, 1H), 7.26 (s, 1H), 6.26 (s, 1H), 4.73 (dd, J = 7.4, 3.4 Hz, 1H), 4.39 (dd, J = 8.7, 3.4 Hz, 1H), 4.28 (t, J = 8.2 Hz, 1H), 4.24 – 4.18 (m, 2H), 3.89 (s, 3H), 1.68 (dt, J = 14.6, 7.2 Hz, 2H), 1.40 (dt, J = 14.8, 7.4 Hz, 2H), 0.98 (t, J = 7.6 Hz, 3H).

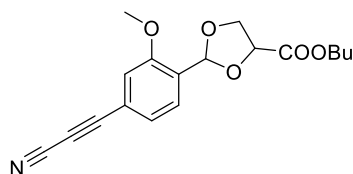
**butyl 2-(4-(3-hydroxyprop-1-yn-1-yl)-2-methoxyphenyl)-1,3-dioxolane-4-carboxylate, 9**

Chemical Formula: C<sub>18</sub>H<sub>22</sub>O<sub>6</sub>  
Exact Mass: 334,1416

Butyl 2-(4-iodo-2-methoxyphenyl)-1,3-dioxolane-4-carboxylate **8** (1 eq., 60 mg, 0.148 mmol) and 2-propyn-1-ol (2 eq., 16.54 mg, 17.4  $\mu$ L, 0.296 mmol) were dissolved in a 1:1 amount of THF and TEA. The solution was degassed and purged with argon. Dichlorobis(triphenylphosphine) palladium (0.01 eq., 1.12 mg, 0.0016 mmol) and CuI (0.02 eq., 0.61 mg, 0.0032 mmol) were added and the solution was degassed again. The reaction mixture was stirred at 25°C under argon for 14 hours.

Then the mixture was diluted with DCM, washed with sat. NH<sub>4</sub>Cl, and deionized water. The organic phase was dried over MgSO<sub>4</sub>, filtered and concentrated under reduced pressure to give methyl 4-(3-hydroxyprop-1-yn-1-yl)-2-methoxybenzoate **9** (36 mg, 0.108 mmol, 73%) in a 1:1 mixture of *cis* and *trans* isomers, as a colourless liquid.

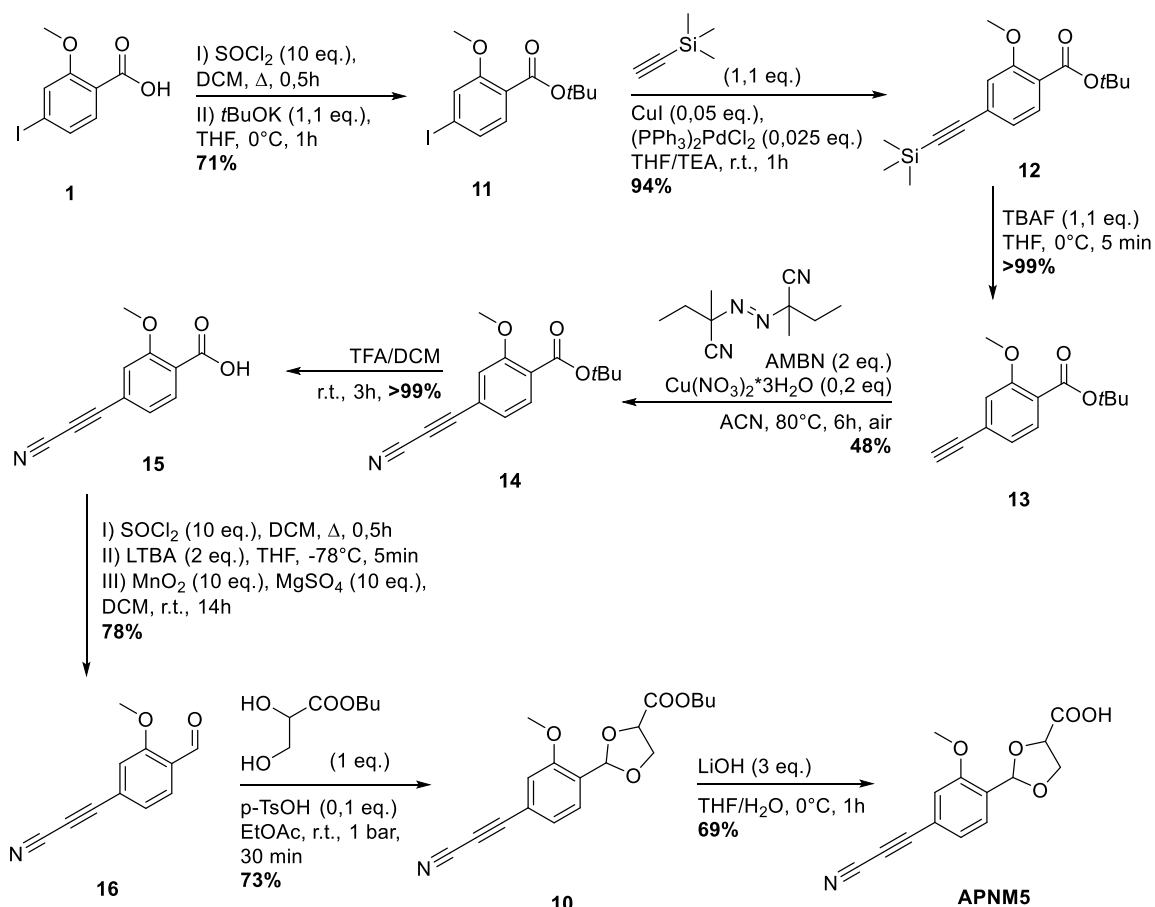
**<sup>1</sup>H NMR (400 MHz, CDCl<sub>3</sub>,  $\delta$  ppm):** 7.75 (d, J = 7.8 Hz, 1H, *trans*), 7.45 (d, J = 7.8 Hz, 1H, *cis*), 7.07 (d, J = 8.0 Hz, 1H, *cis*), 7.04 (d, J = 8.4 Hz, 1H, *trans*), 6.95 (s, 2H, *cis* + *trans*), 6.32 (s, 1H, *trans*), 6.23 (s, 1H, *cis*), 4.76 (t, J = 6.4 Hz, 1H, *trans*), 4.68 (dd, J = 7.5, 3.4 Hz, 1H, *cis*), 4.49 (m, 1H, *cis*), 4.47 (s, 4H, *cis* + *trans*), 4.39 (t, J = 7.9 Hz, 1H, *trans*), 4.34 (dd, J = 8.7, 3.4 Hz, 1H, *cis*), 4.27 – 4.14 (m, 4H, *cis* + *trans*), 4.06 (dd, J = 8.0, 6.0 Hz, 1H, *trans*), 3.82 (s, 3H, *trans*), 3.82 (s, 3H, *cis*), 1.71 – 1.57 (m, 4H, *cis* + *trans*), 1.40 – 1.31 (m, 4H, *cis* + *trans*), 0.92 (m, 6H, *cis* + *trans*).

**butyl 2-(4-(cyanoethynyl)-2-methoxyphenyl)-1,3-dioxolane-4-carboxylate, 10**

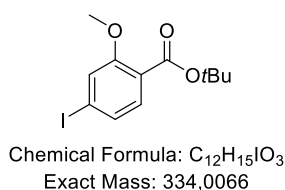
Chemical Formula: C<sub>18</sub>H<sub>19</sub>NO<sub>5</sub>  
Exact Mass: 329,1263

To the solution of butyl 2-(4-(3-hydroxyprop-1-yn-1-yl)-2-methoxyphenyl)-1,3-dioxolane-4-carboxylate **9** (1 eq., 36 mg, 0.107 mmol) in THF was added MgSO<sub>4</sub> (30 eq., 386.4 mg, 3.21 mmol), NH<sub>3</sub> (1.05 eq., 2 M in isopropanol, 56.5  $\mu$ L, 0.113 mmol) and MnO<sub>2</sub> (30 eq., 279 mg, 3.21 mmol). After stirring the mixture at 25 °C for 24 hours, TLC analysis (EtOAc/Cy : 1/9) showed only traces of the product. MgSO<sub>4</sub>, MnO<sub>2</sub> and NH<sub>3</sub> were added (15, 15 and 1 eq. respectively) and the reaction mixture was stirred for 24 hours without any improvement.

## 1.3.2 Final strategy for APNM5 synthesis



Scheme EP 2. Synthesis of APNM5. Final strategy.

*tert*-butyl 4-iodo-2-methoxybenzoate, 11

**I)** Thionyl chloride (10 eq., 4.07 g, 2.48 mL, 34.17 mmol) was added to a solution of 4-iodo-2-methoxybenzoic acid (1 eq., 950 mg, 3.417 mmol) in DCM. The mixture was refluxed for 2 hours and the completeness of reaction was controlled by TLC. Residual  $\text{SOCl}_2$  and DCM were evaporated, of 4-iodo-2-methoxybenzoyl chloride was obtained as a crude brown oil (1g) and was used in the next step without further purification. If needed to be store, special precaution was taken to avoid moisture.

**II)** The crude was dissolved in THF and cooled down to  $0^\circ\text{C}$ . A 0.6 mM solution of potassium *tert*-butoxide (1.1 eq., 422 mg, 3.76 mmol) in dry THF was added dropwise. The temperature

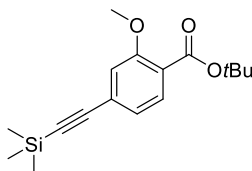


was not allowed to raise over 5 °C. The reaction mixture was stirred for one hour and then the excess of potassium *tert*-butoxide was carefully quenched with water. The solution was concentrated, and the product was extracted with diethyl ether. The organic phase was washed with 5% aqueous solution of NaOH and brine, dried over Na<sub>2</sub>SO<sub>4</sub>, evaporated and the residue purified by flash chromatography to give *tert*-butyl 4-iodo-2-methoxybenzoate (762 mg, 67%) as a yellowish solid.

**<sup>1</sup>H NMR (400 MHz, CDCl<sub>3</sub>, δ ppm):** 7.42 (d, J = 8.1 Hz, 1H), 7.31 (d, J = 8.2 Hz, 1H), 7.27 (d, J = 5.1 Hz, 1H), 3.88 (s, 3H), 1.57 (s, 10H).

**<sup>13</sup>C NMR (101 MHz, CDCl<sub>3</sub>, δ ppm):** 164.78, 159.28, 132.52, 129.41, 121.65, 99.03, 81.42, 56.30, 28.25.

### ***tert*-butyl 2-methoxy-4-((trimethylsilyl)ethynyl)benzoate, 12**

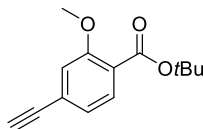


Chemical Formula: C<sub>17</sub>H<sub>24</sub>O<sub>3</sub>Si  
Exact Mass: 304,1495

*Tert*-butyl 4-iodo-2-methoxybenzoate **11** (1 eq., 762 mg, 2.28 mmol) and ethynyltrimethylsilane (1.1 eq., 190.45 mg, 2.51 mmol) were dissolved in a 1:1 amount of THF and TEA. The solution was degassed and purged with argon. Dichlorobis (triphenylphosphine) palladium (0.025 eq., 40.13 mg, 0.057 mmol) and CuI (0.05 eq., 21.7 mg, 0.114 mmol) were added and the solution was degassed again. The reaction mixture was stirred at 25 °C under argon for 14 hours. Then the mixture was diluted with DCM, washed with sat. NH<sub>4</sub>Cl, and brine. The organic phase was dried over Na<sub>2</sub>SO<sub>4</sub>, filtered and concentrated under reduced pressure. Flash chromatography purification gave *tert*-butyl 2-methoxy-4-((trimethyl silyl)ethynyl)benzoate **12** (650 mg, 2.13 mmol, 94%) as an orange oil.

**<sup>1</sup>H NMR (400 MHz, CDCl<sub>3</sub>, δ ppm):** 7.66 (d, J = 7.8 Hz, 1H), 7.08 – 6.98 (m, J = 9.7, 1.6 Hz, 2H), 3.89 (s, 3H), 1.57 (s, 9H), 0.26 (s, 9H).

**<sup>13</sup>C NMR (101 MHz, CDCl<sub>3</sub>, δ ppm):** 164.92, 158.96, 131.49, 127.69, 123.83, 122.07, 115.51, 104.37, 96.66, 81.43, 56.21, 28.40, 0.03.

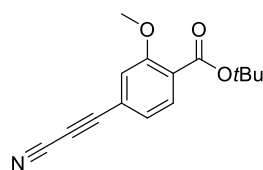
***tert*-butyl 4-ethynyl-2-methoxybenzoate, 13**

Chemical Formula: C<sub>14</sub>H<sub>16</sub>O<sub>3</sub>  
Exact Mass: 232,1099

Tetrabutylammonium fluoride (1.1 eq., 1M solution in THF, 2.35 mL, 2.347 mmol) was added to a solution of *tert*-butyl 2-methoxy-4-((trimethylsilyl)ethynyl)benzoate **11** (1 eq., 642 mg, 2.108 mmol) in dry THF at 0 °C. The reaction mixture was let to stir for 5 minutes after then saturated aqueous NH<sub>4</sub>Cl and water were added (2X volume of THF). The product was extracted with EtOAc and washed with brine. The organic phase was dried over Na<sub>2</sub>SO<sub>4</sub>, filtered and concentrated under reduced pressure. Purification by flash chromatography gave *tert*-butyl 4-ethynyl-2-methoxybenzoate (490 mg, quant. yield) as a yellowish oil.

**<sup>1</sup>H NMR (400 MHz, CDCl<sub>3</sub>, δ ppm):** 7.67 (d, J = 7.8 Hz, 1H), 7.08 (d, J = 9.4 Hz, 1H), 7.06 (s, 1H), 3.89 (s, 3H), 3.17 (s, 1H), 1.58 (s, 9H).

**<sup>13</sup>C NMR (101 MHz, CDCl<sub>3</sub>, δ ppm):** 164.75, 158.77, 131.37, 126.44, 123.85, 122.49, 115.59, 82.99, 81.40, 79.01, 56.09, 28.26.

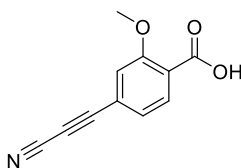
***tert*-butyl 4-(cyanoethynyl)-2-methoxybenzoate, 14**

Chemical Formula: C<sub>15</sub>H<sub>15</sub>NO<sub>3</sub>  
Exact Mass: 257,1052

*tert*-butyl 4-ethynyl-2-methoxybenzoate **13** (1 eq., 489 mg, 2.108 mmol), 2,2'-Azobis(2-methyl butyronitrile) (AMBN, 2 eq., 810 mg, 4.217 mmol) and copper(II) nitrate trihydrate (0.2 eq., 102 mg, 0.422 mmol) were dissolved in acetonitrile. The temperature was raised to 80°C and air supply was ensured. The colour of the solution went from yellow to dark green. The disappearance of starting material was checked by LC-MS and the presence of the product was confirmed by treatment of a sample with cysteine. After 6 hours, the solvent was evaporated, water was added and the product was extracted with ethyl acetate. The organic phase was dried over Na<sub>2</sub>SO<sub>4</sub>, filtered and concentrated under reduced pressure. Purification by flash chromatography gave *tert*-butyl 4-(cyanoethynyl)-2-methoxybenzoate **14** (260 mg, 1.01 mmol, 48%) as a transparent oil.

**<sup>1</sup>H NMR (400 MHz, CDCl<sub>3</sub>, δ ppm):** 7.69 (d, J = 7.8 Hz, 1H), 7.21 (d, J = 7.9 Hz, 1H), 7.14 (s, 1H), 3.91 (s, 3H), 1.58 (s, 9H).

**<sup>13</sup>C NMR (101 MHz, CDCl<sub>3</sub>, δ ppm):** 164.28, 158.50, 131.47, 125.29, 121.24, 120.75, 116.35, 105.17, 82.21, 81.89, 64.18, 56.26, 28.21.

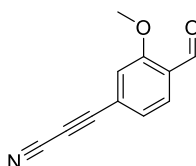
**4-(cyanoethynyl)-2-methoxybenzoic acid, 15**

Chemical Formula: C<sub>11</sub>H<sub>7</sub>NO<sub>3</sub>  
Exact Mass: 201,0426

Trifluoroacetic acid (TFA, 3 mL) was added to a solution of *tert*-butyl 4-(cyanoethynyl)-2-methoxybenzoate **14** (247 mg, 0.96 mmol) in dichloromethane. The solution was stirred at room temperature for three hours. The reaction was checked with TLC and the presence of the product was confirmed by treatment of a sample with cysteine followed by LC-MS analysis. TFA in excess and solvent were evaporated and the crude product was purified by flash chromatography. 4-(cyanoethynyl)-2-methoxybenzoic acid **15** was obtained as a colourless liquid (192 mg, quant. yield).

**<sup>1</sup>H NMR (400 MHz, MeOD-d<sub>4</sub>, δ ppm):** 7.71 (d, J = 7.7 Hz, 1H), 7.35 (s, 1H), 7.25 (d, J = 7.7 Hz, 1H), 3.82 (s, 3H).

**<sup>13</sup>C NMR (101 MHz, MeOD-d<sub>4</sub>, δ ppm):** 158.57, 131.43, 125.13, 121.60, 116.51, 104.37, 81.44, 62.77, 55.44.

**3-(4-formyl-3-methoxyphenyl)propionitrile, 16**

Chemical Formula: C<sub>11</sub>H<sub>7</sub>NO<sub>2</sub>  
Exact Mass: 185,0477

**I)** Thionyl chloride (10 eq., 384.27 mg, 0.23 mL, 3.23 mmol) was added to a solution of 4-(cyanoethynyl)-2-methoxybenzoic acid **15** (1 eq., 65 mg, 0.323 mmol) in DCM. The mixture was refluxed for 2 hours and the completeness of reaction was controlled by TLC.

Residual SOCl<sub>2</sub> and DCM were evaporated, crude intermediary product 4-(cyanoethynyl)-2-methoxybenzoyl chloride was obtained as a brown oil and was used in the next step without further purification. If needed to be store, special precaution was taken to avoid moisture.

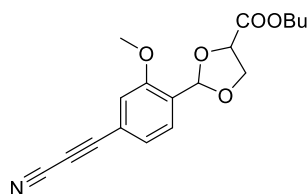
**II)** A solution of 4-(cyanoethynyl)-2-methoxybenzoyl chloride (crude, 1 eq., 71 mg, 0.323 mmol) in THF was cooled to -78 °C. Lithium tri-*tert*-butoxyaluminum hydride (2 eq., 1 M in THF, 646 μL, 0.646 mmol) was added dropwise in 10 minutes. The solution was stirred for another 5 minutes, then saturated NaHCO<sub>3</sub> was added. The obtained reaction mixture was left stirring for several minutes (to let all aluminium salt to precipitate), organic phase was decanted. Et<sub>2</sub>O

was added to the reaction mixture, then decanted. United organic phases were washed with sat NaHCO<sub>3</sub> and brine, dried over MgSO<sub>4</sub> and evaporated to give 3-(4-(hydroxymethyl)-3-methoxyphenyl) propiolonitrile as crude product.

**III)** The crude 3-(4-(hydroxymethyl)-3-methoxyphenyl) propiolonitrile (1 eq., 55 mg, 0.294 mmol) was resolubilized in DCM, then MnO<sub>2</sub> (10 eq., 256 mg, 2.94 mmol) and MgSO<sub>4</sub> (10 eq., 354 mg, 2.94 mmol) were subsequently added. The obtained reaction mixture was left stirring overnight at room temperature, then filtered through celite, washed thoroughly with three portions of DCM. The solvent was evaporated and the crude material was purified by flash chromatography to give 3-(4-formyl-3-methoxyphenyl)propiolonitrile **16** (46,5 mg, 0.251 mmol, 85 %) as a white solid.

**<sup>1</sup>H NMR (400 MHz, CDCl<sub>3</sub>, δ ppm):** 7.85 (d, *J* = 7.8 Hz, 1H), 7.28 (d, *J* = 8.9 Hz, 1H), 7.21 (s, 1H), 3.97 (s, 1H).

### butyl 2-(4-(cyanoethynyl)-2-methoxyphenyl)-1,3-dioxolane-4-carboxylate, **10**



Chemical Formula: C<sub>18</sub>H<sub>19</sub>NO<sub>5</sub>  
Exact Mass: 329,1263

3-(4-formyl-3-methoxyphenyl)propiolonitrile (1 eq., 46.5 mg, 0.251 mmol) and butyl 2,3-dihydroxypropanoate (1 eq., 40.7 mg, 0.251 mmol) were dissolved in EtOAc and concentrated using rotary evaporator in bath conditioned at room temperature. The dissolving/concentration steps were repeated 3 times. The reaction was monitored by LC-MS. After third evaporation the peak of aldehyde completely disappeared and there were two close peaks of *cis* and *trans* product (1:1). Increase of bath temperature (up to 40°C) leads to production of only a *trans*-isomer. Then EtOAc was added and the solution was washed with NaHCO<sub>3</sub>, H<sub>2</sub>O, dried over MgSO<sub>4</sub> and concentrated in vacuo. Silica gel flash chromatography was performed (Cyclohexane/EtOAc) to give butyl 2-[4-(2-cyanoethynyl)-2-methoxyphenyl]-1,3-dioxolane-4-carboxylate (60 mg, 0.182 mmol, 72.6 %) as a mixture of *cis* and *trans* isomers (white solid). A portion of *cis* and *trans* isomers were separated for the NMR characterization.

**(trans)**

### butyl (2R,4S)-2-(4-(cyanoethynyl)-2-methoxyphenyl)-1,3-dioxolane-4-carboxylate

+ enantiomer (2S, 4R)

**<sup>1</sup>H NMR (400 MHz, CDCl<sub>3</sub>, δ ppm):** 7.57 (d, *J* = 7.8 Hz, 1H), 7.23 (d, *J* = 10.9 Hz, 1H), 7.09 (s, 1H), 6.33 (s, 1H), 4.77 (t, *J* = 6.4 Hz, 1H), 4.39 (t, *J* = 7.9 Hz, 1H), 4.22 (t, *J* = 6.5 Hz, 2H), 4.12 – 4.06 (m, 1H), 3.88 (s, 3H), 1.71 – 1.63 (m, 2H), 1.45 – 1.37 (m, 2H), 0.95 (t, *J* = 7.4 Hz, 3H).

**$^{13}\text{C}$  NMR (101 MHz,  $\text{CDCl}_3$ ,  $\delta$  ppm):** 170.88, 157.68, 129.25, 127.66, 126.06, 119.48, 115.01, 105.32, 99.91, 82.55, 74.21, 68.32, 65.49, 55.99, 30.59, 19.06, 13.67.

*(cis)*

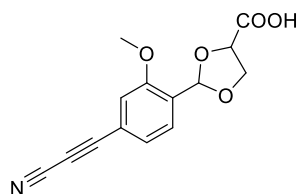
**butyl (2R,4R)-2-(4-(cyanoethynyl)-2-methoxyphenyl)-1,3-dioxolane-4-carboxylate**

**+ enantiomer (2S, 4S)**

**$^1\text{H}$  NMR (400 MHz,  $\text{CDCl}_3$ ,  $\delta$  ppm):** 7.89 (d,  $J = 7.9$  Hz, 1H), 7.27 (d,  $J = 8.1$  Hz, 1H), 7.08 (s, 1H), 6.24 (s, 1H), 4.70 (dd,  $J = 7.3, 3.4$  Hz, 1H), 4.35 (dd,  $J = 8.7, 3.3$  Hz, 1H), 4.25 (t,  $J = 8.2$  Hz, 1H), 4.22 – 4.14 (m, 2H), 3.88 (s, 3H), 1.66 – 1.58 (m, 2H), 1.35 (dt,  $J = 15.2, 7.5$  Hz, 2H), 0.92 (t,  $J = 7.4$  Hz, 3H).

**$^{13}\text{C}$  NMR (101 MHz,  $\text{CDCl}_3$ ,  $\delta$  ppm):** 170.69, 157.64, 129.22, 128.55, 126.22, 119.42, 114.80, 105.34, 100.13, 82.66, 74.07, 69.26, 65.47, 63.29, 55.94, 30.56, 19.04, 13.64.

**2-(4-(cyanoethynyl)-2-methoxyphenyl)-1,3-dioxolane-4-carboxylic acid, APNM5**



Chemical Formula:  $\text{C}_{14}\text{H}_{11}\text{NO}_5$   
Exact Mass: 273.0637

butyl 2-[4-(2-cyanoethynyl)-2-methoxyphenyl]-1,3-dioxolane-4-carboxylate (1 eq., 30 mg, 0.0911 mmol) was dissolved in THF and cooled down to 0 °C. Then lithium hydroxide (3 eq., 0.5 M in water, 0.547 mL, 0.273 mmol) was added. The reaction was let to stir at 0 °C until completeness (checked by TLC). The reaction was carefully neutralized with aqueous HCl (1M), THF was evaporated and the product was extracted with EtOAc. The organic phase was dried over  $\text{MgSO}_4$  and concentrated under vacuum. Purification of the crude product by preparative HPLC gave 2-(4-(cyanoethynyl)-2-methoxyphenyl)-1,3-dioxolane-4-carboxylic acid **APNM5** (17.5 mg, 0.064 mmol, 70.31%) as a 1:1 mixture of *cis* and *trans* isomers (white solid).

**$^1\text{H}$  NMR (400 MHz,  $\text{CDCl}_3$ ,  $\delta$  ppm):** 7.67 (d,  $J = 7.98$  Hz, 1H, *cis*), 7.54 (d,  $J = 7.9$  Hz, 1H, *trans*), 7.30 – 7.22 (m, 2H, *cis* + *trans*), 7.12 (s, 1H, *cis*), 7.07 (s, 1H, *trans*), 6.29 (s, 1H, *trans*), 6.12 (s, 1H, *cis*), 4.79 (t,  $J = 6.5$  Hz, 1H, *trans*), 4.76 – 4.70 (m, 1H, *cis*), 4.48 – 4.40 (m, 2H, *cis* + *trans*), 4.28 (t,  $J = 8.5$  Hz, 1H, *cis*), 4.15 – 4.09 (m, 1H, *trans*), 3.90 (s, 3H, *cis*), 3.87 (s, 3H, *trans*).

**$^{13}\text{C}$  NMR (101 MHz,  $\text{CDCl}_3$ ,  $\delta$  ppm):** 175.05, 174.12, 157.63, 157.60, 128.96, 128.78, 127.87, 127.54, 126.40, 126.10, 120.08, 119.72, 115.28, 115.10, 105.26, 105.24, 101.58, 100.23, 82.37, 82.25, 73.77, 73.54, 69.38, 68.18, 63.64, 63.52, 56.08, 56.07.

**HR-ESI-MS**  $\text{C}_{14}\text{H}_{11}\text{NO}_5$  273.06372 found 273.06364

## User Chromatograms

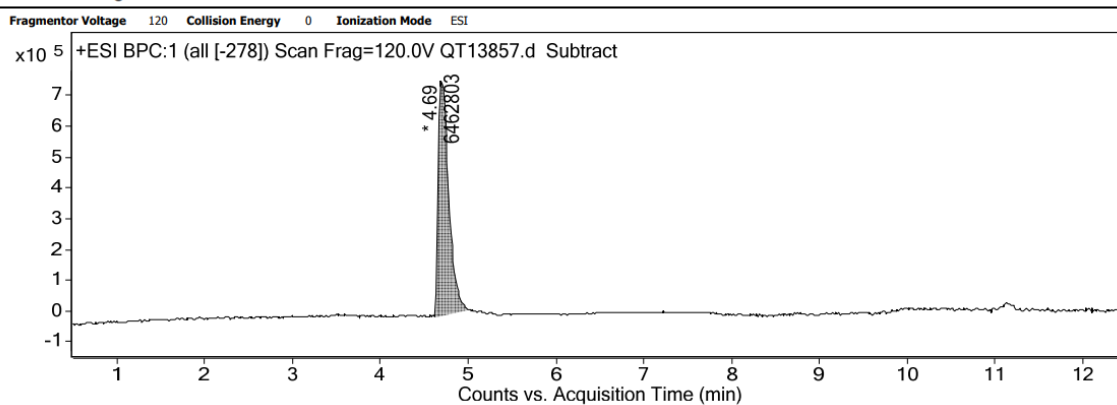
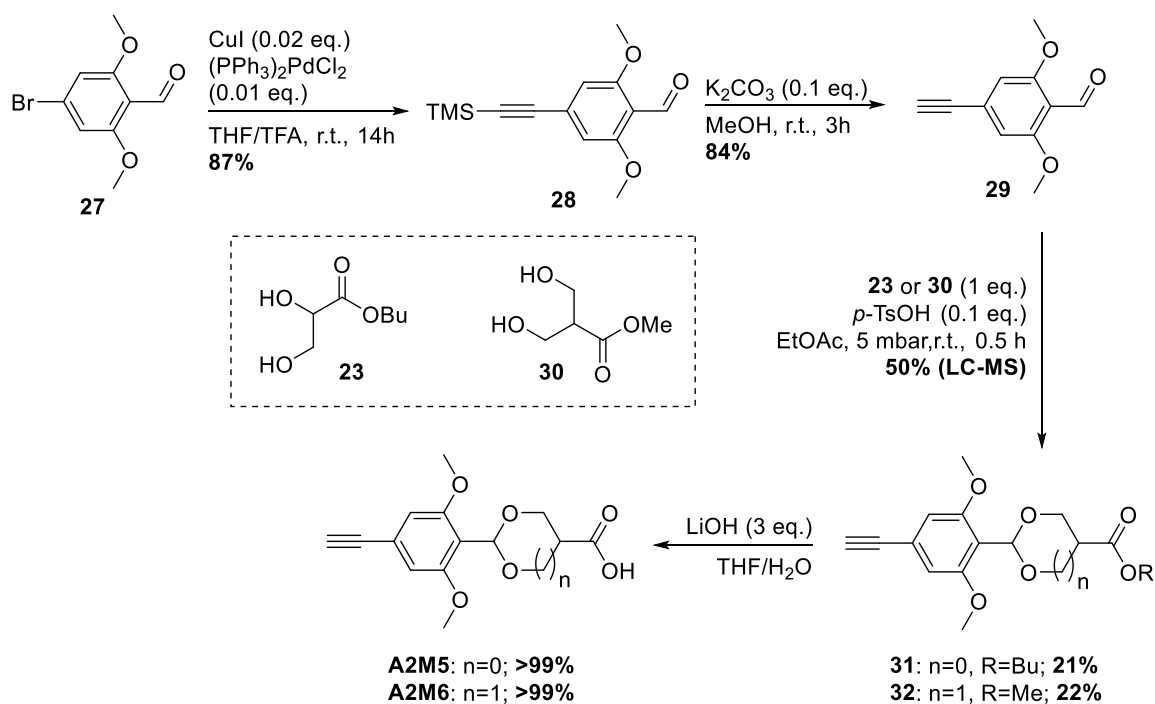
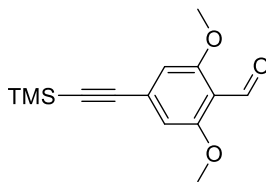


Figure EP 1. HPLC chromatogram of APNM5.

1.4 SYNTHESIS OF **A2M5** AND **A2M6**Scheme EP 3. Synthesis of compounds **A2M5** and **A2M6**.

**2,6-dimethoxy-4-((trimethylsilyl)ethynyl)benzaldehyde, 28**

Chemical Formula:  $C_{14}H_{18}O_3Si$   
Exact Mass: 262,1025

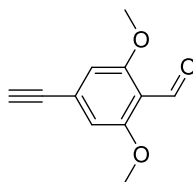
Compound **28** was synthesized starting from 4-bromo-2,6-dimethoxybenzaldehyde **27** following the same Sonogashira coupling procedure used for the synthesis of compound **12**.

Yield: 76-87%

**$^1H$  NMR (400 MHz,  $CDCl_3$ ,  $\delta$  ppm):** 10.45 (s, 1H), 6.66 (s, 2H), 3.90 (s, 6H), 0.27 (s, 9H).

**$^{13}C$  NMR (101 MHz,  $CDCl_3$ ,  $\delta$  ppm):** 188.98, 161.99, 130.38, 114.67, 107.73, 104.28, 98.28, 56.41, 1.22.

**HR-ESI-MS**  $C_{14}H_{18}O_3Si$  262.1025 found 262.1023

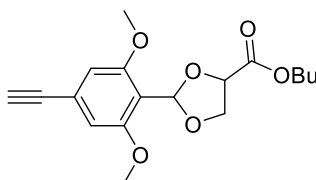
**4-ethynyl-2,6-dimethoxybenzaldehyde, 29**

Chemical Formula:  $C_{11}H_{10}O_3$   
Exact Mass: 190,0630

2,6-dimethoxy-4-((trimethylsilyl)ethynyl)benzaldehyde (1 eq., 301 mg, 1.15 mmol) and  $K_2CO_3$  (0.1 eq., 15.86 mg, 0.11 mmol) were dissolved in MeOH. The reaction was stirred at room temperature for 3 h, and the solvent was removed under vacuum. The solid was redissolved in DCM and was washed with aqueous  $NaHCO_3$  three times. The organic layer was dried over  $Na_2SO_4$  and evaporated under vacuum. Purification by flash chromatography afforded 4-ethynyl-2,6-dimethoxybenzaldehyde (183.72 mg, 0.97 mmol, 84.2%) as a white solid.

**$^1H$  NMR (400 MHz,  $CDCl_3$ ,  $\delta$  ppm):** 10.46 (s, 1H), 6.70 (s, 2H), 3.90 (s, 6H), 3.25 (s, 1H).

**$^{13}C$  NMR (101 MHz,  $CDCl_3$ ,  $\delta$  ppm):** 187.72, 160.78, 128.10, 113.73, 106.71, 81.90, 79.11, 55.20.

**butyl 2-(4-ethynyl-2,6-dimethoxyphenyl)-1,3-dioxolane-4-carboxylate, 31**

Chemical Formula:  $C_{18}H_{22}O_6$   
Exact Mass: 334,1416

Compound **31** was synthesized following the same procedure used for compound **10**. After two purification a mixture 1:0.3 of *trans* and *cis* isomers was obtained.

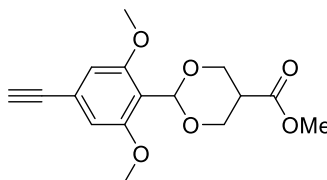
Yield: 21%, colourless oil

**<sup>1</sup>H NMR (400 MHz, CDCl<sub>3</sub>, δ ppm):** 6.71 (s, 1H, *trans*), 6.69 (s, 1H, *cis*), 6.67 (s, 1H, *trans*), 6.66 (s, 1H, *cis*), 4.81 – 4.76 (m, 1H, *trans*), 4.66 (dd, *J* = 7.5, 5.7 Hz, 1H, *cis*), 4.50 – 4.44 (m, 1H, *trans*), 4.40 (dd, *J* = 7.7, 5.7 Hz, 1H, *cis*), 4.26 – 4.22 (m, 1H, *cis*), 4.20 (t, *J* = 6.8 Hz, 4H, *cis* + *trans*), 4.01 (dd, *J* = 7.9, 6.1 Hz, 1H, *trans*), 3.80 (s, 6H, *trans*), 3.76 (s, 6H, *cis*), 3.093 (s, 1H, *trans*), 3.088 (s, 1H, *cis*), 1.70 – 1.60 (m, 4H, *cis* + *trans*), 1.46 – 1.34 (m, 4H, *cis* + *trans*), 0.97 – 0.91 (m, 6H, *cis* + *trans*).

**<sup>13</sup>C NMR (101 MHz, CDCl<sub>3</sub>, δ ppm):** 170.26, 168.69, 158.56, 158.41, 128.86, 127.08, 123.55, 123.48, 113.00, 112.50, 107.25, 98.92, 82.54, 82.49, 76.64, 76.58, 73.97, 73.93, 67.93, 66.89, 64.22, 64.15, 55.12, 54.96, 29.62, 29.56, 18.07, 18.00, 12.68, 12.62.

**HR-ESI-MS** C<sub>18</sub>H<sub>22</sub>O<sub>6</sub> 334.1416 found 334.1411

### methyl 2-(4-ethynyl-2,6-dimethoxyphenyl)-1,3-dioxane-5-carboxylate, **32**



Chemical Formula: C<sub>16</sub>H<sub>18</sub>O<sub>6</sub>

Exact Mass: 306,1103

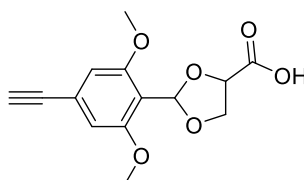
Compound **32** was synthesized following the same procedure used for compound **10**. After two purification a mixture 1:0.45 of *trans* and *cis* isomers was obtained.

Yield: 22%, colourless oil

**<sup>1</sup>H NMR (400 MHz, CDCl<sub>3</sub>, δ ppm):** 6.69 (s, 2H, *trans*), 6.65 (s, 2H, *cis*), 6.10 (s, 1H, *cis*), 6.02 (s, 1H, *trans*), 4.74 (dd, *J* = 11.8, 1.5 Hz, 2H, *cis*), 4.49 – 4.42 (m, 2H, *trans*), 4.07 – 4.02 (m, 2H, *cis*), 3.99 – 3.91 (m, 2H, *trans*), 3.87 (s, 3H, *cis*), 3.84 (s, 6H, *trans*), 3.80 (s, 3H, *trans*), 3.70 (s, 6H, *cis*), 3.27 – 3.18 (m, 2H, *cis* + *trans*), 3.08 (s, 1H, *trans*), 3.06 (s, 1H, *cis*).

**HR-ESI-MS** C<sub>16</sub>H<sub>18</sub>O<sub>6</sub> 306.1103 found 306.1105

### 2-(4-ethynyl-2,6-dimethoxyphenyl)-1,3-dioxolane-4-carboxylic acid, **A2M5**



Chemical Formula: C<sub>14</sub>H<sub>14</sub>O<sub>6</sub>

Exact Mass: 278,0790



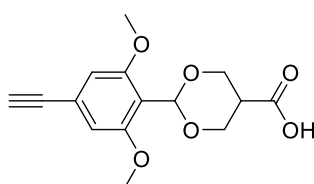
Compound **A2M5** was synthesized from **31** following the same procedure used for compound **APNM5**. After purification by preparative HPLC a mixture 1:0.3 of *trans* and *cis* isomers was obtained.

Yield: >99% (LC-MS), white solid.

**<sup>1</sup>H NMR (400 MHz, DMSO,  $\delta$  ppm):** 6.72 (s, 2H, *trans*), 6.69 (s, 2H, *cis*), 5.92 (s, 1H, *cis*), 5.82 (s, 1H, *trans*), 4.39 (d,  $J = 10.9$  Hz, 2H, *cis*), 4.20 (dd,  $J = 11.2, 4.2$  Hz, 2H, *trans*), 3.92 – 3.86 (m, 1H, *trans*), 3.75 (s, 6H, *trans*), 3.72 (s, 6H, *cis*). Some peaks were covered by peak of ammonium formate used in the mobile phase of the HPLC.

**HR-ESI-MS** C<sub>14</sub>H<sub>14</sub>O<sub>6</sub> 278.0790 found 278.0782

### 2-(4-ethynyl-2,6-dimethoxyphenyl)-1,3-dioxane-5-carboxylic acid, A2M6



Chemical Formula: C<sub>15</sub>H<sub>16</sub>O<sub>6</sub>

Exact Mass: 292.0947

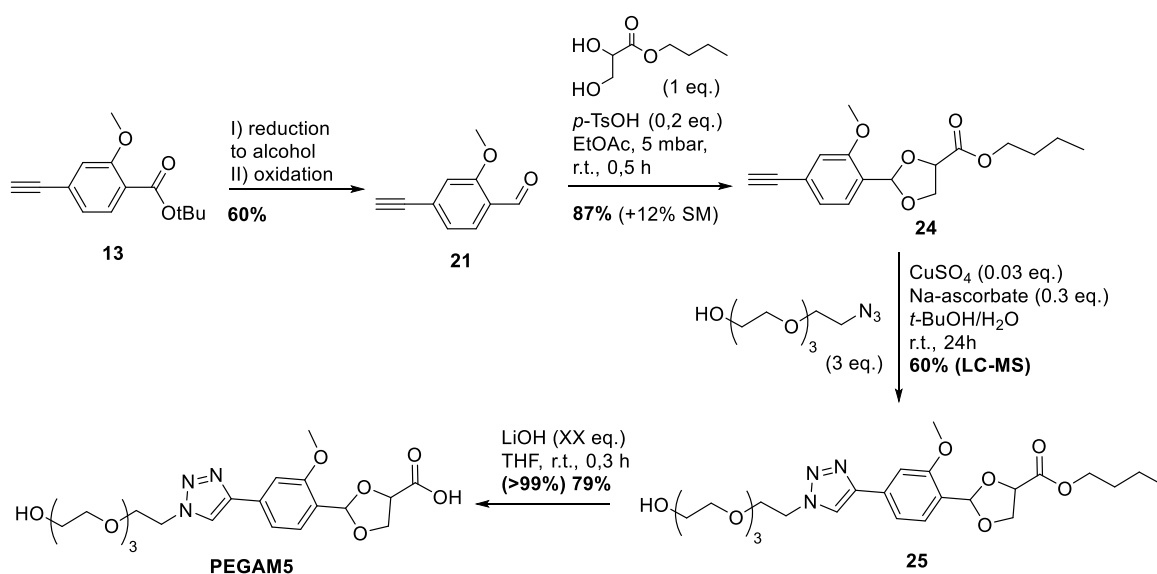
Compound **A2M6** was synthesized from **32** following the same procedure used for compound **APNM5**. After purification by preparative HPLC a mixture 1:0.45 of *trans* and *cis* isomers was obtained.

Yield: >99% (LC-MS), white solid

**<sup>1</sup>H NMR (400 MHz, DMSO,  $\delta$  ppm):** 6.75 (s, 2H, *cis* + *trans*), 6.46 (s, 1H, *trans*), 6.32 (s, 1H, *cis*), 4.55 (t,  $J = 6.0$  Hz, 1H, *trans*), 4.49 (d,  $J = 6.8$  Hz, 1H, *cis*), 4.23 (t,  $J = 7.1$  Hz, 1H, *trans*), 4.03 (d,  $J = 6.9$  Hz, 1H, *cis*), 3.87 – 3.82 (m, 2H, *cis* + *trans*), 3.77 (s, 6H, *trans*), 3.73 (s, 6H, *cis*). Peaks (*cis* and *trans*) corresponding to the proton of the terminal alkyne were covered by peak of ammonium formate used in the mobile phase of the HPLC.

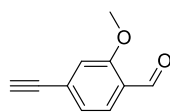
**HR-ESI-MS** C<sub>15</sub>H<sub>16</sub>O<sub>6</sub> 292.0947 found 292.0933

## 1.5 SYNTHESIS OF PEGAM5



Scheme EP 4. Synthesis of PEGAM5.

## 4-ethynyl-2-methoxybenzaldehyde, 21



Chemical Formula: C<sub>10</sub>H<sub>8</sub>O<sub>2</sub>  
 Exact Mass: 160.0524

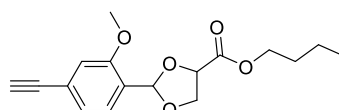
Compound **21** was synthesized following the same procedures used for compound **16**, Final yield: 60%.

**<sup>1</sup>H NMR (400 MHz, CDCl<sub>3</sub>, δ ppm):** 10.44 (d, *J* = 0.8 Hz, 1H), 7.78 (dd, *J* = 7.9, 0.4 Hz, 1H), 7.15 (dt, *J* = 7.9, 1.1 Hz, 1H), 7.10 (d, *J* = 1.3 Hz, 1H), 3.94 (s, 3H), 3.28 (s, 1H).

**<sup>13</sup>C NMR (101 MHz, CDCl<sub>3</sub>, δ ppm):** 188.00, 160.27, 128.41, 127.48, 123.90, 123.54, 114.20, 81.81, 79.65, 76.31, 54.78, 0.00.

**HR-ESI-MS** C<sub>10</sub>H<sub>8</sub>O<sub>2</sub> 160.0524 found 160.0522

## butyl 2-(4-ethynyl-2-methoxyphenyl)-1,3-dioxolane-4-carboxylate, 24



Chemical Formula: C<sub>17</sub>H<sub>20</sub>O<sub>5</sub>  
 Exact Mass: 304.1311

Compound **24** was obtained with the same condensation procedure used for compound **10**. butyl 2-(4-ethynyl-2-methoxyphenyl)-1,3-dioxolane-4-carboxylate was obtained as a 1:1 mixture of *cis* and *trans* isomers, a colourless oil. Yield: 87%.

**(trans)**

**butyl (2R,4S)-2-(4-ethynyl-2-methoxyphenyl)-1,3-dioxolane-4-carboxylate**

**+ enantiomer (2S, 4R)**

**<sup>1</sup>H NMR (400 MHz, CDCl<sub>3</sub>, δ ppm):** 7.48 (d, *J* = 7.9 Hz, 1H), 7.12 (dd, *J* = 7.8, 1.4 Hz, 1H), 7.01 (d, *J* = 1.4 Hz, 1H), 6.34 (s, 1H), 4.77 (dd, *J* = 7.3, 5.6 Hz, 1H), 4.40 (dd, *J* = 8.4, 7.4 Hz, 1H), 4.22 (td, *J* = 6.7, 1.9 Hz, 2H), 4.08 (dd, *J* = 8.4, 5.6 Hz, 1H), 3.86 (s, 3H), 3.10 (s, 1H), 1.74 – 1.61 (m, 2H), 1.48 – 1.34 (m, 2H), 0.95 (t, *J* = 7.4 Hz, 3H).

**<sup>13</sup>C NMR (101 MHz, CDCl<sub>3</sub>, δ ppm):** 170.11, 156.46, 126.04, 124.73, 123.48, 123.26, 113.29, 99.39, 82.39, 76.64, 73.13, 67.22, 64.37, 54.76, 29.58, 18.04, 12.64.

**(cis)**

**butyl (2R,4R)-2-(4-ethynyl-2-methoxyphenyl)-1,3-dioxolane-4-carboxylate**

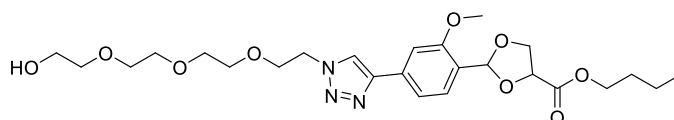
**+ enantiomer (2S, 4S)**

**<sup>1</sup>H NMR (400 MHz, CDCl<sub>3</sub>, δ ppm):** 7.78 (d, *J* = 7.9 Hz, 1H), 7.15 (dd, *J* = 7.9, 1.4 Hz, 1H), 7.01 (d, *J* = 1.4 Hz, 1H), 6.25 (s, 1H), 4.69 (dd, *J* = 7.6, 3.7 Hz, 1H), 4.36 (dd, *J* = 8.7, 3.6 Hz, 1H), 4.27 – 4.22 (m, 1H), 4.22 – 4.14 (m, 2H), 3.86 (s, 3H), 3.10 (s, 1H), 1.70 – 1.58 (m, 2H), 1.45 – 1.30 (m, 2H), 0.93 (t, *J* = 7.4 Hz, 3H).

**<sup>13</sup>C NMR (101 MHz, CDCl<sub>3</sub>, δ ppm):** 170.86, 157.44, 127.85, 125.62, 124.68, 124.24, 114.08, 100.54, 83.49, 77.55, 74.04, 69.11, 65.38, 55.73, 30.55, 19.03, 13.63.

**HR-ESI-MS** C<sub>17</sub>H<sub>20</sub>O<sub>5</sub> 304.1311 found 304.1296

**butyl 2-(4-(1-(2-(2-(2-(2-hydroxyethoxy)ethoxy)ethoxy)ethyl)-1H-1,2,3-triazol-4-yl)-2-methoxyphenyl)-1,3-dioxolane-4-carboxylate, 26**

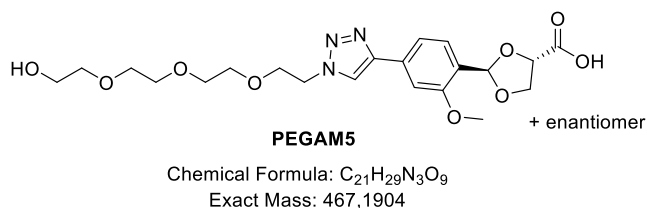


Chemical Formula: C<sub>25</sub>H<sub>37</sub>N<sub>3</sub>O<sub>9</sub>  
Exact Mass: 523.2530

2-{2-[2-(2-azidoethoxy)ethoxy]ethoxy}ethan-1-ol (3 eq., 122 mg, 0.556 mmol) and butyl 2-(4-ethynyl-2-methoxyphenyl)-1,3-dioxolane-4-carboxylate (1 eq., 56 mg, 0.184 mmol) were suspended in 0.5 mL of a 1:1 water/*tert*-butanol mixture. Freshly prepared solution of sodium ascorbate (0.3 eq., 0.1 M in water, 556 μL, 0.0556 mmol) was added, followed by CuSO<sub>4</sub>·5H<sub>2</sub>O (0.03 eq., 0.1 M in water, 55.6 μL, 0.00556 mmol). The suspension was stirred vigorously overnight, and checked by LC-MS. The maximum conversion reached was 60%, after then the product of the side reaction (acetal hydrolysis promoted by copper as Lewis acid) started to appear. The reaction was stopped and the product is extracted with diethyl ether. The organic phase was dried over Na<sub>2</sub>SO<sub>4</sub>, concentrated at low pressure to give crude butyl 2-(4-(1-(2-(2-(2-

(2-hydroxyethoxy)ethoxy)ethoxy)ethyl)-1H-1,2,3-triazol-4-yl)-2-methoxyphenyl)-1,3-dioxolane-4-carboxylate as a colourless oil (mixture of *cis* and *trans* isomers). The obtained product was used in the next step without any further purification.

**(2R,4S)-2-(4-(1-(2-(2-(2-(2-hydroxyethoxy)ethoxy)ethoxy)ethyl)-1H-1,2,3-triazol-4-yl)-2-ethoxyphenyl)-1,3-dioxolane-4-carboxylic acid, and enantiomer (2S,4R), PEGAM5**

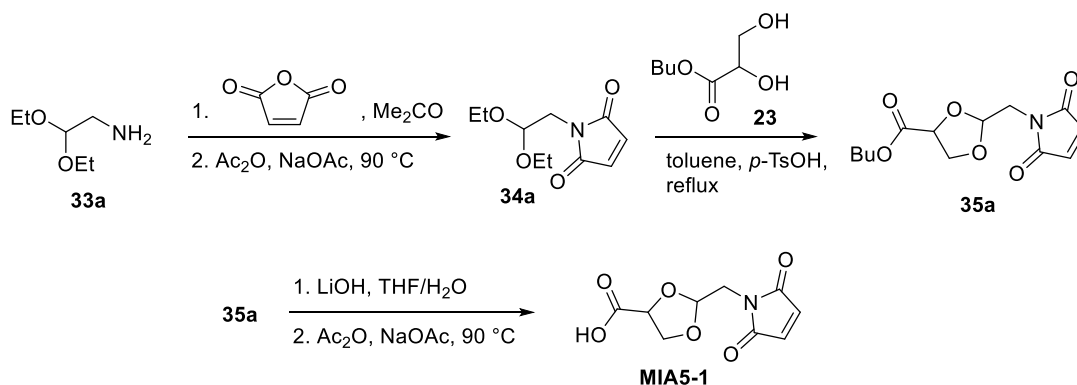


Compound **PEGAM5** (1 eq., 96 mg, 0.18 mmol) was dissolved in THF and cooled down to 0 °C. Then lithium hydroxide (3 eq., 1 M in water, 550 µL, 0.55 mmol) was added. The reaction was let to stir at 0 °C until completeness (checked by LC-MS: quantitative yield). The reaction was carefully neutralized with aqueous HCl (1M), THF was evaporated and the product was extracted with EtOAc. The organic phase was dried over MgSO<sub>4</sub> and concentrated under vacuum. Purification by preparative HPLC gave **PEGAM5** (68 mg, 0.142 mmol, 79.3%, *trans* isomer) as colourless liquid.

**<sup>1</sup>H NMR (400 MHz, DMSO, δ ppm):** 8.62 (s, 1H), 7.49 (dd, *J* = 4.6, 3.3 Hz, 2H), 7.44 (dd, *J* = 7.9, 1.3 Hz, 1H), 6.14 (s, 1H), 4.58 (t, *J* = 5.2 Hz, 2H), 4.32 (t, *J* = 6.7 Hz, 1H), 4.20 (t, *J* = 7.5 Hz, 1H), 3.90 – 3.86 (m, 5H), 3.82 – 3.76 (m, 1H), 3.56 – 3.54 (m, 2H), 3.51 – 3.48 (m, 2H), 3.48 – 3.43 (m, 6H), 3.36 (t, *J* = 5.1 Hz, 2H).

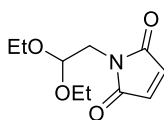
## 1.6 SYNTHESIS OF MIAs

## 1.6.1 Synthesis of linker MIA5-1



Scheme EP 5. Synthesis of linker MIA5-1.

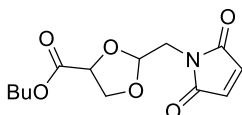
## 1-(2,2-diethoxyethyl)-1H-pyrrole-2,5-dione, 33a



Chemical Formula: C<sub>10</sub>H<sub>15</sub>NO<sub>4</sub>  
Molecular Weight: 213,23

Molecule **33a** was synthesized according to the reported procedures.<sup>44</sup>

## butyl 2-((2,5-dioxo-2,5-dihydro-1H-pyrrol-1-yl)methyl)-1,3-dioxolane-4-carboxylate, 35a



Chemical Formula: C<sub>13</sub>H<sub>17</sub>NO<sub>6</sub>  
Molecular Weight: 283,28

A solution of **33a** (1 eq., 677 mg, 3.18 mmol) and **23** (1 eq., 515 mg, 3.18 mmol) in toluene (50 mL) containing a catalytic amount of *p*-toluenesulfonic acid monohydrate (0.2 eq., 120 mg, 0.635 mmol) was refluxed for 2 h. Ethanol was removed as azeotrope of toluene (b.p. of azeotrope: 76.7°C) and the reaction was monitored by TLC. After disappearing of the starting material, toluene was evaporated at reduced pressure, the residue was redissolved in ethyl acetate and washed with a saturated solution of NaHCO<sub>3</sub> and brine. The organic phase was dried over Na<sub>2</sub>SO<sub>4</sub> and the solvent was evaporated. The crude product was purified by flash chromatography (cyclohexane, then cyclohexane to EtOAc), yielding the wanted product **35a**

in 54% yield and **ethyl 2-((2,5-dioxo-2,5-dihydro-1H-pyrrol-1-yl)methyl)-1,3-dioxolane-4-carboxylate** as by-product (21%), which will be used as well for the following step.

**butyl 2-((2,5-dioxo-2,5-dihydro-1H-pyrrol-1-yl)methyl)-1,3-dioxolane-4-carboxylate**, mixture of *cis*- and *trans*- isomers.

**<sup>1</sup>H NMR (400MHz, CDCl<sub>3</sub>, δ ppm):** 6.73 (s, 4H, *cis* + *trans*), 5.35 (t, J = 4.5 Hz, 1H, *trans*), 5.23 (t, J = 3.6 Hz, 1H, *cis*), 4.66 – 4.59 (m, 1H, *trans*), 4.54 (dd, J = 7.2, 4.0 Hz, 1H, *cis*), 4.27 (t, J = 7.9 Hz, 1H, *trans*), 4.22 – 4.19 (m, 1H, *cis*), 4.15 (q, J = 13.4, 6.7 Hz, 4H, *cis* + *trans*), 4.08 (t, J = 8.1 Hz, 1H, *cis*), 3.95 (dd, J = 8.3, 5.3 Hz, 1H, *trans*), 3.87 (d, J = 4.2 Hz, 2H, *cis*), 3.74 (d, J = 4.4 Hz, 2H, *trans*), 1.68 – 1.58 (m, 4H, *cis* + *trans*), 1.37 (dp, J = 14.3, 7.2 Hz, 4H, *cis* + *trans*), 0.93 (td, J = 7.2, 3.5 Hz, 6H, *cis* + *trans*).

**<sup>13</sup>C NMR (100MHz, CDCl<sub>3</sub>, δ ppm):** 170.54, 170.34, 170.19, 134.26, 134.22, 102.68, 101.96, 74.05, 73.96, 68.64, 68.00, 65.44, 39.70, 39.54, 30.53, 19.02, 13.66, 13.63.

**HR-ESI-MS** C<sub>13</sub>H<sub>17</sub>NO<sub>6</sub> 283.10559 found 283.10564

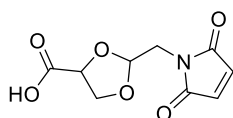
**ethyl 2-((2,5-dioxo-2,5-dihydro-1H-pyrrol-1-yl)methyl)-1,3-dioxolane-4-carboxylate**, mixture of *cis*- and *trans*- isomers.

**<sup>1</sup>H NMR (400MHz, CDCl<sub>3</sub>, δ ppm):** 6.74 (s, 4H, *cis* + *trans*), 5.36 (t, J = 4.6 Hz, 1H, *trans*), 5.25 – 5.21 (m, 1H, *cis*), 4.62 (dd, J = 7.2, 5.3 Hz, 1H, *trans*), 4.54 (dd, J = 7.5, 3.9 Hz, 1H, *cis*), 4.27 (dd, J = 8.4, 7.4 Hz, 1H, *trans*), 4.20 (ddt, J = 7.2, 4.6, 2.4 Hz, 4H, *cis* + *trans*), 4.16 (dd, J = 8.2, 4.2 Hz, 1H, *cis*), 4.07 (dd, J = 8.8, 7.5 Hz, 1H, *cis*), 3.95 (dd, J = 8.5, 5.3 Hz, 1H, *trans*), 3.87 (dd, J = 3.7, 3.0 Hz, 2H, *cis*), 3.74 (d, J = 4.6 Hz, 2H, *trans*), 1.28 (td, J = 7.1, 2.8 Hz, 6H, *cis* + *trans*).

**<sup>13</sup>C NMR (100MHz, CDCl<sub>3</sub>, δ ppm):** 170.45, 170.35, 170.27, 170.20, 134.27, 134.23, 102.67, 101.97, 74.02, 73.95, 68.64, 67.97, 61.61, 61.58, 39.68, 39.52, 14.14, 14.13.

**HR-ESI-MS** C<sub>11</sub>H<sub>13</sub>NO<sub>6</sub> 255.07429 found 255.07428

**2-((2,5-dioxo-2,5-dihydro-1H-pyrrol-1-yl)methyl)-1,3-dioxolane-4-carboxylic acid, MIA5-1**



Chemical Formula: C<sub>9</sub>H<sub>9</sub>NO<sub>6</sub>  
Molecular Weight: 227,17

A solution of LiOH (14 eq., 219 mg, 9.16 mmol) in water (7 mL) was poured to a solution of ethyl 2-[(2,5-dioxo-2,5-dihydro-1H-pyrrol-1-yl)methyl]-1,3-dioxolane-4-carboxylate (1 eq., 167 mg, 0.654 mmol) and 4a (2.61 eq., 483 mg, 1.71 mmol) in THF (10 mL) and the reaction mixture was stirred for 30 minutes at r.t.. Completion of the reaction was checked by TLC, then EtOAc was added and the mixture was acidified with aqueous 3M solution of HCl to pH 2. The aqueous phase was extracted with EtOAc and the combined organic layers were washed with water and with brine, dried over Na<sub>2</sub>SO<sub>4</sub> and concentrated to give the intermediate product used in the next step without further purification.

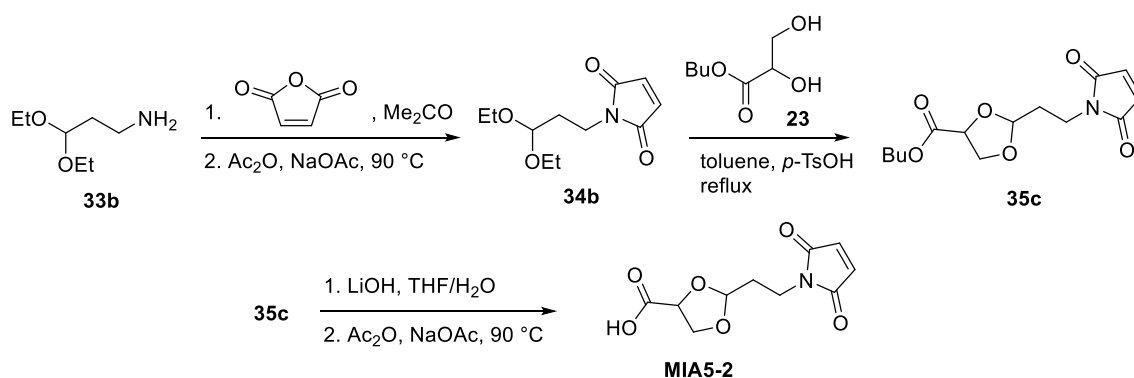
The intermediate product 2-[[{(2Z)-3-carboxyprop-2-enamido]methyl]-1,3-dioxolane-4-carboxylic acid (1 eq., 165 mg, 0.673 mmol) was treated with sodium acetate (2.4 eq., 132 mg, 1.62 mmol) in acetic anhydride (10 mL). The mixture was stirred for 15 min at r.t. and then for 2 h at 80 °C. The acetic anhydride was evaporated under reduced pressure and 5 mL of water were added. The mixture was stirred for 30 min at r.t. and then extracted with ethyl acetate. The solvent was evaporated and the resulting crude material was purified by preparative HPLC to afford 5a as a light-yellow oil in 37% overall yield (mixture of *cis*- and *trans*-isomers).

**<sup>1</sup>H NMR (400MHz, MeOH-d<sub>4</sub>, δ ppm):** 6.87 (s, 2H, *trans*), 6.85 (s, 2H, *cis*), 5.29 (s, 1H, *trans*), 5.20 (s, 1H, *cis*), 4.66 (t, J = 5.4 Hz, 1H, *trans*), 4.57 (bs, 1H, *cis*), 4.29 (t, J = 7.8 Hz, 1H, *trans*), 4.16 (bs, 1H, *cis*), 4.11 (t, J = 8.2 Hz, 1H, *cis*), 4.01 – 3.94 (m, 1H, *trans*), 3.78 (t, J = 12.7 Hz, 2H, *cis*), 3.70 (d, J = 2.7 Hz, 2H, *trans*).

**<sup>13</sup>C NMR (100MHz, MeOH-d<sub>4</sub>, δ ppm):** 170.77, 170.63, 134.13, 102.47, 101.70, 73.66, 68.23, 67.59, 39.27, 39.14.

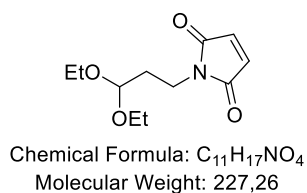
**HR-ESI-MS** C<sub>9</sub>H<sub>9</sub>NO<sub>6</sub> 227.04299 found 227.04251

### 1.6.2 Synthesis of linker MIA5-2



**Scheme EP 6.** Synthesis of linker **MIA5-2**.

#### 1-(3,3-diethoxypropyl)-1H-pyrrole-2,5-dione, 34b



Maleic anhydride (1 eq., 3.31 g, 33.7 mmol) was dissolved in acetone (23.2 mL) and 1-amino-3,3-diethoxypropane (1 eq., 4.97 g, 5.46 mL, 33.7 mmol) was added at 0 °C. The mixture was stirred for five minutes, then the solvent was evaporated to afford a crude residue. The residue was dissolved in acetic anhydride (6.8 mL) and sodium acetate (1.2 eq., 200 mg, 2.45 mmol) was added. The reaction mixture was warmed up to 90 °C and stirred for 2 h. (N.B. prolonging the reaction time leads to product decomposition). The reaction mixture was then filtrated

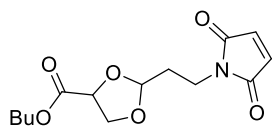
with toluene and the solvent was evaporated. The obtained dark brown liquid was purified by flash chromatography (cyclohexane, then cyclohexane to EtOAc), to give product **34b** as a yellow liquid in overall yield of 47%.

**<sup>1</sup>H NMR (400MHz, CDCl<sub>3</sub>, δ ppm):** 6.68 (s, 2H), 4.50 (t, J = 5.4 Hz, 1H), 3.60 (q, J = 6.7 Hz, 4H), 3.52 – 3.40 (m, 2H), 1.90 (q, J = 6.4 Hz, 2H), 1.17 (t, J = 7.0 Hz, 6H).

**<sup>13</sup>C NMR (100MHz, CDCl<sub>3</sub>, δ ppm):** 169.69, 133.13, 100.03, 60.25, 33.10, 31.34, 14.30.

**HR-ESI-MS** C<sub>11</sub>H<sub>17</sub>NO<sub>4</sub> 227.11576 found 227.11531

**butyl 2-(2-(2,5-dioxo-2,5-dihydro-1H-pyrrol-1-yl)ethyl)-1,3-dioxolane-4-carboxylate, 35c**



Chemical Formula: C<sub>14</sub>H<sub>19</sub>NO<sub>6</sub>  
Molecular Weight: 297,31

A solution of **34b** (1 eq., 271 mg, 1.19 mmol) and **23** (1 eq., 193 mg, 1.19 mmol) in toluene (3.97 mL) containing a catalytic amount of *p*-toluensulfonic acid monohydrate (0.2 eq., 45.4 mg, 0.238 mmol) was refluxed for 2 h. Ethanol was removed as azeotrope of toluene (b.p. of azeotrope: 76.7°C) and the reaction was monitored by TLC. After disappearing of the starting material, toluene was evaporated at reduced pressure. The residue was dissolved in ethyl acetate and washed with a saturated solution of NaHCO<sub>3</sub> and brine. The organic phase was dried over Na<sub>2</sub>SO<sub>4</sub> and the solvent was evaporated. The crude product was purified by flash chromatography (cyclohexane, then cyclohexane to EtOAc) to afford **35c** in 51% yield and ethyl 2-(2-(2,5-dioxo-2,5-dihydro-1H-pyrrol-1-yl)ethyl)-1,3-dioxolane-4-carboxylate as by-product (45%), which will be used as well for the following step.

**butyl 2-(2-(2,5-dioxo-2,5-dihydro-1H-pyrrol-1-yl)ethyl)-1,3-dioxolane-4-carboxylate, mixture of *cis*- and *trans*-isomers.**

**<sup>1</sup>H NMR (400MHz, CDCl<sub>3</sub>, δ ppm):** 6.67 (s, 4H, *cis* + *trans*), 5.12 (t, J = 3.7 Hz, 1H, *trans*), 5.05 (t, J = 4.5 Hz, 1H, *cis*), 4.56 (t, J = 6.9 Hz, 1H, *trans*), 4.51 (dd, J = 7.6, 3.5 Hz, 1H, *cis*), 4.28 (t, J = 8.0 Hz, 1H, *trans*), 4.16 (t, J = 6.6 Hz, 4H, *cis* + *trans* + 1H, *cis*), 4.02 (t, J = 8.1 Hz, 1H, *cis*), 3.87 – 3.79 (m, 1H, *trans*), 3.77 – 3.66 (m, J = 19.1, 6.7 Hz, 4H, *cis* + *trans*), 2.15 – 1.99 (m, 4H, *cis* + *trans*), 1.69 – 1.59 (m, 4H, *cis* + *trans*), 1.38 (dt, J = 14.9, 7.6 Hz, 4H, *cis* + *trans*), 0.93 (t, J = 7.3 Hz, 6H, *cis* + *trans*).

**<sup>13</sup>C NMR (100MHz, CDCl<sub>3</sub>, δ ppm):** 171.17, 170.63, 134.17, 134.15, 104.58, 103.90, 73.85, 73.78, 68.66, 68.13, 65.35, 65.29, 33.03, 32.48, 32.32, 31.44, 30.57, 30.55, 19.04, 13.65.

**HR-ESI-MS** C<sub>14</sub>H<sub>19</sub>NO<sub>6</sub> 297.12124 found 297.12116

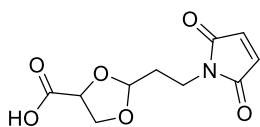


**ethyl 2-(2-(2,5-dioxo-2,5-dihydro-1H-pyrrol-1-yl)ethyl)-1,3-dioxolane-4-carboxylate**, mixture of *cis*- and *trans*-isomers.

**<sup>1</sup>H NMR (400MHz, CDCl<sub>3</sub>, δ ppm):** 6.67 (s, 4H, *cis* + *trans*), 5.11 (t, J = 3.7 Hz, 1H, *trans*), 5.04 (t, J = 4.3 Hz, 1H, *cis*), 4.56 – 4.52 (m, 1H, *trans*), 4.50 (dd, J = 7.5, 3.6 Hz, 1H, *cis*), 4.30 – 4.24 (m, 1H, *trans*), 4.21 (dd, J = 14.4, 7.3 Hz, 4H, *cis* + *trans*), 4.18 – 4.13 (m, 1H, *cis*), 4.01 (t, J = 8.1 Hz, 1H, *cis*), 3.85 – 3.79 (m, 1H, *trans*), 3.73 (dt, J = 6.7, 2.0 Hz, 2H, *cis*), 3.69 (t, J = 6.7 Hz, 2H, *trans*), 2.15 – 1.98 (m, 4H, *cis* + *trans*), 1.28 (t, J = 7.1 Hz, 6H, *cis* + *trans*).

**<sup>13</sup>C NMR (100MHz, CDCl<sub>3</sub>, δ ppm):** 171.08, 170.65, 170.58, 134.15, 104.58, 103.89, 73.83, 73.74, 68.63, 68.09, 61.49, 61.44, 33.00, 32.47, 32.27, 31.43, 14.17, 14.13.

**HR-ESI-MS** C<sub>12</sub>H<sub>15</sub>NO<sub>6</sub> 269.08994 found 269.08979

**2-(2-(2,5-dioxo-2,5-dihydro-1H-pyrrol-1-yl)ethyl)-1,3-dioxolane-4-carboxylic acid, MIA5-2**

Chemical Formula: C<sub>10</sub>H<sub>11</sub>NO<sub>6</sub>  
Molecular Weight: 241,20

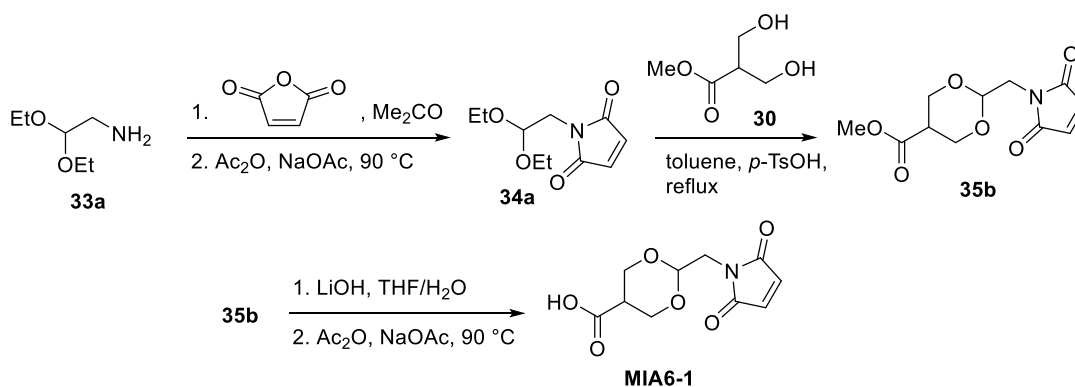
A solution of LiOH (2.5 eq., 50.7 mg, 0.0355 mL, 2.12 mmol) in water (1.41 mL) was poured to a solution of **35c** and ethyl 2-(2-(2,5-dioxo-2,5-dihydro-1H-pyrrol-1-yl)ethyl)-1,3-dioxolane-4-carboxylate (in total 252 mg, 1 eq.) in THF (1.41 mL) and the reaction mixture was stirred at r.t. for 30 minutes. Completion of the reaction was checked by TLC, then EtOAc was added and the mixture was acidified with aqueous 3M solution of HCl to pH 2. The aqueous phase was extracted with EtOAc and the combined organic layers were washed with water and with brine, dried over Na<sub>2</sub>SO<sub>4</sub> and concentrated to give the intermediate product used in the next step without further purification.

**2-{2-[(2Z)-3-carboxyprop-2-enamido]ethyl}-1,3-dioxolane-4-carboxylic acid** (1 eq., 130 mg, 0.502 mmol) was dissolved in acetic anhydride (6.78 mL) and sodium acetate (2.4 eq., 98.7 mg, 1.2 mmol) was added. The reaction mixture was stirred at 90 °C for 2 h and controlled by TLC. Acetic anhydride was evaporated under reduced pressure and 5 mL of water was added to the residue. The mixture was stirred at r.t. for 30 min and then extracted with ethyl acetate. After solvent evaporation the resulting crude material was purified by preparative HPLC to afford **MIA5-2** as a light-yellow oil in 54% overall yield (mixture of *cis* and *trans*-isomers).

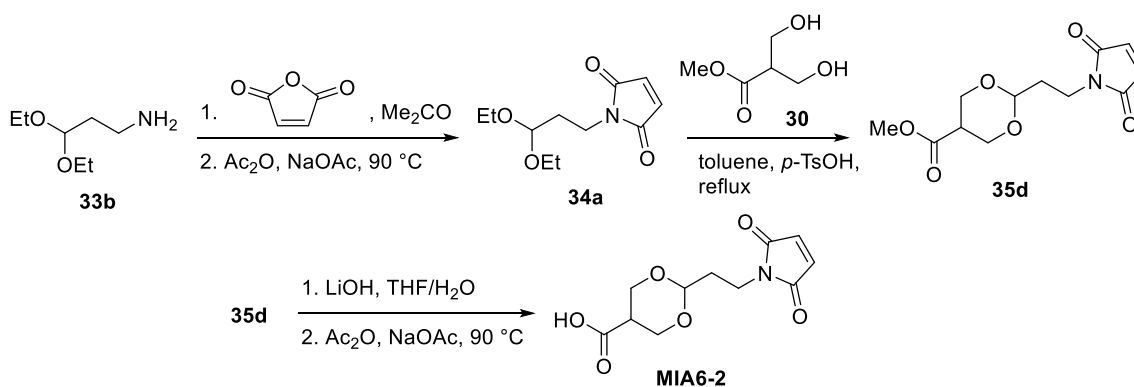
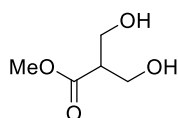
**<sup>1</sup>H NMR (400MHz, MeOD-d<sub>4</sub>, δ ppm):** 6.81 (s, 4H, *cis* + *trans*), 5.08 (s, 1H, *trans*), 5.02 (s, 1H, *cis*), 4.57 (t, J = 7.6 Hz, 1H, *trans*), 4.53 (d, J = 3.8 Hz, 1H, *cis*), 4.30 (t, J = 8.0 Hz, 1H, *trans*), 4.15 (d, J = 8.0 Hz, 1H, *cis*), 4.06 (t, J = 8.1 Hz, 1H, *cis*), 3.84 (t, J = 7.2 Hz, 1H, *trans*), 3.77 – 3.63 (m, 4H, *cis* + *trans*), 2.09 – 1.96 (m, 4H, *cis* + *trans*).

**<sup>13</sup>C NMR (100MHz, MeOD-d<sub>4</sub>, δ ppm):** 173.26, 172.74, 171.07, 134.08, 134.05, 104.26, 103.62, 73.36, 68.22, 67.80, 32.50, 32.00, 31.81, 31.08.

**HR-ESI-MS** C<sub>10</sub>H<sub>11</sub>NO<sub>6</sub> 241.05864 found 241.05785

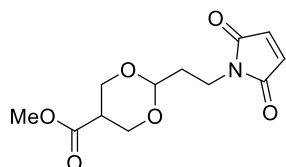
1.6.3 Synthesis of linker **MIA6-1**Scheme EP 7. Synthesis of linker **MIA6-1**.

The linker **MIA6-1** was synthesized according to the reported procedures.<sup>44</sup>

1.6.4 Synthesis of linker **MIA6-2**Scheme EP 8. Synthesis of linker **MIA6-2**.methyl 3-hydroxy-2-(hydroxymethyl)propanoate, **30**

Chemical Formula:  $\text{C}_5\text{H}_{10}\text{O}_4$   
Molecular Weight: 134,13

Molecule **30** was synthesized according to the reported procedures.<sup>44</sup>

**methyl 2-(2-(2,5-dioxo-2,5-dihydro-1H-pyrrol-1-yl)ethyl)-1,3-dioxane-5-carboxylate, 35d**

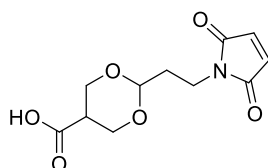
Chemical Formula: C<sub>12</sub>H<sub>15</sub>NO<sub>6</sub>  
Molecular Weight: 269,25

A solution of **34b** (1 eq., 500 mg, 2.2 mmol) and **30** (0.895 eq., 264 mg, 1.97 mmol) in toluene (7.33 mL) containing catalytic amount of *p*-toluensulfonic acid monohydrate (0.2 eq., 83.7 mg, 0.44 mmol) was refluxed for 2 h. Ethanol was removed as azeotrope of toluene (b.p. of azeotrope: 76.7°C). After the reaction was complete, toluene was evaporated and the residue was dissolved in EtOAc and washed with a saturated solution of NaHCO<sub>3</sub> and with brine. The organic phase was dried over Na<sub>2</sub>SO<sub>4</sub>, filtrated and the solvent was evaporated at reduced pressure. The crude product was purified by flash chromatography (cyclohexane, then cyclohexane to EtOAc) to give **35d** (362 mg, 1.34 mmol, 68 %) as a yellow liquid (mixture of *cis* and *trans*-isomers).

**<sup>1</sup>H NMR (400MHz, CDCl<sub>3</sub>, δ ppm):** 6.67 (d, J = 3.6 Hz, 2H, *cis* + *trans*), 4.59 – 4.51 (m, 1H, *cis*), 4.49 (t, J = 4.7 Hz, 1H, *trans*), 4.24 (dd, J = 11.6, 4.6 Hz, 2H, *trans*), 3.84 (d, J = 10.3 Hz, 1H, *cis*), 3.79 (s, 1H, *cis*), 3.74 – 3.67 (m, 2H, *trans*), 3.68 – 3.57 (m, 5H, *cis* + *trans*), 3.03 – 2.88 (m, 1H, *trans*), 2.27 (s, 1H, *cis*), 1.94 – 1.82 (m, 2H, *cis* + *trans*).

**<sup>13</sup>C NMR (100MHz, CDCl<sub>3</sub>, δ ppm):** 170.68, 170.24, 134.16, 134.13, 100.87, 100.15, 67.50, 66.83, 52.35, 51.83, 39.90, 39.77, 33.37, 33.20, 33.16, 33.08.

**HR-ESI-MS** C<sub>12</sub>H<sub>15</sub>NO<sub>6</sub> 269.08994 found 269.09001

**2-(2-(2,5-dioxo-2,5-dihydro-1H-pyrrol-1-yl)ethyl)-1,3-dioxane-5-carboxylic acid, MIA6-2**

Chemical Formula: C<sub>11</sub>H<sub>13</sub>NO<sub>6</sub>  
Molecular Weight: 255,23

Using the similar procedure as for **MIA5-1**, the linker **MIA6-2** was synthesized as a light-yellow oil in 79% overall yield (mixture of *cis* and *trans*-isomers).

**<sup>1</sup>H NMR (400MHz, MeOD-d<sub>4</sub>, δ ppm):** 6.75 (s, 2H, *trans*), 6.74 (s, 2H, *cis*), 4.57 (t, J = 5.0 Hz, 1H, *cis*), 4.48 (t, J = 4.8 Hz, 1H, *trans*), 4.41 (d, J = 10.7 Hz, 2H, *cis*), 4.17 (dd, J = 11.8, 4.8 Hz, 2H, *trans*), 3.87 – 3.81 (m, 2H, *cis*), 3.67 (t, J = 11.6 Hz, 2H, *trans*), 3.56 (dt, J = 13.9, 6.9 Hz, 4H, *cis* + *trans*),

2.90 – 2.81 (m, 1H, *trans*), 2.32 – 2.29 (m, 1H, *cis*), 1.80 (d,  $J = 4.9$  Hz, 2H, *trans*), 1.76 (td,  $J = 6.9$ , 5.0 Hz, 2H, *cis*).

**$^{13}\text{C}$  NMR (100MHz, MeOD- $d_4$ ,  $\delta$  ppm):** 171.07, 134.06, 134.03, 100.59, 100.03, 67.38, 66.63, 39.66, 39.04, 33.01, 32.66, 32.60.

**HR-ESI-MS**  $\text{C}_{11}\text{H}_{13}\text{NO}_6$  255.07429 found 255.071341

## 1.7 SYNTHESIS OF FRET PROBES

### **1.7.1 General procedures for synthesis of FRET probes**

#### **Procedure A**

Starting acid (1 eq., 0.1 M in dry DMSO) was added to a solution of BEP (1 eq., 0.1 M in dry DMSO) and DIPEA (5 eq.) and stirred for few minutes, then **TAMRA-NH<sub>2</sub>** (0.95 eq., 0.1 M in dry DMSO) was added. The mixture was stirred for 15 minutes. Amide coupling was monitored by LC-MS. **BHQ-2-SH** (1.1 eq., 0.007 M in dry DMSO) was added to the mixture and let to stir until reaction was complete (monitored by LC-MS).

The reaction mixture was then purified by preparative HPLC to give the product as a violet solid. The aqueous mobile phase used in the purification was neutral and contained ammonium formate (0.025 mM).

#### **Procedure B**

A solution of  $\text{CuSO}_4$  (1 M, 1 eq.), tris(benzyltriazolylmethyl)amine (TBTA, 1 M, 2 eq.) and sodium ascorbate (1 M, 5 eq.) in water was prepared and added to a solution of the starting acid (1 eq.) and **BHQ-2-N<sub>3</sub>** (1.2 eq.) in DMF. The mixture was let to stir at room temperature until cycloaddition was complete (LC-MS check). The product was then quickly extracted with DCM to get rid of the copper and the ascorbate salts. The organic phase was concentrated under vacuum and the **BHQ-ACID** adduct was redissolved in DMF. BEP (1.2 eq.), **TAMRA-NH<sub>2</sub>** (1.1 eq.) and DIPEA (1.1 eq.) were added and the solution was stirred at r.t. for 15 min. Reaction was monitored by LC-MS. The reaction mixture was then purified by preparative HPLC to give the product as a violet solid. The aqueous mobile phase used in the purification was neutral and contained ammonium formate (0.025 mM).

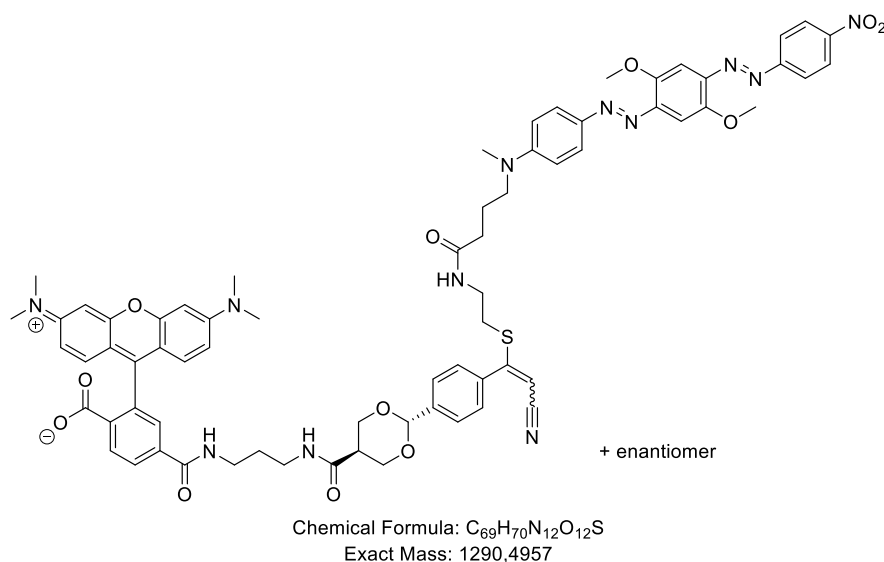
#### **Procedure C**

Solutions of starting acid (1 eq., 10 mg/mL in dry DMSO) and DIPEA (1 eq., 0.1 M in dry ACN) were mixed under argon at room temperature, after few minutes  $\text{N,N}'$ -disuccinimidyl carbonate (1.2 eq.) was added and the reaction mixture was stirred for 1 hour. Then **TAMRA-NH<sub>2</sub>** (1.05 eq., 0.1 M in dry ACN) was added and the reaction was let to stir, the formation of TAMRA adduct was checked with LC-MS. If after 1 hour, no product was detected, 5 eq. of DIPEA were added (to neutralize TFA molecules coming from HPLC purification of **TAMRA-NH<sub>2</sub>**). When the intermediary product was formed, **BHQ-2-SH** (1 eq., 0.025 M in dry DMSO) and DIPEA (5 eq., 0.1 M in dry ACN) were added and let to stir until formation of the product was

detected with LC-MS. The reaction mixture was then purified by preparative HPLC to give the product as a violet solid.

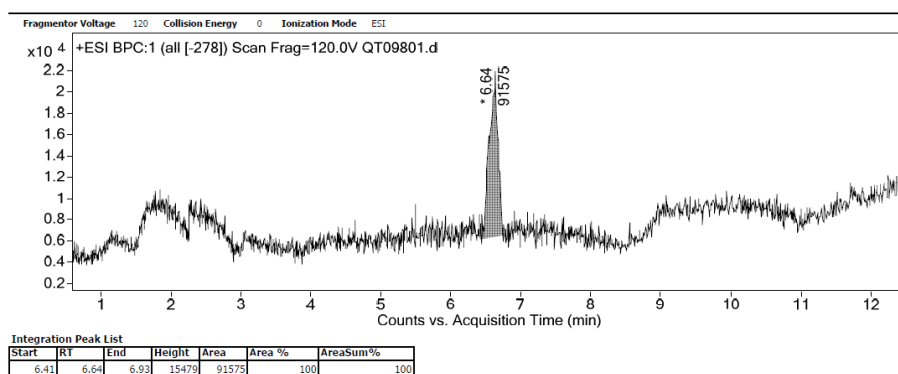
### 1.7.2 F-APN6

**4-((3-((2*r*,5*r*)-2-(4-(2-cyano-1-((2-(4-((4-((*E*)-(2,5-dimethoxy-4-((*E*)-(4-nitrophenyl)diazenyl)phenyl)diazenyl)phenyl)(methylamino)butanamido)ethyl)thio)vi-nyl)phenyl)-1,3-dioxane-5-carboxamido)propyl)carbonyl)-2-(6-(dimethylamino)-3-(dimethyliminio)-3*H*-xanthen-9-yl)benzoate**  
and enantiomer



**F-APN6** was provided by Dr. Igor Dovgan, HR-ESI-MS chromatogram is shown below.

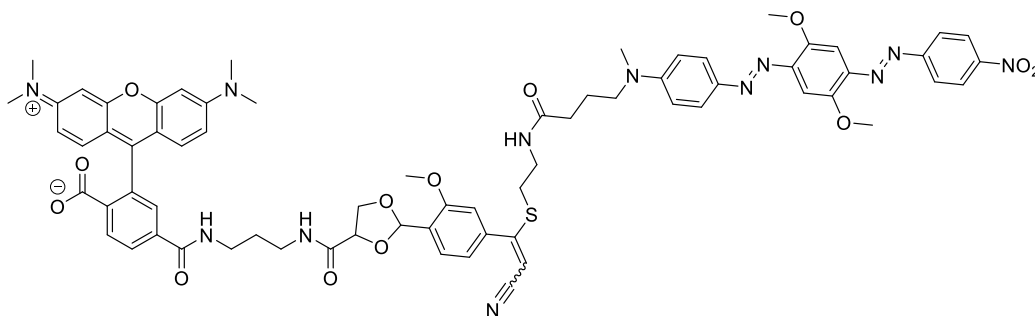
**HR-ESI-MS** C<sub>69</sub>H<sub>70</sub>N<sub>12</sub>O<sub>12</sub>S 1290.49569 found 1290.49306



**Figure EP 2.** HR-ESI-MS chromatogram of **F-APN6**.

## 1.7.3 F-APNMS

4-((3-(2-(4-(2-cyano-1-((2-(4-((4-((E)-(2,5-dimethoxy-4-((E)-(4-nitrophenyl)diazenyl)phenyl)diazenyl)phenyl)(methyl)amino)butanamido)ethyl)thio)vinyl)-2-methoxyphenyl)-1,3-dioxolane-4-carboxamido)propyl)carbamoyl)-2-(6-(dimethylamino)-3-(dimethyliminio)-3H-xanthen-9-yl)benzoate



Chemical Formula: C<sub>69</sub>H<sub>70</sub>N<sub>12</sub>O<sub>13</sub>S  
Exact Mass: 1306,4906

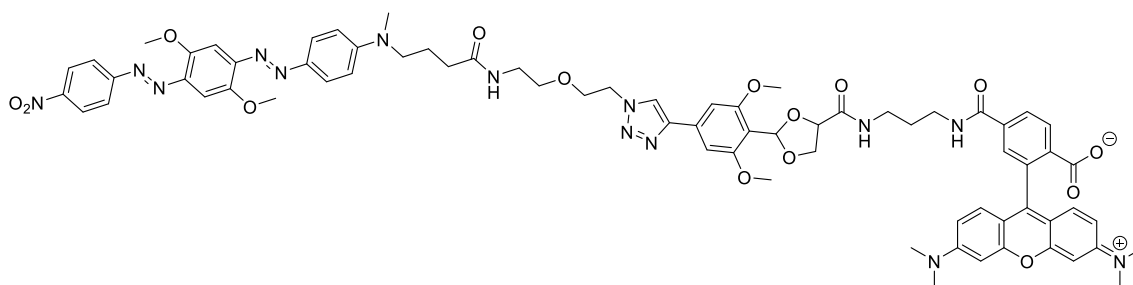
**Procedure A, Yield 29%**

**<sup>1</sup>H NMR (400 MHz, DMSO-d<sub>6</sub>, δ ppm):** 8.83 (d, *J* = 6.9 Hz, 1H), 8.46 (d, *J* = 1.8 Hz, 1H), 8.45 – 8.42 (m, 1H), 8.23 (dd, *J* = 7.9, 1.6 Hz, 1H), 8.12 – 8.04 (m, 2H), 8.01 (dt, *J* = 11.0, 5.6 Hz, 1H), 7.89 (t, *J* = 6.0 Hz, 1H), 7.83 – 7.79 (m, 1H), 7.79 – 7.75 (m, 1H), 7.56 (d, *J* = 8.2 Hz, 1H), 7.45 (s, 1H), 7.39 (d, *J* = 1.8 Hz, 1H), 7.33 (d, *J* = 8.0 Hz, 1H), 7.22 – 7.14 (m, 2H), 6.86 (dd, *J* = 9.2, 6.9 Hz, 2H), 6.54 – 6.44 (m, 5H), 6.12 (d, *J* = 2.8 Hz, 1H), 6.11 (s, 1H), 4.68 (t, *J* = 6.5 Hz, 1H), 4.61 (dd, *J* = 7.6, 4.7 Hz, 1H), 4.31 (t, *J* = 7.8 Hz, 1H), 4.18 (dd, *J* = 13.0, 5.0 Hz, 1H), 4.16 – 4.11 (m, 1H), 4.01 (s, 3H), 3.95 (s, 3H), 3.89 (s, 3H), 3.35 (s, 12H), 3.24 (q, *J* = 6.5 Hz, 2H), 3.16 (dt, *J* = 13.6, 6.7 Hz, 3H), 3.04 (d, *J* = 7.2 Hz, 3H), 2.94 (s, 9H), 2.79 (t, *J* = 6.7 Hz, 2H), 2.13 (q, *J* = 7.4 Hz, 2H), 1.77 (q, *J* = 7.7 Hz, 2H), 1.73 – 1.67 (m, 2H), 1.24 (s, 1H).

**HR-ESI-MS** C<sub>69</sub>H<sub>70</sub>N<sub>12</sub>O<sub>13</sub>S 1306.4906 found 1306.48834

**1.7.4 F-A2M5**

**4-((3-(2-(4-(1-(2-(2-(4-((E)-(2,5-dimethoxy-4-((E)-(4-nitrophenyl)diazenyl)phenyl)diazenyl)phenyl)(methyl)amino)butanamido)ethoxy)ethyl)-1H-1,2,3-triazol-4-yl)-2,6-dimethoxyphenyl)-1,3-dioxolane-4-carboxamido)propyl)carbamoyl)-2-(6-(dimethylamino)-3-(dimethyliminio)-3H-xanthen-9-yl)benzoate**



Chemical Formula:  $C_{71}H_{76}N_{14}O_{15}$   
Exact Mass: 1364,5615

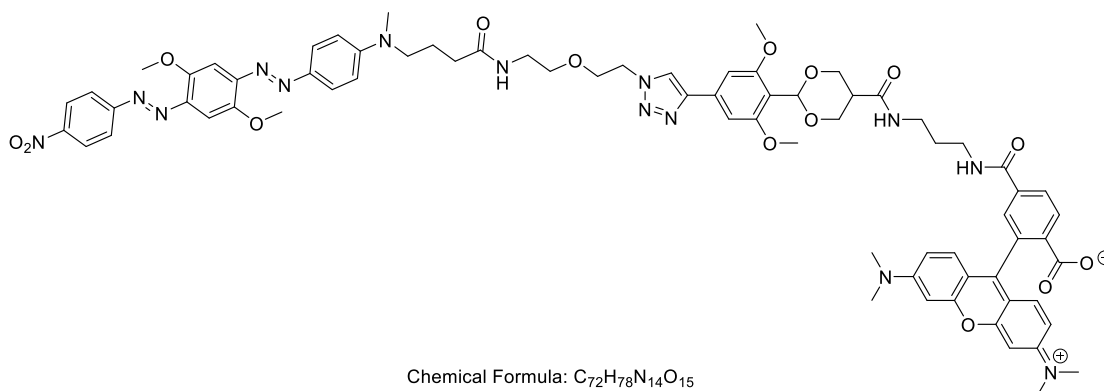
**Procedure B, Yield >99% (LC-MS)**

**$^1H$  NMR (400 MHz, DMSO- $d_6$ ,  $\delta$  ppm):** 8.83 (d,  $J$  = 6.9 Hz, 1H), 8.46 (d,  $J$  = 1.8 Hz, 1H), 8.44 (s,  $J$  = 2.1 Hz, 1H), 8.23 (dd,  $J$  = 7.9, 1.6 Hz, 1H), 8.09 – 8.05 (m, 2H), 8.01 (dt,  $J$  = 11.0, 5.6 Hz, 1H), 7.89 (t,  $J$  = 6.0 Hz, 1H), 7.83 – 7.79 (m, 1H), 7.78 (d,  $J$  = 7.9 Hz, 1H), 7.56 (d,  $J$  = 8.2 Hz, 1H), 7.45 (s, 1H), 7.39 (d,  $J$  = 1.8 Hz, 2H), 7.33 (d,  $J$  = 8.0 Hz, 1H), 7.20 – 7.15 (m, 2H), 6.86 (dd,  $J$  = 9.2, 6.9 Hz, 2H), 6.49 (ddd,  $J$  = 11.4, 10.6, 5.7 Hz, 5H), 6.12 (d,  $J$  = 2.8 Hz, 1H), 6.11 (s, 1H), 4.68 (t,  $J$  = 6.5 Hz, 1H), 4.61 (dd,  $J$  = 7.6, 4.7 Hz, 1H), 4.31 (t,  $J$  = 7.8 Hz, 1H), 4.19 (t,  $J$  = 8.0 Hz, 1H), 4.15 (dd,  $J$  = 8.2, 4.8 Hz, 1H), 4.01 (s, 3H), 3.95 (s, 3H), 3.89 (s, 3H), 3.35 (s, 12H), 3.24 (dd,  $J$  = 12.8, 6.5 Hz, 1H), 3.16 (dt,  $J$  = 13.5, 6.6 Hz, 2H), 3.04 (d,  $J$  = 7.2 Hz, 2H), 2.94 (s, 6H), 2.79 (t,  $J$  = 6.7 Hz, 3H), 2.13 (q,  $J$  = 7.4 Hz, 2H), 1.81 – 1.74 (m, 1H), 1.71 (dd,  $J$  = 12.8, 6.3 Hz, 1H), 1.24 (s, 1H).

**HR-ESI-MS**  $C_{71}H_{76}N_{14}O_{15}$  1364.5615 found 1364.5584

## 1.7.5 F-A2M6

4-((3-(2-(4-(1-(2-(2-(4-((E)-(2,5-dimethoxy-4-((E)-(4-nitrophenyl)diazenyl)phenyl)diazenyl)phenyl)(methyl)amino)butanamido)ethoxy)ethyl)-1H-1,2,3-triazol-4-yl)-2,6-dimethoxyphenyl)-1,3-dioxane-5-carboxamido)propyl)carbamoyl)-2-(6-(dimethylamino)-3-(dimethyliminio)-3H-xanthen-9-yl)benzoate



**Procedure B, Yield >99% (LC-MS)**

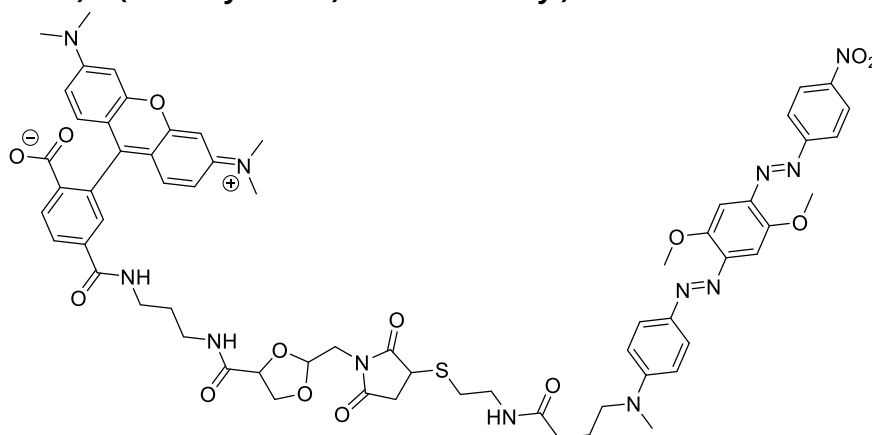
**$^1\text{H NMR}$  (400 MHz, DMSO- $d_6$ ,  $\delta$  ppm):** 8.83 (s, 1H), 8.46 (t,  $J = 2.3$  Hz, 1H), 8.45 – 8.43 (m, 2H), 8.23 (dd,  $J = 7.9, 1.6$  Hz, 1H), 8.09 – 8.05 (m, 2H), 8.01 (dt,  $J = 11.0, 5.6$  Hz, 1H), 7.89 (t,  $J = 6.0$  Hz, 1H), 7.84 – 7.76 (m, 2H), 7.56 (d,  $J = 8.2$  Hz, 1H), 7.45 (s, 1H), 7.39 (d,  $J = 1.8$  Hz, 1H), 7.33 (d,  $J = 8.0$  Hz, 1H), 7.21 – 7.15 (m, 2H), 6.86 (dd,  $J = 9.2, 6.9$  Hz, 2H), 6.49 (ddd,  $J = 11.4, 10.6, 5.7$  Hz, 5H), 6.12 (d,  $J = 2.8$  Hz, 1H), 6.11 (s, 1H), 4.68 (t,  $J = 6.5$  Hz, 1H), 4.61 (dd,  $J = 7.6, 4.7$  Hz, 1H), 4.31 (t,  $J = 7.8$  Hz, 1H), 4.19 (t,  $J = 8.0$  Hz, 1H), 4.17 – 4.11 (m, 1H), 4.01 (s, 3H), 3.95 (s, 3H), 3.89 (s, 3H), 3.35 (s, 12H), 3.24 (dd,  $J = 12.8, 6.5$  Hz, 2H), 3.16 (dt,  $J = 13.5, 6.6$  Hz, 3H), 3.04 (d,  $J = 7.2$  Hz, 2H), 2.94 (s, 6H), 2.79 (t,  $J = 6.7$  Hz, 2H), 2.13 (q,  $J = 7.4$  Hz, 2H), 1.81 – 1.74 (m, 2H), 1.71 (dd,  $J = 12.8, 6.3$  Hz, 2H), 1.24 (s, 1H).

**HR-ESI-MS**  $C_{72}H_{78}N_{14}O_{15}$  1378.5771 found 1378.5746



**1.7.6 F-MIA5-1**

**4-((3-(2-((3-((2-4-((4-((E)-(2,5-dimethoxy-4-((E)-(4-nitrophenyl)diazenyl)phenyl)diazenyl)phenyl) (methylamino)butanamido)ethyl)thio)-2,5-dioxopyrrolidin-1-yl)methyl)-1,3-dioxolane-4-carboxamido)propyl)carbamoyl)-2-(6-(dimethylamino)-3-(dimethyliminio)-3H-xanthen-9-yl)benzoate**



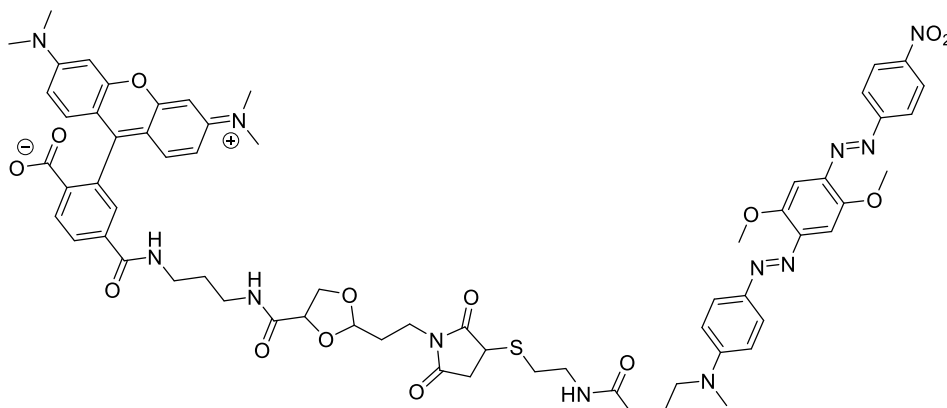
**Procedure C, Yield 55%**

**<sup>1</sup>H NMR (400 MHz, DMSO-d<sub>6</sub>, δ ppm):** 8.78 (s, 1H), 8.44 (d, J = 8.1 Hz, 2H), 8.27 (d, J = 17.9 Hz, 2H), 8.06 (d, J = 7.7 Hz, 3H), 7.92 (s, 1H), 7.80 (d, J = 8.5 Hz, 2H), 7.39 (d, J = 26.4 Hz, 2H), 7.02 (s, 3H), 6.96 – 6.82 (m, 4H), 5.28 (s, 1H), 5.07 (t, 1H), 4.51 – 4.40 (m, 2H), 4.18 – 4.11 (m, 2H), 4.11 – 4.02 (m, 3H), 3.99 (s, 3H), 3.93 (s, 3H), 3.24 (s, 12H), 3.06 (s, 3H), 2.17 (s, 2H), 1.86 – 1.77 (m, 1H), 1.77 – 1.62 (m, 1H), 1.29 – 1.21 (m, 1H).

**HR-ESI-MS** C<sub>64</sub>H<sub>68</sub>N<sub>12</sub>O<sub>14</sub>S 1260.46987 found 1260.4714

**1.7.7 F-MIA5-2**

**4-((3-(2-(2-(3-((2-4-((4-((E)-(2,5-dimethoxy-4-((E)-(4-nitrophenyl)diazenyl)phenyl)diazenyl)phenyl) (methylamino)butanamido)ethyl)thio)-2,5-dioxopyrrolidin-1-yl)ethyl)-1,3-dioxolane-4-carboxamido)propyl)carbamoyl)-2-(6-(dimethylamino)-3-(dimethyliminio)-3H-xanthen-9-yl) benzoate**



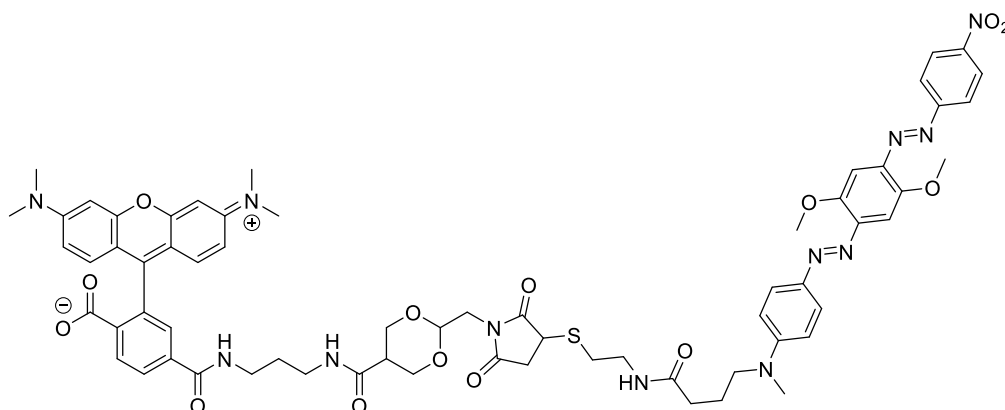
**Procedure C, Yield: 63%**

**<sup>1</sup>H NMR (400 MHz, DMSO-d<sub>6</sub>, δ ppm):** 8.77 (s, 1H), 8.44 (d, J = 8.8 Hz, 2H), 8.25 (t, J = 12.4 Hz, 2H), 8.06 (d, J = 8.8 Hz, 2H), 7.91 (s, 1H), 7.80 (d, J = 8.8 Hz, 2H), 7.39 (d, J = 26.2 Hz, 2H), 7.02 (s, 3H), 6.95 – 6.83 (m, 3H), 4.92 (d, J = 12.3 Hz, 1H), 4.46 – 4.33 (m, 1H), 4.23 – 4.16 (m, 1H), 3.99 (s, 3H), 3.93 (s, 3H), 3.69 – 3.62 (m, 1H), 3.24 (s, 12H), 3.17 (d, J = 6.7 Hz, 3H), 3.06 (s, 3H), 2.93 – 2.80 (m, 1H), 2.77 – 2.70 (m, 1H), 2.16 (t, J = 7.1 Hz, 2H), 1.96 – 1.87 (m, J = 22.0 Hz, 1H), 1.86 – 1.75 (m, 2H), 1.74 – 1.62 (m, 2H), 1.24 (s, 2H).

**HR-ESI-MS** C<sub>65</sub>H<sub>70</sub>N<sub>12</sub>O<sub>14</sub>S, 1274.48552; found 1274.48542.

**1.7.8 F-MIA6-1**

**4-((3-(2-((3-((2-(4-((E)-(2,5-dimethoxy-4-((E)-(4-nitrophenyl)diazenyl)phenyl)diaz-enyl)phenyl)(methyl)amino)butanamido)ethyl)thio)-2,5-dioxopyrrolidin-1-yl)methyl)-1,3-dioxane-5-carboxamido)propyl)carbamoyl)-2-(6-(dimethylamino)-3-(dimethyliminio)-3H-xanthen-9-yl) benzoate**

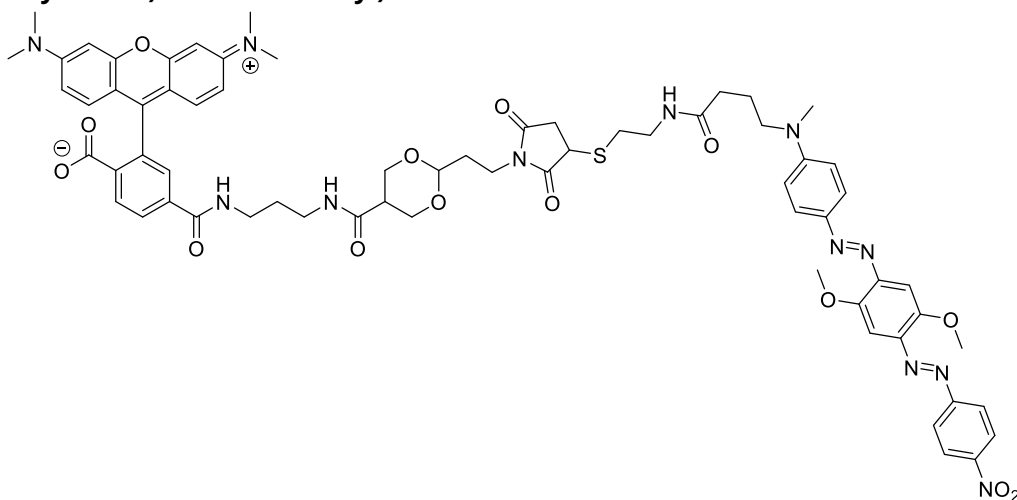
**Procedure C, Yield: 76%**

**<sup>1</sup>H NMR (400MHz, DMSO-d<sub>6</sub>, δ ppm):** 8.81 (t, J=5.3 Hz, 1 H), 8.43 (d, J=8.8 Hz, 2 H), 8.29 - 8.33 (m, 1 H), 8.24 - 8.29 (m, 1 H), 8.00 - 8.12 (m, 3 H), 7.95 (s, 1 H), 7.80 (d, J=9.0 Hz, 2 H), 7.72 (t, J=5.4 Hz, 1 H), 7.42 (s, 1 H), 7.36 (s, 1 H), 7.03 (s, 4 H), 6.91 (s, 2 H), 6.87 (d, J=9.0 Hz, 2 H), 4.75 (t, J=5.1 Hz, 1 H), 4.29 (d, J=11.5 Hz, 2 H), 4.02 - 4.07 (m, 1 H), 3.99 (s, 3 H), 3.94 (s, 3 H), 3.81-3.84 (m, 2H), 3.44 - 3.51 (m, 4 H), 3.30 - 3.36 (m, 4 H), 3.24 (s, 12H), 3.20 (d, J=8.3 Hz, 2 H), 3.07 (s, 3 H), 2.84 (dt, J=13.0, 6.4 Hz, 1 H), 2.71 (dt, J=13.2, 6.7 Hz, 1 H), 2.55-2.57 (m, 2H), 2.34 (br.s, 1H), 2.18 (d, J=5.5 Hz, 2 H), 1.76 - 1.86 (m, 2 H), 1.66 - 1.76 (m, 2 H)

**HR-ESI-MS:** C<sub>65</sub>H<sub>70</sub>N<sub>12</sub>O<sub>14</sub>S, 1274.48552; found 1274.48491.

## 1.7.9 F-MIA6-2

4-((3-(2-(2-(3-((2-(4-((E)-(2,5-dimethoxy-4-((E)-(4-nitrophenyl)diazenyl)phenyl) diazenyl)phenyl)(methyl)amino)butanamido)ethyl)thio)-2,5-dioxopyrrolidin-1-yl)ethyl)-1,3-dioxane-5-carboxamido)propyl)carbonyl)-2-(6-(dimethylamino)-3-(dimethyliminio)-3H-xanthen-9-yl)benzoate



**Procedure C, Yield:** 71%

**<sup>1</sup>H NMR (400MHz, DMSO-d<sub>6</sub>, δ ppm):** 8.75 (s, 2H), 8.44 (d, J = 8.7 Hz, 2H), 8.27 (d, J = 15.6 Hz, 2H), 8.06 (d, J = 8.4 Hz, 3H), 7.91 (s, 1H), 7.80 (d, J = 9.1 Hz, 2H), 7.64 (s, 1H), 7.39 (d, J = 26.4 Hz, 2H), 7.02 (s, 3H), 6.94 – 6.83 (m, 4H), 4.56 (s, 1H), 4.47 (s, 1H), 4.28 (d, J = 11.7 Hz, 2H), 3.99 (s, 4H), 3.93 (s, 3H), 3.80 (d, J = 10.4 Hz, 2H), 3.63 (t, J = 11.0 Hz, 1H), 3.24 (s, 9H), 3.07 (s, 4H), 2.86 (dd, J = 13.2, 6.7 Hz, 2H), 2.72 (dd, J = 13.3, 6.4 Hz, 2H), 2.21 – 2.12 (m, 3H), 1.80 (s, 3H), 1.68 (s, 5H), 1.24 (s, 1H).

**HR-ESI-MS** C<sub>66</sub>H<sub>72</sub>N<sub>12</sub>O<sub>14</sub>S, 1288.50117; found 1288.49841

## 1.8 SYNTHESIS OF SUPPORTED ACIDS AND SOLID CATALISTS

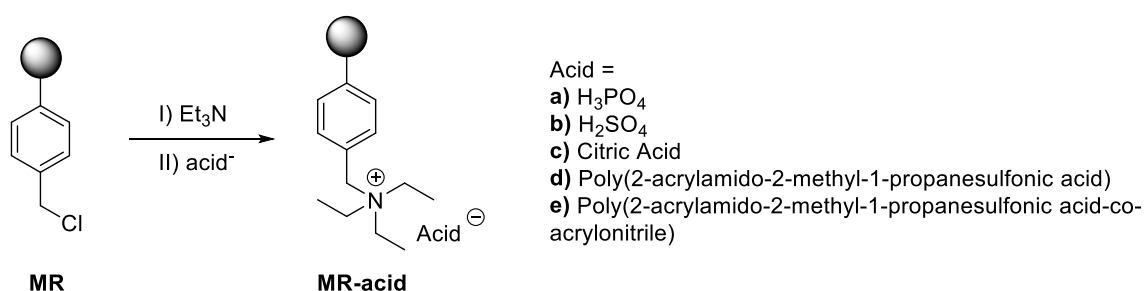
### 1.8.1 Silica supported acids

Silica supported acids were synthesized according to procedures present in literature.

Catalyst	Preparation	References
PMA/SiO <sub>2</sub>	PMA (H <sub>3</sub> PMO <sub>12</sub> O <sub>40</sub> , 229 mg) was added to a slurry solution of silica (2 g) in MeOH (40 mL) and stirred for 6 hours at room temperature, after which MeOH was evaporated under vacuum.	Kumar (2008) <sup>69</sup>
H <sub>2</sub> SO <sub>4</sub> /SiO <sub>2</sub>	100 mL two neck RBF was charged with 10 g of silica and equipped with a dropping funnel and a way out for HCl (to a flask filled with water). The dropping funnel was charged with 3 mL of ClSO <sub>3</sub> H, which was dropped to the stirring silica. The mixture was let to stir for 3 hours.	Mirjalili (2002) <sup>70</sup> Mirjalili (2004) <sup>71</sup>
HClO <sub>4</sub> /SiO <sub>2</sub>	To a suspension of silica gel (3 g, 230–400 mesh) in Et <sub>2</sub> O (10 mL), was added HClO <sub>4</sub> (125 mg, 1.25 mmol, 178 μL of a 70% aq. solution of HClO <sub>4</sub> ) and the mixture was stirred magnetically for 30 min at room temperature. The Et <sub>2</sub> O was removed under reduced pressure (rotary evaporator) and the residue heated at 100 °C for 72 h under vacuum to afford HClO <sub>4</sub> -SiO <sub>2</sub> (0.42 mmol/g) as a free-flowing powder.	Agarwal (2005) <sup>72</sup> Agnihotri (2006) <sup>73</sup> Kumar (2007) <sup>74</sup>
BF <sub>3</sub> /SiO <sub>2</sub>	A mixture of BF <sub>3</sub> .OEt <sub>2</sub> (8.4 mmol) and silica gel (1 g) in MeOH (10 mL) was prepared and stirred for 1 h at room temperature. The generated suspension was then filtered and dried at ambient temperature for 6 h, after which it was stored in a dry and covered container at room temperature.	Khan (2016) <sup>75</sup>

**Table EP 1.** Syntheses of silica supported acids.

### 1.8.2 Modified Merrifield resins



**Scheme EP 9.** Modification of Merrifield resin.

Merrifield resin was modified with five different acids as illustrated in **Scheme EP 9**. No more information is available.

### 1.8.3 Catalysts provided by Dr. Camelia Ghimbeu (IS2M)

#### HASG-400

HASG-400 is a porous commercial graphite from Timcal.

#### HASG-400-ox

HASG-400-ox was obtained by oxidation treatment of HASG-400 using concentrated nitric acid ( $\text{HNO}_3$ ). The carbon and acid mixture was heated under reflux at 60 °C for 1 h, then temperature was raised to 100 °C for 30 min. This treatment with nitric acid is well known in the carbon field for introducing oxygen groups of acidic surfaces.<sup>76</sup>

#### Lignine-400

Lignin alkali (Lignin Kraft) low sulphonate content (from Aldrich) was pre-carbonized at 400 °C for 1 h under argon using a heating rate of 5 K/min. This lignin has about 4 wt.% of sulphur in its structure. Heating at 400° C ensures the decomposition of lignin (see TGA figure below) to obtain a carbon rich in oxygen and sulphur compounds.

(Camélia Matei Ghimbeu et al., Valorizing low cost and renewable lignin as hard carbon for Na-ion batteries: impact of lignin grade, Submitted article, *Carbon*, 2019)

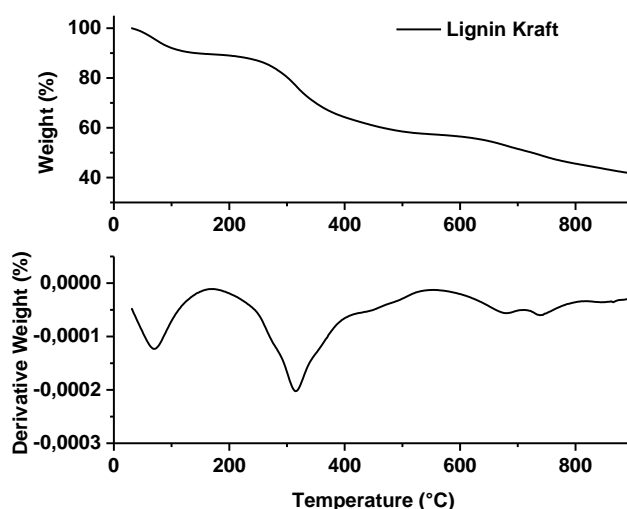


Figure EP 3. Thermogravimetric analysis (TGA) of Lignine-400.

### 1.8.4 PAASA encapsulated in alginate beads

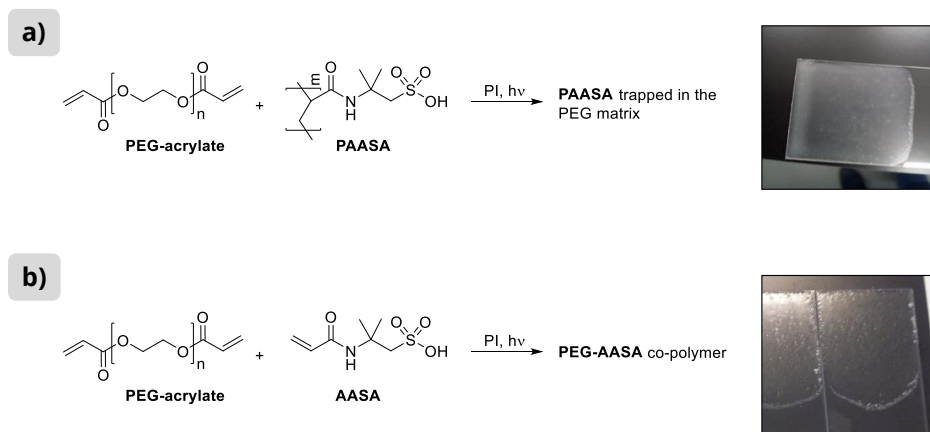
Alginate macrobeads containing PAASA were prepared according to reported procedure.<sup>87</sup>

A solution of alginate (15 wt. %) and PAASA (0.1 wt.%, considering the original commercially available 15 wt.% solution in water) is dripped into a stirred aqueous solution of 0.1 M calcium chloride at room temperature. After formation, the beads were left for curing in the  $\text{CaCl}_2$  solution for 24 hours in order to allow optimal cross-linking of the alginate chains by the

calcium ions. Then the beads were separated by vacuum filtration and washed with Milli-Q water.

### 1.8.5 PEG-PAASA and PEG-AASA provided by Dr. Lavinia Balan (IS2M)

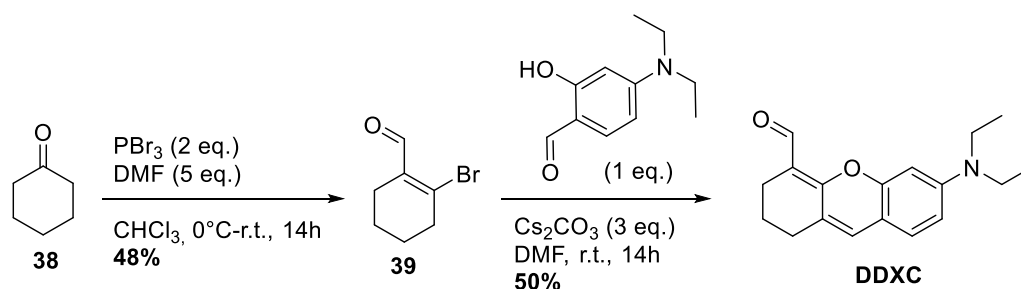
The following figure and described procedure are the only information in our possess at this moment about the preparation of PEG-based polymers provided by Dr. Lavinia Balan (IS2M, Université Haute-Alsace).



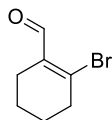
**Figure EP 4.** **a)** Synthesis and photo of **PEG-PAASA** film: polymerization of PEG-acrylate with encapsulation of **PAASA** within the matrix. **b)** Synthesis and photo of the co-polymer **PEG-AASA**.

A solution of PEG-acrylate, acid (PAASA or AASA in different wt. %) and a photoinitiator was stirred for one hour at room temperature to ensure homogeneous mixing of all the components. Few drops of the solution were spread on a glass support to create film of a defined thickness (100  $\mu\text{M}$ ) or small drops were deposited on a highly hydrophobic surface in order to create small spheres. The solutions were subjected to a UV source and photopolymerization was monitored by FT-IR analysis until disappearance of the characteristic peaks of the alkenyl C=C stretching (1680-1620  $\text{cm}^{-1}$ ). No more details about the synthesis are available.

### 1.9 SYNTHESIS OF **DDXC**



**Scheme EP 10.** Synthesis of **DDXC**.

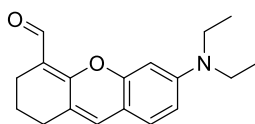
**2-bromocyclohex-1-ene-1-carbaldehyde, 39**Chemical Formula: C<sub>7</sub>H<sub>9</sub>BrO

Exact Mass: 187,9837

Compound **39** was synthesized according to the reported procedure.<sup>152</sup> A solution of dry DMF (5 eq., 1.83 g, 1.93 mL, 25 mmol) in anhydrous chloroform was cooled to 0 °C in the ice-bath. PBr<sub>3</sub> (2 eq., 2.71 g, 0.94 mL, 10 mmol) was added dropwise over a period of 10 minutes. The resulting white suspension was warmed to room temperature and stirred for additional 30 min. A solution of cyclohexanone (1 eq., 0.49 g, 0.518 mL, 5 mmol) in chloroform was added drop-wise and stirred for 12 h at room temperature. The reaction mixture was then poured in ice water. Solid sodium bicarbonate was carefully added to neutralize the acids and the mixture was extracted three times with chloroform. The organic part was then washed with cold water, dried with sodium sulphate and evaporated. Purification of the residue was done by column chromatography (EtOAc/cyclohexane 5/95), obtaining 2-bromocyclohex-1-ene-1-carbaldehyde (452 mg, 2.39 mmol, 47.82 %) as a colourless liquid.

**<sup>1</sup>H NMR (400 MHz, CDCl<sub>3</sub>, δ ppm):** 10.02 (s, 1H), 2.74 (tt, *J* = 6.2, 2.3 Hz, 2H), 2.28 (ddd, *J* = 8.3, 6.0, 2.3 Hz, 2H), 1.80 – 1.72 (m, 2H), 1.72 – 1.64 (m, 2H).

**<sup>13</sup>C NMR (101 MHz, CDCl<sub>3</sub>, δ ppm):** 193.72, 143.56, 135.31, 38.85, 25.02, 24.29, 21.12.

**6-(diethylamino)-2,3-dihydro-1H-xanthene-4-carbaldehyde, DDXC**Chemical Formula: C<sub>18</sub>H<sub>21</sub>NO<sub>2</sub>

Exact Mass: 283,1572

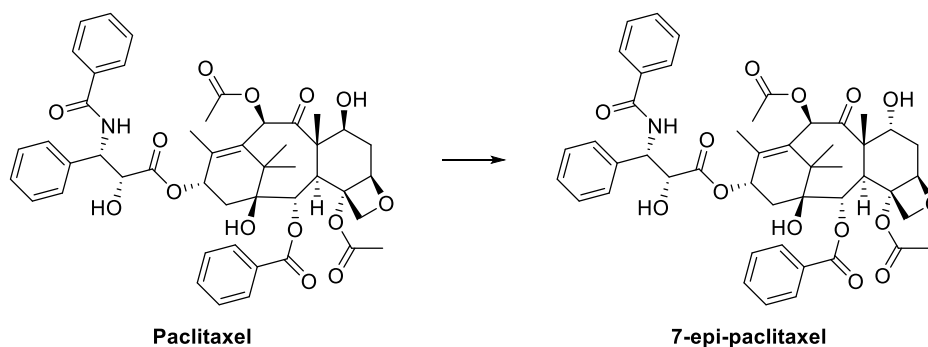
Cs<sub>2</sub>CO<sub>3</sub> (3 eq., 861 mg, 2.64 mmol) and 2-bromocyclohex-1-ene-1-carbaldehyde (1.2 eq., 200 mg, 1.06 mmol) were added to a solution of 4-(diethylamino)-2-hydroxybenzaldehyde (1 eq., 170 mg, 0.882 mmol) in DMF. The reaction mixture was stirred at r.t. overnight.

The mixture was filtered through a pad of silica gel and the filtrate was concentrated under reduced pressure. The residue was re-dissolved in DCM (20 mL), washed with water (2x10 mL), dried over anhydrous sodium sulphate, filtered and concentrated in vacuo. Purification of the residue by chromatography afforded 6-(diethylamino)-2,3-dihydro-1H-xanthene-4-carbaldehyde (124 mg, 0.441 mmol, 50 %) as an orange solid.

**<sup>1</sup>H NMR (400 MHz, CDCl<sub>3</sub>, δ ppm):** 10.27 (s, 1H), 6.98 (dd, *J* = 8.6, 4.9 Hz, 1H), 6.61 (s, 1H), 6.40 (dd, *J* = 8.6, 2.5 Hz, 1H), 6.35 (d, *J* = 2.4 Hz, 1H), 3.38 (q, *J* = 7.1 Hz, 4H), 2.56 – 2.50 (m, 1H), 2.44 (t, *J* = 6.1 Hz, 1H), 1.73 – 1.65 (m, 1H), 1.19 (t, *J* = 7.1 Hz, 6H).

**<sup>13</sup>C NMR (101 MHz, CDCl<sub>3</sub>, δ ppm):** 187.13, 162.04, 154.21, 149.64, 128.13, 127.61, 123.17, 111.39, 110.32, 107.81, 97.23, 44.63, 29.88, 21.67, 20.72, 12.63.

### 1.10 ISOMERIZATION OF PACLITAXEL



**Scheme EP 11.** Epimerization at C7 of Paclitaxel.

#### 1.10.1 Azidation attempt on micro scale

The late stage metal-free azidation of paclitaxel was carried out applying the protocol described in literature<sup>115</sup> to the cytotoxic protocol and microscale conditions.

Solutions of reagents were prepared as follow:

- paclitaxel, 50 mM in acetonitrile (CITOTOXIC PROTOCOL)
- *p*-toluensulfonyl azide, 500 mM in acetonitrile
- sodium bicarbonate, 500 mM in water
- potassium persulfate, 167 mM in water

In a glass vial were added, in order:

- 12.75  $\mu$ L of the azide solution (1.5 eq., 1.26 mg)
- 8.5  $\mu$ L of bicarbonate solution (1 eq., 0.36 mg)
- 76.5  $\mu$ L of persulfate solution (3 eq., 3.45 mg)
- 29.75  $\mu$ L of acetonitrile (in order to have a 3/2 mixture ACN/water)
- 85  $\mu$ L of paclitaxel solution (1 eq., 3.63 mg); final concentration of paclitaxel: 20 mM.

The vial was sealed and fluxed with Argon for a few minutes. Temperature was set to 85°C and the reaction mixture was left to stir for 4 hours. Reaction was monitored by LC-MS, a new peak was detected with the same *m/z* of the starting material and a similar retention time. There was no sign of a possible paclitaxel-azide adduct.

The reaction was repeated on a small scale without the azide source and at room temperature, obtaining the same chromatographic profile.

#### 1.10.2 Paclitaxel isomerization on 20 mg scale

Solutions of reagents were prepared as follow:

- paclitaxel, 50 mM in acetonitrile (CYTOTOXIC PROTOCOL)
- sodium bicarbonate, 0.5 M in water
- potassium persulfate, 0.1M in water

In a glass vial were added, in order:



- 46.9  $\mu\text{L}$  of bicarbonate solution (1 eq., 1.97 mg in water)
- 702.5  $\mu\text{L}$  of persulfate solution (3 eq., 18.99 mg in water)
- 655.5  $\mu\text{L}$  of acetonitrile (in order to have a 3/2 mixture ACN/water)
- 468  $\mu\text{L}$  of paclitaxel solution (1 eq., 20 mg); final concentration of paclitaxel: 12 mM.

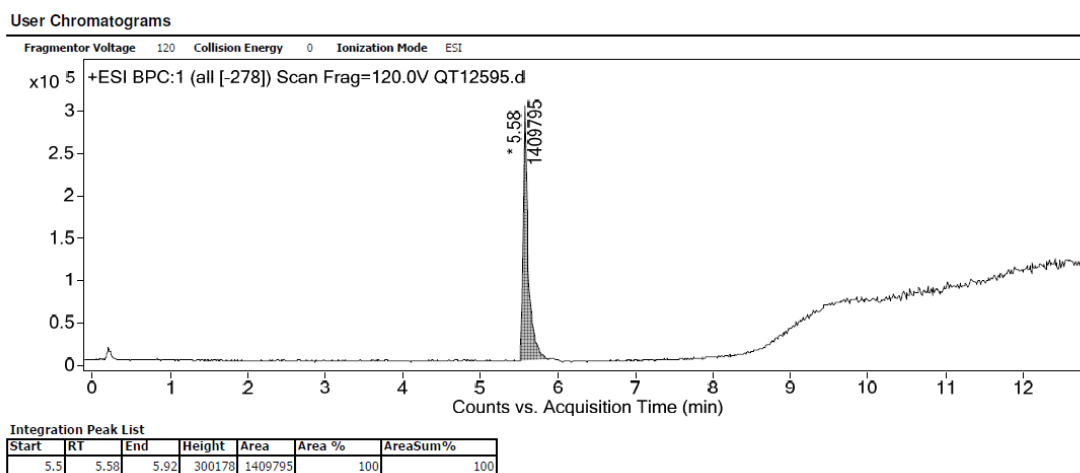
The vial was sealed and fluxed with argon for a few minutes and the reaction mixture was left to stir for 4 hours at room temperature. Reaction was monitored by LC-MS and the product was purified by preparative HPLC.

### Paclitaxel

**(2aR,4S,4aS,6R,9S,11S,12S,12aR,12bS)-9-(((2R,3S)-3-benzamido-2-hydroxy-3-phenylpropanoyl)oxy)-12-(benzoyloxy)-4,11-dihydroxy-4a,8,13,13-tetramethyl-5-oxo-3,4,4a,5,6,9,10,11,12,12a-decahydro-1H-7,11-methanocyclodeca [3,4]benzo[1,2-b]oxete - 6,12b(2aH)-diyl diacetate**

**$^1\text{H}$  NMR (400MHz, DMSO- $d_6$ ,  $\delta$  ppm):** 8.85 (d,  $J$  = 8.6 Hz, 1H), 7.91 (d,  $J$  = 7.2 Hz, 2H), 7.82 (d,  $J$  = 7.1 Hz, 2H), 7.65 (t,  $J$  = 7.4 Hz, 1H), 7.56 (t,  $J$  = 7.5 Hz, 2H), 7.49 (t,  $J$  = 7.2 Hz, 1H), 7.42 (t,  $J$  = 7.3 Hz, 2H), 7.36 – 7.30 (m, 4H), 7.15 (dt,  $J$  = 11.4, 4.3 Hz, 1H), 6.23 (s, 1H), 6.12 (d,  $J$  = 7.6 Hz, 1H), 5.83 (t,  $J$  = 8.9 Hz, 1H), 5.35 (dd,  $J$  = 7.7, 3.3 Hz, 2H), 4.86 (t,  $J$  = 6.6 Hz, 2H), 4.64 (s, 1H), 4.52 (t,  $J$  = 7.6 Hz, 1H), 4.09 – 4.00 (m, 1H), 3.95 (dd,  $J$  = 15.0, 8.2 Hz, 2H), 3.55 (d,  $J$  = 7.1 Hz, 1H), 2.31 – 2.20 (m, 1H), 2.16 (s, 3H), 2.05 (s, 3H), 1.83 (dd,  $J$  = 15.1, 9.3 Hz, 1H), 1.72 (s, 3H), 1.65 (dd,  $J$  = 15.6, 9.2 Hz, 1H), 1.57 (t,  $J$  = 13.0 Hz, 1H), 1.44 (s, 3H), 0.96 (s, 3H), 0.95 (s, 3H).

**HR-ESI-MS**  $\text{C}_{47}\text{H}_{51}\text{NO}_{14}$ , 853,33096; found 853.33135



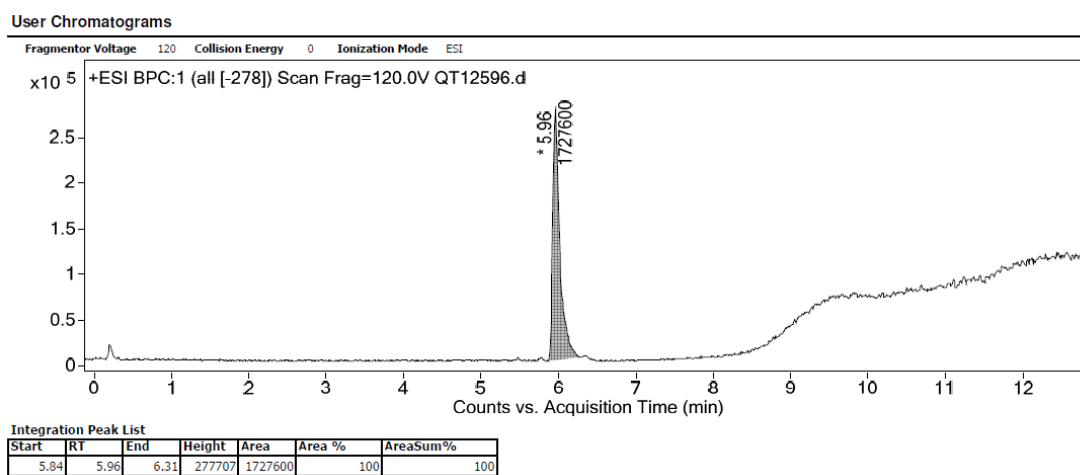
**Figure EP 5.** HR-MS chromatogram of Paclitaxel.

**7-epi-paclitaxel**

**(2aR,4R,4aS,6R,9S,11S,12S,12aR,12bS)-9-(((2R,3S)-3-benzamido-2-hydroxy-3-phenylpropanoyl)oxy)-12-(benzoyloxy)-4,11-dihydroxy-4a,8,13,13-tetramethyl-5-oxo-3,4,4a,5,6,9,10,11,12,12a-decahydro-1H-7,11-methanocyclodeca[3,4]benzo[1,2-b]oxete-6,12b(2aH)-diyl diacetate**

**<sup>1</sup>H NMR (400MHz, DMSO-d<sub>6</sub>, δ ppm):** 8.81 (d, J = 8.6 Hz, 1H), 7.93 (d, J = 7.3 Hz, 2H), 7.82 (d, J = 7.2 Hz, 2H), 7.66 (t, J = 7.4 Hz, 1H), 7.58 (t, J = 7.5 Hz, 2H), 7.48 (t, J = 7.3 Hz, 1H), 7.42 (t, J = 7.4 Hz, 2H), 7.33 (dd, J = 8.5, 5.5 Hz, 4H), 7.15 (td, J = 5.9, 2.8 Hz, 1H), 6.56 (s, 1H), 6.06 (d, J = 7.5 Hz, 1H), 5.83 (t, J = 8.8 Hz, 1H), 5.43 (d, J = 7.5 Hz, 1H), 5.37 (t, J = 8.0 Hz, 1H), 4.93 (dd, J = 9.2, 3.4 Hz, 1H), 4.89 (d, J = 9.2 Hz, 1H), 4.68 (s, 1H), 4.55 (t, J = 6.8 Hz, 1H), 4.21 (d, J = 8.3 Hz, 1H), 4.07 (d, J = 8.3 Hz, 1H), 3.67 (d, J = 7.4 Hz, 1H), 3.42 (dd, J = 9.2, 3.1 Hz, 1H), 2.27 (d, J = 7.4 Hz, 3H), 2.14 (dd, J = 14.8, 9.6 Hz, 1H), 2.05 (s, 3H), 2.03 – 1.99 (m, 1H), 1.94 (dd, J = 15.3, 9.3 Hz, 1H), 1.70 (dd, J = 15.3, 8.7 Hz, 1H), 1.61 (s, 3H), 1.43 (s, 3H), 0.95 (s, 3H), 0.92 (s, 3H).

**HR-ESI-MS** C<sub>47</sub>H<sub>51</sub>NO<sub>14</sub>, 853,33096; found 853.32930



**Figure EP 6.** HR-MS chromatogram of 7-epi-paclitaxel.

## 2. STABILITY OF FRET PROBES IN AQUEOUS MEDIA

### 2.1 MATERIALS AND METHODS

Aqueous buffers were prepared following **Table EP 2.**, pH was measured with a pH-meter.

Calculated pH	Measured pH	Composition
0	<0.7	1 M solution of HCl
1	1.19	0.1 M solution of HCl
2	2.00	0.01 M solution of HCl
3	3.03	30 mL of KH phthalate std + 10 mL of 0,1 M HCl
4	4.12	KH phthalate (std solution for pH-meter)
5	5.03	0.78 mL of Na <sub>2</sub> HPO <sub>4</sub> 0,1 M + 39.4 mL of NaH <sub>2</sub> PO <sub>4</sub>
7.4	7.32	31 mL of Na <sub>2</sub> HPO <sub>4</sub> 0,1 M + 9 mL of NaH <sub>2</sub> PO <sub>4</sub>
9	9.03	0.485 g of TRIS base in 15 mL of miliQ water, pH adjusted to 9 with 1 M solution of HCl and then diluted with miliQ water to 40 mL

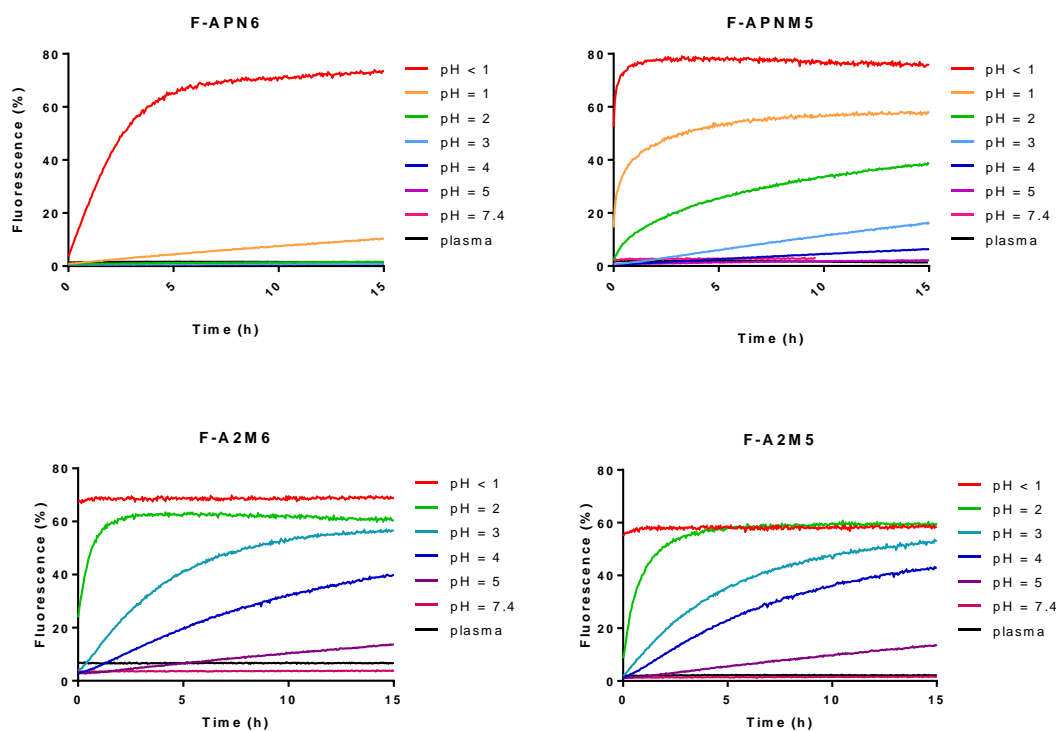
**Table EP 2.** Preparation of buffer solutions for the stability tests.

Fluorescence measurements were done using 96-well plates black Nunclon Delta Surface from Thermo Scientific and a fluorometer Perkin Elmer VictorX2 2030 Multilabel Reader or a 2-Monochromators multidetection reader for microplates SAFAS Xenius XML.

### 2.2 STABILITY TESTS IN AQUEOUS BUFFERS

#### 2.2.1 FRET probes *F-APN6*, *F-APNM5*, *F-A2M5*, *F-A2M6*

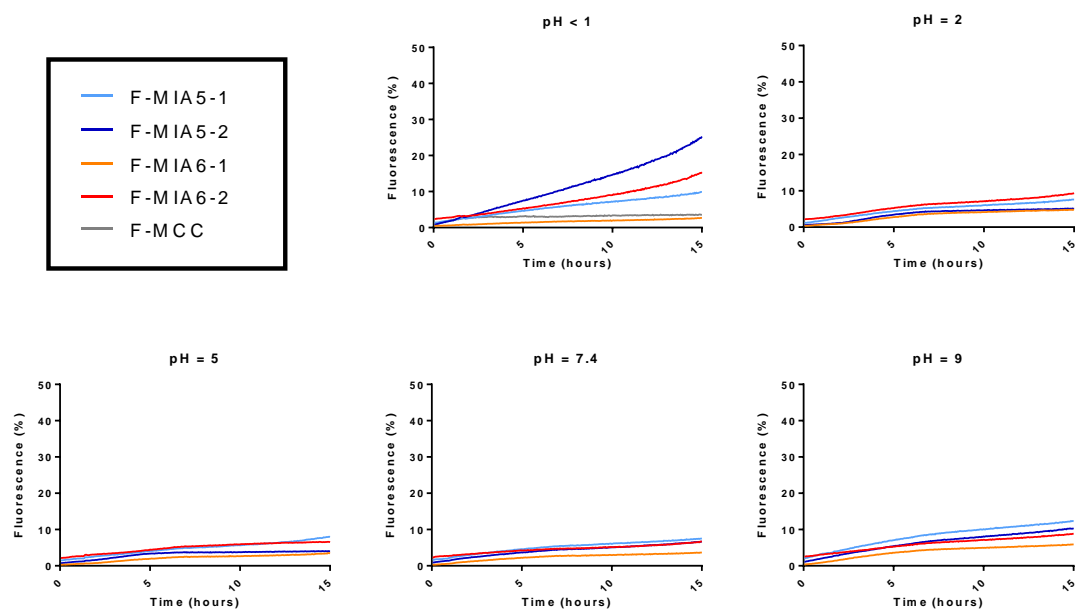
Working solutions (40  $\mu$ M in DMSO) of FRET probes **F-APN6**, **F-APNM5**, **F-A2M5** and **F-A2M6** were prepared. 25  $\mu$ L of each working solution was added to 975  $\mu$ L of aqueous media (final concentration 1  $\mu$ M), vortexed and distributed onto 96-well plates (in triplicates). The instrument temperature could not be set (SAFAS Xenius XML); however, the temperature of the room was maintained constant (23°C). Excitation/emission wavelengths were set to those for TAMRA (550/580 nm). The fluorescence was measured every 3 minutes for 15 hours and normalized to the fluorescence of a solution of TAMRA-NH<sub>2</sub> (1  $\mu$ M) and BHQ-2-SH (1  $\mu$ M) in the corresponding media (2.5 % DMSO, positive control) recorded in the same conditions. For stability test at pH < 1 the fluorescence of MCC-FRET probe was monitored in parallel. The obtained results are shown in **Figure EP 7**.



**Figure EP 7.** Profile of FRET probes **F-APN6**, **F-APNM5**, **F-A2M5** and **F-A2M6** stability at different pH.

### 2.2.2 FRET probes **F-MIA5-1**, **F-MIA5-2**, **F-MIA6-1**, **F-MIA6-2**

Working solutions (40  $\mu\text{M}$  in DMSO) of FRET probes **F-MIA5-1**, **F-MIA5-2**, **F-MIA6-1** and **F-MIA6-2** were prepared. 25  $\mu\text{L}$  of each working solution was added to 975  $\mu\text{L}$  of aqueous media (final concentration 1  $\mu\text{M}$ ), vortexed and distributed onto 96-well plates (in triplicates). The instrument temperature was set to 25°C and excitation/emission wavelengths were set to those for TAMRA (550/580 nm). The fluorescence was measured every 3 minutes for 15 hours and normalized to the fluorescence of a solution of TAMRA-NH<sub>2</sub> (1  $\mu\text{M}$ ) and BHQ-2-SH (1  $\mu\text{M}$ ) in the corresponding media (2.5% DMSO, positive control) recorded under the same conditions. For stability test at pH < 1 the fluorescence of MCC-FRET probe was monitored in parallel. The obtained results are shown in **Figure EP 8**.



**Figure EP 8.** Profile of FRET probes **F-MIA5-1**, **F-MIA5-2**, **F-MIA6-1** and **F-MIA6-2** stability at different pH.

### 2.2.3 FRET probes **F-APN6** and **F-APNM5** at 37 °C

The working solutions (40  $\mu\text{M}$  in DMSO) of **F-APN6**, **F-APNM5** and TAMRA+BHQ (positive control) were diluted with the aqueous media to obtain 5 mL of 1  $\mu\text{M}$  concentration solutions. The solutions were agitated at 37 °C, 600  $\mu\text{L}$  aliquots were taken each hour for 6 hours and distributed on a 96-well plate (triplicates of 200  $\mu\text{L}$  each). The fluorescence was measured ( $\text{ex}_{550}/\text{em}_{580}$ ) and normalized to the fluorescence of the positive control.

## 2.3 RATE OF SUCCINIMIDE RING-OPENING

### 2.3.1 Rate of succinimide ring-opening in PBS buffer

The solution (2 mL) of each FRET probes probes **F-MIA5-1**, **F-MIA5-2**, **F-MIA6-1** and **F-MIA6-2** (50  $\mu\text{M}$ , final concentration) in PBS 1x buffer (pH 7.4, DMSO 10%) was incubated at 37 °C. After certain intervals of time the aliquots (100  $\mu\text{L}$ ) were taken, diluted with 100  $\mu\text{L}$  of acetonitrile and then were analysed by LC-MS. The conversion was calculated as the peak-area under hydrolyzed product (M+18) divided by the total peak-area.

### 2.3.2 Rate of succinimide ring-opening in human plasma

The solution (2 mL) of each FRET probe **F-MIA5-1**, **F-MIA5-2**, **F-MIA6-1** and **F-MIA6-2** (1  $\mu\text{M}$ , final concentration) in human plasma (DMSO 10%) was incubated at 37 °C. After certain

intervals of time 100  $\mu$ L aliquots were taken and mixed with 100  $\mu$ L of acetonitrile, allowing the precipitation of proteins, the resulting mixture was centrifuged and the supernatant was analysed by LC-MS. The conversion was calculated as the area under opened product divided by the total area.

Human plasma was supplied by Etablissement Français du Sang (EFS Strasbourg).

## 2.4 STABILITY OF **F-MIA5-1** AND **HF-MIA5-1** IN PLASMA

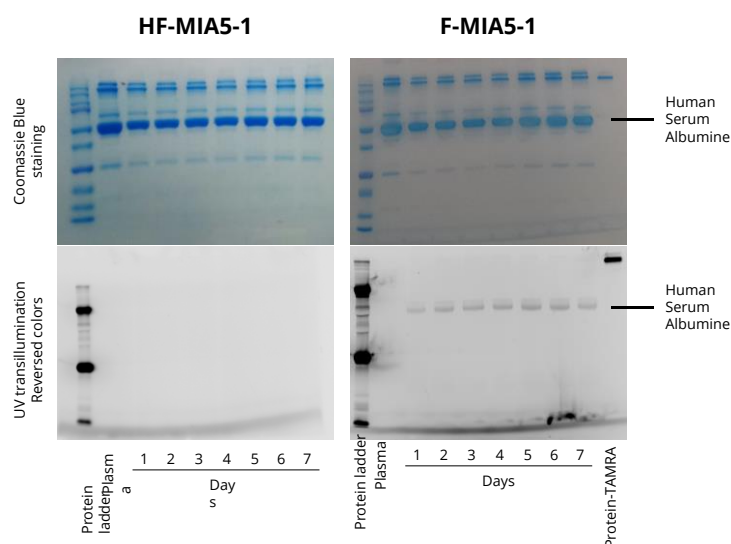
### Procedure

1) Preparation of probe **HF-MIA5-1**. 5  $\mu\text{L}$  of 10 mM stock solution of FRET probe P(5-1) was added to 15  $\mu\text{L}$  of PBS 1x buffer (pH 7.4) and 13.5  $\mu\text{L}$  of DMSO in a vial for LC-MS (final concentration 0.5 mM). The resulting solution was incubated at 37  $^{\circ}\text{C}$  and analysed by LC-MS until 100% hydrolysis was achieved.

2) Preparation of probe **F-MIA5-1**. Aliquots from 10 mM stock solutions of FRET probe P(5-1) was diluted to reach the final concentration of 0.5 mM (PBS/DMSO 1:1).

3) Incubation in human plasma. For every 0.5 mM solution of probes, 10  $\mu\text{L}$  were taken and added to 90  $\mu\text{L}$  of human plasma (final concentration of probes: 50  $\mu\text{M}$ ), the resulting solutions were incubated at 37  $^{\circ}\text{C}$ . Each day aliquots of 2  $\mu\text{L}$  were taken, diluted 100 times with water and stocked at -20  $^{\circ}\text{C}$ .

4) SDS-PAGE analysis Non-reducing SDS-PAGE was performed on 12% Mini-PROTEAN® TGX™ Gel (Bio-Rad ref 4561044) following standard lab procedures. For each solution of samples (including neat plasma diluted 10 times with water and a 0,1 mg/mL solution of antibody-TAMRA conjugate (standard control, with average degree of conjugation of 0,86) 24  $\mu\text{L}$  of aliquot was taken and mixed with 8  $\mu\text{L}$  of 4x non-reducing Laemmli SDS sample buffer (ref J63615, Alfa Aesar). The samples were heated at 95  $^{\circ}\text{C}$  for 5 minutes and loaded into the gel well (10  $\mu\text{L}$ ). The gel was run at constant voltage (200 V) for 40 min using TRIS 0.25 M - Glycine 1.92 M - SDS 1% as a running buffer. Fluorescence was measured on GeneGenius bio-imaging system (Syngene) and then normalized to standard control prior to staining with Coomassie Blue (**Figure EP 9**).



**Figure EP 9.** HSA bands revealed by Coomassie Blue staining of gel with **HF-MIA5-1** probe and fluorescence of HSA bands on gel with **HF-MIA5-1** and **F-MIA5-1** probes.

### 3. SCREENING OF CATALYSTS AND HYDROLYSIS TESTS

#### 3.1 MATERIALS AND METHODS

Catalysts were obtained from commercial sources and used without any further treatment or synthesized in the laboratory according to procedures described above or received from Dr. Jean-Michel Becht and Dr. Lavinia Balan from IS2M (Université Haute-Alsace).

Human plasma was supplied by Etablissement Français du Sang (EFS Strasbourg).

Washing solutions were prepared as follow:

- *NaCl sat.*: NaCl (for molecular biology, >99% purity) was dissolved in 1 L of ultrapure water until saturation. Dilutions of this stock solution were done using ultrapure water.

- *PBS*: prepared from commercial tablets. One tablet dissolved in 200 mL of ultrapure water yields 0.01 M phosphate buffer, 0.0027 M potassium chloride and 0.137 M sodium chloride, pH 7.4, at 25 °C. Dilutions of this stock solution were done using ultrapure water.

Fluorescence measurements were done using 96-well plates black Nunclon Delta Surface from Thermo Scientific and a 2-Monochromators multidetection reader for microplates SAFAS Xenius XML.

Leica TCS SPE Confocal Laser Scanning Microscope was used to collect images of the solids. Magnification: 20X; Laser: 561 nm; emission collection channel: 570-590; PMI is equally fixed within acquisitions of the same kind of solid.

#### 3.2 GENERAL SCREENING PROCEDURES

##### **3.2.1 Screening of CSA and homogeneous catalysts**

FRET probes were dissolved in a solution of the catalyst in the appropriate solvent.

- Volume: 0.3 mL
- FRET concentration: 10  $\mu$ M (from a stock solution  $\sim$ 1 mM in DMSO)
- Catalyst concentration: 50 mM

The Eppendorf tubes were agitated at 750 rpm at 37 °C. At given time point, 35  $\mu$ L of the solution was taken, diluted 10 times with 315  $\mu$ L of water, vortexed and distributed onto 96-well plates (two replicates of 150  $\mu$ L each). If the solvent was plasma, the 35  $\mu$ L aliquot was mixed with 315  $\mu$ L of acetonitrile, allowing the precipitation of proteins, the resulting mixture was centrifuged and the supernatant was distributed onto 96-well plates (two replicates of 150  $\mu$ L each).

Fluorescence was measured and related to that of the positive control.

##### **Positive control:**

Positive control was a 10  $\mu$ M solution of TAMRA-NH<sub>2</sub> and BHQ-2-SH in the appropriate solvent, put under agitation at 37 °C. At given time, a 35  $\mu$ L aliquot was taken and treated according to



the solvent used (as described above). Fluorescence was measured and used as 100% hydrolysis value.

### **Comparison control**

FRET probes (10  $\mu\text{M}$ ) in 0.3 mL of the appropriate solvent containing CSA (50 mM) were treated as described for the other samples and used as comparison for the evaluation of the hydrolysis.

### **Negative control**

Negative control consisted in a 10  $\mu\text{M}$  solution of the FRET probe in the appropriate solvent treated as described above and used to check that no auto-hydrolysis takes place within the timeframe of the experiment.

**CSA test** was done the same way, using different concentration of the acid: 0.1 M, 10 mM, 1 mM, 0.1 mM, 10  $\mu\text{M}$ .

### **3.2.2 Screening of heterogeneous catalysts**

- 10 mg of solid catalyst  
 - or 1 bead (in case of Nafion NR50)  
 - or the amount of solid catalyst corresponding to 5K equivalents of acidic protons  
 were dispersed in 0.3 mL of the appropriate solvent and let to incubate for 5 minutes at 37 °C. Then the FRET probes were added (final concentration: 10  $\mu\text{M}$ ) and the mixture was let under mechanical agitation at 37 °C. At given time the reaction was monitored according to the type of catalyst as follow:

- Non-adsorbent catalyst: Fluorescence was measured with a spectrophotometer as described for the screening of homogeneous catalysts.

- Adsorbent catalysts: Fluorescence was evaluated by placing the plastic tube under a UV lamp and comparing the fluorescence to that emitted by the same solid catalyst soaked with an equimolar mixture of TAMRA and BHQ (positive control).

Comparison and negative control were the same as for the screening of homogeneous catalysts.

### **3.2.3 Screening of PEG-based catalysts**

#### **PEG-PAASA (film) – PEG-AASA (film and beads)**

- PEG-PAASA and PEG-AASA in form of films were supplied by Dr. Lavinia Balan in a glass support. The polymer was detached from the support by wetting it with 3 mL of plasma. This procedure was indeed a pre-washing of the catalyst. In some case the polymer detached spontaneously from the support, so the pre-washing was not performed.
- PEG-AASA beads were supplied by Dr. Lavinia Balan as free beads and stored in a glass container at r.t. When required, beads were pre-washed (cf. paragraph 3.3.2).

Defined amount of the detached film *or* of PEG-AASA beads were dispersed into 0.3 mL of plasma, the acetal substrate was added (10  $\mu\text{M}$  in case of a FRET probe, 0.28 mM in case of PEGAM5) and the reaction vials were agitated (750 rpm) at 37 °C for a maximum of 7 days.

Reaction monitoring was done at given times according to the nature of the substrate:

*For FRET:* 35  $\mu\text{L}$  of the solution were taken and mixed with 315  $\mu\text{L}$  of acetonitrile, allowing the precipitation of proteins, the resulting mixture was centrifuged and the supernatant was distributed onto 96-well plates (two replicates of 150  $\mu\text{L}$  each). Fluorescence was measured and related to that of the positive control (10  $\mu\text{M}$  solution of TAMRA and BHQ in plasma).

*For PEGAM5:* See following paragraph.

### 3.2.4 PEGAM5's hydrolysis monitoring

Tests with **PEGAM5** as substrate were done the same way as above, but the concentration of PEGAM5 was increased to 0.28 mM (5  $\mu\text{L}$  of a 16.8 mM stock solution in DMSO were dissolved in 285  $\mu\text{L}$  of plasma). At given times 10  $\mu\text{L}$  aliquots were taken, mixed with 90  $\mu\text{L}$  of acetonitrile, allowing the precipitation of proteins. The resulting mixture was centrifuged and the supernatant was analysed by LC-MS (fixed injection volume: 5  $\mu\text{L}$ ). Peak areas of the starting material and of the product are measured and percentage was extrapolated from the calibration curves built as follow.

#### Calibration curve for PEGAM5 (Starting Material – SM)

X  $\mu\text{L}$  of a stock solution of PEGAM5 in DMSO (16.8 mM) were added to (300 – X)  $\mu\text{L}$  of plasma. Three different solution were prepared, corresponding to different amount of PEGAM5 (cf. **Table EP 3**). The solutions were incubated at 37 °C for 1 hour, then 10  $\mu\text{L}$  aliquots were taken, diluted in 90  $\mu\text{L}$  of acetonitrile, allowing the precipitation of proteins. The resulting mixtures were centrifuged and the supernatant was analysed by LC-MS (fixed injection volume of 5  $\mu\text{L}$ ). The values of the peak area corresponding to PEGAM5 were plotted against the percentage.

Percentage	PEGAM5 stock sol. ( $\mu\text{L}$ )	Plasma ( $\mu\text{L}$ )
100%	5	295
50%	2.5	297.5
20%	1	299

**Table EP 3.** Composition of the solutions for the calibration curve of PEGAM5.

#### Calibration curve for 36 (Product of PEGAM5 hydrolysis – P)

5  $\mu\text{L}$  of 3 M HCl aq. solution was added to 10  $\mu\text{L}$  of a 16.8 mM stock solution of **PEGAM5** in DMSO. The solution was incubated at 37 °C for 1 hour, to insure complete acidic hydrolysis of **PEGAM5**. Then it was neutralized by adding 15  $\mu\text{L}$  of a 1 M KOH aq. solution.

The solution of hydrolysed **PEGAM5** was used for the calibration curve of the hydrolysis product (aldehyde **36 – P**)

X  $\mu\text{L}$  of the prepared solution were added to  $(300 - X)$   $\mu\text{L}$  of plasma. Four different solutions were prepared, corresponding to different amounts of **36** (cf. **Table EP 4**). The solutions were incubated at  $37^\circ\text{C}$  for 1 hour, then 10  $\mu\text{L}$  aliquots were taken, diluted in 90  $\mu\text{L}$  of acetonitrile, allowing the precipitation of proteins. The resulting mixtures were centrifuged and the supernatant was analysed by LC-MS (fixed injection volume of 5  $\mu\text{L}$ ). The values of the peak area corresponding to aldehyde **36** were plotted against the percentage.

Percentage	XX solution ( $\mu\text{L}$ )	Plasma ( $\mu\text{L}$ )
100%	15	285
50%	7.5	292.5
20%	3	297
10%	1.5	298.5

**Table EP 4.** Composition of the solutions for the calibration curve of XX.

### 3.3 WASHING PRE-TREATMENT

#### **3.3.1 Washing pre-treatment for Nafion**

##### **Method A**

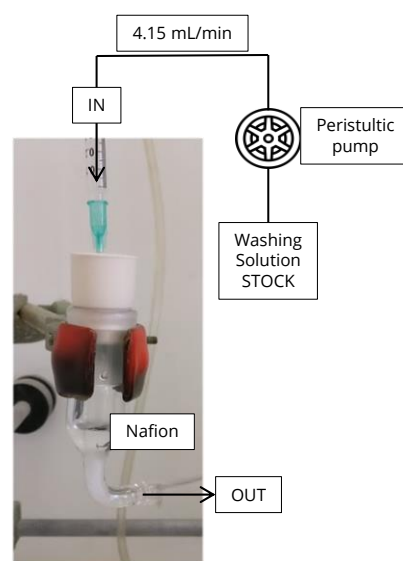
20 commercial Nafion NR50 beads were put on a flask; 30 mL of the washing solution were added and let to stir at room temperature for 18 hours. Then the washing solution was decanted, the beads were let to dry and were stocked in at room temperature in a close glass container until use.

##### **Method B**

20 beads are put on a Buchner funnel and 100 mL of the washing solution was used to wash the beads. Total time: approximately 1 minute. Then the beads were let to dry and were stocked in at room temperature in a close glass container until use.

##### **Method C**

20 beads or 20 mg of POWDion (40-60 mesh) were put on a glass container with an entrance and a way out for the washing solution. The washing solution was pumped at a flow rate of 4.15 mL/min by a peristaltic pump into the glass container, getting in contact with the catalyst, and out (**Figure EP 10**). At given times, the flow was stopped, the system was opened to take out part of the catalyst. Then the system was closed and the flow was started again to continue the washing (total time of the operation: maximum 1 minute). The beads were let to dry and were stocked in at room temperature in a close glass container until use.



**Figure EP 10.** Photo and scheme of the system used to wash the catalyst with method C. The washing solution is pumped at 4.15 mL/min to a closed glass container in which it gets in contact with the solid catalyst and then exit.

### 3.3.2 Washing pre-treatment for PEG-AASA (beads)

The amount of PEG-AASA beads required for the reaction was weighted and the washing was performed in the vial to be used for the reaction, following one of the procedure described below.

*Fast washing.* 1 mL of plasma was added and the suspension was vigorously agitated at room temperature for 15 seconds. Then plasma was removed.

*10 minutes washing.* 1 mL of plasma was added and the suspension was put at 37 °C under mechanical shaking (750 rpm) for 10 minutes. Then plasma was removed.

*30 minutes washing.* 1 mL of plasma was added and the suspension was put at 37 °C under mechanical shaking (750 rpm) for 30 minutes. Then plasma was removed.

### 3.4 NAFION NR50 AND AMBERLYST A-15 ADSORBANCE AND RELEASING RATE

The following solutions were prepared:

- 1 mL of TAMRA (10  $\mu$ M) and BHQ (10  $\mu$ M) in water
- 0.8 mL of F-APNM5 (10  $\mu$ M) in water

Each solution was distributed in two vials (0.3 mL each). In one vial was added a bead of Nafion NR50 and in the other a bead of Amberlyst A-15. 0.3 mL of the TAMRA+BHQ solution was also kept as positive control.

The 5 vials were agitated (750 rpm) at 37 °C. At given time point ( $t = 0$  h, 1.5 h and 3 h) 35  $\mu$ L of the solution was taken, diluted 10 times with 315  $\mu$ L of water, vortexed and distributed onto 96-well plates (two replicates of 150  $\mu$ L each). Fluorescence was measured with SAFAS Xenius

XML spectrophotometer. Values were compared to those obtained from the fluorescence measurement of the positive control.

After 3 hours, the beads were taken from the solution and put into 1 mL of 1:1 mixture of DMSO and HCl aq. (3 M). They were left at room temperature under agitation (750 rpm) for 24 hours. Then, 100  $\mu$ L of the solution was taken, diluted 3 times with 300  $\mu$ L of water, vortexed and distributed onto 96-well plates (two replicates of 150  $\mu$ L each). Fluorescence was measured with SAFAS Xenius XML spectrophotometer and compared to that of a 1  $\mu$ M solution of TAMRA and BHQ in an equal composition of solvents (1:1:4 DMSO/3 M HCl aq./water).

### 3.5 DETECTION OF HYDROLYSIS WITH UV TRANSILLUMINATOR AND CONFOCAL MICROSCOPE

#### **3.5.1 Preparation of Nafion beads for the calibration curve**

0.3 mL solutions of TAMRA and BHQ in water at different concentration were prepared, ranging from 1  $\mu$ M to 10  $\mu$ M (**Table EP 5**). For each solution, a Nafion bead was added and let to soak all the TAMRA and BHQ (37 °C, agitation, 15 minutes), then analysed.

Entry	Volume	[TAMRA+BHQ]	Theoretical conversion
1	0.3 mL	//	0%
2	0.3 mL	1 $\mu$ M	10%
3	0.3 mL	2.5 $\mu$ M	25%
4	0.3 mL	5 $\mu$ M	50%
5	0.3 mL	7.5 $\mu$ M	75%
6	0.3 mL	10 $\mu$ M	100%

**Table EP 5.** List of solutions used to build the calibration curve.

#### **3.5.2 Fluorescence detection at UV transilluminator**

The beads were taken out from their solutions, dried and placed on defined positions on the viewing surface of the GeneGenius bio-imaging system (Syngene) transilluminator and several snapshot were taken. For each image taken, the positions of beads on the viewing surface were rotated clockwise until each bead was analysed on each position.

Also, for each position, at least two images were taken differing in the orientation of the bead.

#### **3.5.3 Fluorescence detection at confocal microscope**

The beads were taken out from their solutions, dried and analysed with the confocal microscope (cf. section 3.1, page 221). The photomultiplier intensity was set in order to allow to detect fluorescence on the bead soaked with the amount of TAMRA and BHQ corresponding to 10% of hydrolysis (**Table EP 5**, entry 2).

## 4. RATIOMETRIC ANALYSIS

### 4.1 MATERIAL AND METHODS

Ratiometric probe **DDXC** was synthesized as described previously in section 1.9 and stocked as a 0.5 M solution in DMSO.

Leica TCS SPE Confocal Laser Scanning Microscope was used to collect images of the solids. Magnification: 20X; Laser: 405 nm; emission collection channels: 502-522 nm and 570-590; PMI is equally fixed for both collection channels and within acquisitions of the same kind of solid. It may vary from one kind of solid to the other according to the degree of emission.

Images were edited with ImageJ® software, using a macro specifically conceived by Romain Vauchelles at the Faculty of Pharmacy of the University of Strasbourg for ratiometric analysis.

### 4.2 PREPARATION OF THE SOLID CATALYSTS, IMAGE ACQUISITION AND EDITING

#### **Preparation of the solid catalysts**

##### **Nafion**

Nafion NR50 beads (one per vial), Nafion NR50 CH beads (one per vial) were incubated in 0.5 mL of a 0.5 mM solution of **DDXC** in water at 37 °C until complete adsorption of the probe (usually from 5 to 30 minutes).

POWDion forms of Nafion (2 mg/vial) were incubated in 0.3 mL of a 0.5 mM solution of **DDXC** in water at 37 °C until complete adsorption of the probe (usually 30 minutes).

##### **PEG-AASA**

3 mg/vial of PEG-AASA beads were incubated in 0.5 mL of a 0.5 mM solution of **DDXC** in water at 37 °C until appreciable adsorption of the probe (usually 3 hours).

Probe adsorption was checked either by looking at the colour of the solution (from light orange to colourless) and of the solid (from colourless to light orange), either by using a UV lamp to check fluorescence emission from the solid.

#### **Image acquisition and editing**

Images of soaked beads were taken at the Confocal Laser Scanning Microscope using the settings described above. For each bead, images were taken at different depths and in different points. The process has to be as fast as possible since exposition to the laser light affect the **DDXC** probe (emission is lowered when exposition time is increased).

Images were edited with ImageJ software using a macro for ratiometric analysis.

## 5. IN VITRO AND IN VIVO EXPERIMENTS

### 5.1 CELL VIABILITY WITH F-A2M5 AND F-A2M6

This experiment was performed by **Dr. Fabien Thoreau** (CNRS, UMR7199)

#### Cell Culture

All cells were maintained in American Type Culture Collection recommended cell culture media and conditions, which are listed in Table A. Cells were all cultured at 37 °C in a humidified atmosphere containing 5% CO<sub>2</sub>. Corning® T25 or T75 were used.

Cell line	Description	Source	Culture
BNL CL.2	Mouse normal liver cell line	ATCC	DMEM, 10% FBS, 1% PS
LS174	Human Dukes' type B, colorectal adenocarcinoma cell line	ATCC	MEM, 10% FBS, 1% PS
HUH7	Human well differentiated hepatocyte derived cellular carcinoma cell line	ATCC	DMEM, 10% FBS, 1% PS
MDA-MB-231	Human breast adenocarcinoma, derived from metastatic site: pleural effusion	ATCC	DMEM, 10% FBS, 1% PS
SKBR3	Human breast adenocarcinoma, derived from metastatic site: pleural effusion	ATCC	DMEM, 10% FBS, 1% PS

**Table EP 6.** Origin and characteristic of tested cell lines

#### Flow cytometry

Cells were plated in 48 well plates (Costar® 3548) on day 1 (100K cells per well for LS174, HUH7, MDA-MB-231 and SKBR3, 50K cells per well for BNL CL.2) and cultured until day 3 at 37 °C in a humidified atmosphere containing 5% CO<sub>2</sub> (in the suited Media as noticed in table 1). A different plate was used for each cell line to avoid contamination.

On day 3, media was removed and cells were incubated with 250 µL per well of a 1 µM solution of tested compound for 1.5 h at 37 °C (compound solutions were prepared freshly in MEM or DMEM media in accordance with the media used to culture the treated cells, cf. **Table EP 6**). Each seeded well of a plate was treated with a different compound solution except one which was incubated with media (control condition of the corresponding cell line).

After 1.5 h incubation, the compound solutions were removed from the wells and cells were rinsed with 300 µL PBS. After removing PBS, cells were trypsinized (80 µL of trypsin per well) for 5-7 min at 37 °C.

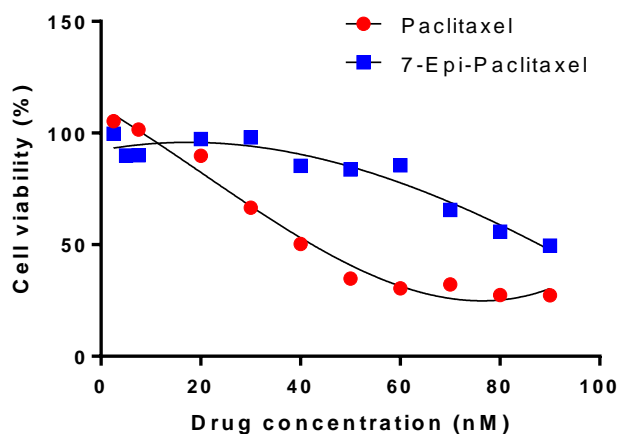
After trypsinization, 500 µL of a PBS/DMEM (without phenol red) (5/5) was added in each well. Cells were flushed and transferred in tubes suited for flow cytometry (Falcon® 5mL). FACS studies were realised on a Fortessa cytometer (BD Biosciences®).

All compounds have been tested on all cell lines several times: at least a biological triplicate in any case.

## 5.2 CELL VIABILITY WITH PACLITAXEL AND 7-EPI-PACLITAXEL

This experiment was performed by **Dr. Manon Ripoll** (former CNRS, UMR7199)

MTT assay after 48 h drug exposure on HeLa cell line. Results (each value is the media of three replicates) are shown in **Figure EP 11**. Unfortunately, no further information is available.



**Figure EP 11.** Cell viability of Paclitaxel and 7-Epi-Paclitaxel.

## 5.3 IN VIVO EXPERIMENT: SAMPLES PREPARATION

### Nafion NR50 pre-washed beads

Nafion NR50 beads were pre-washed for 90 minutes in flow at a rate of 4.15 mL/min (washing method C, cf. section 3.3.1), then they were incubated with 100  $\mu$ L of human Fibroblast Growth Factor (hFGF, 100 ng/ $\mu$ L) at 37 °C for 1 hour, according to the procedure reported by Paria *et al.*<sup>153</sup>

### F-APNM5 solution for injection in mice

3 mg of **F-APNM5** obtained by lyophilization (following preparative HPLC purification) were dissolved into 229  $\mu$ L of a 10% solution of Kolliphor EL® in PBS. To help the solubilization, the solution was warmed up to 50 °C and used right after to run test with Nafion beads. The solution was then stored at -20°C.

Nafion bead soaked with hFGF were tested for hydrolysis in plasma in presence of F-APNM5 from the stock solution for injection in mice, using the procedure previously described for the catalyst screening (section 3.2.2, page 222). As comparison, a Nafion-90 (not soaked with hFGF) bead was tested with F-APNM5 from the stock solution in DMSO. After 24 hours reaction the bead was analysed at the confocal microscope.



## 6. LATE STAGE FUNCTIONALIZATION

### 6.1 SOLVENTS AND TEMPERATURES STABILITY TESTS

10  $\mu\text{L}$  of 10 mM solutions of cytotoxic drug (Abiraterone, Octeotride Acetate, Paclitaxel, Topotecan\*HCl and Vinblastine) in different solvents (water, pyridine, methanol and dimethyl sulfoxide) were let stir for one hour at a given temperature (r.t., 50°C, 80°C, 110°C). Total number of samples: 20.

0.5  $\mu\text{L}$  of each solution was taken, diluted 100 times with acetonitrile and analyzed at LC-MS. Chromatograms were compared to those of the drugs taken before the experiment. All chromatograms can be found on Appendix C (page 261).

## TABLE OF ILLUSTRATIONS

<b>Figure 1.</b> Representation of the objectives pursued. The first band on the left represents the range of pH covered by cells and extracellular environment. The second red band represents the range of pH covered by the abiotic acid catalyst. The three blue bands on the right represent the pH ranges in which the hydrolysis of different abiotic acetal substrates is supposed to be triggered. Grey faded horizontal bands are used to show the matching between the abiotic substrates and the corresponding hydrolysis promoters. ....	11
<b>Figure 2.</b> Representation of the four possible scenarios given by the combination of the substrate and the solid catalyst. Hydrophobic catalyst is symbolized by a sphere with a plain contour, while the hydrophilic catalyst's symbol has a dotted contour. The substrate and the product are represented as, respectively, blue and green dots. Dots are plain for the hydrophobic substrate and striped for the hydrophilic one. <b>a)</b> Hydrophobic substrate + hydrophobic catalysts; <b>b)</b> hydrophobic substrate + hydrophilic catalysts; <b>c)</b> hydrophilic substrate + hydrophobic catalyst and <b>d)</b> hydrophilic substrate + hydrophilic catalyst. ....	13
<b>Figure 3.</b> FRET principle applied on cyclic acetals. The acetal is the link between the donor (in fuchsia) and the acceptor (in violet). The excitation and relaxation are represented with Jablonski diagrams. When hydrolysis occurs, the donor and acceptor are no longer in close proximity and the energy transfer does not happen, allowing the detection of the donor fluorescence emission.....	29
<b>Figure 4.</b> Chemical structure of the donor/acceptor pair chosen, TAMRA and BHQ-2. ....	30
<b>Figure 5.</b> Chemical structure of amino-to-thiol acetal linker model <b>APN6</b> . ....	31
<b>Figure 6.</b> Conjugation to natural amines and thiols of activated linker <b>APN6</b> . ....	31
<b>Figure 7.</b> Modification of TAMRA and BHQ-2 and conjugation to <b>APN6</b> to obtain the corresponding FRET probe <b>F-APN6</b> .....	32
<b>Figure 8.</b> Hydrolysis profiles of acetal <b>F-APN6</b> in different concentration of proton at 23°C. ....	33
<b>Figure 9.</b> Hydrolysis profiles of acetal <b>F-APN6</b> in three different acidic solutions; comparison between 23°C and 37 °C. ....	34
<b>Figure 10.</b> New amino-to-thiol linker model <b>APNM5</b> , designed to be more prone to hydrolysis than its parent <b>APN6</b> . "APN" stands for "arylpropionitrile", "M" indicates the presence of a methoxy substituent and "5" accounts for the size of the acetal ring. ....	35
<b>Figure 11.</b> First outline of the synthetic pathway for compound <b>APNM5</b> . ....	36
<b>Scheme 1.</b> Generic scheme of the three possible synthetic pathways for the preparation of arylpropionitrile compounds.....	36
<b>Scheme 2.</b> Formation of arylpropionitrile from aryl propargylic alcohol in a one-pot domino reaction involving three transformations. Manganese oxide is used for the two oxidations, ammonia is used for the imine formation and magnesium sulphate is used as drying agent. ....	37
<b>Scheme 3.</b> First attempt of APN synthesis: <b>i)</b> esterification on the benzoic acid, followed by <b>ii)</b> a Sonogashira coupling to give compound <b>3</b> (isolated); <b>iii)</b> domino one-pot reaction to obtain the intermediate <b>4</b> (not successful). ....	38
<b>Scheme 4.</b> Step-by-step formation of arylpropionitrile <b>4</b> . The reaction proceeds well till the formation of the imine, while the last oxidation does not occur. ....	38
<b>Scheme 5.</b> Second strategy for the synthesis of <b>APNM5</b> . ....	40

<b>Scheme 6.</b> Complete synthesis of target compound <b>APNM5</b> .	41
<b>Figure 12.</b> Chemical structures of the four possible isomers of the cyclic acetal <b>G8</b> and <b>APNM5</b> : two <i>cis</i> isomers and two <i>trans</i> isomers with respect to the acetal ring substituents in positions 2 and 4.	42
<b>Figure 13.</b> <b>a)</b> Generic reaction between cysteine and arylpropionitriles, the change in molecular mass is indicated. <b>b)</b> LC chromatogram of a sample of <b>APNM5</b> with <b>c)</b> the MS extract of the main peak. <b>d)</b> LC chromatogram of a sample of <b>APNM5</b> treated with cysteine and <b>e)</b> the MS extract of the corresponding peak with the expected m/z value well visible.	44
<b>Scheme 7.</b> Synthesis of the FRET probe <b>F-APNM5</b> of acetal amino-to-thiol linker <b>APNM5</b> .	45
<b>Figure 14.</b> Chromatograms of the preparative HPLC outcome when using <b>a)</b> an acidic mobile phase and <b>b)</b> a neutral mobile phase. All the chemical species are detected by HR/MS and shown in the figure.	46
<b>Figure 15.</b> Hydrolysis profiles of acetals <b>F-APN6</b> and <b>F-APNM5</b> in different concentration of proton at 23°C.	47
<b>Figure 16.</b> Hydrolysis profiles of acetals <b>F-APN6</b> and <b>F-APNM5</b> in three different acidic solution; comparison between 23°C and 37 °C.	48
<b>Figure 17.</b> <b>a)</b> Structure of <b>PEGAM5</b> , the hydrophilic version of acetal model <b>APNM5</b> , and calculated LogP value; <b>b)</b> comparison with FRET acetal <b>F-APNM5</b> structure and estimated LogP value.	49
<b>Figure 18.</b> Calculation of Huckel charges on carbons 1, 2 and 6 of the aromatic ring in four model compounds; positive charges are enlightened in green, negative charges are in orange. Calculations were made with ChemDraw® 3D software. <b>a)</b> Model compound <b>17</b> for APN-acetals conjugated to <b>BHQ-2-SH</b> . This model applied to FRET probes <b>F-APN6</b> and <b>F-APNM5</b> . <b>b)</b> Model compound <b>18</b> for triazole-aryl compounds. This model applies to acetal <b>PEGAM5</b> and to FRET probes <b>F-A2M5</b> and <b>F-A2M6</b> (describe later in section 4 of this chapter, page 44). As comparison, Huckel charges were calculated also for <b>c)</b> trimethyl(phenyl)silane ( <b>19</b> ) and <b>d)</b> fluorobenzene ( <b>20</b> ) to give a comparison of charge values on the aromatic carbons close to respectively an electron-donating group and an electron-withdrawing group.	50
<b>Scheme 8.</b> Synthesis of <b>PEGAM5</b> .	51
<b>Figure 19.</b> HR-ESI-MS chromatogram of isolated <b>PEGAM5</b> . The two peaks correspond to the two stereoisomers obtained.	52
<b>Figure 20.</b> New cyclic acetal linker models <b>A2M5</b> and <b>A2M6</b> .	53
<b>Scheme 9.</b> Synthesis of compounds <b>A2M5</b> and <b>A2M6</b> .	54
<b>Figure 21.</b> HR-ESI-MS chromatograms of isolated compound <b>A2M5</b> ( <b>a</b> ) and <b>A2M6</b> ( <b>b</b> ).	55
<b>Scheme 10.</b> Synthesis of FRET probes <b>F-A2M5</b> and <b>F-A2M6</b> .	56
<b>Figure 22.</b> HR-ESI-MS chromatograms of isolated compound <b>F-A2M5</b> ( <b>a</b> ) and <b>F-A2M6</b> ( <b>b</b> ).	57
<b>Figure 23.</b> Hydrolysis profiles of acetals <b>F-A2M5</b> and <b>F-A2M6</b> in different aqueous solutions in plasma at 23°C.	57
<b>Figure 24.</b> Chemical structure of FRET probes <b>F-Val-Cit</b> and <b>F-amide</b> .	58
<b>Table 1.</b> Cell lines tested for the acetal cleavage.	59
<b>Figure 25.</b> Cell viability of <b>F-amide</b> , <b>F-Val-Cit</b> , <b>F-A2M5</b> and <b>F-A2M6</b> on five cell lines. Two set of data are showed: plain bars indicate the value of fluorescence calculated trough flow cytometry (scale on the left); dots represent the relative cleavability of the new two acetals <b>F-A2M5</b> and <b>F-A2M6</b> with respect to the cleavable probe <b>F-Val-Cit</b> (scale on the	

right). All values are subtracted of the corresponding values obtained from the control (cells incubated only in presence of the media). .....	59
<b>Figure 26.</b> Illustration of the two reaction pathways of the ADC containing the thiosuccinimidyl linkage. In human plasma, the ADC can undergo either thiol exchange with thiol-bearing biomolecules (human serum albumin for example in the figure), or succinimidyl ring-opening, which precludes thiol exchange. ....	62
<b>Figure 27.</b> Molecular structure of <b>MCC</b> and <b>MD</b> and relative LogP values. ....	62
<b>Table 2.</b> Chemical structures of <b>MD</b> and three new amine-to-thiol cross-linkers based on <b>MD</b> . Code names are given on the following base: “ <b>MI</b> ” for “maleimide”, “ <b>A</b> ” for “acetal”, “ <b>5</b> ” or “ <b>6</b> ” for the ring size and “ <b>1</b> ” or “ <b>2</b> ” for the carbon-chain length. So <b>MD</b> will be named also “ <b>MIA6-1</b> ” to help the reader quickly identifying its structural composition. ....	64
<b>Scheme 11.</b> Synthesis of <b>MIA</b> linkers. ....	64
<b>Scheme 12.</b> One-pot three-step synthesis of the FRET probes. ....	66
<b>Figure 28.</b> Stability essay in 1 M HCl aqueous solution (pH<1). ....	67
<b>Figure 29.</b> Ring-opening rate of the succinimidyl ring in PBS for the four probes (50 $\mu$ M solution).....	68
<b>Figure 30.</b> Ring-opening rate of the succinimidyl ring in plasma for the four probes and for <b>F-MCC</b> (1 $\mu$ M solution). ....	70
<b>Figure 31. a)</b> Illustration of thiol-exchange reaction with human serum albumin (HSA). <b>b)</b> HSA bands revealed by Coomassie Blue staining of gel with <b>HF-MIA5-1</b> probe and fluorescence of HSA bands on gel with <b>HF-MIA5-1</b> and <b>F-MIA5-1</b> probes (for a complete illustration, see Experimental Procedures, section 2.4, page 200). <b>c)</b> Analysis of fluorescence intensity reported as percentage of thiol exchange. ....	71
<b>Figure 32.</b> Summary of the investigation on maleimide-acetal linkers for hydrophilicity and stability in acidic media -towards acetal hydrolysis- and in serum towards thiol exchange. ....	72
<b>Table 3.</b> Synopsis of the cyclic acetals investigated. The table includes: denomination; chemical structure (acetal and significant motifs are enlightened in red, fuchsia sphere represents the fluorophore TAMRA and violet spheres represents BHQ-2 quencher); pH in which hydrolysis occurs; hydrophobic or hydrophilic nature of the acetal (with calculated and estimated LogP values) and the contemplated applications. ....	73
<b>Figure 33.</b> Representation of the objectives pursued and achieved. The first band on the left represent the range of pH covered by cells and extracellular environment. The second red band in the centre represents the range of pH covered by the abiotic acid catalyst. The three striped blue bands on the right represent the pH ranges in which the hydrolysis of different abiotic acetal substrates is supposed to be triggered. Plain blue bands represent the pH ranges in which the hydrolysis of the identified acetals actually occurs, with the corresponding chemical structures. Grey faded horizontal bands are used to shows the matching between the pH activity ranges of xenobiotic substrates and the corresponding hydrolysis promoters.....	74
<b>Figure 34.</b> Chemical structure of camphor sulfonic acid (CSA). ....	77
<b>Figure 35.</b> Graph of the hydrolysis of <b>F-APN6</b> in MeOH in the presence of different amount of camphor sulfonic acid.....	78
<b>Table 4.</b> Screening of possible co-solvents. Percentage of hydrolysis is calculated from fluorescence measured after 1h at 37 °C and normalised to the fluorescence given by an equimolar solution of TAMRA and BHQ treated in the same conditions.....	79

<b>Figure 36. a)</b> Legend of the symbol used to describe the efficiency of a catalyst, its interaction with the FRET probe and with the proton concentration of the solvent. <b>b)</b> Representation of the wanted reaction outcome. ....	83
<b>Table 5.</b> Screening of homogeneous acidic catalysts. Reactions were monitored after 3 hours. pH value is determined with a universal indicator a few minutes after the addition of the catalyst, there are no changes in pH after 3 hours. "X" is for "not tested". ....	83
<b>Figure 37.</b> Chemical structure of <b>a) PAASA</b> and <b>b) PAcMA</b> linear polymers. ....	84
<b>Figure 38.</b> Chemical structure of heterogeneous catalysts <b>a) Nafion NR50</b> and <b>b) PAASAcAN</b> . ....	85
<b>Table 6.</b> Screening of commercial heterogeneous catalysts. "X" stands for "not tested". ....	86
<b>Figure 39.</b> Representation of the cationic exchange between the proton of the sulfonic acid and metal ion present in the buffered solutions. ....	87
<b>Table 7.</b> Screening of functionalized silica with FRET probe <b>F-APN6</b> . PMA/SiO <sub>2</sub> (entry 34) and H <sub>2</sub> SO <sub>4</sub> /SiO <sub>2</sub> (entry 37) gave a good level of hydrolysis, unfortunately this was due to leaking of the acid from the support material, as proved by the results obtained after catalyst's washing (entries 35, 36, 38, 39). "X" is for "not tested". ....	88
<b>Table 8.</b> Heterogeneous catalysts provided by Dr. Becht (IS2M, Université Haute-Alsace, Mulhouse). ....	89
<b>Table 9.</b> Screening of synthetic acid catalysts provided by IS2M. ....	90
<b>Figure 40.</b> Representation of the modification of Merrifield resin. <b>MR</b> = Merrifield resin; <b>MR-acid</b> = Merrifield resin functionalized with acid. ....	90
<b>Figure 41.</b> Chemical structures of Merrifield resin modified with <b>a) H<sub>2</sub>SO<sub>4</sub></b> , <b>b) H<sub>3</sub>PO<sub>4</sub></b> , <b>c) citric acid</b> , <b>d) PAASA</b> and <b>PAASAcAN</b> . ....	91
<b>Table 10.</b> Screening of modified Merrifield resins. ....	91
<b>Table 11.</b> Recall of the acidic catalysts who showed good hydrolysis in water and PBS. ....	92
<b>Table 12.</b> Comparison between Amberlyst A-15 and Nafion NR50. ....	94
<b>Figure 42. a)</b> Adsorption profiles of Nafion NR50 and Amberlyst A-15 by means of fluorescence emitted by TAMRA remained in solution. <b>b)</b> Pictures of the samples taken at t = 0, t = 2 minutes and t = 3 hours under artificial light and at t = 3 hours under UV light (using a laboratory UV lamp). The vials are identified by coloured dots. Blue and light blue dots identify Amberlyst A15 samples, red and orange dots identify Nafion NR50 samples. ....	95
<b>Figure 43.</b> Pictures of Nafion NR50 and Amberlyst A15 in the releasing solvent mixture at t = 0 (under artificial light) and at t = 5 hours (under artificial and UV light). Vials are identified by coloured dots according to the legend. ....	97
<b>Table 13.</b> Fluorescence values measured after 24 hours are reported as percentage of the positive control (equimolar solution of <b>TAMRA</b> and <b>BHQ</b> in 1 mL of the releasing solvent mixture. Ratio between the values of <b>TAMRA+BHQ</b> and <b>F-APNM5</b> are reported. ....	98
<b>Table 14.</b> List of solutions used to build the calibration curve. For each solution, a Nafion bead was added and let to soak all the TAMRA and BHQ (37 °C, agitation, 15 minutes), then analysed. ....	99
<b>Figure 44.</b> Sample of images taken at the UV transilluminator. Beads are identified by the corresponding percentage of conversion. Colour is modified according to the intensity (red = high intensity, blue = low intensity). ....	99
<b>Figure 45.</b> Calibration curve built with the aid of UV transilluminator. ....	100
<b>Figure 46.</b> Confocal laser scanning microscopy applied on Nafion beads. The microscope records images of the bead by scanning it at different depths ( <b>z</b> dimension). The grey area	

represent the external part of the bead, the core is not scanned by the microscope because of the bead dimension. ....	102
<b>Figure 47.</b> Images of Nafion beads soaked with solutions of TAMRA and BHQ at different concentrations. The colour code applied highlights the saturated areas. ....	102
<b>Figure 39.</b> Representation of the cationic exchange between the proton of the sulfonic acid and metal ion present in the buffered solutions. ....	104
<b>Figure 48.</b> Representation of possible scenarios of acetal hydrolysis triggered by three different Nafion beads: <b>a)</b> commercial or not washed enough, <b>b)</b> partially neutralized (ideal-washing) and <b>c)</b> almost completely neutralized (over-washing). ....	105
<b>Figure 49.</b> Schematic representation of the three different methods employed for the pre-treatment of Nafion beads. ....	106
<b>Figure 50. a)</b> Legend of the symbols used to represent the pH of the reaction media and the hydrolysis (= fluorescence) at given times. <b>b)</b> Symbol of the ideal reaction outcome. <b>c)</b> Examples of fluorescence emission level detected under UV lamp related to the corresponding symbol. ....	106
<b>Table 15.</b> Screening of washing procedures of Nafion – Method A. Fluorescence of the bead is checked under UV light at t = 3h, 24h. pH is checked with pH paper at t = 3h. “X” is for “not tested”. ....	107
<b>Table 16.</b> Screening of washing procedures of Nafion – Method B. Fluorescence of the bead is checked under UV light at t = 3h, 24h. pH is checked with pH paper at t = 3h. “X” is for “not tested”. ....	108
<b>Table 17.</b> Screening of washing procedures of Nafion – Method C. Fluorescence of the bead is checked under UV light at t = 3h, 24h. pH is checked with pH paper at t = 3h. “X” is for “not tested”. ....	109
<b>Figure 51.</b> Photos of Nafion beads used in the hydrolysis of acetal <b>F-APNM5</b> (cf. <b>Table 17</b> , entries 20-24). Nafion beads are pre-washed with a PBS solution diluted 10 times for different amount of time (Method C). Pictures are taken under a UV lamp at given reaction times. ....	111
<b>Figure 52. a)</b> Nafion-120 and <b>b)</b> Nafion-90 analysed at confocal microscope after 24 hours reaction with <b>F-APNM5</b> in plasma. <b>c)</b> Fluorescence intensity of the whole images measured with ImageJ®. ....	111
<b>Table 18.</b> Different types of acidic resin Nafion. ....	113
<b>Table 19.</b> Hydrolysis of FRET acetal <b>F-APNM5</b> in plasma carried out by different forms of Nafion. Conditions: [substrate] = 10 $\mu$ M, T = 37 $^{\circ}$ C, V = 0.3 mL, t = 24 hours. pH is measured at t = 3 h (pH paper). ....	113
<b>Figure 53. a)</b> Hydrolysis reaction of <b>PEGAM5</b> . Of the two products, only the aldehyde is visible at the LC-MS, the diol does not adsorbe at 254 nm. <b>b)</b> Calibration curves for the starting material ( <b>SM</b> ) and the product ( <b>P</b> ). <b>c)</b> Hydrolysis reaction of <b>PEGAM5</b> catalyzed by pre-treated Nafion and control ( <b>Ctrl</b> ). ....	115
<b>Figure 54. a)</b> Synthesis and photo of <b>PEG-PAASA</b> film: polymerization of PEG-acrylate with encapsulation of <b>PAASA</b> within the matrix. <b>b)</b> Synthesis and photo of the co-polymer <b>PEG-AASA</b> . ....	118
<b>Table 20.</b> Test of the different compositions of <b>PEG-PAASA</b> and <b>PEG-AASA</b> . The composition giving the highest yield is enlightened in red. pH of the solution is measured after 24 hours with pH paper. ....	119
<b>Table 21.</b> Test of different amount of PEG-AASA-20% in form of beads with acetal <b>F-APNM5</b> . pH of the solution is measured after 24 hours with pH paper. ....	121



<b>Table 22.</b> Test of PEG-AASA-20% in form of film and beads with the cleavable hydrophobic probes <b>F-A2M5</b> and <b>F-A2M6</b> . Results obtained with the more stable <b>F-APNM5</b> are listed as comparison. ....	122
<b>Table 23.</b> Reaction condition for <b>PEGAM5</b> hydrolysis carried out by PEG-AASA beads. ....	123
<b>Figure 55.</b> <b>a)</b> Hydrolysis reaction of <b>PEGAM5 (SM)</b> gives aldehyde <b>36 (P)</b> and diol <b>37</b> as products. <b>b)</b> Calibration curves for the starting material ( <b>SM</b> ) and the aldehyde product ( <b>P</b> ) of the reaction in plasma. <b>c)</b> Negative control: no auto-hydrolysis is detected over 7 days. <b>d)</b> Acetal hydrolysis with PEG-AASA beads in different conditions. ....	124
<b>Figure 56.</b> A fast, qualitative proof of Nafion's acidity in buffered media. <b>a)</b> Commercial Nafion in a PBS solution. The cationic exchange kills the buffer within minutes. <b>b)</b> Washed Nafion in a PBS solution. The buffer is maintained while the bead keeps its acidity (light red colour). The solution remains the same even after months. ....	126
<b>Figure 46.</b> Confocal laser scanning microscopy applied on Nafion beads. The microscope records images of the bead by scanning it at different depths (z dimension). Given the bead's dimension it is possible to take image of only a portion. ....	127
<b>Figure 57.</b> <b>DDXC</b> probe keto-enol tautomerization, with excitation and emission wavelengths. ....	128
<b>Figure 58.</b> <b>a)</b> Emission spectra recorded with a UV spectrophotometer at excitation wavelength of 400 nm. The arrows indicate the change in relation to the pH. <b>b)</b> The ratio between the emission at 512 nm and at 580 nm are plotted in function of the pH. The graph can be used to determine the pH of a solution by extrapolation. <b>c)</b> <b>DDXC</b> probe dissolved in aqueous solution of pH = 1; 3; 5; 7.4. Pictures are taken under artificial and UV light to show the change in colour related to the proton concentration. ....	129
<b>Figure 59.</b> Above: confocal microscope settings for excitation (laser at 405 nm) and emission (two channels at 512±10 and 580±10). Below: merged images of <b>DDXC</b> solutions' drop from acidic pH < 1 (on the left end) to pH = 5 (on the right end). ....	130
<b>Figure 60.</b> <b>a)</b> Processed images of <b>DDXC</b> solutions' drops. The colour is in function of the ratio between the intensities of fluorescence recorded at 512 nm and 580 nm. <b>b)</b> Graph of the population of each image according to the value of the ratio. The value of ratio corresponding to the maximum incidence is attributed at the corresponding value of pH, allowing to build the calibration curve. <b>c)</b> Calibration curve obtained with the confocal microscope, compared to the one obtained with the spectrophotometer (Cf. <b>Figure 58</b> ). <b>d)</b> Colour scale in function of the ratio $Em_{512}/Em_{580}$ and of the corresponding pH values. ....	131
<b>Figure 61.</b> Confocal microscopy images of Nafion soaked with <b>DDXC</b> expected with <b>a)</b> commercial untreated acidic Nafion, <b>b)</b> neutralized Nafion and <b>c)</b> partially deactivated Nafion-90 keeping inner acidity. pH colour scale is the same derived from the processed images of <b>DDXC</b> at different pHs (Cf. <b>Figure 60</b> ). ....	132
<b>Figure 62.</b> Ratiometric images of commercial Nafion NR50. Colour code is represented both as in function of the ratio and of the pH. ....	132
<b>Figure 63.</b> Ratiometric images of Nafion NR50 washed for 30, 60, and 90 minutes. Colour code is represented both as in function of the ratio and of the pH. ....	133
<b>Figure 64.</b> Ratiometric images of Nafion NR50 washed for 120 minutes. Colour code is represented both as in function of the ratio and of the pH. ....	134
<b>Figure 65.</b> Graph of the ratio intensities of different Nafion beads. The maxima correspond to a value of ratio which is directly correlated to the proton concentration (Cf. <b>Figure 60</b> ). ....	134
<b>Table 24.</b> Acidity of solid catalyst Nafion NR50 according to the ratiometric analysis. ....	135

<b>Figure 66.</b> Nafion NR50 - CH and POWDion™ 40-60 mesh soaked with DDXC and analysed at confocal microscope; the graph shows the ratiometric distribution and extrapolated pH values.....	135
<b>Figure 67.</b> POWDion™ 40-60 mesh SOL. and POWDion™ 200 mesh SOL. soaked with DDXC and analysed at confocal microscope; ratiometric distribution and extrapolated pH values.....	136
<b>Figure 68.</b> Ratiometric images, ratio distribution and extrapolated pH value for PEG-AASA beads not washed (first two images) and quickly washed in plasma (last two images). .....	137
<b>Figure 69.</b> Ratiometric images, ratio distribution and extrapolated pH value for PEG-AASA beads washed in plasma for 30 minutes.....	138
<b>Figure 2.</b> Representation of the four possible scenarios given by the combination of the substrate and the solid catalyst. Hydrophobic catalyst is symbolized by a sphere with a plain contour, while the hydrophilic catalyst's symbol has a dotted contour. The substrate and the product are represented as, respectively, blue and green dots. Dots are plain for the hydrophobic substrate and striped for the hydrophilic one. <b>a)</b> Hydrophobic substrate + hydrophobic catalysts; <b>b)</b> hydrophobic substrate + hydrophilic catalysts; <b>c)</b> hydrophilic substrate + hydrophobic catalyst and <b>d)</b> hydrophilic substrate + hydrophilic catalyst. ....	139
<b>Table 25.</b> Condensed collection of results obtained by treating acetals F-APNM5 and PEGAM5 in plasma with heterogeneous catalysts Nafion-90 and PEG-AASA-20% (in form of film and beads). Entries in which the hydrophobic or hydrophilic nature of the substrate and the catalyst matches are enlightened in grey. ....	140
<b>Figure 70.</b> <b>a)</b> biological pH values; <b>b)</b> pH ranges of hydrolytic activity of commercial and pre-treated Nafion NR50 related to the pH range of F-APNM5 cleavability; <b>c)</b> pH ranges of hydrolytic activity of PEG-AASA-20% washed and not-washed related to the pH range of PEGAM5 cleavability. ....	141
<b>Figure 71.</b> <b>a)</b> Nafion-hFGF and <b>b)</b> Nafion-90 analysed at confocal microscope after 24 hours reaction with F-APNM5 in plasma. <b>c)</b> Fluorescence intensity of the whole images measured with ImageJ®. ....	146
<b>Table 26.</b> List of the planned experiments. Each entry line corresponds to one kind of experiment (to be reproduced in triplicates) and displays if the catalyst is implanted (marked with X) and which chemical is injected into the mice (marked with X). ....	147
<b>Figure 72.</b> Chemical structure of Abiraterone.....	155
<b>Figure 73.</b> Chemical structure of Octeotride.....	155
<b>Figure 74.</b> Chemical structure of Paclitaxel.....	156
<b>Figure 75.</b> Chemical structure of Topotecan.....	156
<b>Figure 76.</b> Chemical structure of Vinblastine.....	157
<b>Figure 77.</b> Chemical structure of Leuprorelin.....	157
<b>Figure 78.</b> Chemical structure of Salinomycin.....	158
<b>Figure 79.</b> Chemical structure of Temsirolimus.....	158
<b>Table 27.</b> HR-MS Analysis outcome of Paclitaxel and obtained Paclitaxel isomer.....	159
<b>Figure 80.</b> NMR spectra of Paclitaxel (in green) and its isomer (in red), with an interesting region enlightened (ppm 3,4 - 4,35). ....	159
<b>Figure 81.</b> Chemical structure of 7-epi-paclitaxel.....	160
<b>Figure 82.</b> Selection of chromatograms of cytotoxic drugs. Vinblastine in DMSO shows degradation with increasing temperature, so procedures in DMSO at >70°C are discouraged. Abiraterone in the same solvent is stable even at 120°C. ....	161
<b>Figure 83.</b> Selection of chromatograms of cytotoxic drugs. The appearance of new interesting peaks is observed with Topotecan in both water and DMSO: profile changes	



remarkably with increasing temperature. For all the obtained chromatograms, see Experimental Procedures, section 6.1, page 210) .....	162
<b>Figure 84.</b> Final overview of the thesis work. The different scenarios hypothesized in the introduction are depicted and related to a pH scale (in the centre up part of the image). Xenobiotics are depicted as the acetal linker bearing two star-symbols (colour of the star is random), unless otherwise specified. The abiotic solid catalyst is depicted as a plain form. The colour of the catalyst, extracellular environment and cell's compartments corresponds to their pH value, according to the pH scale in the centre. Confocal ratiometric images of Nafion-90 and PEG-AASA-20% are also inserted. ....	167
<b>Figure EP 2.</b> HR-ESI-MS chromatogram of <b>F-APN6</b> .....	202
<b>Figure EP 8.</b> Profile of FRET probes <b>F-MIA5-1</b> , <b>F-MIA5-2</b> , <b>F-MIA6-1</b> and <b>F-MIA6-2</b> stability at different pH. ....	218

## REFERENCES

1. Sletten, E. M. & Bertozzi, C. R. Bioorthogonal Chemistry: Fishing for Selectivity in a Sea of Functionality. *Angew. Chemie Int. Ed.* **48**, 6974–6998 (2009).
2. Bertozzi, C. R. & Wu, P. In vivo chemistry. *Curr. Opin. Chem. Biol.* **17**, 717–718 (2013).
3. Shieh, P. & Bertozzi, C. R. Design strategies for bioorthogonal smart probes. *Org. Biomol. Chem.* **12**, 9307–9320 (2014).
4. Mejia Oneto, J. M., Khan, I., Seebald, L. & Royzen, M. In Vivo Bioorthogonal Chemistry Enables Local Hydrogel and Systemic Pro-Drug To Treat Soft Tissue Sarcoma. *ACS Cent. Sci.* **2**, 476–482 (2016).
5. Ursuegui, S., Recher, M., Krężel, W. & Wagner, A. An in vivo strategy to counteract post-administration anticoagulant activity of azido-Warfarin. *Nat. Commun.* **8**, 15242 (2017).
6. Tsuji, J. *Transition Metal Reagents and Catalysts: Innovations in Organic Synthesis*. (John Wiley & Sons, 2003). doi:10.1002/0470854766
7. Sasmal, P. K., Streu, C. N. & Meggers, E. Metal complex catalysis in living biological systems. *Chem. Commun.* **49**, 1581–1587 (2013).
8. Yusop, R. M., Unciti-Broceta, A., Johansson, E. M. V., Sánchez-Martín, R. M. & Bradley, M. Palladium-mediated intracellular chemistry. *Nat. Chem.* **3**, 241–245 (2011).
9. Chankeshwara, S. V., Indrigo, E. & Bradley, M. Palladium-mediated chemistry in living cells. *Curr. Opin. Chem. Biol.* **21**, 128–135 (2014).
10. Yang, M., Li, J., Chen, P. R., Maiyun Yang, J. L. and P. R. C. & Considerable. Transition metal-mediated bioorthogonal protein chemistry in living cells. *Chem. Soc. Rev.* **43**, 6511–6526 (2014).
11. Völker, T. & Meggers, E. Transition-metal-mediated uncaging in living human cells—an emerging alternative to photolabile protecting groups. *Curr. Opin. Chem. Biol.* **25**, 48–54 (2015).
12. Weiss, J. T. *et al.* Extracellular palladium-catalysed dealkylation of 5-fluoro-1-propargyl-uracil as a bioorthogonally activated prodrug approach. *Nat. Commun.* **5**, 3277 (2014).
13. Miller, M. A. *et al.* Nano-palladium is a cellular catalyst for in vivo chemistry. *Nat. Commun.* **8**, 15906–12919 (2017).
14. Tsubokura, K. *et al.* In Vivo Gold Complex Catalysis within Live Mice. *Angew. Chemie Int. Ed.* **56**, 3579–3584 (2017).
15. Rebelein, J. G. & Ward, T. R. In vivo catalyzed new-to-nature reactions. *Curr. Opin. Biotechnol.* **53**, 106–114 (2018).
16. Lin, H., Chen, Y. & Shi, J. Nanoparticle-triggered in situ catalytic chemical reactions for tumour-specific therapy. *Chem. Soc. Rev.* **47**, 1938–1958 (2018).
17. Vidal, C., Tomás-Gamasa, M., Destito, P., López, F. & Mascareñas, J. L. Concurrent and orthogonal gold(I) and ruthenium(II) catalysis inside living cells. *Nat. Commun.* **9**, 1913 (2018).
18. Nelson, D. L. & Cox, M. M. *Lehninger Principles of Biochemistry*. (W. H. Freeman, 2017).
19. Casey, J. R., Grinstein, S. & Orłowski, J. Sensors and regulators of intracellular pH. *Nat. Rev. Mol. Cell Biol.* **11**, 50–61 (2009).
20. Leriche, G., Chisholm, L. & Wagner, A. Cleavable linkers in chemical biology. *Bioorg. Med. Chem.* **20**, 571–582 (2012).
21. Gillies, E. R., Goodwin, A. P. & Fréchet, J. M. J. Acetals as pH-Sensitive Linkages for Drug Delivery. *Bioconjug. Chem.* **15**, 1254–1263 (2004).
22. Lee, S., Wang, W., Lee, Y. & Sampson, N. S. Cyclic acetals as cleavable linkers for affinity capture. *Org. Biomol. Chem.* **13**, 8445–8452 (2015).
23. Tamura, T. & Hamachi, I. Chemistry for Covalent Modification of Endogenous/Native Proteins: From Test Tubes to Complex Biological Systems. *J. Am. Chem. Soc.* (2018). doi:10.1021/jacs.8b11747
24. Skoog, D. A., Crouch, S. R. & Holler, F. J. *Principles of Instrumental Analysis*. (Cengage

- Learning US, 2017).
25. Valeur, B. & Berberan-Santos, M. N. *Molecular Fluorescence: Principles and Applications*. (Wiley-VCH Verlag GmbH & Co. KGaA, 2012). doi:10.1002/9783527650002
  26. Förster, T. Zwischenmolekulare Energiewanderung und Fluoreszenz. *Ann. Phys.* **437**, 55–75 (1948).
  27. Selvin, P. R. Fluorescence resonance energy transfer. *Methods Enzymol.* **246**, 300–34 (1995).
  28. Griep, M. H. *et al.* Förster Resonance Energy Transfer between Core/Shell Quantum Dots and Bacteriorhodopsin. *Mol. Biol. Int.* **2012**, 1–7 (2012).
  29. Kotresh, M. G. Fluorescence and Laser Spectroscopic Investigation of Nanoparticles. (Karnatak University, 2018).
  30. Lakowicz, J. R. *Principles of Fluorescence Spectroscopy*. (Springer US, 2006). doi:10.1007/978-0-387-46312-4
  31. Bird, A. Fluorescence Resonance Energy Transfer (FRET) systems for biomedical sensor applications. (Dublin City University, 2010).
  32. Lee, L., Johnston, A. P. R. R. & Caruso, F. Probing the Dynamic Nature of DNA Multilayer Films Using Förster Resonance Energy Transfer. *Langmuir* **28**, 12527–12535 (2012).
  33. Hermanson, G. T. *Bioconjugate Techniques*. (Academic Press, Elsevier, 2008).
  34. Koniev, O. *et al.* Selective Irreversible Chemical Tagging of Cysteine with 3-Arylpropionitriles. *Bioconjug. Chem.* **25**, 202–206 (2014).
  35. Jacques, S. A. *et al.* From solution to in-cell study of the chemical reactivity of acid sensitive functional groups: a rational approach towards improved cleavable linkers for biospecific endosomal release. *Org. Biomol. Chem.* **14**, 4794–4803 (2016).
  36. Koniev, O. *et al.* Selective Irreversible Chemical Tagging of Cysteine with 3-Arylpropionitriles. 202–206 (2014). doi:10.1021/bc400469d
  37. Okamoto, K., Watanabe, M., Sakata, N., Murai, M. & Ohe, K. Copper-Catalyzed C–H Cyanation of Terminal Alkynes with Cyanogen Iodide. *Org. Lett.* **15**, 5810–5813 (2013).
  38. Li, Y. *et al.* Copper mediated oxidative coupling between terminal alkynes and CuCN. *Tetrahedron Lett.* **56**, 390–392 (2015).
  39. Rong, G., Mao, J., Zheng, Y., Yao, R. & Xu, X. Cu-Catalyzed direct cyanation of terminal alkynes with AMBN or AIBN as the cyanation reagent. *Chem. Commun.* **51**, 13822–13825 (2015).
  40. Montalbetti, C. A. G. N. & Falque, V. Amide bond formation and peptide coupling. *Tetrahedron* **61**, 10827–10852 (2005).
  41. Chintareddy, V. R., Wadhwa, K. & Verkade, J. G. Tetrabutylammonium Fluoride (TBAF)-Catalyzed Addition of Substituted Trialkylsilylalkynes to Aldehydes, Ketones, and Trifluoromethyl Ketones. *J. Org. Chem.* **76**, 4482–4488 (2011).
  42. Francisco, J. A. *et al.* cAC10-vcMMAE, an anti-CD30-monomethyl auristatin E conjugate with potent and selective antitumor activity. *Blood* **102**, 1458–1465 (2003).
  43. Tsuchikama, K. & An, Z. Antibody-drug conjugates: recent advances in conjugation and linker chemistries. *Protein Cell* **9**, 33–46 (2018).
  44. Dovgan, I., Kolodych, S., Koniev, O. & Wagner, A. 2-(Maleimidomethyl)-1,3-Dioxanes (MD): a Serum-Stable Self-hydrolysable Hydrophilic Alternative to Classical Maleimide Conjugation. *Sci. Rep.* **6**, 2–7 (2016).
  45. Tobaldi, E., Dovgan, I., Mosser, M., Becht, J.-M. & Wagner, A. Structural investigation of cyclo-dioxo maleimide cross-linkers for acid and serum stability. *Org. Biomol. Chem.* **15**, 9305–9310 (2017).
  46. Peterson, E. C. *et al.* Simple Radiometric Method for Accurately Quantitating Epitope Densities of Hapten–Protein Conjugates with Sulfhydryl Linkages. *Bioconjug. Chem.* **25**, 2112–2115 (2014).
  47. Hambuchen, M. D. *et al.* Combining Active Immunization with Monoclonal Antibody Therapy To Facilitate Early Initiation of a Long-Acting Anti-Methamphetamine Antibody Response. *J. Med. Chem.* **58**, 4665–4677 (2015).

48. Zhao, Z. *et al.* Engineering of a hybrid nanoparticle-based nicotine nanovaccine as a next-generation immunotherapeutic strategy against nicotine addiction: A focus on hapten density. *Biomaterials* **123**, 107–117 (2017).
49. Jones, D. S. *et al.* A Method for Producing Protein Nanoparticles with Applications in Vaccines. *PLoS One* **11**, 10.1371/journal.pone.0138761 (2016).
50. Richards, D. A., Maruani, A. & Chudasama, V. Antibody fragments as nanoparticle targeting ligands: a step in the right direction. *Chem. Sci.* **00**, 1–15 (2016).
51. Koniev, O. *et al.* MAPN: First-in-class reagent for kinetically resolved thiol-to-thiol conjugation. *Bioconjug. Chem.* **26**, 1863–1867 (2015).
52. Beck, A., Goetsch, L., Dumontet, C. & Corvaia, N. Strategies and challenges for the next generation of antibody–drug conjugates. *Nat. Publ. Gr.* **16**, 315–337 (2017).
53. Niculescu-Duvaz, I. Trastuzumab emtansine, an antibody-drug conjugate for the treatment of HER2+ metastatic breast cancer. *Curr. Opin. Mol. Ther.* **12**, 350–60 (2010).
54. Shen, B. *et al.* Conjugation site modulates the in vivo stability and therapeutic activity of antibody-drug conjugates. *Nat. Biotechnol.* **30**, 184–189 (2012).
55. Chudasama, V. L. *et al.* Semi-mechanistic Population Pharmacokinetic Model of Multivalent Trastuzumab Emtansine in Patients with Metastatic Breast cancer. *Clin. Pharmacol. Ther.* **92**, 520–527 (2012).
56. Ponte, J. F. *et al.* Understanding How the Stability of the Thiol-Maleimide Linkage Impacts the Pharmacokinetics of Lysine-Linked Antibody – Maytansinoid Conjugates. *Bioconjug. Chem.* **27**, 1588–1598 (2016).
57. Baldwin, A. D. & Kiick, K. L. Tunable degradation of maleimide-Thiol adducts in reducing environments. *Bioconjug. Chem.* **22**, 1946–1953 (2011).
58. Fontaine, S. D., Reid, R., Robinson, L., Ashley, G. W. & Santi, D. V. Long-term stabilization of maleimide-thiol conjugates. *Bioconjug. Chem.* **26**, 145–152 (2015).
59. Tan, X. *et al.* Hydrolytic degradation of N,N'-ethylenedimaleimide: Crystal structures of key intermediates and proposed mechanisms. *J. Mol. Struct.* **1125**, 514–521 (2016).
60. Lyon, R. P. P. *et al.* Self-hydrolyzing maleimides improve the stability and pharmacological properties of antibody-drug conjugates. *Nat. Biotechnol.* **30**, 1–7 (2014).
61. Tumey, L. N. *et al.* Mild Method for Succinimide Hydrolysis on ADCs: Impact on ADC Potency, Stability, Exposure, and Efficacy. *Bioconjug. Chem.* **25**, 1871–1880 (2014).
62. Fife, H., California, S. & Angeles, L. Steric Effects in Ketal Hydrolysis. *J. Org. Chem.* **31**, 1772–1775 (1966).
63. Liu, B. & Thayumanavan, S. Substituent Effects on the pH Sensitivity of Acetals and Ketals and Their Correlation with Encapsulation Stability in Polymeric Nanogels. *J. Am. Chem. Soc.* **139**, 2306–2317 (2017).
64. Rzepa, H. How to stop (some) acetals hydrolysing. Available at: <http://www.ch.imperial.ac.uk/rzepa/blog/?p=14740>.
65. Knowles, J. P. & Whiting, A. The Effects of Ring Size and Substituents on the Rates of Acid-Catalysed Hydrolysis of Five- and Six-Membered Ring Cyclic Ketone Acetals. *European J. Org. Chem.* **2007**, 3365–3368 (2007).
66. Beller, M., Renken, A. & van Santen, R. A. *Catalysis: From Principles to Applications*. (Wiley-VCH, 2012).
67. Horie, K. *et al.* Definitions of terms relating to reactions of polymers and to functional polymeric materials (IUPAC Recommendations 2003). *Pure Appl. Chem.* **76**, 889–906 (2004).
68. Anastas, P. T. & Warner, J. C. *Green Chemistry: Theory and Practice*. (Oxford University Press, 2000).
69. Kumar, P. S., Kumar, G. D. K. & Baskaran, S. Truly catalytic and chemoselective cleavage of benzylidene acetal with phosphomolybdic acid supported on silica gel. *European J. Org. Chem.* 6063–6067 (2008). doi:10.1002/ejoc.200800963
70. Mirjalili, B. B. F., Zolfigol, M. A. & Bamoniri, A. Deprotection of acetals and ketals by silica sulfuric acid and wet SiO<sub>2</sub>. *Molecules* **7**, 751–755 (2002).

71. Mirjalili, B. B. F., Zolfigol, M. A., Bamoniri, A. & Hazar, A. Acetalization of carbonyl compounds by using silica-bound sulfuric acid under green condition. *Bull. Korean Chem. Soc.* **25**, 865–868 (2004).
72. Agarwal, A. & Vankar, Y. D. Selective deprotection of terminal isopropylidene acetals and trityl ethers using HClO<sub>4</sub> supported on silica gel. *Carbohydr. Res.* **340**, 1661–1667 (2005).
73. Agnihotri, G. & Misra, A. K. Mild and efficient method for the cleavage of benzylidene acetals using HClO<sub>4</sub>-SiO<sub>2</sub> and direct conversion of acetals to acetates. *Tetrahedron Lett.* **47**, 3653–3658 (2006).
74. Kumar, R., Kumar, D. & Chakraborti, A. Perchloric Acid Adsorbed on Silica Gel (HClO<sub>4</sub>·4-SiO<sub>2</sub>) as an Inexpensive, Extremely Efficient, and Reusable Dual Catalyst System for Acetal/Ketal Formation and Their Deprotection to Aldehydes/Ketones. *Synthesis (Stuttg.)* **2007**, 299–303 (2007).
75. Khan, A. U., Alam, M. & Lee, D.-U. A bench-top catalyst: BF<sub>3</sub>·SiO<sub>2</sub>-assisted synthesis, biological assay, and computational simulations of azacholestanes. *Appl. Biol. Chem.* **59**, 117–127 (2016).
76. Figueiredo, J. ., Pereira, M. F. ., Freitas, M. M. . & Órfão, J. J. . Modification of the surface chemistry of activated carbons. *Carbon N. Y.* **37**, 1379–1389 (1999).
77. Vaino, A. R. & Janda, K. D. Solid-Phase Organic Synthesis: A Critical Understanding of the Resin. *J. Comb. Chem.* **2**, 579–596 (2000).
78. Merrifield, R. B. in *Advances in Enzymology - and Related Areas of Molecular Biology*, volume 32 (ed. Nord, F. F.) 221–296 (John Wiley & Sons, 2006). doi:10.1002/9780470122778.ch6
79. Harmer, M. A. & Sun, Q. Solid acid catalysis using ion-exchange resins. *Appl. Catal. A Gen.* **221**, 45–62 (2001).
80. Scott, R. H. & Balasubramanian, S. Properties of fluorophores on solid phase resins; implications for screening, encoding and reaction monitoring. *Bioorg. Med. Chem. Lett.* **7**, 1567–1572 (1997).
81. Minsky, M. Memoir on Inventing the Confocal Scanning Microscope. *Scanning* **10**, 128–138 (1988).
82. Pawley, J. *Handbook of Biological Confocal Microscopy*. (Springer US, 2010).
83. Cavanagh, H. D., Petroll, W. M. & Jester, J. V. The application of confocal microscopy to the study of living systems. *Neurosci. Biobehav. Rev.* **17**, 483–98 (1993).
84. Rajadhyaksha, M., Grossman, M., Esterowitz, D., Webb, R. H. & Anderson, R. R. In vivo confocal scanning laser microscopy of human skin: Melanin provides strong contrast. *J. Invest. Dermatol.* **104**, 946–952 (1995).
85. Gombotz, W. R. & Wee, S. F. Protein release from alginate matrices. *Adv. Drug Deliv. Rev.* **31**, 267–285 (1998).
86. Nokhodchi, A. & Tailor, A. In situ cross-linking of sodium alginate with calcium and aluminum ions to sustain the release of theophylline from polymeric matrices. *Farmaco* **59**, 999–1004 (2004).
87. Machado, A. H. E. *et al.* Encapsulation of DNA in macroscopic and nanosized calcium alginate gel particles. *Langmuir* **29**, 15926–15935 (2013).
88. Working, P. K., Newman, M. S., Johnson, J. & Cornacoff, J. B. in *Poly(ethylene glycol) Chemistry and Biological Applications* (eds. Harris, J. M. & Zalipsky, S.) **680**, 45–57 (American Chemical Society, 1997).
89. Kadajji, V. G. & Betageri, G. V. Water Soluble Polymers for Pharmaceutical Applications. *Polymers (Basel)*. **3**, 1972–2009 (2011).
90. Jang, H.-J., Shin, C. Y. & Kim, K.-B. Safety Evaluation of Polyethylene Glycol (PEG) Compounds for Cosmetic Use. *Toxicol. Res.* **31**, 105–136 (2015).
91. Grillo-Hill, B. K., Webb, B. A. & Barber, D. L. in *Methods in Cell Biology* 429–448 (Elsevier, 2014). doi:10.1016/B978-0-12-420138-5.00023-9
92. Lee, M. H., Kim, J. S. & Sessler, J. L. Small molecule-based ratiometric fluorescence probes for cations, anions, and biomolecules. *Chem. Soc. Rev.* **44**, 4185–4191 (2015).



93. Charier, S. *et al.* An Efficient Fluorescent Probe for Ratiometric pH Measurements in Aqueous Solutions. *Angew. Chemie Int. Ed.* **43**, 4785–4788 (2004).
94. Chao, J. *et al.* A ratiometric pH probe for intracellular pH imaging. *Sensors Actuators B Chem.* **221**, 427–433 (2015).
95. Niu, W. *et al.* Ratiometric Emission Fluorescent pH Probe for Imaging of Living Cells in Extreme Acidity. *Anal. Chem.* **87**, 2788–2793 (2015).
96. Tong, Z.-X. *et al.* A ratiometric fluorescent pH probe based on keto–enol tautomerization for imaging of living cells in extreme acidity. *Analyst* **142**, 3906–3912 (2017).
97. Stegmann, T. J. New Approaches to Coronary Heart Disease. *BioDrugs* **11**, 301–308 (1999).
98. Galloway, W. R. J. D., Isidro-Llobet, A. & Spring, D. R. Diversity-oriented synthesis as a tool for the discovery of novel biologically active small molecules. *Nat. Commun.* **1**, 1–13 (2010).
99. Hajduk, P. J., Galloway, W. R. J. D. & Spring, D. R. Drug discovery: A question of library design. *Nature* **470**, 42–43 (2011).
100. Erlanson, D. A. in 1–32 (2011). doi:10.1007/128\_2011\_180
101. Herrmann, A. Dynamic combinatorial/covalent chemistry: a tool to read, generate and modulate the bioactivity of compounds and compound mixtures. *Chem. Soc. Rev.* **43**, 1899–1933 (2014).
102. Li, J. W.-H. & Vederas, J. C. Drug Discovery and Natural Products: End of an Era or an Endless Frontier? *Science (80-. )*. **325**, 161–165 (2009).
103. Newman, D. J. & Cragg, G. M. Natural Products as Sources of New Drugs from 1981 to 2014. *J. Nat. Prod.* **79**, 629–661 (2016).
104. Godula, K. C-H Bond Functionalization in Complex Organic Synthesis. *Science (80-. )*. **312**, 67–72 (2006).
105. Dai, H.-X., Stepan, A. F., Plummer, M. S., Zhang, Y.-H. & Yu, J.-Q. Divergent C-H Functionalizations Directed by Sulfonamide Pharmacophores: Late-Stage Diversification as a Tool for Drug Discovery. *J. Am. Chem. Soc.* **133**, 7222–7228 (2011).
106. Abid Masood, M. *et al.* Lead diversification. Application to existing drug molecules: Mifepristone 1 and antalarmin 8. *Bioorg. Med. Chem. Lett.* **22**, 723–728 (2012).
107. Wencel-Delord, J. & Glorius, F. C-H bond activation enables the rapid construction and late-stage diversification of functional molecules. *Nat. Chem.* **5**, 369–375 (2013).
108. Jorgensen, L. *et al.* 14-Step Synthesis of (+)-Ingenol from (+)-3-Carene. *Science (80-. )*. **341**, 878–882 (2013).
109. White, K. L. & Movassaghi, M. Concise Total Syntheses of (+)-Haplocidine and (+)-Haplocine via Late-Stage Oxidation of (+)-Fendleridine Derivatives. *J. Am. Chem. Soc.* **138**, 11383–11389 (2016).
110. Blizzard, T. A. *et al.* Chemical modification of paraherquamide. 1. Unusual reactions and absolute stereochemistry. *J. Org. Chem.* **54**, 2657–2663 (1989).
111. Fier, P. S. & Hartwig, J. F. Synthesis and late-stage functionalization of complex molecules through C-H fluorination and nucleophilic aromatic substitution. *J. Am. Chem. Soc.* **136**, 10139–47 (2014).
112. Song, S., Sun, X., Li, X., Yuan, Y. & Jiao, N. Efficient and Practical Oxidative Bromination and Iodination of Arenes and Heteroarenes with DMSO and Hydrogen Halide: A Mild Protocol for Late-Stage Functionalization. *Org. Lett.* **17**, 2886–2889 (2015).
113. Zhang, X., Guo, S. & Tang, P. Transition-metal free oxidative aliphatic C–H fluorination. *Org. Chem. Front.* **2**, 806–810 (2015).
114. Sharma, A. & Hartwig, J. F. Metal-catalysed azidation of tertiary C–H bonds suitable for late-stage functionalization. *Nature* **517**, 600–604 (2015).
115. Zhang, X., Yang, H. & Tang, P. Transition-Metal-Free Oxidative Aliphatic C–H Azidation. *Org. Lett.* **17**, 5828–5831 (2015).
116. Dhineshkumar, J. & Prabhu, K. R. An Efficient Tertiary Azidation of 1,3-Dicarbonyl Compounds in Water Catalyzed by Tetrabutylammonium Iodide. *European J. Org.*

- Chem.* **2016**, 447–452 (2016).
117. Michaudel, Q., Thevenet, D. & Baran, P. S. Intermolecular Ritter-Type C–H Amination of Unactivated sp<sup>3</sup> Carbons. *J. Am. Chem. Soc.* **134**, 2547–2550 (2012).
  118. Nagib, D. A. & MacMillan, D. W. C. Trifluoromethylation of arenes and heteroarenes by means of photoredox catalysis. *Nature* **480**, 224–228 (2011).
  119. Parsons, A. T. & Buchwald, S. L. Copper-Catalyzed Trifluoromethylation of Unactivated Olefins. *Angew. Chemie Int. Ed.* **50**, 9120–9123 (2011).
  120. Wang, X. *et al.* Copper-Catalyzed C(sp<sup>3</sup>)–C(sp<sup>3</sup>) Bond Formation Using a Hypervalent Iodine Reagent: An Efficient Allylic Trifluoromethylation. *J. Am. Chem. Soc.* **133**, 16410–16413 (2011).
  121. Xu, J. *et al.* Copper-Catalyzed Trifluoromethylation of Terminal Alkenes through Allylic C–H Bond Activation. *J. Am. Chem. Soc.* **133**, 15300–15303 (2011).
  122. Chu, L. & Qing, F. L. Copper-catalyzed oxidative trifluoromethylation of terminal alkenes using nucleophilic CF<sub>3</sub>SiMe<sub>3</sub>: Efficient C(sp<sup>3</sup>)-CF<sub>3</sub> bond formation. *Org. Lett.* **14**, 2106–2109 (2012).
  123. Wu, H. *et al.* Direct trifluoromethylthiolation of unactivated C(sp<sup>3</sup>)-H using silver(I) trifluoromethanethiolate and potassium persulfate. *Angew. Chem. Int. Ed. Engl.* **54**, 4070–4 (2015).
  124. Liu, J.-B., Xu, X.-H., Chen, Z.-H. & Qing, F.-L. Direct dehydroxytrifluoromethylthiolation of alcohols using silver(I) trifluoromethanethiolate and tetra-n-butylammonium iodide. *Angew. Chem. Int. Ed. Engl.* **54**, 897–900 (2015).
  125. Allen, J. M. & Lambert, T. H. Tropylium Ion Mediated  $\alpha$ -Cyanation of Amines. *J. Am. Chem. Soc.* **133**, 1260–1262 (2011).
  126. Kang, T., Kim, Y., Lee, D., Wang, Z. & Chang, S. Iridium-catalyzed intermolecular amidation of sp<sup>3</sup> C-H bonds: Late-stage functionalization of an unactivated methyl group. *J. Am. Chem. Soc.* **136**, 4141–4144 (2014).
  127. McMurray, L., O'Hara, F. & Gaunt, M. J. Recent developments in natural product synthesis using metal-catalysed C–H bond functionalisation. *Chem. Soc. Rev.* **40**, 1885 (2011).
  128. Yamaguchi, J., Yamaguchi, A. D. & Itami, K. C-H bond functionalization: Emerging synthetic tools for natural products and pharmaceuticals. *Angew. Chemie - Int. Ed.* **51**, 8960–9009 (2012).
  129. Cernak, T., Dykstra, K. D., Tyagarajan, S., Vachal, P. & Krska, S. W. The medicinal chemist's toolbox for late stage functionalization of drug-like molecules. *Chem. Soc. Rev.* **45**, 546–576 (2015).
  130. Wang, J. *et al.* Chemical Remodeling of Cell-Surface Sialic Acids through a Palladium-Triggered Bioorthogonal Elimination Reaction. *Angew. Chemie Int. Ed.* **54**, 5364–5368 (2015).
  131. Gensch, T., Hopkinson, M. N., Glorius, F. & Wencel-Delord, J. Mild metal-catalyzed C–H activation: examples and concepts. *Chem. Soc. Rev.* **45**, 2900–2936 (2016).
  132. Yuan, X. *et al.* Androgen receptor functions in castration-resistant prostate cancer and mechanisms of resistance to new agents targeting the androgen axis. *Oncogene* **33**, 2815–25 (2014).
  133. Rehman, Y. & Rosenberg, J. E. Abiraterone acetate: oral androgen biosynthesis inhibitor for treatment of castration-resistant prostate cancer. *Drug Des. Devel. Ther.* **6**, 13–8 (2012).
  134. van der Lely, A. J., de Herder, W. W. & Lamberts, S. W. J. A Risk-Benefit Assessment of Octreotide in the Treatment of Acromegaly. *Drug Saf.* **17**, 317–324 (1997).
  135. Wang, J. *et al.* Octreotide acts as an antitumor angiogenesis compound and suppresses tumor growth in nude mice bearing human hepatocellular carcinoma xenografts. *J. Cancer Res. Clin. Oncol.* **129**, 327–334 (2003).
  136. Kingston, D. G. I. Taxol: The chemistry and structure-activity relationships of a novel anticancer agent. *Trends Biotechnol.* **12**, 222–227 (1994).
  137. Cragg, G. M. Paclitaxel (Taxol): a success story with valuable lessons for natural

- product drug discovery and development. *Med. Res. Rev.* **18**, 315–31 (1998).
138. Weaver, B. A. How Taxol/paclitaxel kills cancer cells. *Mol. Biol. Cell* **25**, 2677–2681 (2014).
  139. Kollmannsberger, C., Mross, K., Jakob, A., Kanz, L. & Bokemeyer, C. Topotecan - A novel topoisomerase I inhibitor: pharmacology and clinical experience. *Oncology* **56**, 1–12 (1999).
  140. Coleman, R. L. Emerging Role of Topotecan in Front-Line Treatment of Carcinoma of the Ovary. *Oncologist* **7**, 46–55 (2002).
  141. Wilson, L., Creswell, K. M. & Chin, D. Mechanism of action of vinblastine. Binding of [acetyl- 3 H]-vinblastine to embryonic chick brain tubulin and tubulin from sea urchin sperm tail outer doublet microtubules. *Biochemistry* **14**, 5586–5592 (1975).
  142. Noble, R. L. The discovery of the vinca alkaloids—chemotherapeutic agents against cancer. *Biochem. Cell Biol.* **68**, 1344–1351 (1990).
  143. Wilson, A. C., Vadakkadath Meethal, S., Bowen, R. L. & Atwood, C. S. Leuprolide acetate: a drug of diverse clinical applications. *Expert Opin. Investig. Drugs* **16**, 1851–1863 (2007).
  144. Huczynski, A. Salinomycin: a new cancer drug candidate. *Chem. Biol. Drug Des.* **79**, 235–8 (2012).
  145. Zhou, S. *et al.* Salinomycin: a novel anti-cancer agent with known anti-coccidial activities. *Curr Med Chem* **20**, 4095–4101 (2013).
  146. Antoszczak, M. *et al.* Synthesis, Anticancer and Antibacterial Activity of Salinomycin N-Benzyl Amides. *Molecules* **19**, 19435–19459 (2014).
  147. Cai, P., Tsao, R. & Ruppen, M. E. In vitro metabolic study of temsirolimus: Preparation, isolation, and identification of the metabolites. *Drug Metab. Dispos.* **35**, 1554–1563 (2007).
  148. Rini, B. I. Temsirolimus, an inhibitor of mammalian target of rapamycin. *Clin. Cancer Res.* **14**, 1286–1290 (2008).
  149. Huang, C. H. O., Kingston, D. G. I., Magri, N. F., Samaranayake, G. & Boettner, F. E. New Taxanes from *Taxus brevifolia*, 2. *J. Nat. Prod.* **49**, 665–669 (1986).
  150. MacEachern-Keith, G. J., Wagner Butterfield, L. J. & Incorvia Mattina, M. J. Paclitaxel Stability in Solution. *Anal. Chem.* **69**, 72–77 (1997).
  151. Tian, J. & Stella, V. J. Degradation of paclitaxel and related compounds in aqueous solutions I: Epimerization. *J. Pharm. Sci.* **97**, 1224–1235 (2008).
  152. Gogoi, J., Gogoi, P. & Boruah, R. C. One-Pot Stereoselective Synthesis of (Z)- $\beta$ -Ketoenamides from  $\beta$ -Halo  $\alpha,\beta$ -Unsaturated Aldehydes. *European J. Org. Chem.* **2014**, 3483–3490 (2014).
  153. Paria, B. C. *et al.* Cellular and molecular responses of the uterus to embryo implantation can be elicited by locally applied growth factors. *Proc. Natl. Acad. Sci.* **98**, 1047–1052 (2001).





## APPENDIX

### A. CATALYSTS' SCREENING

A complete list of all the tests performed on catalysts, listed in alphabetical order according to the catalyst's name. First table explains the information given in the table: "substrate" indicates the acetal substrate used; "case" indicate the nature of the catalyst; "pH" is the pH of the solution measured by pH paper; "hydrolysis" column gives information about the observed fluorescence at given time.

Legend		
<b>Case</b>	<b>A</b>	homogeneous/soluble in the solvent
	<b>B</b>	heterogeneous non-adsorbent
	<b>C</b>	heterogeneous adsorbent
<b>pH</b>	//	not measured
	<b>N</b>	neutral
	<b>A</b>	acidic
<b>Hydrolysis</b>	//	not observed
	<b>F+</b>	hydrolysis observed by means of detection of fluorescence. F+ = low fluorescence → F+++ = high fluorescence
	<b>F++</b>	
	<b>F+++</b>	

Substrate	Catalyst	Case	Solvent	pH	Hydrolysis
F-APN6	ALA014	C	MeOH	//	No
F-APNM5	ALA014	C	MeOH	//	F+
F-APNM5	ALA014	C	Water	N	//
F-APNM5	ALA014	C	PBS	N	//
F-APN6	AlCl <sub>3</sub>	A	MeOH	//	//
F-APN6	Amberlyst A15	C	MeOH	//	F+++
F-APN6	Amberlyst A15	C	Water	N	F+++
F-APN6	Amberlyst A15	C	PBS	A	F+++
F-APNM5	Amberlyst A15	C	MeOH	//	F+++
F-APNM5	Amberlyst A15	C	Water	N	F+++
F-APNM5	Amberlyst A15	C	PBS	A	F+++
F-APN6	Amberlyte CG-50	C	MeOH	//	//
F-APNM5	Amberlyte CG-50	C	MeOH	//	//
F-APN6	BF <sub>3</sub> /SiO <sub>2</sub> (fresh)	B	MeOH	//	F++
F-APN6	BF <sub>3</sub> /SiO <sub>2</sub> (washed)	B	MeOH	//	//

Continue...

Substrate	Catalyst	Case	Solvent	pH	Hydrolysis
F-APN6	BF3/SiO2 (washing sol.)	B	MeOH	//	F+
F-APN6	CAN	A	MeOH	//	//
F-APN6	CeCl3/NaI	A	MeOH	//	//
F-APN6	CSA	A	MeOH	//	F+++
F-APN6	CSA	A	Water	A	//
F-APN6	CSA	A	PBS	A	//
F-APN6	CSA	A	Plasma	A	//
F-APNM5	CSA	A	MeOH	//	F+++
F-APNM5	CSA	A	Water	A	F+++
F-APNM5	CSA	A	PBS	A	F+++
F-APNM5	CSA	A	Plasma	A	F+
F-APNM5	Dowex	C	MeOH	//	F+
F-APNM5	Dowex	C	Water	N	//
F-APNM5	Dowex	C	PBS	N	//
F-APN6	Dowex 50WX8-200	C	MeOH	//	//
F-APN6	FeBr3	A	MeOH	//	//
F-APN6	FeCl3	A	MeOH	//	//
F-APN6	H2SO4/SiO2 (fresh)	B	MeOH	//	F+++
F-APN6	H2SO4/SiO2 (washed)	B	MeOH	//	F+
F-APN6	H2SO4/SiO2 (washing sol.)	B	MeOH	//	F++
F-APN6	HClO4/SiO2	B	MeOH	//	//
F-APN6	HSA6	C	MeOH	//	//
F-APNM5	HSA6	C	MeOH	//	//
F-APN6	HSA6OX	C	MeOH	//	//
F-APNM5	HSA6OX	C	MeOH	//	//
F-APN6	In(OTf)3	A	MeOH	//	//
F-APN6	JH003	C	MeOH	//	//
F-APNM5	JH003	C	MeOH	//	//
F-APN6	Lignine 400	C	MeOH	//	//
F-APNM5	Lignine 400	C	MeOH	//	//
F-APN6	Montmorillonite K10	C	MeOH	//	//
F-APNM5	Montmorillonite K10	C	MeOH	//	//

Continue...

Substrate	Catalyst	Case	Solvent	pH	Hydrolysis
F-APN6	Montmorillonite KSF	C	MeOH	//	//
F-APNM5	Montmorillonite KSF	C	MeOH	//	//
F-APN6	MR-Citric Acid	C	MeOH	//	//
F-APN6	MR-Citric Acid	C	Water	N	//
F-APNM5	MR-Citric Acid	C	MeOH	//	//
F-APNM5	MR-Citric Acid	C	Water	N	//
F-APN6	MR-H2SO4	C	MeOH	//	//
F-APN6	MR-H2SO4	C	Water	N	//
F-APNM5	MR-H2SO4	C	MeOH	//	//
F-APNM5	MR-H2SO4	C	Water	N	//
F-APN6	MR-H3PO4	C	MeOH	//	//
F-APN6	MR-H3PO4	C	Water	N	//
F-APNM5	MR-H3PO4	C	MeOH	//	//
F-APNM5	MR-H3PO4	C	Water	N	//
F-APN6	MR-PAASA	C	MeOH	//	//
F-APN6	MR-PAASA	C	Water	N	//
F-APNM5	MR-PAASA	C	MeOH	//	F+
F-APNM5	MR-PAASA	C	Water	N	//
F-APN6	MR-PAASAcAN	C	MeOH	//	//
F-APN6	MR-PAASAcAN	C	Water	N	//
F-APNM5	MR-PAASAcAN	C	MeOH	//	//
F-APNM5	MR-PAASAcAN	C	Water	N	//
F-APN6	Nafion NR-50	C	MeOH	//	F+++
F-APN6	Nafion NR-50	C	Water	N	F+++
F-APN6	Nafion NR-50	C	PBS	A	F+++
F-APNM5	Nafion NR-50	C	MeOH	//	F+++
F-APNM5	Nafion NR-50	C	Water	N	F+++
F-APNM5	Nafion NR-50	C	PBS	A	F+++
F-APNM5	Nafion NR-50	C	Plasma	A	//
F-APN6	Nb2O5	B	MeOH	//	//
F-APN6	PAASA	A	MeOH	//	F+++
F-APN6	PAASA	A	Water	A	//
F-APN6	PAASA	A	PBS	A	//

Continue...

Substrate	Catalyst	Case	Solvent	pH	Hydrolysis
F-APNM5	PAASA	A	MeOH	//	F+++
F-APNM5	PAASA	A	Water	A	F+++
F-APNM5	PAASA	A	PBS	A	F+++
F-APN6	PAASAcAN	C	MeOH	//	F+
F-APN6	PAASAcAN	C	Water	N	No
F-APNM5	PAASAcAN	C	MeOH	//	F++
F-APNM5	PAASAcAN	C	Water	N	F+
F-APNM5	PAASAcAN	C	PBS	N	//
F-APN6	PAcMA	A	MeOH	//	//
F-APNM5	PAcMA	A	MeOH	//	F+
F-APNM5	PAcMA	A	Water	N	//
F-APN6	PMA/SiO <sub>2</sub>	B	MeOH	//	//
F-APN6	Sc(OTf) <sub>3</sub>	A	MeOH	//	//
F-APN6	Ti(IV) silicate	B	MeOH	//	//
F-APN6	Yt(OTf) <sub>3</sub>	A	MeOH	//	//
F-APN6	Zn(OTf) <sub>3</sub>	A	MeOH	//	//
F-APN6	ZnBr <sub>2</sub>	A	MeOH	//	//

## B. NAFION NR50'S WASHING PRE-TREATMENT SCREENING

Complete list of all the tests performed on the washing pre-treatment.

Explanation of all the given information is included in the following legend.

The main table is ordered according to the method used (A – B – C), then to the washing solution and then to the dilution (increased).

Legend		
<b>Nafion NR50</b>	C = Commercial CR = Re-activated	
<b>WASHING</b>	<b>Method</b>	A, B or C
	<b>Washing solvent</b>	Washing solvent: <i>UP water</i> (ultrapure water); <i>PBS 1X</i> ; <i>NaCl sat.</i> (saturated solution of NaCl in ultrapure water).
	<b>Details</b>	Details on the amount of washing solvent, time and rate.
	<b>Dilution</b>	<i>N</i> times dilution of the washing solvent
	<b>[NaCl]</b>	Concentration of NaCl
	<b>Washing pH</b>	pH of the washing solvent after washing (measured with a pH meter)
<b>HYDROLYSIS w/ F-APNM5</b>	<b>Solvent</b>	<i>MeOH</i> , <i>Water</i> , <i>PBS</i> or <i>plasma</i>
	<b>Pre-equil. (min.)</b>	Pre-equilibration of the beads in plasma (minutes)
	<b>Time</b>	<i>3h</i> , <i>6h</i> or <i>24h</i> check for fluorescence
	<b>pH (t=3h)</b>	pH of the solution at t=3h, checked with pH paper
	<b>Fluo</b>	Fluorescence of the bead (=hydrolysis): // (no fluo); <i>F+</i> , <i>F++</i> , <i>F+++</i> (from little to good fluorescence)

Nafion NR-50	WASHING				HYDROLYSIS w/ F-APNIM5						
	Method	Details	Washing solvent	Dilution	[NaCl]	Washing pH	Solvent	Pre-equil. (min.)	Time	pH (t=3h)	Fluo
C	A	30mL 18h	UP water	//	//	4,45	Water	//	3h	~5	F++
C	A	30mL 18h	UP water	//	//	4,45	Water	//	24h	~5	F+++
C	A	30mL 18h	UP water	//	//	4,45	PBS	//	3h	1-2	F+++
C	A	30mL 18h	UP water	//	//	4,45	PBS	//	24h	1-2	F+++
C	A	30mL 18h	NaCl sat	//	6,57M	3,28	Water	//	3h	~5	F+
C	A	30mL 18h	NaCl sat	//	6,57M	3,28	Water	//	24h	~5	F++
C	A	30mL 18h	NaCl sat	//	6,57M	3,28	PBS	//	3h	7,4	//
C	A	30mL 18h	NaCl sat	//	6,57M	3,28	PBS	//	24h	7,4	//
C	A	30mL 18h	NaCl sat	100	65,7mM	2,45	Water	//	3h	~5	F++
C	A	30mL 18h	NaCl sat	100	65,7mM	2,45	Water	//	24h	~5	F+++
C	A	30mL 18h	NaCl sat	100	65,7mM	2,45	PBS	//	3h	6-7	//
C	A	30mL 18h	NaCl sat	100	65,7mM	2,45	PBS	//	24h	6-7	F+
C	A	30mL 18h	NaCl sat	10K	657µM	3,25	Water	//	3h	~5	F++
C	A	30mL 18h	NaCl sat	10K	657µM	3,25	Water	//	24h	~5	F+++
C	A	30mL 18h	NaCl sat	10K	657µM	3,25	PBS	//	3h	1-2	F+++
C	A	30mL 18h	NaCl sat	10K	657µM	3,25	PBS	//	24h	1-2	F+++
C	A	30mL 18h	NaCl sat	1M	6,57µM	4,69	Water	//	3h	~5	F++
C	A	30mL 18h	NaCl sat	1M	6,57µM	4,69	Water	//	24h	~5	F+++
C	A	30mL 18h	NaCl sat	1M	6,57µM	4,69	PBS	//	3h	1-2	F+++

Nafion NR-50	WASHING				HYDROLYSIS w/ F-APNM5						
	Method	Details	Washing solvent	Dilution	[NaCl]	Washing pH	Solvent	Pre-equil. Time (min.)	pH (t=3h)	Fluo	
C	A	30mL 18h	NaCl sat	1M	6,57µM	4,69	PBS	//	24h	1-2	F+++
C	A	30mL 18h	PBS 1X	//	137mM	5,63	Water	//	3h	~5	F++
C	A	30mL 18h	PBS 1X	//	137mM	5,63	Water	//	24h	~5	F+++
C	A	30mL 18h	PBS 1X	//	137mM	6,14	Water	//	3h	~5	F+
C	A	30mL 18h	PBS 1X	//	137mM	6,14	Water	//	24h	~5	F++
C	A	30mL 18h	PBS 1X	//	137mM	5,63	PBS	//	3h	7,4	//
C	A	30mL 18h	PBS 1X	//	137mM	5,63	PBS	//	24h	7,4	//
C	A	30mL 18h	PBS 1X	//	137mM	6,14	PBS	//	3h	7,4	//
C	A	30mL 18h	PBS 1X	//	137mM	6,14	PBS	//	24h	7,4	//
C	A	30mL 18h	PBS 1X	//	137mM	5,63	Plasma	//	3h	7,4	//
C	A	30mL 18h	PBS 1X	//	137mM	5,63	Plasma	//	24h	7,4	//
C	A	30mL 18h	PBS 1X	//	137mM	6,14	Plasma	//	3h	7,4	//
C	A	30mL 18h	PBS 1X	//	137mM	6,14	Plasma	//	24h	7,4	//
C	A	30mL 18h	PBS 1X	10	13,7mM	2,27	Water	//	3h	~5	F++
C	A	30mL 18h	PBS 1X	10	13,7mM	2,27	Water	//	24h	~5	F++
C	A	30mL 18h	PBS 1X	10	13,7mM	2,27	PBS	//	3h	1-2	F++
C	A	30mL 18h	PBS 1X	10	13,7mM	2,27	PBS	//	24h	1-2	F++
C	A	30mL 18h	PBS 1X	10	13,7mM	2,27	Plasma	//	3h	6-7	F+
C	A	30mL 18h	PBS 1X	10	13,7mM	2,27	Plasma	//	24h	6-7	F+



Nafion NR-50	WASHING				HYDROLYSIS w/ F-APNIM5						
	Method	Details	Washing solvent	Dilution	[NaCl]	Washing pH	Solvent	Pre-equil. (min.)	Time	pH (t=3h)	Fluo
C	A	30mL 18h	PBS 1X	100	1,37mM	2,86	Water	//	3h	~5	F++
C	A	30mL 18h	PBS 1X	100	1,37mM	2,86	Water	//	24h	~5	F+++
C	A	30mL 18h	PBS 1X	100	1,37mM	2,89	Water	//	3h	~5	F++
C	A	30mL 18h	PBS 1X	100	1,37mM	2,89	Water	//	24h	~5	F++
C	A	30mL 18h	PBS 1X	100	1,37mM	2,86	PBS	//	3h	1-2	F+
C	A	30mL 18h	PBS 1X	100	1,37mM	2,86	PBS	//	24h	1-2	F++
C	A	30mL 18h	PBS 1X	100	1,37mM	2,89	PBS	//	3h	1-2	F++
C	A	30mL 18h	PBS 1X	100	1,37mM	2,89	PBS	//	24h	1-2	F++
C	A	30mL 18h	PBS 1X	100	1,37mM	2,89	Plasma	//	3h	3-4	F++
C	A	30mL 18h	PBS 1X	100	1,37mM	2,89	Plasma	//	24h	3-4	F++
C	A	30mL 18h	PBS 1X	1K	137µM	3,9	Water	//	3h	~5	F++
C	A	30mL 18h	PBS 1X	1K	137µM	3,9	Water	//	24h	~5	F+++
C	A	30mL 18h	PBS 1X	1K	137µM	3,9	PBS	//	3h	1-2	F++
C	A	30mL 18h	PBS 1X	1K	137µM	3,9	PBS	//	24h	1-2	F+++
C	A	30mL 18h	PBS 1X	1K	137µM	3,9	Plasma	//	3h	1-2	F+
C	A	30mL 18h	PBS 1X	1K	137µM	3,9	Plasma	//	24h	1-2	F+
C	A	30mL 18h	PBS 1X	10K	13,7µM	3,7	Water	//	3h	~5	F++
C	A	30mL 18h	PBS 1X	10K	13,7µM	3,7	Water	//	24h	~5	F+++
C	A	30mL 18h	PBS 1X	10K	13,7µM	3,7	PBS	//	3h	1-2	F++

Nafion NR-50	WASHING				HYDROLYSIS w/ F-APNM5						
	Method	Details	Washing solvent	Dilution	[NaCl]	Washing pH	Solvent	Pre-equil. Time (min.)	pH (t=3h)	Fluo	
C	A	30mL 18h	PBS 1X	10K	13,7µM	3,7	PBS	//	24h	1-2	F+++
C	A	30mL 18h	PBS 1X	10K	13,7µM	3,7	Plasma	//	3h	1-2	F+
C	A	30mL 18h	PBS 1X	10K	13,7µM	3,7	Plasma	//	24h	1-2	F+
C	B	100mL 1min	UP water	//	//	4,87	MeOH	//	3h	//	F+++
C	B	100mL 1min	UP water	//	//	4,87	MeOH	//	24h	//	F+++
C	B	100mL 1min	UP water	//	//	4,87	Water	//	3h	3-4	F+++
C	B	100mL 1min	UP water	//	//	4,87	Water	//	24h	3-4	F+++
C	B	100mL 1min	UP water	//	//	4,87	PBS	//	3h	1-2	F+++
C	B	100mL 1min	UP water	//	//	4,87	PBS	//	24h	1-2	F+++
C	B	100mL 1min	NaCl sat	//	6,57M	2,4	MeOH	//	3h	//	F+++
C	B	100mL 1min	NaCl sat	//	6,57M	2,4	MeOH	//	3h	//	F+++
C	B	100mL 1min	NaCl sat	//	6,57M	2,4	Water	//	24h	3-4	F+++
C	B	100mL 1min	NaCl sat	//	6,57M	2,4	Water	//	3h	3-4	F+++
C	B	100mL 1min	NaCl sat	//	6,57M	2,4	PBS	//	24h	1-2	F+++
C	B	100mL 1min	NaCl sat	//	6,57M	2,4	PBS	//	3h	1-2	F+++
C	B	100mL 1min	NaCl sat	100	65,7mM	3,53	MeOH	//	3h	//	F+++
C	B	100mL 1min	NaCl sat	100	65,7mM	3,53	MeOH	//	3h	//	F+++
C	B	100mL 1min	NaCl sat	100	65,7mM	3,53	Water	//	24h	3-4	F+++
C	B	100mL 1min	NaCl sat	100	65,7mM	3,53	Water	//	3h	3-4	F+++

Nafion NR-50	WASHING				HYDROLYSIS w/ F-APNM5						
	Method	Details	Washing solvent	Dilution	[NaCl]	Washing pH	Solvent	Pre-equil. (min.)	Time	pH (t=3h)	Fluo
C	B	100mL 1min	NaCl sat	100	65,7mM	3,53	PBS	//	24h	1-2	F+++
C	B	100mL 1min	NaCl sat	100	65,7mM	3,53	PBS	//	3h	1-2	F+++
C	B	100mL 1min	NaCl sat	10K	657µM	4,79	MeOH	//	3h	//	F+++
C	B	100mL 1min	NaCl sat	10K	657µM	4,79	MeOH	//	3h	//	F+++
C	B	100mL 1min	NaCl sat	10K	657µM	4,79	Water	//	24h	3-4	F+++
C	B	100mL 1min	NaCl sat	10K	657µM	4,79	Water	//	3h	3-4	F+++
C	B	100mL 1min	NaCl sat	10K	657µM	4,79	PBS	//	24h	1-2	F+++
C	B	100mL 1min	NaCl sat	10K	657µM	4,79	PBS	//	3h	1-2	F+++
C	B	100mL 1min	NaCl sat	1M	6,57µM	5,25	MeOH	//	3h	//	F+++
C	B	100mL 1min	NaCl sat	1M	6,57µM	5,25	MeOH	//	3h	//	F+++
C	B	100mL 1min	NaCl sat	1M	6,57µM	5,25	Water	//	24h	3-4	F+++
C	B	100mL 1min	NaCl sat	1M	6,57µM	5,25	Water	//	3h	3-4	F+++
C	B	100mL 1min	NaCl sat	1M	6,57µM	5,25	PBS	//	24h	1-2	F+++
C	B	100mL 1min	NaCl sat	1M	6,57µM	5,25	PBS	//	3h	1-2	F+++
C	C	4,15mL/min 5min	PBS 1X	//	137mM	1,53	Water	//	3h	~5	F++
C	C	4,15mL/min 5min	PBS 1X	//	137mM	1,53	Water	//	24h	~5	F+++
C	C	4,15mL/min 5min	PBS 1X	//	137mM	1,53	PBS	//	3h	1-2	F++
C	C	4,15mL/min 5min	PBS 1X	//	137mM	1,53	PBS	//	24h	1-2	F+++
C	C	4,15mL/min 15min	PBS 1X	//	137mM	2,41	Water	//	3h	~5	F++

Nafion NR-50	WASHING				HYDROLYSIS w/ F-APNM5						
	Method	Details	Washing solvent	Dilution	[NaCl]	Washing pH	Solvent	Pre-equil. Time (min.)	pH (t=3h)	Fluo	
C	C	4,15mL/min 15min	PBS 1X	//	137mM	2,41	Water	//	24h	~5	F+++
C	C	4,15mL/min 15min	PBS 1X	//	137mM	2,41	PBS	//	3h	1-2	F++
C	C	4,15mL/min 15min	PBS 1X	//	137mM	2,41	PBS	//	24h	1-2	F+++
C	C	4,15mL/min 15min	PBS 1X	//	137mM	2,41	Plasma	//	3h	~5	F+
C	C	4,15mL/min 15min	PBS 1X	//	137mM	2,41	Plasma	//	24h	~5	F++
C	C	4,15mL/min 30min	PBS 1X	//	137mM	6,79	Water	//	3h	~5	F++
C	C	4,15mL/min 30min	PBS 1X	//	137mM	6,79	Water	//	24h	~5	F+++
C	C	4,15mL/min 30min	PBS 1X	//	137mM	6,79	PBS	//	3h	1-2	F+
C	C	4,15mL/min 30min	PBS 1X	//	137mM	6,79	PBS	//	24h	1-2	F+++
C	C	4,15mL/min 30min	PBS 1X	//	137mM	6,79	Plasma	//	3h	6-7	//
C	C	4,15mL/min 30min	PBS 1X	//	137mM	6,79	Plasma	//	24h	6-7	F+
C	C	4,15mL/min 60min	PBS 1X	//	137mM	7,34	Water	//	3h	~5	F++
C	C	4,15mL/min 60min	PBS 1X	//	137mM	7,34	Water	//	24h	~5	F+++
C	C	4,15mL/min 60min	PBS 1X	//	137mM	7,34	PBS	//	3h	7,4	//
C	C	4,15mL/min 60min	PBS 1X	//	137mM	7,34	PBS	//	24h	7,4	//
C	C	4,15mL/min 60min	PBS 1X	//	137mM	7,34	Plasma	//	3h	7,4	//
C	C	4,15mL/min 60min	PBS 1X	//	137mM	7,34	Plasma	//	24h	7,4	//
CR	C	4,15mL/min 15min	PBS 1X	10	13,7mM	2,63	PBS	Yes (20 min)	3h	1-2	F++
CR	C	4,15mL/min 15min	PBS 1X	10	13,7mM	2,63	PBS	Yes (20 min)	6h	1-2	F+++

Nafion NR-50	WASHING					HYDROLYSIS w/ F-APNM5					
	Method	Details	Washing solvent	Dilution	[NaCl]	Washing pH	Solvent	Pre-equil. (min.)	Time	pH (t=3h)	Fluo
CR	C	4,15mL/min 15min	PBS 1X	10	13,7mM	2,63	PBS	Yes (20 min)	24h	1-2	F+++
CR	C	4,15mL/min 15min	PBS 1X	10	13,7mM	2,63	Plasma	Yes (20 min)	3h	3-4	F+
CR	C	4,15mL/min 15min	PBS 1X	10	13,7mM	2,63	Plasma	Yes (20 min)	6h	3-4	F+
CR	C	4,15mL/min 15min	PBS 1X	10	13,7mM	2,63	Plasma	Yes (20 min)	24h	3-4	F++
CR	C	4,15mL/min 30min	PBS 1X	10	13,7mM	2,81	PBS	Yes (20 min)	3h	1-2	F++
CR	C	4,15mL/min 30min	PBS 1X	10	13,7mM	2,81	PBS	Yes (20 min)	6h	1-2	F+++
CR	C	4,15mL/min 30min	PBS 1X	10	13,7mM	2,81	PBS	Yes (20 min)	24h	1-2	F+++
CR	C	4,15mL/min 30min	PBS 1X	10	13,7mM	2,81	Plasma	Yes (20 min)	3h	~5	F+
CR	C	4,15mL/min 30min	PBS 1X	10	13,7mM	2,81	Plasma	Yes (20 min)	6h	~5	F+
CR	C	4,15mL/min 30min	PBS 1X	10	13,7mM	2,81	Plasma	Yes (20 min)	24h	~5	F++
CR	C	4,15mL/min 45min	PBS 1X	10	13,7mM	3,4	PBS	Yes (20 min)	3h	1-2	F++
CR	C	4,15mL/min 45min	PBS 1X	10	13,7mM	3,4	PBS	Yes (20 min)	6h	1-2	F+++
CR	C	4,15mL/min 45min	PBS 1X	10	13,7mM	3,4	PBS	Yes (20 min)	24h	1-2	F+++
CR	C	4,15mL/min 45min	PBS 1X	10	13,7mM	3,4	Plasma	Yes (20 min)	3h	~5	F+
CR	C	4,15mL/min 45min	PBS 1X	10	13,7mM	3,4	Plasma	Yes (20 min)	6h	~5	F+
CR	C	4,15mL/min 45min	PBS 1X	10	13,7mM	3,4	Plasma	Yes (20 min)	24h	~5	F++
CR	C	4,15mL/min 60min	PBS 1X	10	13,7mM	5,9	Plasma	Yes (20 min)	3h	~5	F+
CR	C	4,15mL/min 60min	PBS 1X	10	13,7mM	5,9	Plasma	Yes (20 min)	6h	~5	F+
CR	C	4,15mL/min 60min	PBS 1X	10	13,7mM	5,9	Plasma	Yes (20 min)	24h	~5	F+

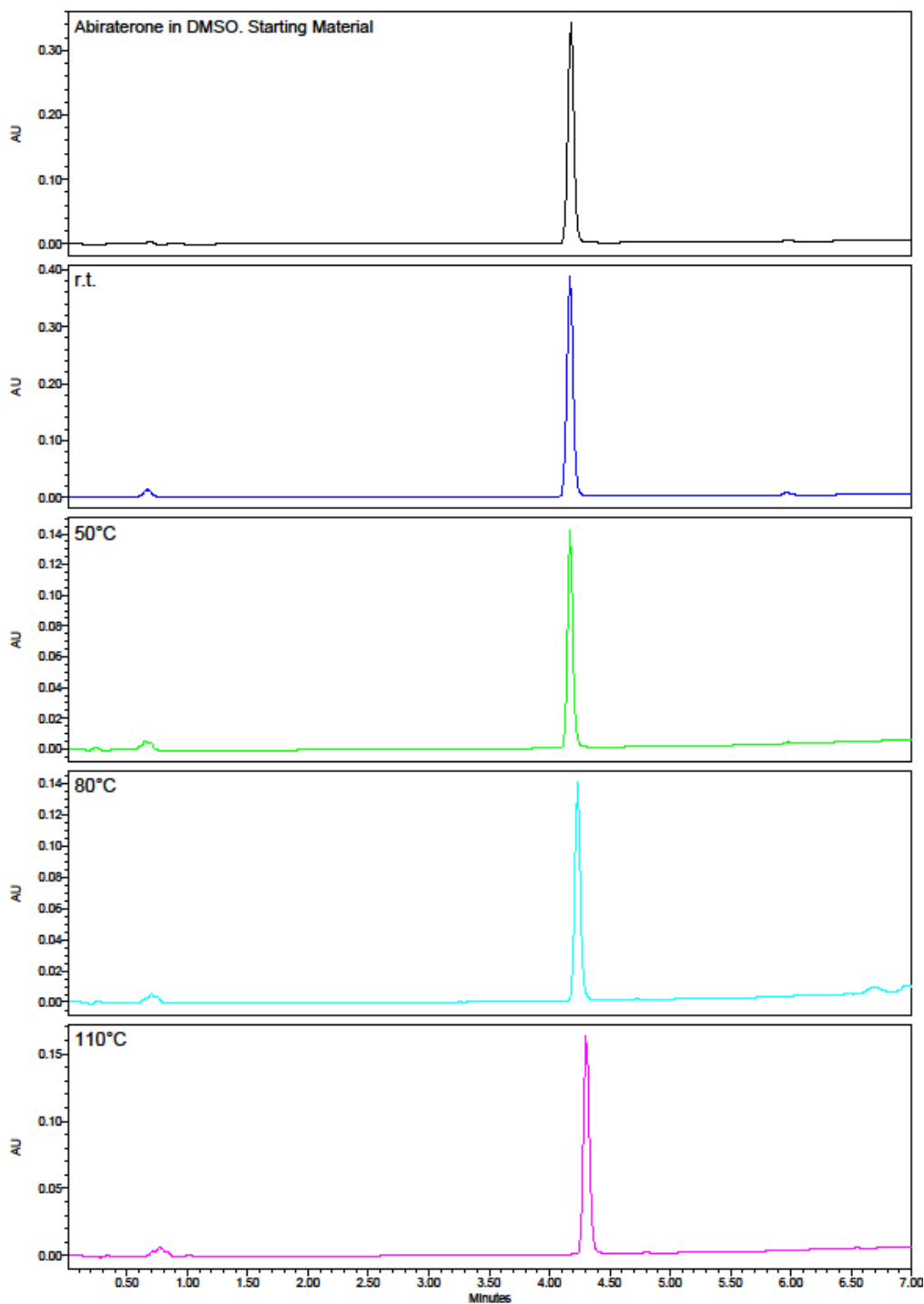
Nafion NR-50	WASHING				HYDROLYSIS w/ F-APN5						
	Method	Details	Washing solvent	Dilution	[NaCl]	Washing pH	Solvent	Pre-equil. (min.)	Time	pH (t=3h)	Fluo
CR	C	4,15mL/min 75min	PBS 1X	10	13,7mM	6,21	PBS	Yes (20 min)	3h	1-2	F++
CR	C	4,15mL/min 75min	PBS 1X	10	13,7mM	6,21	PBS	Yes (20 min)	6h	1-2	F+++
CR	C	4,15mL/min 75min	PBS 1X	10	13,7mM	6,21	PBS	Yes (20 min)	24h	1-2	F+++
CR	C	4,15mL/min 75min	PBS 1X	10	13,7mM	6,21	Plasma	Yes (20 min)	3h	6-7	F+
CR	C	4,15mL/min 75min	PBS 1X	10	13,7mM	6,21	Plasma	Yes (20 min)	6h	6-7	F+
CR	C	4,15mL/min 75min	PBS 1X	10	13,7mM	6,21	Plasma	Yes (20 min)	24h	6-7	F+
C	C	4,15mL/min 90min	PBS 1X	10	13,7mM	6,84	PBS	Yes (30 min)	3h	3-4	F++
C	C	4,15mL/min 90min	PBS 1X	10	13,7mM	6,84	PBS	Yes (30 min)	24h	3-4	F+++
CR	C	4,15mL/min 90min	PBS 1X	10	13,7mM	6,95	PBS	Yes (20 min)	3h	6-7	//
CR	C	4,15mL/min 90min	PBS 1X	10	13,7mM	6,95	PBS	Yes (20 min)	6h	6-7	//
CR	C	4,15mL/min 90min	PBS 1X	10	13,7mM	6,95	PBS	Yes (20 min)	24h	6-7	//
C	C	4,15mL/min 90min	PBS 1X	10	13,7mM	6,73	Plasma	Yes (30 min)	3h	6-7	F+
C	C	4,15mL/min 90min	PBS 1X	10	13,7mM	6,73	Plasma	Yes (30 min)	24h	6-7	F+
C	C	4,15mL/min 90min	PBS 1X	10	13,7mM	6,84	Plasma	Yes (30 min)	3h	6-7	F+
C	C	4,15mL/min 90min	PBS 1X	10	13,7mM	6,84	Plasma	Yes (30 min)	24h	6-7	F+
CR	C	4,15mL/min 90min	PBS 1X	10	13,7mM	6,95	Plasma	Yes (20 min)	3h	7	F+
CR	C	4,15mL/min 90min	PBS 1X	10	13,7mM	6,95	Plasma	Yes (20 min)	24h	7	F+
CR	C	4,15mL/min 90min	PBS 1X	10	13,7mM	6,95	Plasma	Yes (20 min)	3h	7,4	F+
CR	C	4,15mL/min 90min	PBS 1X	10	13,7mM	6,95	Plasma	Yes (20 min)	24h	7,4	F+

Nafion NR-50	WASHING				HYDROLYSIS w/ F-APNM5						
	Method	Details	Washing solvent	Dilution	[NaCl]	Washing pH	Solvent	Pre-equil. (min.)	Time	pH (t=3h)	Fluo
CR	C	4,15mL/min 90min	PBS 1X	10	13,7mM	6,95	Plasma	Yes (80 min)	3h	7	F+
CR	C	4,15mL/min 90min	PBS 1X	10	13,7mM	6,95	Plasma	Yes (80 min)	24h	7	F+
CR	C	4,15mL/min 90min	PBS 1X	10	13,7mM	6,95	Plasma	Yes (80 min)	3h	7,4	F+
CR	C	4,15mL/min 90min	PBS 1X	10	13,7mM	6,95	Plasma	Yes (80 min)	24h	7,4	F+
CR	C	4,15mL/min 90min	PBS 1X	10	13,7mM	6,95	Plasma	Yes (180 min)	3h	7,4	F+
CR	C	4,15mL/min 90min	PBS 1X	10	13,7mM	6,95	Plasma	Yes (180 min)	24h	7,4	F+
CR	C	4,15mL/min 90min	PBS 1X	10	13,7mM	6,95	Plasma	Yes (180 min)	3h	7,4	F+
CR	C	4,15mL/min 90min	PBS 1X	10	13,7mM	6,95	Plasma	Yes (180 min)	24h	7,4	F+
C	C	4,15mL/min 90min	PBS 1X	10	13,7mM	6,95	PBS	//	3h	5	//
C	C	4,15mL/min 90min	PBS 1X	10	13,7mM	6,95	PBS	//	24h	5	F++
C	C	4,15mL/min 90min	PBS 1X	10	13,7mM	6,95	Plasma	//	3h	7,4	//
C	C	4,15mL/min 90min	PBS 1X	10	13,7mM	6,95	Plasma	//	24h	7,4	//

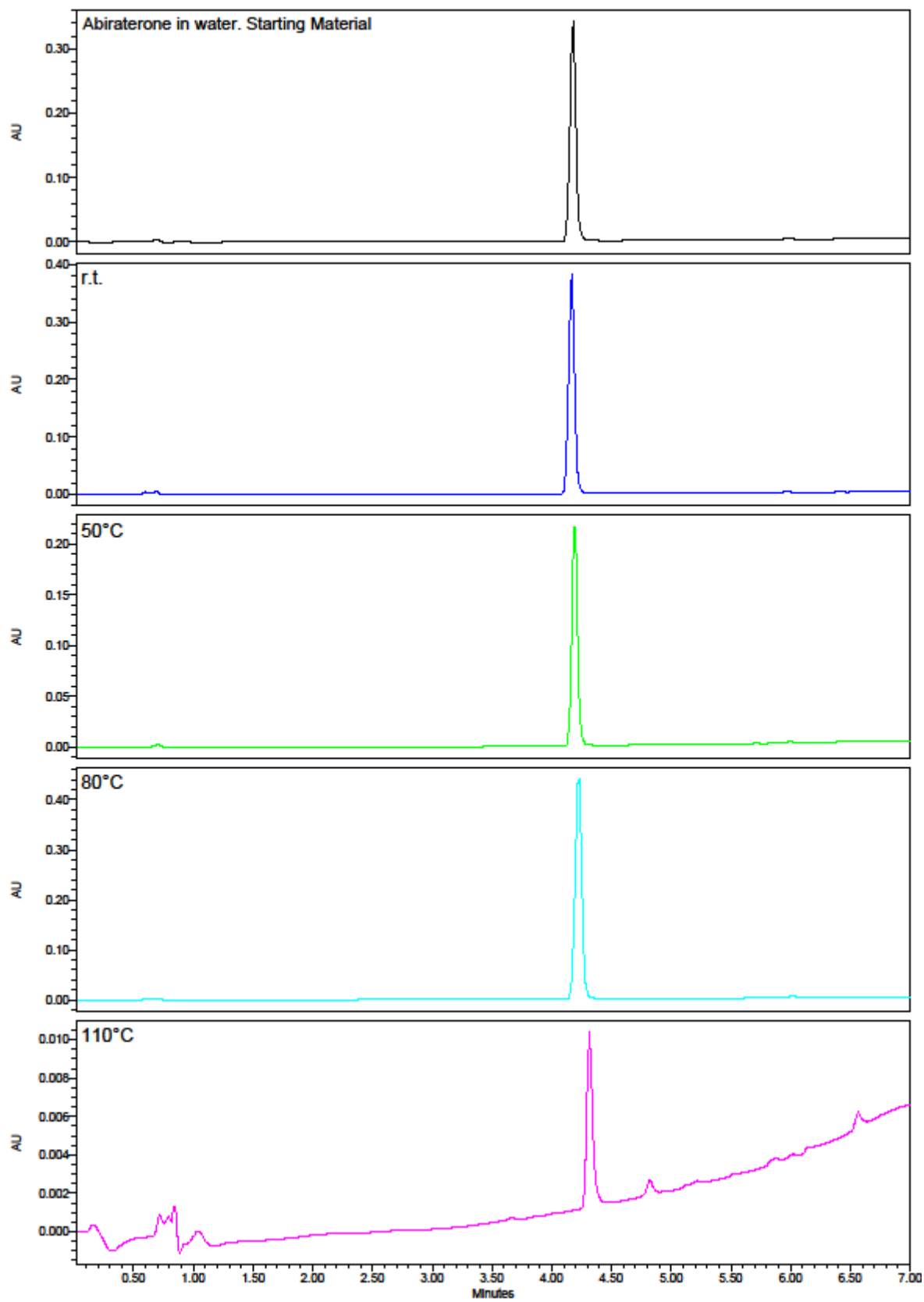
## C. LATE STAGE FUNCTIONALIZATION: SOLVENT AND TEMPERATURE

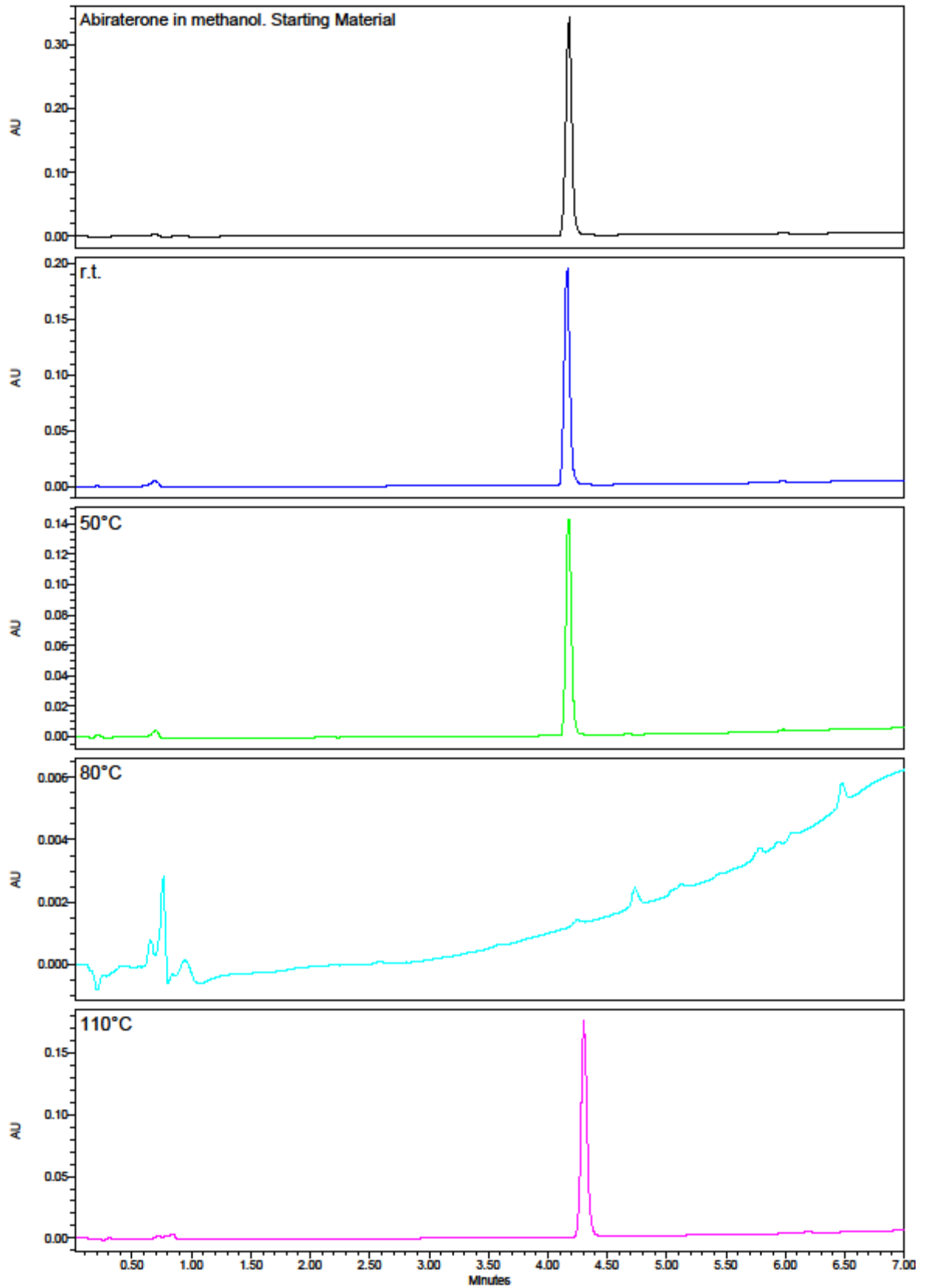
### STABILITY TESTS

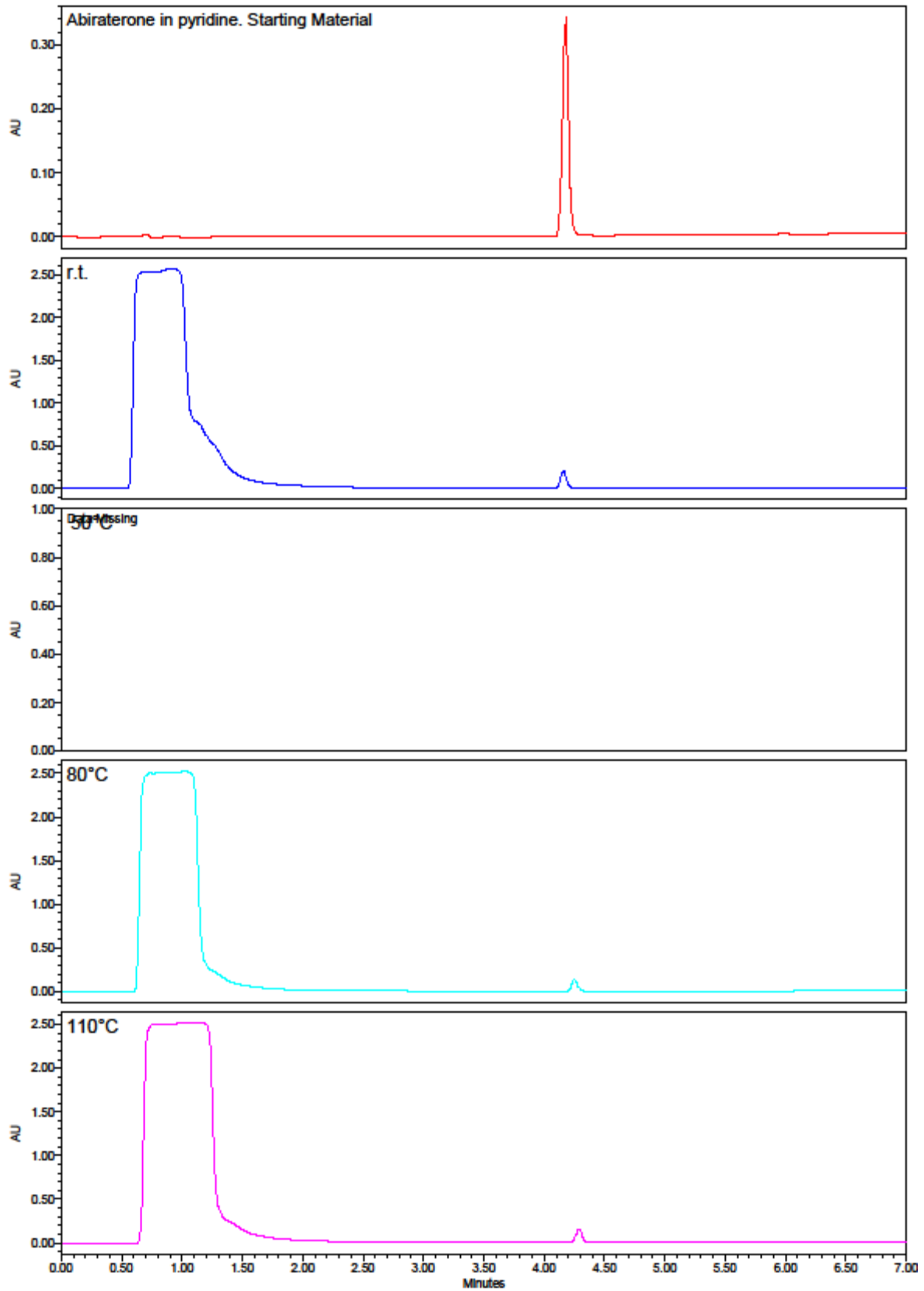
LC-MS chromatograms obtained by the stability tests in different solvents at different temperatures. Drug names and temperatures are indicated on the up left side of each chromatogram.

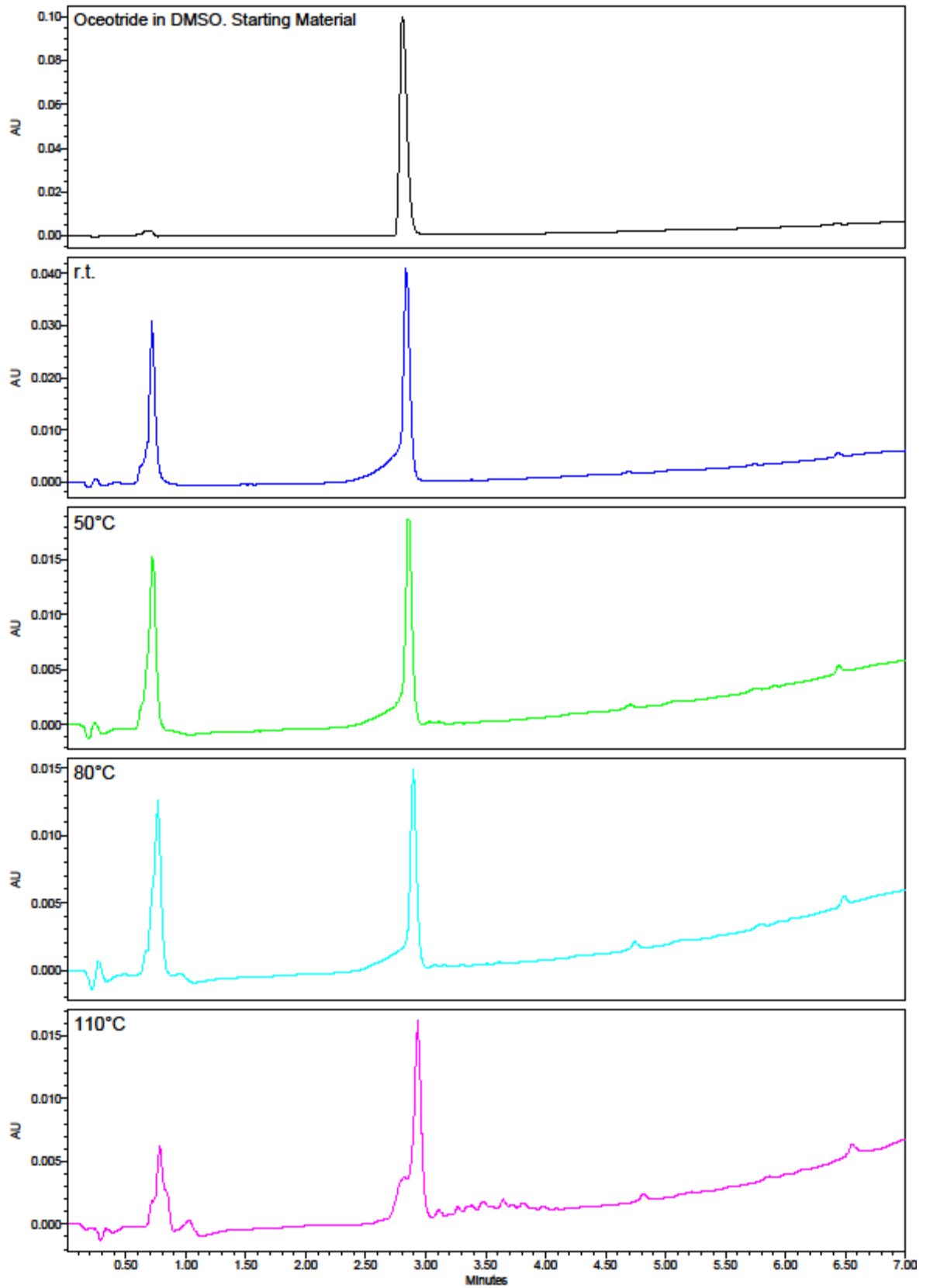


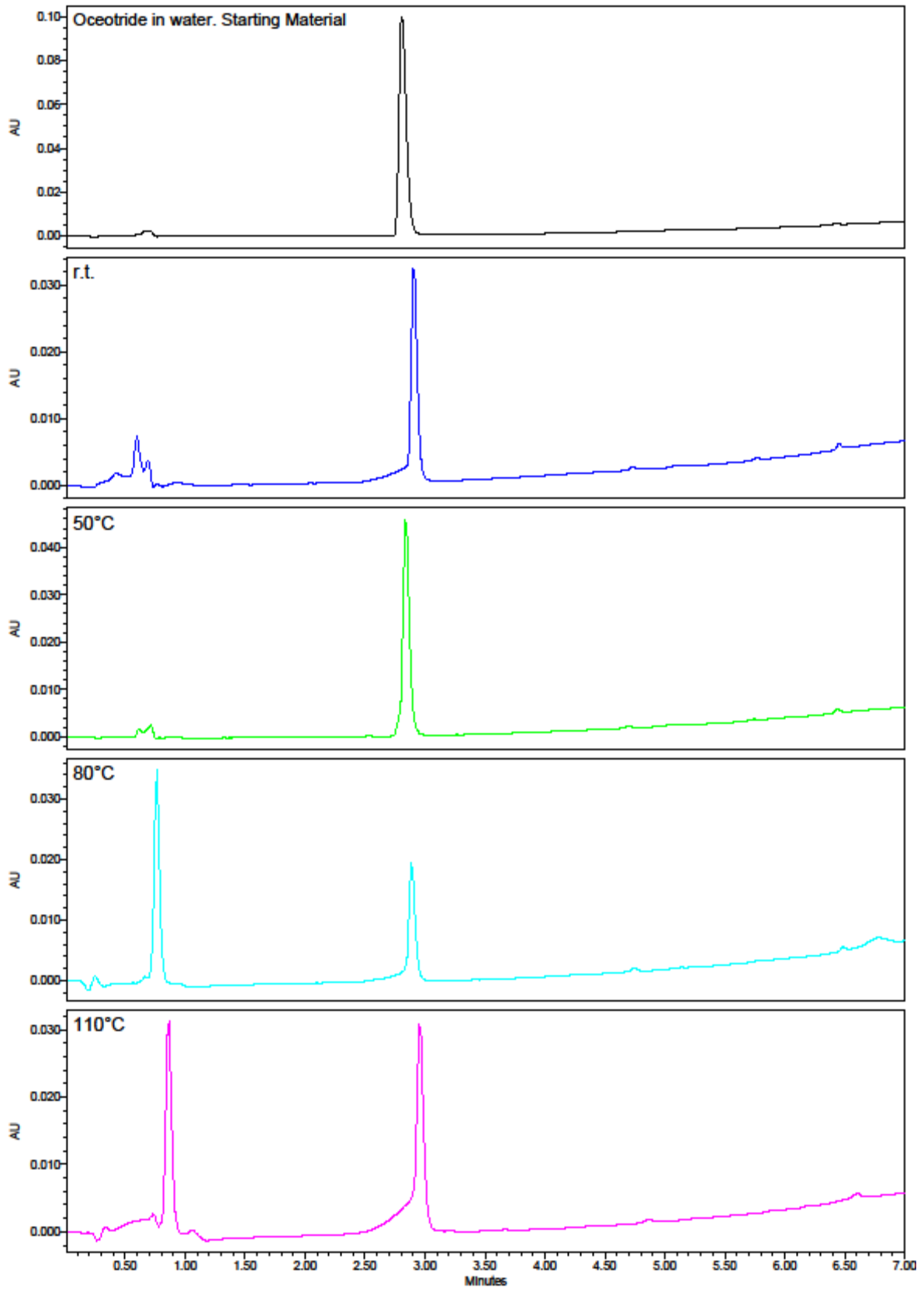


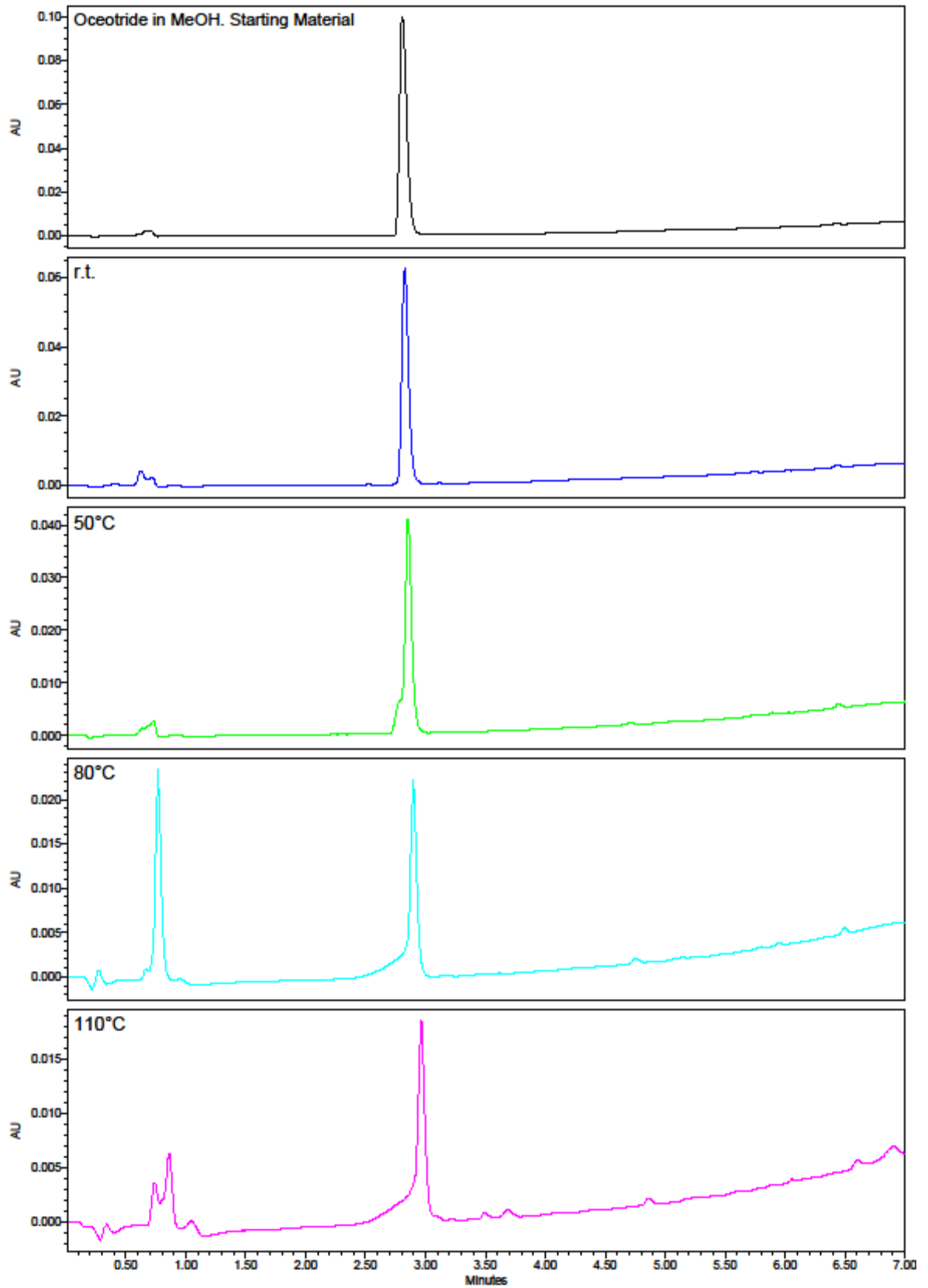


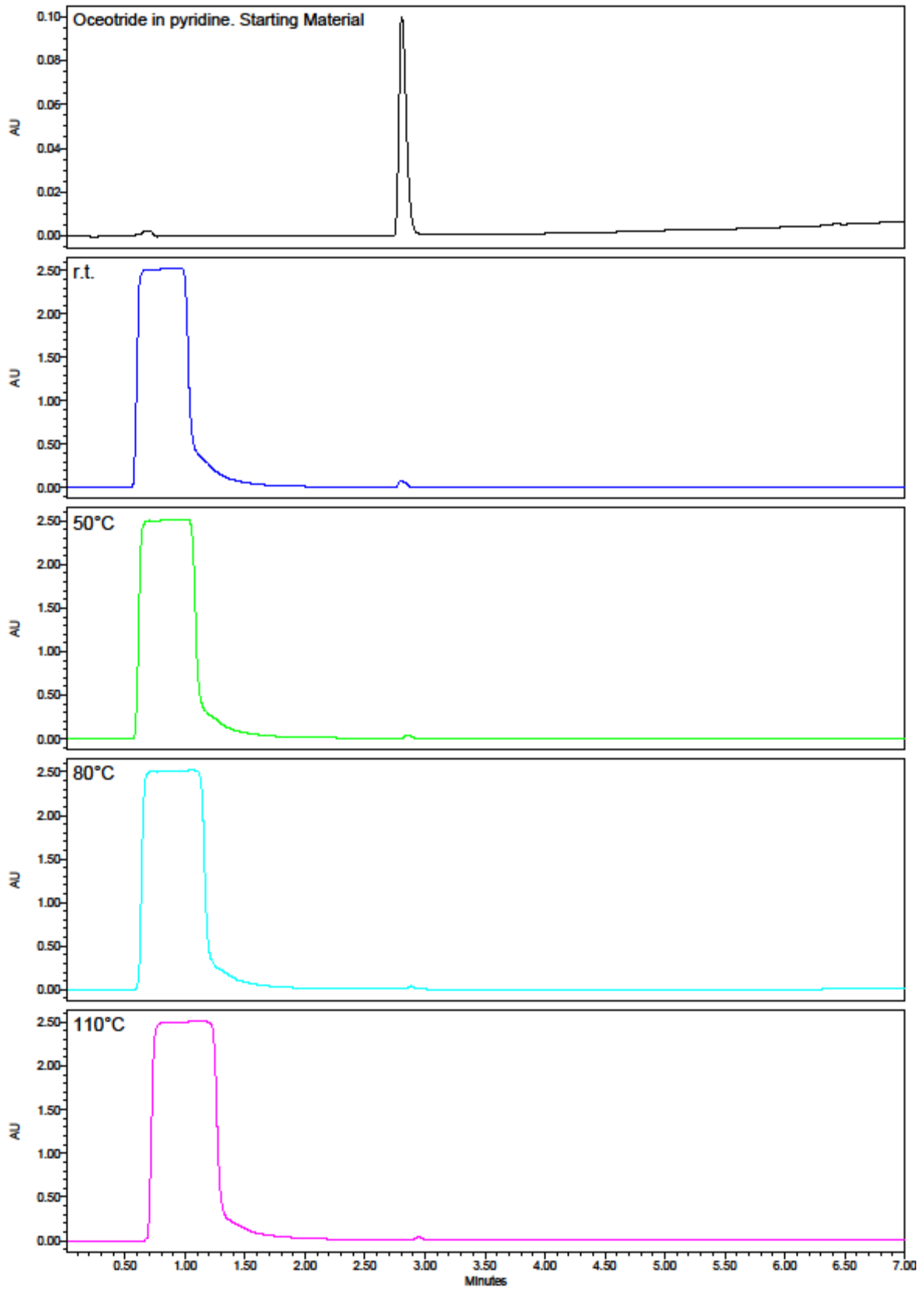


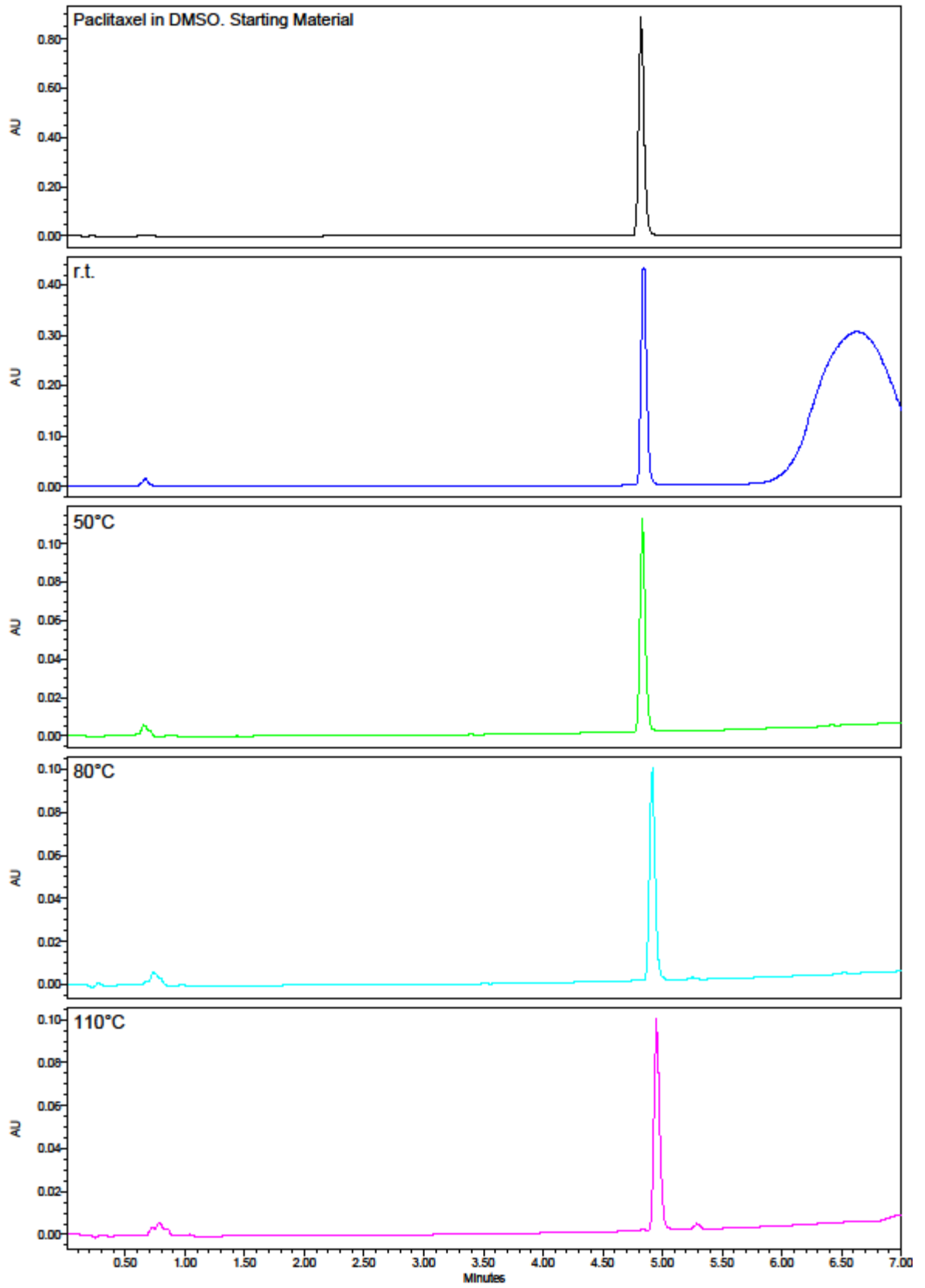




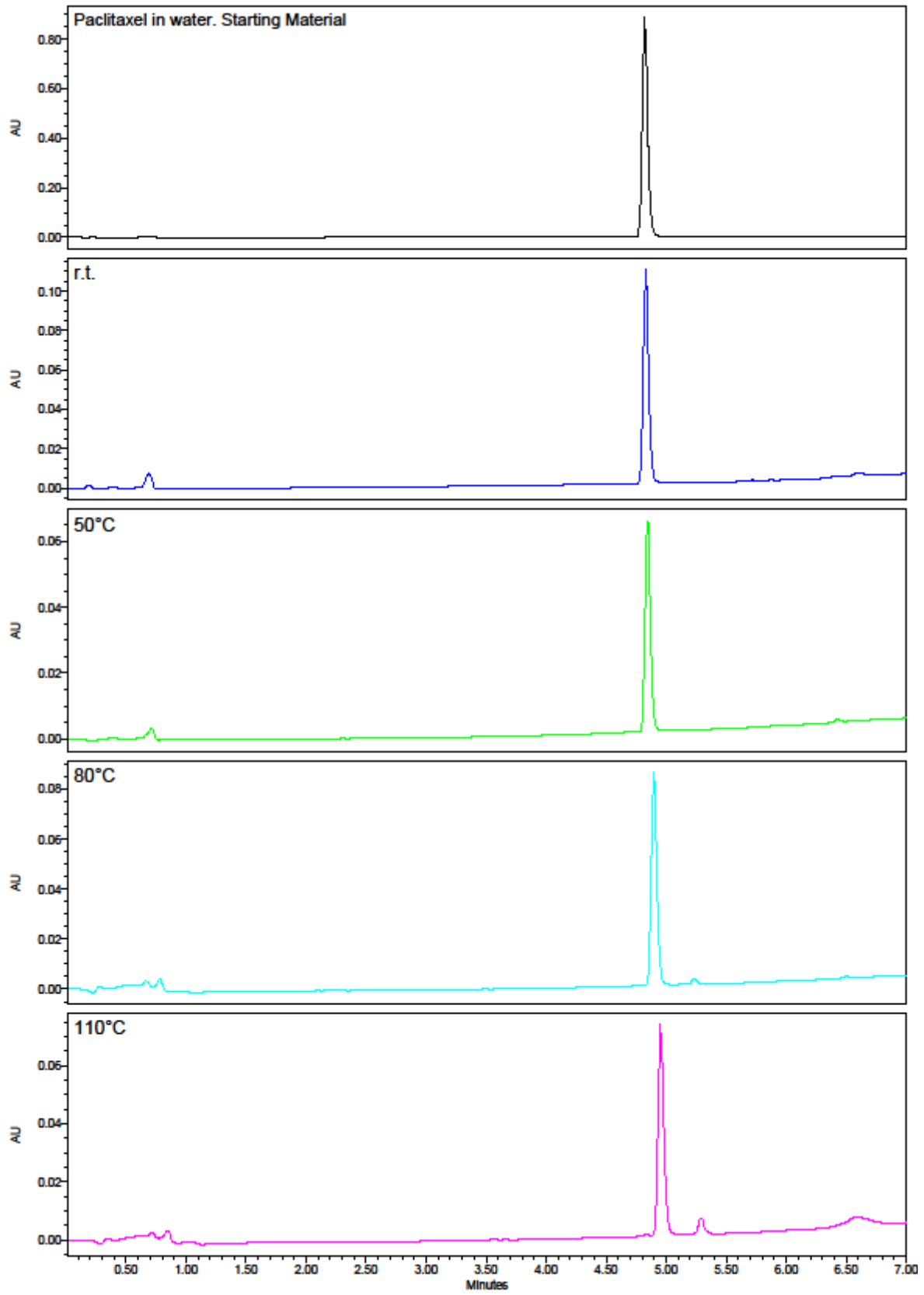


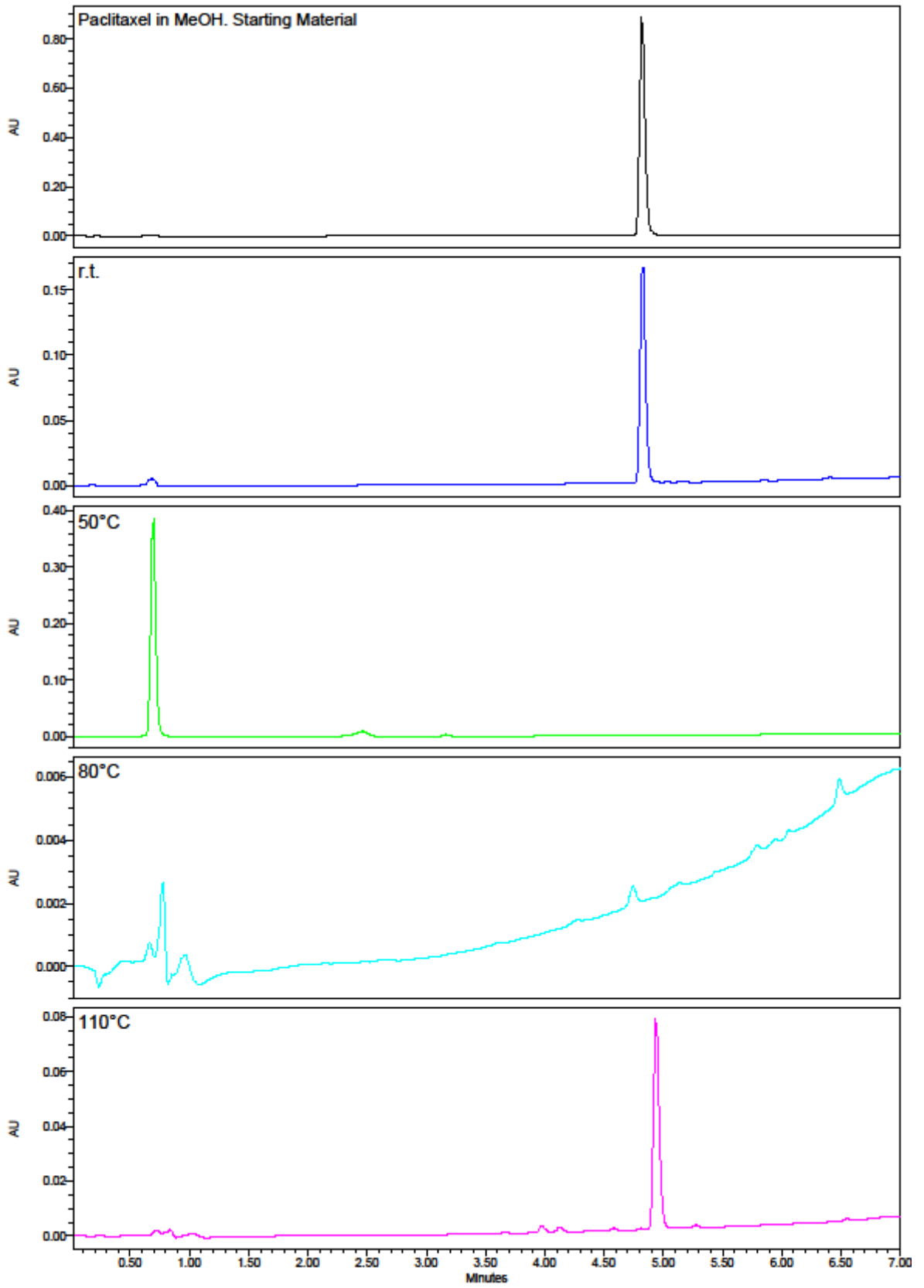


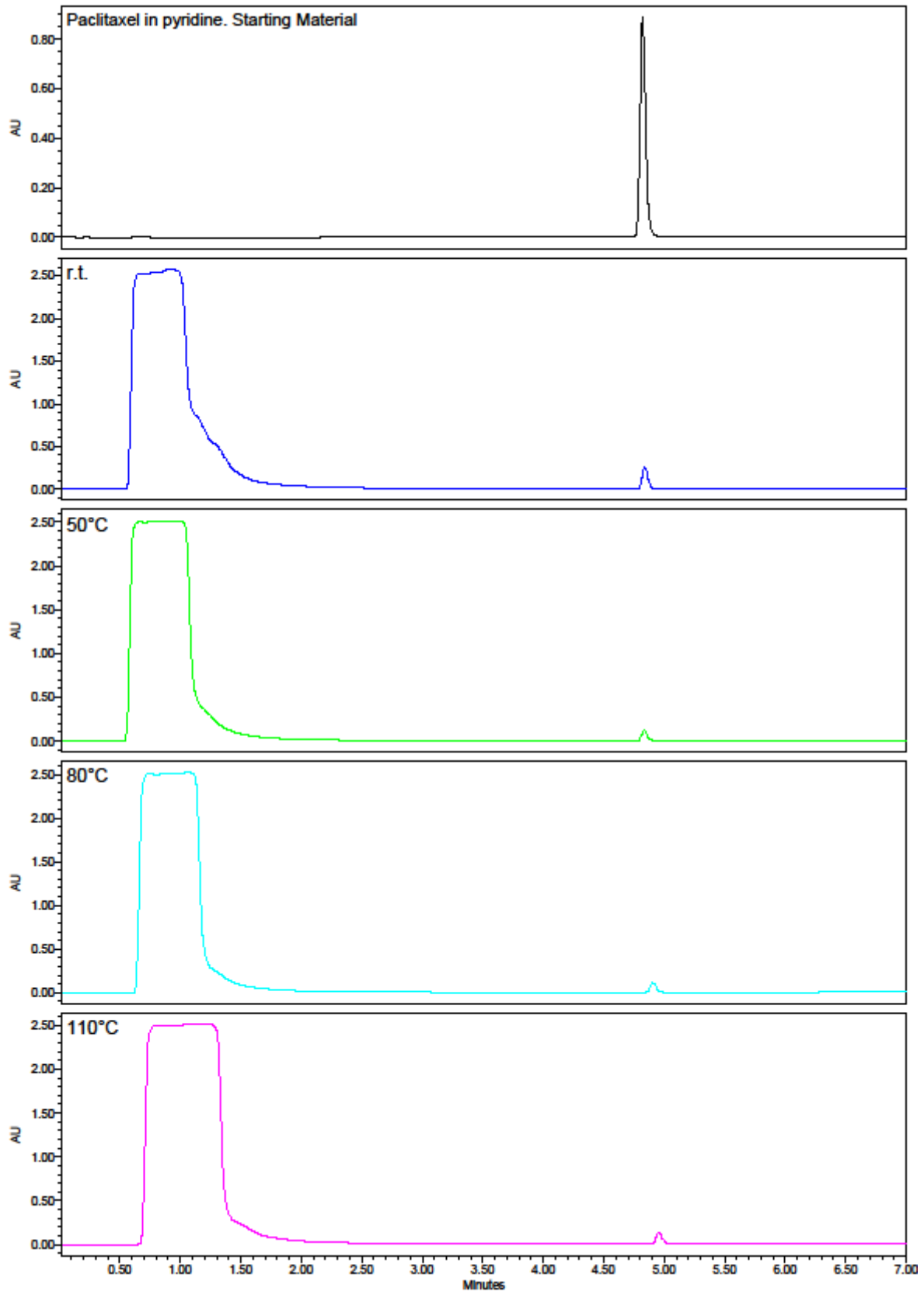


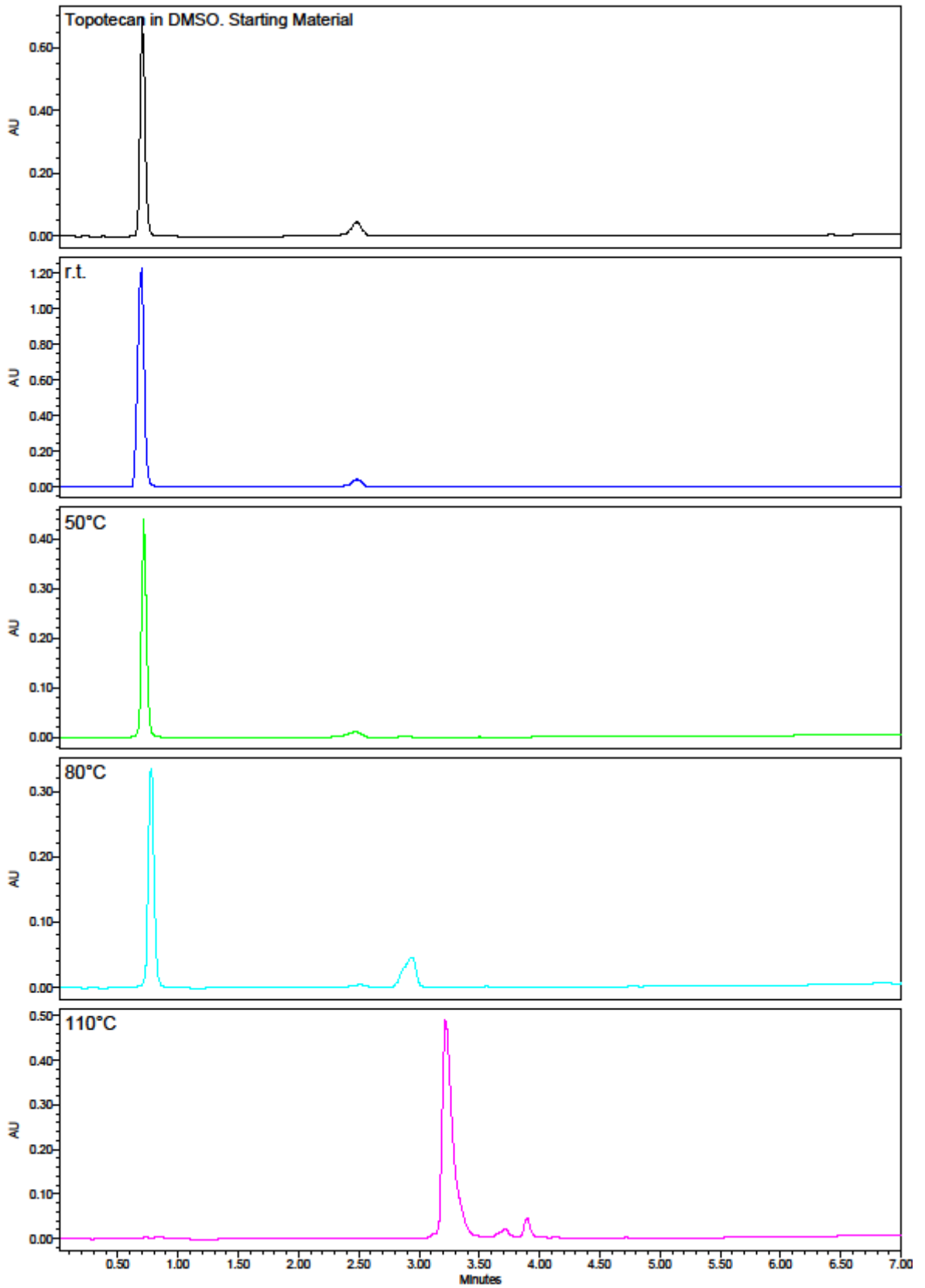


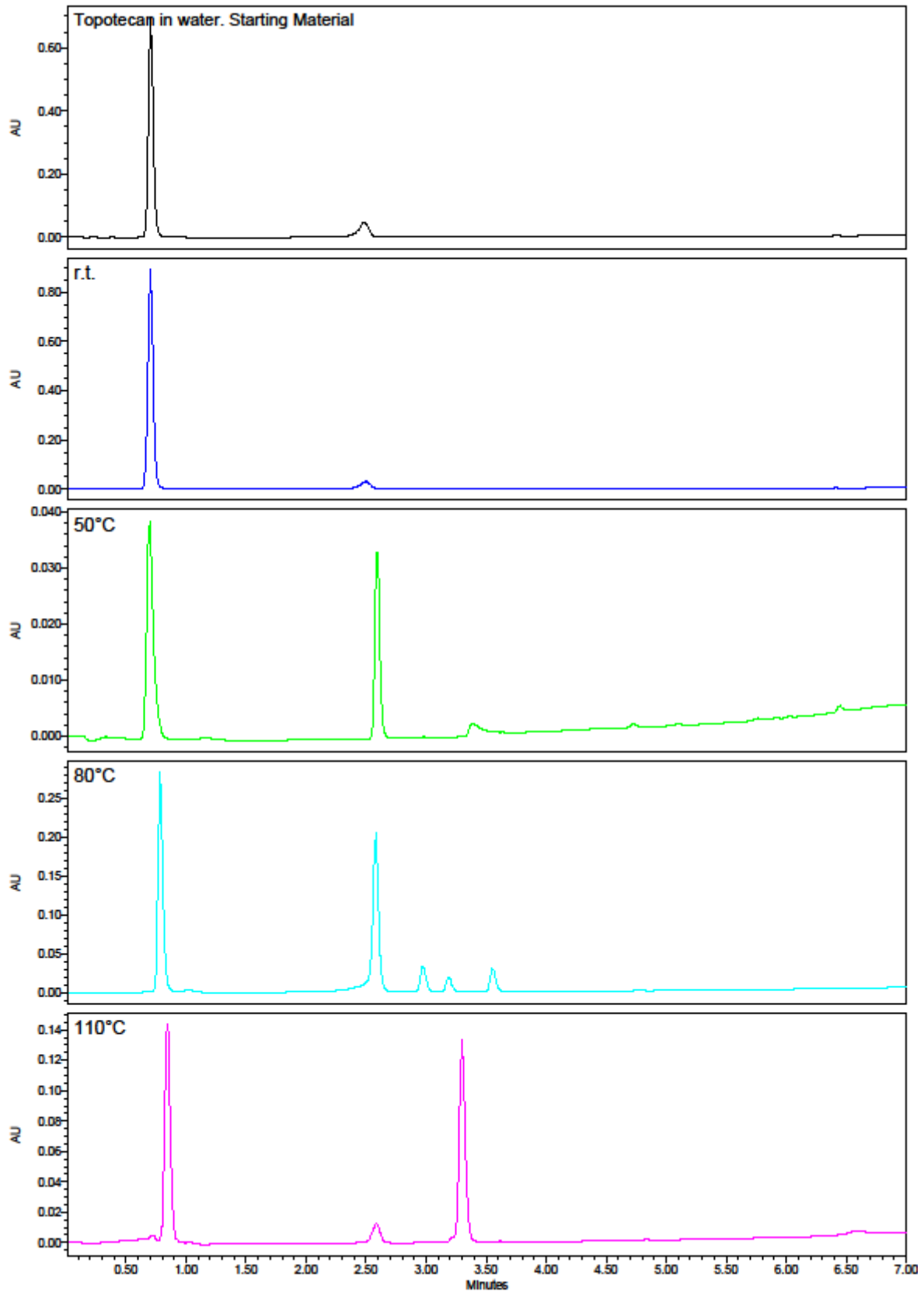


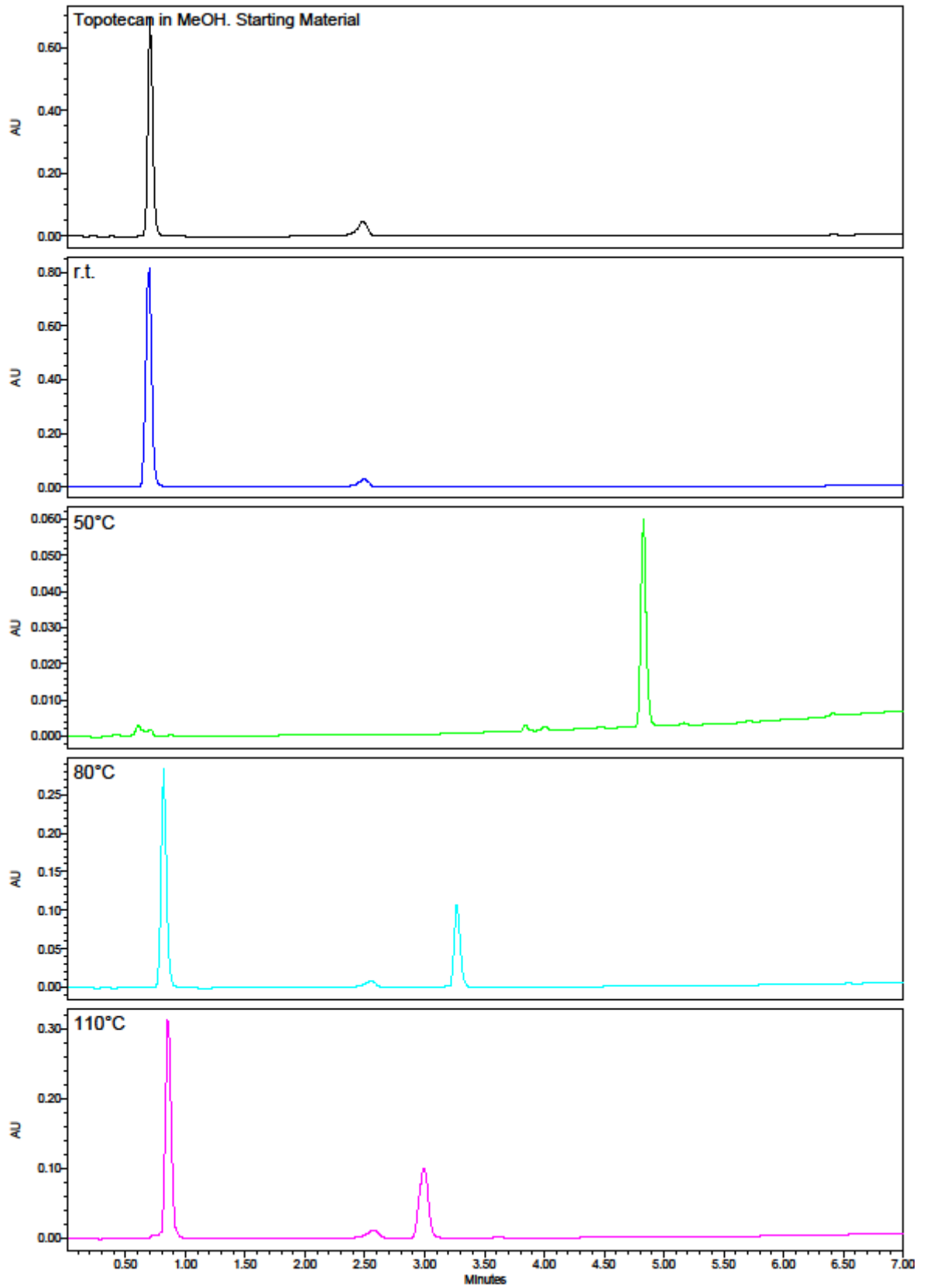


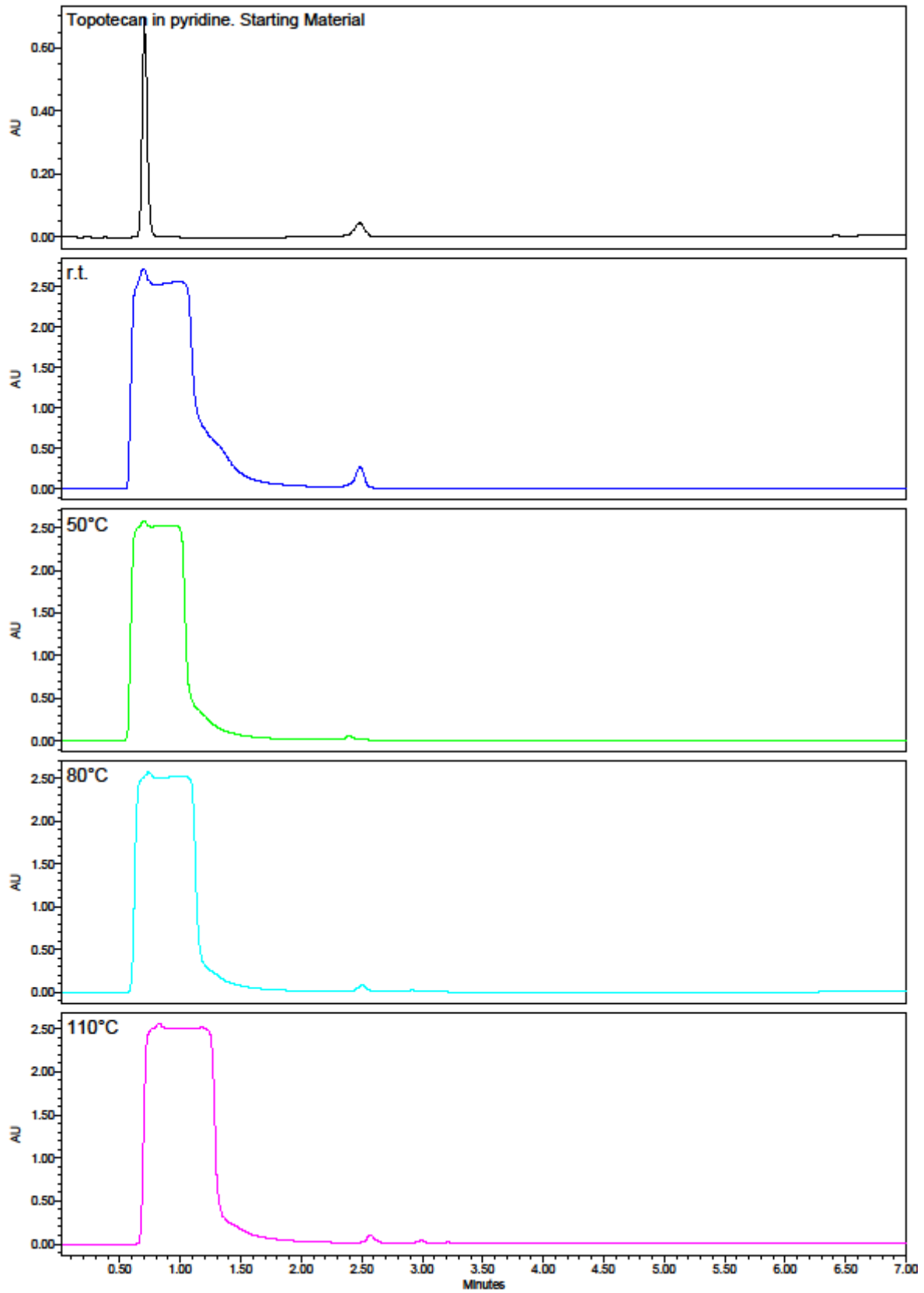


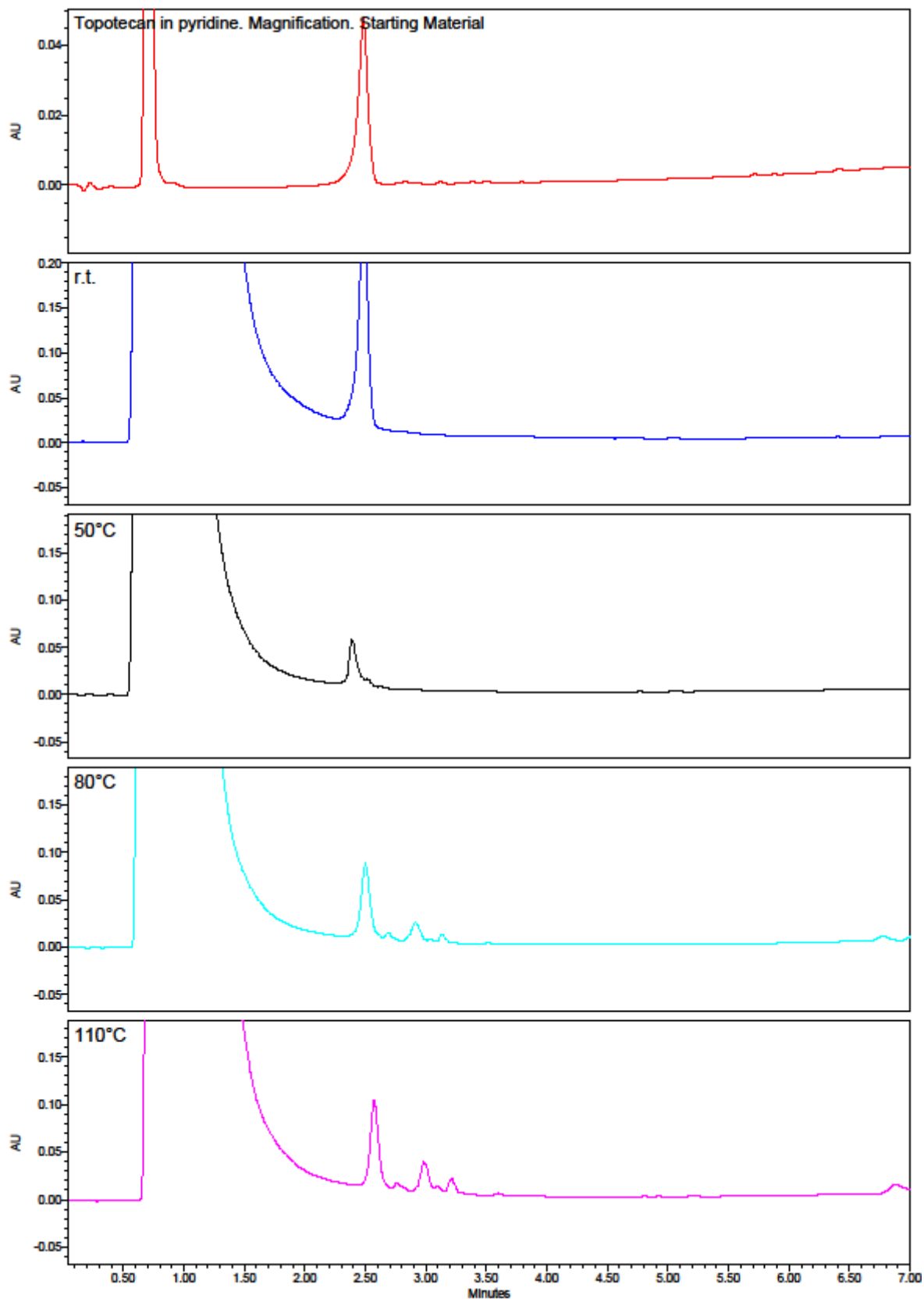




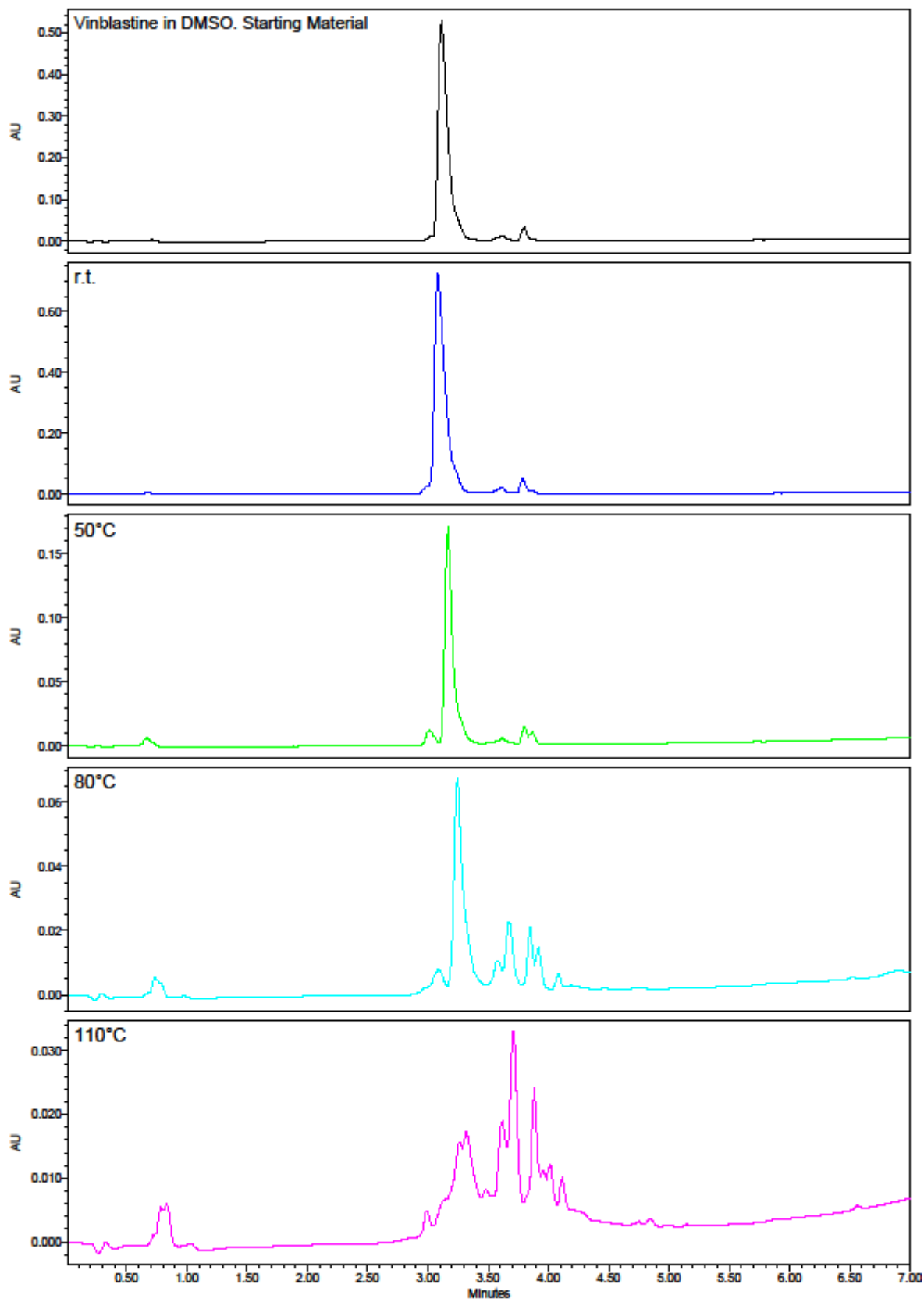


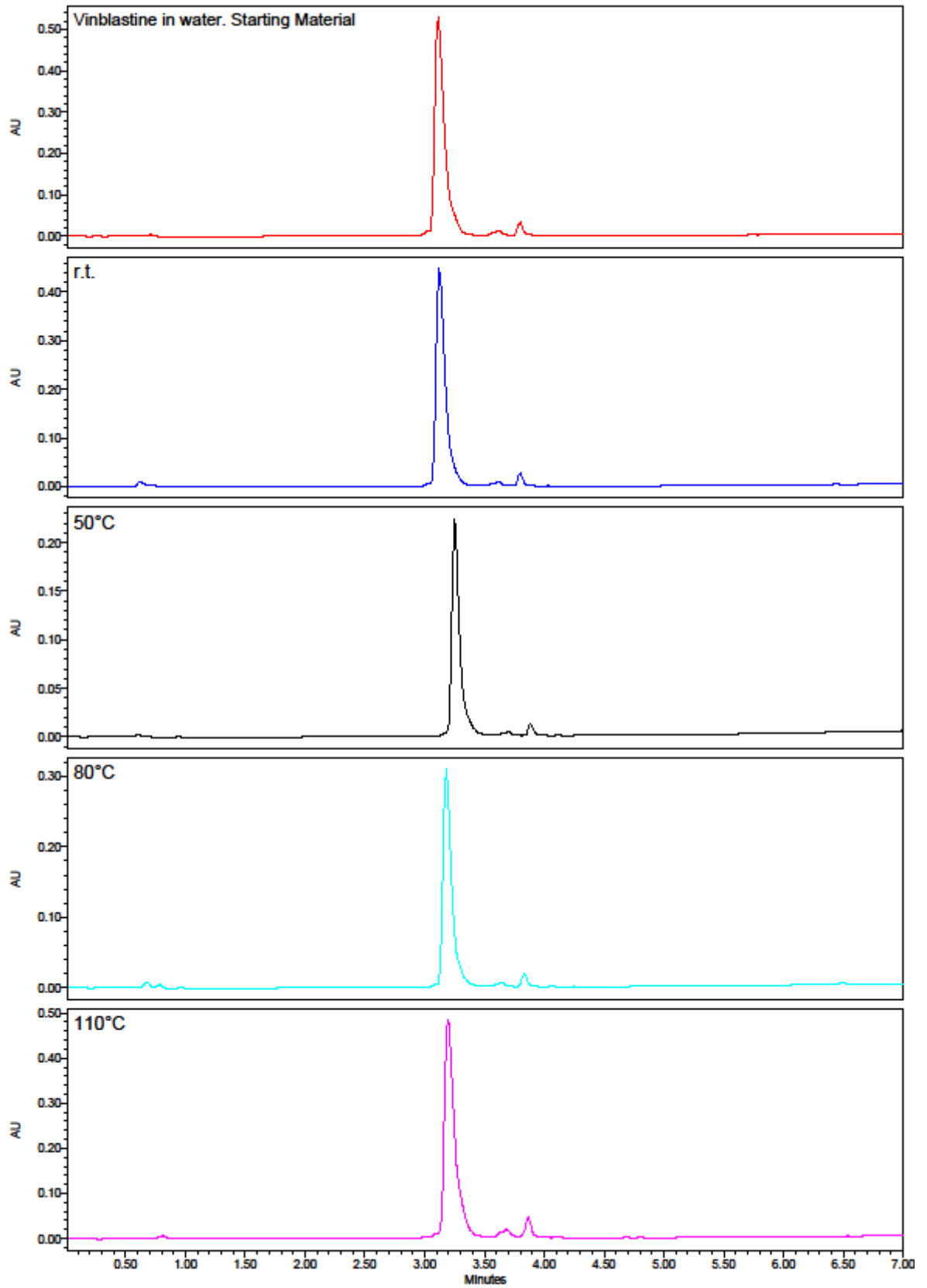


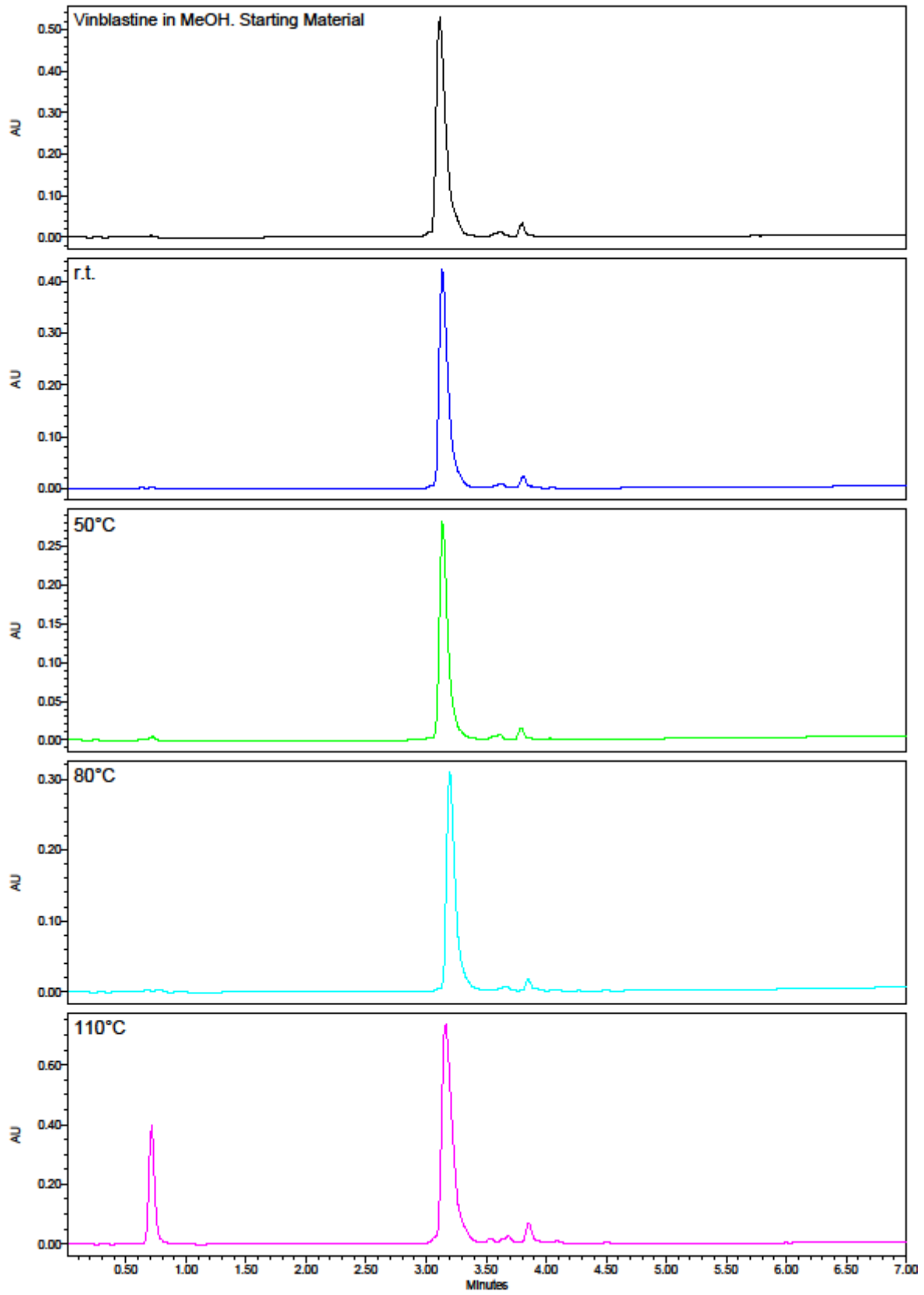


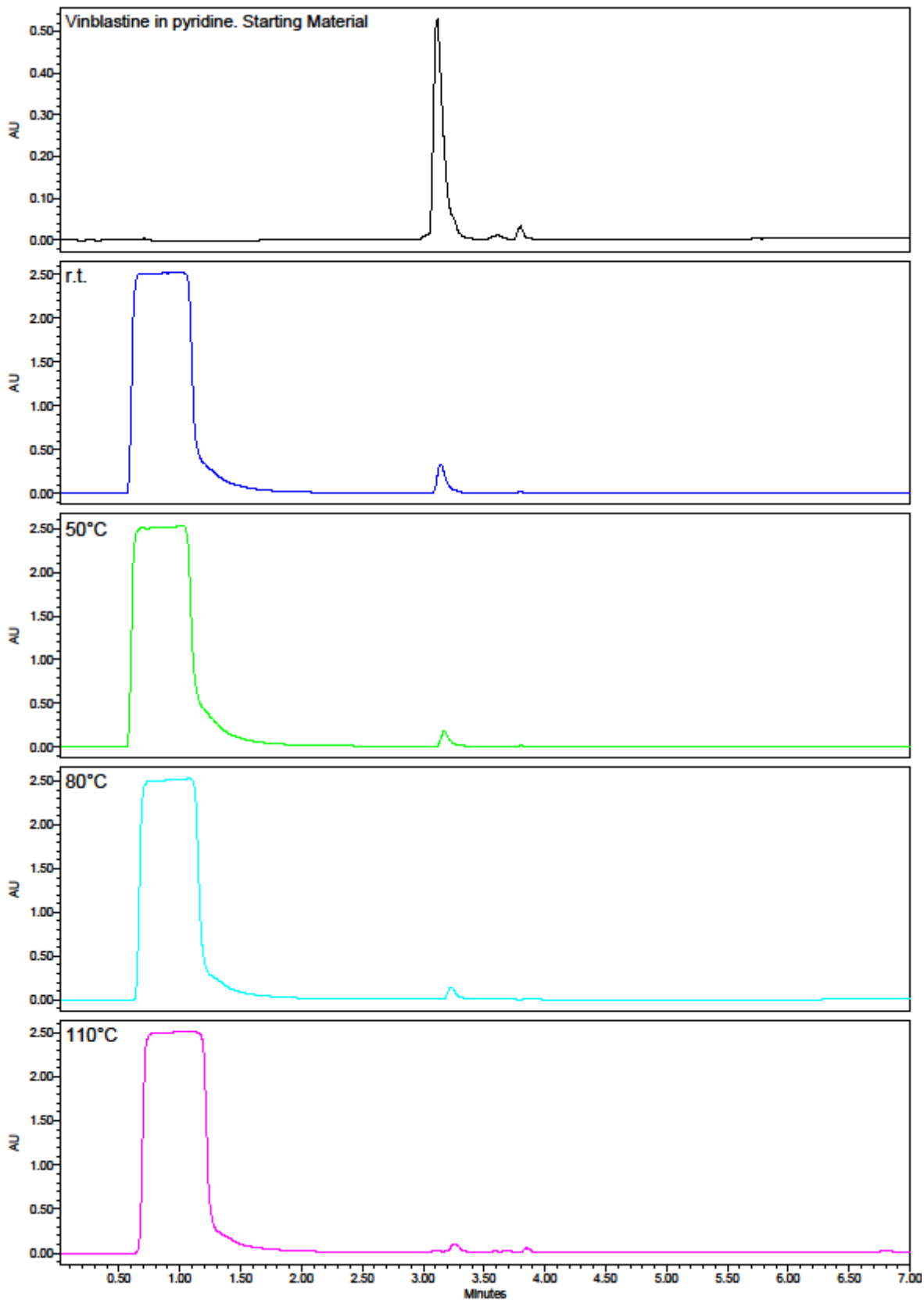


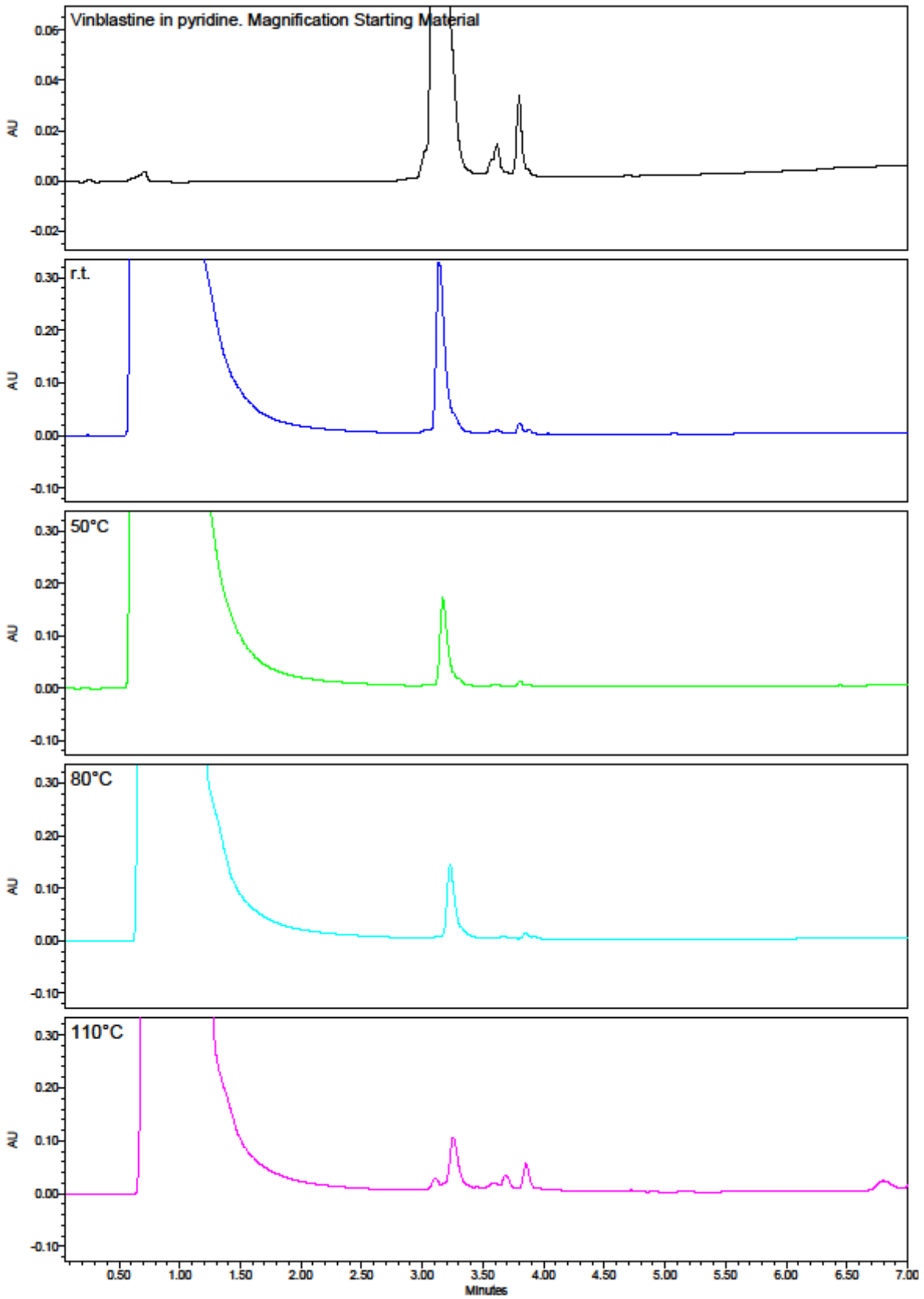












## ACKNOWLEDGMENTS

Firstly, I would like to express my sincere gratitude to my advisors Dr. Alain Wagner and Dr. Jean-Michel Becht for the continuous support of my Ph.D study and for their guidance during these three years.

Besides my advisors, I would like to thank Prof. Thomas Ward, and Dr. Frédéric Taran for accepting to be part of my thesis committee, as well as Dr. Gaëtan Mislin and Dr. Frédéric Bolze for taking part in the two “mid-thesis” committees and giving me many useful advices.

My sincere thanks also go to all those who collaborated to this thesis with their expertise: Dr. Camelia Ghimbeu, Prof. Jocelyne Brendle, Dr. Lavinia Balan and Dr. Sébastien Dautrey for providing the solid catalysts. A special thank in particular to the group of Dr. Balan that synthesized the PEG polymers and that I had the honour to know personally.

Dr. Fabien Thoreau and Dr. Manon Ripoll for the tests in cell, Dr. Igor Dovgan for providing me some probes and so many insights about their synthesis.

Dr. François Daubeuf for quite saving my work by directing me to the right formulation for *in vivo* tests and Dr. Wojciech Krezel and Joanna Sobska, for helping me discovering the world of tests in animals.

Dr. Jean-Marc Nuzillard, for identifying our “mysterious” paclitaxel isomer.

Romain Vauchelles, from creating the macro that allowed me to fill this thesis with colourful images and for introducing me with infinite patience to confocal microscopy.

I thank all of my fellow labmates in the BFC laboratory and in all the corridor of F3 of the Faculty of Pharmacy, from the very first one I spoke to (Zolo), to the last arrived.

To all my friends here in Strasbourg and in Italy: THANKS!

Last but not the least, I would like to thank my family: my parents, my brother and sisters for supporting me spiritually throughout these years.

**Elisabetta TOBALDI**

**Acid Catalysed Abiotic Reactions in  
Biological System:  
From Design to In Vivo Proof of Concept**

Titre en français

**Réactions abiotiques catalysées par un acide dans les systèmes biologiques : de la conception à la preuve de concept in vivo**

## Résumé

Cette thèse porte sur les réactions abiotiques catalysées par un acide dans les systèmes biologiques. Elles sont définies comme des systèmes réactionnels composés d'un substrat xénobiotique - un acétal cyclique dans ce travail - stable dans des conditions biologiques et clivable à un pH bas et d'un catalyseur acide hétérogène correspondant biocompatible. Le défi de cette approche est de maintenir le catalyseur actif dans un milieu biologique tamponné et toujours capable d'hydrolyser le substrat xénobiotique d'acétal et de maintenir le pH tamponné du système vivant dans son état d'origine.

Dans la première partie de ce travail, nous nous concentrons sur le réglage précis des acétals cycliques. Nous identifions 4 structures acétales et montrons que les changements structuraux conduisent à une réactivité différente dans différentes gammes de pH, chacune correspondant à des applications possibles in vivo, notamment des lieurs stables pour les conjugués anticorps-médicaments et des lieurs clivables dans des conditions physiologiques pour la bioconjugaison.

La deuxième partie est axée sur le catalyseur biocompatible. Ici, nous identifions deux catalyseurs biocompatibles solides, ayant différents degrés d'hydrophobie et de propriétés d'adsorption : le copolymère Nafion NR-50 et le copolymère PEG-AASA. Nous démontrons qu'avec un traitement approprié, ils peuvent maintenir un pH interne inférieur à 4, hydrolyser le substrat et ne pas affecter le biofluide hautement tamponné utilisé comme solvant.

**Mots-clés** : réactions abiotiques, hydrolyse abiotique de l'acétal, catalyseurs acides biocompatibles, pH extrême in vivo

This thesis' object is acid-catalysed abiotic reactions in biological systems. They are defined as reaction systems composed by a xenobiotic substrate – a cyclic acetal in this work - stable in biological conditions and cleavable at low pH and a corresponding biocompatible heterogeneous acid catalyst. The challenge of this approach is to keep the catalyst active in a buffered biological media and still capable of hydrolysing the xenobiotic acetal substrate and to maintain the buffered pH of the living system in its original state.

In the first part of this work we focus on the fine-tuning of cyclic acetals. We identify 4 acetal structures and we show that structural changes lead to a different reactivity in different pH ranges, each corresponding to possible applications in vivo, including stable linkers for antibody drug conjugates and linkers cleavable in physiological conditions for bioconjugation.

The second part is focused on the biocompatible catalyst. Herein we identify two solid biocompatible catalysts, with different degree of hydrophobicity and adsorbance properties: Nafion NR-50 and PEG-AASA co-polymer. We demonstrate that, upon proper treatment, they can maintain an inner pH < 4, hydrolyse the substrate and do not affect the highly buffered biofluid used as solvent.

**Keywords**: abiotic reactions, abiotic acetal hydrolysis, biocompatible acid catalysts, extreme pH in vivo